Universidade de Aveiro
Departamento de
Engenharia Mecânica
2017

Daniel Gil Afonso

Aplicabilidade Industrial de Estampagem Incremental: Análise Funcional e Energética

Industrial Applicability of Single Point Incremental Forming: Functional and Energetic Approach

Daniel Gil Afonso

Industrial Applicability of Single Point Incremental Forming: Functional and Energetic Approach

Industrial Applicability of Single Point Incremental Forming: Functional and Energetic Approach

Tese apresentada à Universidade de Aveiro para cumprimento dos requisitos necessários à obtenção do grau de Doutor em Engenharia Mecânica, realizada sob a orientação científica do Doutor Ricardo Alves de Sousa, Professor Auxiliar do Departamento de Engenharia Mecânica da Universidade de Aveiro e do Doutor Ricardo Torcaro, Professor Adjunto da Escola Superior de Design, Gestão e Tecnologias da Produção de Aveiro - Norte da Universidade de Aveiro.

o júri / the jury

presidente / president

Doutor José Carlos Esteves Duarte Pedro
Professor Catedrático, Universidade de Aveiro (por delegação da Reitora da Universidade de Aveiro)

vogais / examiners committee

Doutor Ricardo José Alves de Sousa
Professor Auxiliar, Universidade de Aveiro (orientador)

Doutor Fábio Jorge Pereira Simões
Professor Adjunto, Instituto Politécnico de Leiria

Doutor Pedro Manuel Cardoso Teixeira
Engenheiro Sénior, HPS - High Performance Structures, Lda.

Doutor José Pedro Ovelheiro Maques de Sousa
Professor Auxiliar, Universidade do Porto - Faculdade de Arquitetura

Doutor Jorge Augusto Fernandes Ferreira
Professor Auxiliar, Universidade de Aveiro

agradecimentos / acknowledgements

First of all, I would like to express my gratitude to my advisors Prof. Ricardo Sousa and Prof. Ricardo Torcato for the support of my Ph.D study and related research, for their contributions, motivation, share of knowledge and fast reviews. Their guidance helped me in all the time of research and writing of this thesis. I could not have imagined having a better advisors and mentors for my Ph.D study.

I would also like to thank all people at the Department of Mechanical Engineering of the University of Aveiro who help me with their insightful comments and encouragement and lead me to seek the research from various perspectives.

Besides, I would also like to thank all colleagues at the School of Design, Management and Production Technologies Northern Aveiro who fallowed some of the experimental work and results, helping with both conducting experiments, and commenting on the results.

I thank my family: my parents and my sister for supporting me during the Ph.D. work with positive incentive.

I also thank my friends for the recreation moments during the Ph.D., providing the needed energy for the sleepless nights before deadlines.

Last but not the least, I would like to express appreciation to my beloved girlfriend Carla Santos who speed nights sleeping on the couch next to me while working late and was always my support in the moments when there was no one to answer my queries.

Palavras-chave

Estampagem incremental, Estampagem incremental por ponto único, Linhas orientadoras de design, Fabrico de peças, Fabrico rápido de ferramentas

Resumo

Os processos de estampagem incremental de chapa, como a estampagem incremental por ponto único, têm sido estudados em profundidade desde o início dos anos 2000. Para além da aplicação no desenvolvimento de protótipos, os processo de estampagem incremental apresentam potencial de aplicação no fabrico de produto únicos ou pequenos lotes. Esta possibilidade oferece vantagens ao permitir acelerar o processo de design e desenvolvimento de produto e ao tornar economicamente viável a produção de pequenas séries. Para além disso, esta possibilidade permite a criação de novas tipologias de negócio, possibilitando o desenvolvimento e fabrico de produtos exclusivos ou customizados. No entanto, principalmente devido à novidade do processo, a estampagem incremental ainda não tem muitos exemplos de aplicação em empresas.

O principal objetivo do trabalho apresentado é desenvolver ferramentas que possam ser utilizadas para a industrialização do processo de estampagem incremental por ponto único e apresentar exemplos de aplicações em diferentes áreas industriais.

A máquina SPIF-A desenvolvida no Departamento de Engenharia Mecânica da Universidade de Aveiro é utilizada para o estudo do processo de estampagem incremental. Apesar do potencial do processo de estampagem para fabricar superfícies de forma livre, existem algumas limitações. Estas devem-se maioritariamente ao comportamento do material e ao processo e parâmetros de estampagem. São definidas linhas orientadoras para o design de peças, bem como as possíveis configurações, de forma a possibilitar o desenvolvimento de peças factíveis. O equipamento necessário para a realização de trabalhos de estampagem incremental e os parâmetros de trabalho são estudados com recurso a análise de estado da arte e a trabalho experimental.

Como exemplo de aplicação industrial da estampagem incremental, são desenvolvidas e fabricadas peças. Os produtos são desenvolvidos e avaliados de forma a garantir o cumprimento dos requisitos definidos.

São propostas novas aplicações para a utilização de estampagem incremental para o fabrico rápido de ferramentas, tipicamente exclusivo do processos de fabrico aditivo. A analogia entre a estampagem incremental e o fabrico aditivo permite encontrar aplicações industriais para além da prototipagem, com grande potencial para o desenvolvimento e fabrico de ferramentas. Esta novidade contribui para a redução do tempo de comercialização, reduzindo custos e permitindo uma maior flexibilidade do desenho de um produto. O conceito de fabrico de moldes em chapa para diversos materiais termoplásticos e compósitos é desenvolvido e analisado.

Keywords Incremental sheet forming, Single point incremental forming, Design Guidelines, Part manufacturing, Rapid tooling

Abstract

Incremental sheet forming processes like single point incremental forming have been majorly studied since the beginning of the 2000's. Besides the applications in the prototyping field, ISF processes can also be used to the manufacture of unique parts and small batches. This possibility has a great potential for speed up new product development and to make products in smaller series economically viable. Also, this capability leads to a new business possibilities, enable the development of exclusive or custom products. However, mainly due to its novelty, SPIF industrial operation is still very apprehensive with just a few examples of application.

The main purpose of the present work is to create tools that can be used for the SPIF process management and present examples of usage in different industrial fields.

The SPIF process is studied using the SPIF-A machine design and built at the Department of Mechanical Engineering at the University of Aveiro. Despite being a free form manufacture process, SPIF has some geometric limitations, manly due to the forming mechanics and formability limit of the materials. The possible part configurations and the design orientation are settled, allowing a suitable part development. The hardware to perform incremental forming operations is outlined and the forming process is described, presenting alternative solutions both based on experimental work and state of the art review.

A group of parts are developed and manufactured using SPIF as examples of industrial application. Parts are developed and evaluated to meet design and development requirements.

New applications using SPIF as a rapid tooling process, typically exclusive form additive manufacturing technologies, are developed. The parity between SPIF and AM processes encounter industrial applications not only in prototyping or part manufacturing but also in tool development and fabrication. This novelty allows to decrease the time to market, decrease tooling cost and increase tooling complexity and consequential part design freedom in sheet metal moulds. The concept is developed and proof for a variety of thermoplastic and composite materials processing technologies.

Mots-clés Formage incrémental de tôle, Formage incrémental un point, Lignes directrices de conception, Fabrication de pièces, Outillage rapide

Résumé

Les processus de formage incrémental de tôle, come formage incrémental un point, sont étudiés en profondeur dès le début des années 2000. Les processus ont son application dans le développement des prototypes et présentent aussi du vrai potentiel dans la fabrication des produits uniques et dans des petits lots. Cette possibilité offre des avantages parce que permit d'accélérer le processus de design et développement de produit et de faire le projet des petites séries économiquement viables. En plus, formage incrémental possibilité la création des nouvelles typologies de affaires à cause de ça contribution dans la fabrication des produits personnalisés et exclusives. Malgré ça et comme celui est un processus très récent, pour l'instant, le formage incrémental n'a pas beaucoup de utilisation industrielle.

L'objectif principal du travail présenté est de développer des moyens que peut être utilisés pour auxilié l'industrialisation do processus de formage incrémental un point et présenter des exemples pour des distinctes applications industrielles.

La machine SPIF-A développé dans le Département de Ingénierie Mécanique de l'Université d'Aveiro est utilisée pour l'étude du processus de formage incrémental. Nonobstant le potentiel du processus de formage incrémental pour fabriquer des surfaces de forme libre il y a quelques limitations géométriques. Ça dépend du comportement du matériel et les paramètres de travail. Les configurations géométriques possibles et les lignes directrices de conception sont définies de façon a possibilité le dessein des pièces faisables. L'Equipment nécessaire pour la réalisation des travaux de formage incrémenta et les paramètres de travail sont étudiés en utilisant l'analyse de l'état de l'art et des travaux expérimentaux.

Comme exemple des applications industrielles du formage incrémental, sont développées et fabriqués des pièces. Les produits sont développés et avalisés de façon à assurer qu'il respecte les exigences définis.

Ils sont proposés des nouvelles applications pour l'utilisation du formage incrémental pour l'outillage rapide, normalement exclusive des processus de fabrication additive. L'analogie avec le formage incrémental et la fabrication additive permet de trouver des applications industrielles qui sont plus que seulement du prototypage, avec du grand potentiel pour le développement et fabrication des outils. Cette nouveauté contribue pour la réduction du temps d'arrivage au marché en permettant de réduire les couts et concédant une liberté de dessein de produit. La conception de fabrication des moules en tôle pour des divers technologies pour des matériaux thermoplastiques et composites est développé et avalisé.

Contents

List of Figures

List of Tables

Nomenclature

AISF	Asymmetric Incremental Sheet Forming
ASM	Applied Scientific Method
CAD	Computer Aided Design
CAM	Computer Aided Manufacturing
CNC	Computer Numerical Control
DFM	Design for Manufacturing
DOE	Design of Experiments
DPIF	Dual Point Incremental Forming
FFF	Fast Freeform Fabrication
FFL	Forming Fracture Line
FLC	Forming Limit Curve
FLD	Forming Limit Diagram
FMS	Force Measuring Sensor
FMSs	Flexible Manufacturing Systems
ISF	Incremental Sheet Forming
ISMF	Incremental Sheet Metal Forming
LDR	Limiting Draw Ratio
NC	Numerical Control
RT	Rapid Tooling
SL	Stretching Limit
SPIF	Single Point Incremental Forming
TPIF	Two Point Incremental Forming
TRL	Technology Readiness Level

Chapter 1

Introduction

Sheet metal forming is a metalworking process that permanently shapes a part by changing its shape, typically from a flat blank. No material is either added or removed, so mass remains unchanged during forming process. Metal forming processes use force to induce plastic deformation on a blank to archive the desired shape. Complementary processes are used for both acquiring the blank before the forming operation and cutting out the part outline for part finishing. Mainly cutting and joining operations are used as accessory operations.

Metal forming produces stiff and tough parts, thanks to the great mechanical properties typical of metals and the high moment of inertia given by its shape. Furthermore, as sheets used have low thicknesses, total parts weight is also low, thus enabling a good solution for both structural and functional parts. As several processes exist, allowing the manufacturing of different shapes, sheet metal forming is also used to produce fairings and other ornamental parts [1].

Metalworking is known for being an ancient art, with great industrial development since the industrial revolution. Several different sheet metal forming exist with different operation principles and enabling the achievement of different geometries. In the mid XX century incremental sheet forming (ISF) processes have been introduced [2]. However, due to the technological issues, ISF processes have been majorly studied since the beginning of the XXI century [3]. ISF are dieless processes that consists on gradually form a sheet to the desired shape, by following a tool path with a simple, typically ball tip tool. ISF processes rely on computer numerical control (CNC) to manage the tool motion. Several variations have been developed, each with specific operation features and leading to different results. Single point incremental forming (SPIF) is one of the best studied ISF processes. A flat blank is formed by a simple CNC controlled punch while peripherally held all around and supported by a backing plate with the part cavity boundary. A comprehensive review paper on SPIF has been published in 2005 [4].

The industrial application of the forming processes are influenced by the geometrical limits and considerations. Besides, as most processes involve the use of self proposed dies and tools, the viability of a forming process is strongly overweight by the production quantity. On the other hand, some processes that doesn't need dies or tools have great cycle time that also influence the number of parts to build.

Is is known that the product life time is highly dependent on the customers request. While mass production is used for most of the industrial products, the demand for custom products is increasing. The concept of mass customisation introduces the possibility of creating indi-

vidually customised products, with mass production volume, cost, and efficiency. The use of flexible manufacturing systems (FMSs) allows converting individually customised designs into individually customised products, with mass customisation volume, cost, efficiency, accuracy, and reliability [5]. ISF systems are strong candidates to integrate FMSs for the manufacture of sheet metal parts.

Since the ISF processes are new when compared to conventional forming processes, not many industrial applications have been developed yet. However, with the consistent results it is now possible to obtain, the process dissemination around the industrial companies is starting. Thanks to the dieless operation, ISF allow the manufacture of sheet metal parts with minimal initial investment. Thus, incremental forming applications differ from conventional forming processes. Besides the applications in the prototyping field, SPIF can also be used for the manufacture of unique parts and small batches. This capability leads to a new business possibilities, enable the development of exclusive or custom products.

Despite being a free form manufacture processes, ISF has some geometric limitations, manly due to the forming mechanics and formability limit of the materials [4]. Thus, it is important to establish well-defined guidelines to grant a feasible part design. Moreover, it is also important to understand the operation procedures to chose and apply the best forming parameters to each part. Finally, if integrated with other forming and finishing processes, ISF can lead to great versatility in the part design and lead to production of high value parts.

This thesis reports the contributions made to the SPIF process and explore possibilities for industrial applications. The work plan includes studies in three different branches: analyse and enhance the SPIF process, test the use of SPIF for sheet metal parts manufacturing and test SPIF as a rapid tooling (RT) process. Briefing, the work plan indents to contribute to the SPIF establishment as an industry ready smart manufacture technology.

In what regards the contribution to the SPIF process, experimental work is performed using the SPIF-A machine [6]. The main objective is to settle a base framework for the remaining work and define a guidance referential to be used both for designing SPIF parts and for the SPIF process handling. Contribution intend to add to design for manufacturing (DFM) guidelines, aiming for a more reliable and feasible forming process. In this sense, SPIF can be seen as a reliable competitor among a technology selection phase during a part design and development [7]. This analysis apprehend not only a functional approach of the SPIF process but also an energetic evaluation associated to the forming performance and result. This first stage of the research is continued along all PhD assignments, contributing to an improved work while reinforcing and completing the results.

The current SPIF technology research may be defined primarily within a design-driven fields, addressing the definition of new and complex systems by combining known elements. The investigation searches solutions in a philosophy of problem solving. This method can be applied by founding the research in concrete examples from industrial partners. On the other hand, new applications can also be provided by researchers. This can legitimise the technology and lower the threshold for other companies to try it. Research plays an important strategic role in identifying future threats and opportunities wherein companies need to upgrade their competence [8].

In this context, the PhD works includes the development of case study parts, contributing to applied research and for the support of the SPIF primary purpose. The case studies are both driven in cooperation with industrial companies or self purposed.

The manufactured parts are used as an example of the possible SPIF application at industrial environment. Each case study describes specific goals and the work method used

for the part and process development. An overall evaluation of the results is performed at both functional and energetic approaches, evaluating the final part quality and the full manufacturing process.

A third field of study involves the use of SPIF as a rapid tooling process. The RT concept is traditionally associated to the rapid manufacturing (RM) or additive manufacturing (AM) technologies. Nevertheless, the RT is overally defined as a combination of processes to produce tools and moulds for conventional manufacturing processes in less time and at a lower cost compared to traditional machining methods [9]. The main advantages of a shorter tool development time and lesser tool cost is the decrease of the time to first product and the practicable batch size. The main disadvantages involve a smaller tool life, wider tolerances and worst surface finishing [10].

Being compatible with FMSs, with parts manufactured from CAD models without considerable dedicated tools in short time, ISF processes can be seen analogously to AM technologies. Thus, it is reasonable to apply the RT therm when describing the fabrication of tools for different industrial processes using ISF techniques.

The use of sheet metal and other thin walled moulds has considerable application in industrial processes, particularly in processing of thermoplastics and composite materials. These tools have usually attractive wight/strength ratios with low material costs and, when applicable, low thermal inertia. However, conventional manufacturing processes have limited geometric freedom or are very time consuming and expensive. Furthermore, traditional RT techniques, using AM processes, struggle to achieve thin geometric features, becoming weak competitors for the mould manufacture.

The ISF processes, in particular SPIF, have great appetence for the fabrication of these geometries. In such a way, the work plan studies the development of sheet metal moulds for various manufacturing process using SPIF and discuss their advantages. SPIF is used as a direct tooling process for the development of moulds. The moulds are used for different manufacturing processes, evaluated and compared against conventional tools.

The PhD work program Industrial Applicability of Single Point Incremental Forming: Functional and Energetic Approach covers the current possibility of SPIF industrialisation, leveraging its implementation. Usable knowledge for practical application is settled and examples of use in different fields are presented. Moreover, the research work founds future developments on SPIF usage and applications, contributing both to the academic and industrial areas.

1.1 Motivation and scope

This thesis follows up the development of a purpose built SPIF machine at the Department of Mechanical Engineering of the University of Aveiro: SPIF-A [11], developed within the project "Innovative Techniques and Efficient Strategies For Numerical Modeling and Experimental Analysis of Incremental Sheet Forming Processes", PTDC/EME-TME/098845/2008 [6,11,12]. The SPIF process requirement were studied and a Stewart Platform based machine, further described on the state of the art chapter, was design and built. Along the project, some research was done, aiming to give a relevant contribution to the state-of-the-art and knowledge level of the SPIF process. In addition to numerical methods simulation applied to SPIF, studies included CAD/CAM strategies for a parallel kinematics SPIF machine [13], analysis of the forming parameters and influence on time efficiency [14], lubrication aspects in the

SPIF process [15] and others.

These studies, onward other developments in the ISF field, lead to a industry ready stage of the SPIF process, where preliminary part production case studies were tested. The PhD work plan aims to contribute to this goal. The work focus on contributing to enhancing the SPIF process and analyse possible industrial applications.

An exhaustive analysis on the SPIF process, particularly using the SPIF-A machine, is performed not only to add to the academic field knowledge but also to define detailed process guidelines for the process implementation. This definition is performed in both a functional and energetic approach. A background knowledge about design and process guidelines for several other manufacturing processes provides a recognition off their importance to both part design and development and the industrialisation. This awareness works as a catalyst to develop analogous information about SPIF, aiming to its industrial dissemination.

Alongside the SPIF process study, industrial applications were developed. The developed guidelines for both process and part design are used as foundation in case study examples. These applications aims not only to consolidate the initial purpose of the ISF technology but also to engage in the process dissemination among industrial entities and product designers.

Lastly, the PhD work aims to propose new employments for ISF, particularly in the development of moulds and tools for other manufacturing processes, aiming to expand the field of interest on the process. In addition to introducing and validating concrete applications, this effort, placing SPIF side by side with other processes of high enthusiasm as AM, aims to extol and draw attention to the incremental forming processes.

1.2 Thesis organisation

The PhD thesis is organised in seven chapters. The first three chapters (1, 2, 3) introduce the study topics. The successive three chapters (4, 5, 6) present the developed work, with partial conclusion at the end of each section. The last chapter (7) presents overall conclusions from the developed work.

The current chapter, *Introduction*, provides a framework to the developed research. A historical background on sheet metal work is described and the emergence of the incremental sheet metal forming technologies is introduced. The ISF initial industrial purpose is presented, defining the path for the thesis goals.

The second chapter, *State of the art*, includes a comprehensive review of the state of the art of sheet metal process, particularly the SPIF process. A fundamental analysis about the sheet behaviour under stress is described and an overall description on sheet metal forming processes is provided, including conventional press forming processes, low cost die processes and dieless and other farfetched forming processes. The state of the art finishes with an exhaustive review on the SPIF process, including the analysis on the working principle and forming mechanics, process parameters and current applications.

The third chapter, *Objectives and methodology*, presents the thesis goals and describe the research methodology. Specific goals are well defined within the three foundation objectives. The methodology used to achieve each objective is described and the different measurement and calculus methods are stated.

Chapters four to six describe the research work completed along the thesis for the goals fulfilment. The perform activities are defined, with a detailed description on both execution and results. Each individual study ends with partial conclusions in order to contribute to

the overall objective. Chapter four, *Developing SPIF*, presents the contributions to the SPIF process development. This chapter includes an energetic analysis about the SPIF process, particularly applied in the SPIFA machine; the proposal of new part configuration and optimisation study on forming parameters; a definition of well defined design guidelines for SPIF parts and efficient CAD/CAM strategies for SPIF. Chapter five, *Fabrication of sheet metal parts*, describes the use of SPIF in some case study industrial application, analysing both the process and the results. Chapter six, *SPIF for rapid tooling applications*, presents the development of sheet metal tools for various manufacturing processes. Moulds for different industrial processes are design to be manufactured by SPIF and experimental work is performed for proof of concept. The chapter includes the development and analysis of tools for composite material layup, thermoforming, rotomoulding and rotocasting.

The final chapter, *Conclusions*, summarises the overall achievements of the thesis work and sets the contributions for the SPIF process and its industrial applications. The research results are compiled and discussed with final considerations, including perspectives for industrial applications of SPIF and for future research works.

Chapter 2

State of the Art

2.1 Sheet metal forming processes

Sheet metal parts have the advantage of using a high strength materials while being light thanks to thin thicknesses. These technical features give them a good strength-to-weight ratio, making them a very viable option for the manufacture of structural pars.

A large variety of forming processes exist to shape metal sheets to the desired form. From the simplest low tech hammering metal shaping to highly precise tools for continuous operation or numerical control (NC) incremental forming to unique parts, processes allow the manufacture of different geometric features at different production rates. The choice of one technology for the manufacture of a metal part must be made in consideration with the geometric features and complexity, production volume and maximum part cost. Despite this, any process has its intrinsic limitations that should be taken into account for a good part design.

2.1.1 Press forming processes

Most mass production operations with sheet metal forming are made using press tools. Press tool basics anatomy include a die, a punch and a blank holder. A more complex tool may need the use of strippers, knockouts, ejectors or other features. Press tools can be used for single operations or organised in progressive tools or compound tools. Press tools are expensive to produce due to both their complexity and necessary precision and the hardened material and tool manufacturing. However, their productivity is high making them well suited to large volume continuous production. Thus, these processes are mostly used in high volume production industries like automotive and domestic appliances to answer their request for high production quantities and complex shaped metal parts [16].

The two main processes for sheet metal forming with press tools are drawing and stretching. Drawing is mostly used for deep parts with limited shape complexity while stretching is better suited for shallow intricate parts. Besides depth, the working principle also differs between drawing and stretch forming: on the first the blank is allowed to draw into the die and thickness is nominally unchanged. On the second, the operation involves stretching in some areas at expense of sheet thickness [1].

When the forming parts are simpler with straight line bents only, specially purposed build tools for stretching or drawing operations are not needed. A variety bending operations exist and can be used to form parts using multiple purpose forming tools.

Drawing

Drawing or deep drawing is used to form a sheet metal into a cavity. It is mostly used when the depth is significant. In other words, when the depth is greater then the cavity average diameter. It allows the fabrication of both shallow or deep parts with relatively simple shapes. As high tooling and equipment costs are needed to deep draw a metal sheet, production is suited for large volume and continuous production.

In the drawing process, a punch force a sheet metal blank into a suitably shaped die. The blank must be cut to the correct size before forming operation. Figure 2.1 represents the drawing principle with and without blankholder. As the punch pushes the sheet, material drawn over the die radius and flows into the die. While the punch movement continues, material is straightened again. Due to this material flow, theoretically sheet thickness doesn't change during the process. In practice some thinning occur in the side walls depending on the clearance between punch and die and their radius [17].

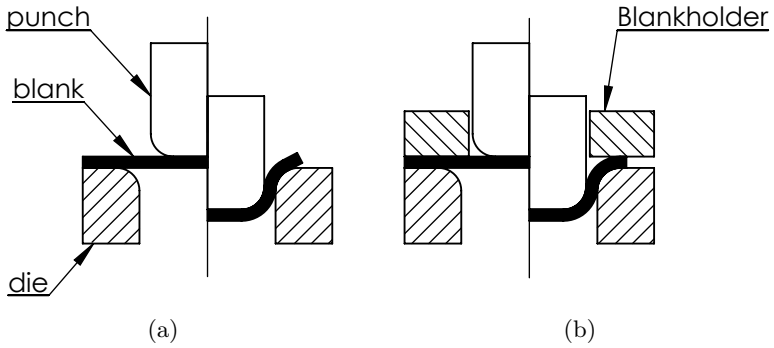

Figure 2.1: Basic drawing process: (a) without blankholder, (b) with blankholder

During drawing operation the material is subjected to different states of stress. The base of the formed part is under almost zero stress, with some biaxial tension. The vertical wall is under tensile stress as it pulls the rest of the blank into the die. The portion of the blank yet to be drawn is under a combination of tensile forces in the axial direction and compression strength on the radial direction as its peripheral size is reduced. This state of stress cause the blank to lift and to wrinkling. The use of a lubricated pressure ring as a blank holder prevents the unbent blank to deform undesirably. The applied pressure must be enough to prevent wrinkling but must allow the free flow of the sheet into the die. Besides wrinkling, possible failures in drawing operations are earing, due to the anisotropy of material, tearing, due to insufficient die or punch radii and surface scratches, due to insufficient lubrication or tool surface smoothness, as presented in figure 2.14 [16].

In order to perform safe drawing operations, some guidelines should be followed. The ratio between blank diameter and formed diameter is restricted by the limiting draw ratio (LDR) (figure 2.3), which is influenced by material, part and tool geometry [1]. Besides, parts should be dimensioned to the inside wall and the internal radius between vertical walls should be 6 times greater then the sheet thickness. A minimum radius (4 times greater than the thickness) should also be applied between vertical walls and the base and between vertical walls and the flange. Drawing slope angle walls or even variable slope walls or multiple slope walls is possible at greater tool cost [18].

Stretch forming

A large variety of container type parts with a great diversity of 3D shapes are stretch formed. In pure stretch forming, the sheet is completely clamped on its frame and the part slope is developed at expense of sheet thickness.

Figure 2.2 illustrates the stretch forming principle in a variety of ways. Figure 2.2 (a) represents the mass production stretch forming process, typical from the automotive and appliance industries. The blank is held unmovable by a blankholder with the aid of locking draw beads. The punch acts as a male die and pushes the sheet into the female die. The punch cooperates with the female die to define the shape, stretching the material around the dies. For simpler cavities, the sheets stretch only around the punch. On more complex parts with inflection points on surface curvature, material stretch to the convex area of each die. This operation has potential for making a wide variety of complex shapes, at the cost of greater tool cost.

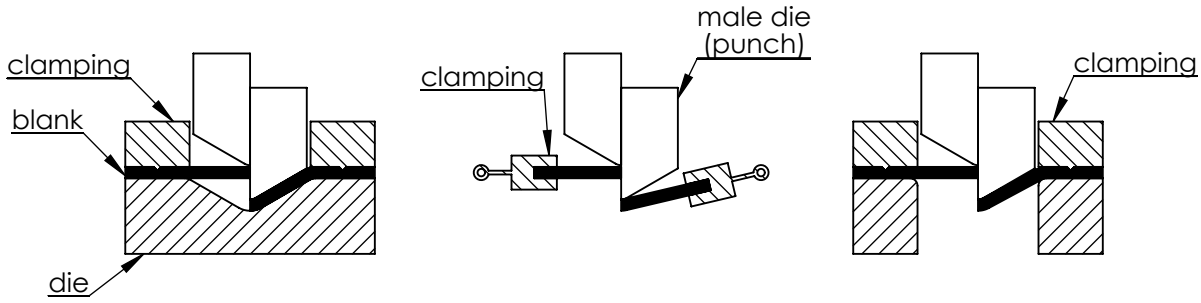

Figure 2.2: Basic stretch forming process: (a) using lock bead blankholder and both female and male dies, (b) using clamps and male die only, (c) using lock bead blankholder and male dies only

Figures 2.2 (b) and (c) represents much simpler operation principles of stretch forming, with more moderate tool cost be limited part complexity. The sheet is also clamped around its edge using a swiveling clamps or a simple blankholder. As only one die is used, the process is simpler and allows the fabrication of large parts. Material stretches around the punch to the desired shape. This procedure is cheaper but has lower productivity, making it better suited for low-volume production as in the aircraft industry.

A third variant of the process is embossing. It uses the sheet features itself through multiple contact points to restrict the movement and stretch the material against the dies. The process is mostly used for the definition of small details or reinforcement ribs on the sheet metal parts [1].

During the process, the punch movement generates biaxial tensile forces at the center that generates the deformation of the sheet. Contact stress between the punch and the sheet exist but much lower than the yield of the sheet. This way, forming is caused manly by the forces transmitted through the sheet. As tensile forces are resisted by the material around the edge, compressive hoop stresses are developed in the border. This will cause a tendency for the outer region to buckle. Besides, specially on gently curved shapes, large springback may occur [19].

As for drawing, some guidelines should be followed in order to safely perform stretching operation. A stretching limit (SL) (figure 2.3) can be determined by pressing a ball into a camped sheet until a localised necking occurs. The SL is defined as the ratio between the height of the stretch h_s and the diameter of the die D_s. This ratio should be taken into account for part design. Besides, a minimum bent radii of 2 times the thickness should be used and if possible relief cuts should be made in the higher strain areas. Finally, for good part manufacture, formed features should distant at least 2.5 times the sheet thickness from each other and from the trimmed edge.

Stamping

In most applications, sheet forming is neither pure stretching nor pure drawing. The sheet is not entirely clamped, thus it isn't a pure stretch forming process, but is also not allowed to flow freely, therefore it isn't a pure drawing operation. In addition to drawing and stretching,stamping operations, also know as press forming also includes a variety of operations, such as punching, blanking, embossing, bending, flanging, and coining. This allows the manufacturing of both simple or complex shapes formed at high production rates. Tooling and equipment costs can be high, but labor costs are low. Most stamping processes are made using progressive tools, where different operations are performed at different stages.

The formability is a property of a material that strongly influence its use in forming operations. The forming limit diagram FLD can be used for comparison between various materials and thicknesses and for diagnosing the failure cause, allowing the proposal of improvements. To obtain a FLD, experimental methods like Erichsen, Nakazima and Bulge tests may be used [20, 21]. Sheet specimens are clamped all around and stretched with a well oiled punch till failure. This operation gives a balanced biaxial tension point. A circle-grid pattern is applied to the blank before forming. Major and minor strains are calculated by measuring the ellipses created after circle deformation. A special transparent ruler as been developed for measuring deformed circles or optical measurement systems can be used. As a more recent alternative, the measurement is performed using Digital Image Correlation using a stereo image which allows not only the read the final strain but also its evolution. Using two image sensors with known imaging parameters and known relative orientation, the position of each object point in three dimensions can be calculated. Using a stochastic intensity pattern on the object surface, the position of each object point in the two images can be identified by applying a correlation algorithm and therefor determine strain [20–22]. The process is repeated diminishing the sheet width to be clamped on one direction only. The minor strain decreases until it reaches zero at a certain width, where the test strain results are similar to a tensile test. The obtained data enables to set thresholds between safe strain and fail condition, as exemplified in figure 2.4, where the stain under the line are in a safe zone. A curve can be obtain for both necking and fracture. The forming limit curve (FLC) can also be determined by numerical simulations [21, 23].

The FLC is influenced by either material properties and sheet thickness. The effect of strength, plastic behaviour of material and sheet thickness on the forming limits is shown in figure 2.5. The increase of the yield strength of the material typically creates a vertical descent of the FLC (sub figure (a)). On the contrary, the increase of sheet thickness leads to a vertical rise of the limit curve (sub figure (b)). The increase of strain hardening and strain rate sensitivity exponents cause the FLC to rise allowing greater major strain and lean to the allowance of greater minor strain aswell.

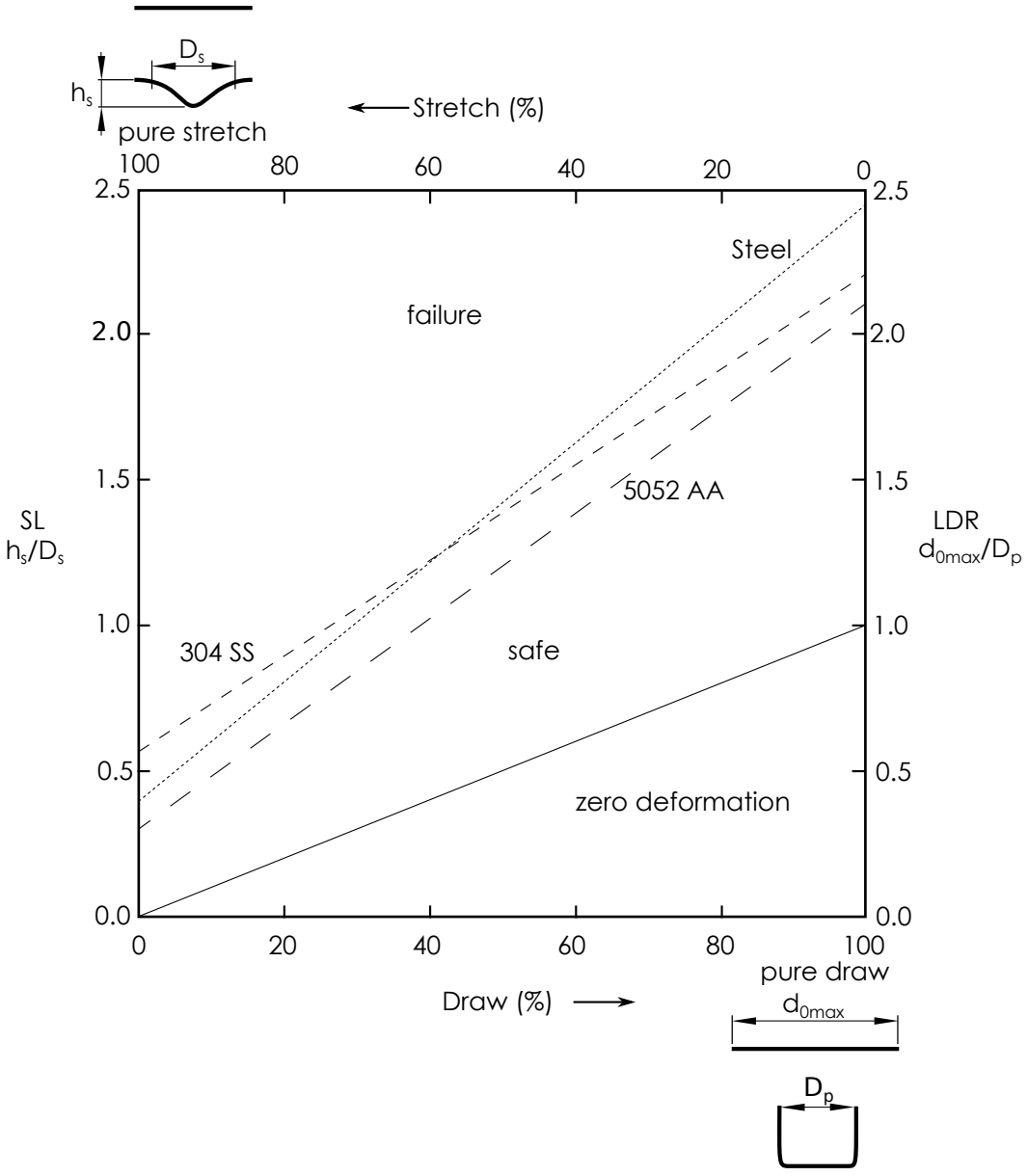

Figure 2.3: Stretch-draw limit diagram for deep drawing Al-killed steel, 304 Stainless steel and 5052-H24 Aluminium Alloy [1]

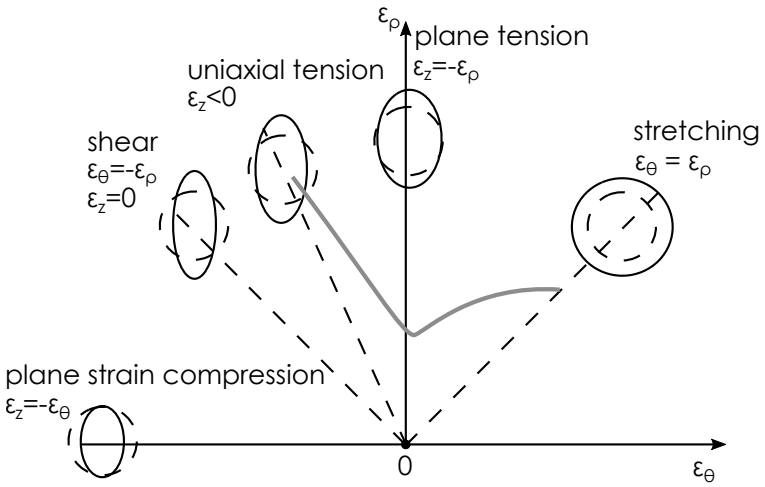

Figure 2.4: Forming limit diagram

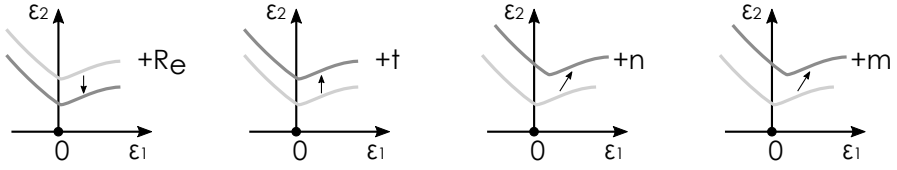

(a) (b) (c) (d)

Figure 2.5: Forming limit curves behaviour with the change in material properties or geometric features: (a) yield strength, (b) sheet thickness, (c) strain hardening, (d) strain rate

Forming operation themselves also influence the forming limit. Usually, if a sheet is first drawn the FLC will rise, allowing the execution of large stretching. Contrariwise, if a sheet is first stretch, the thinning cause the limit line to drop, preventing posterior drawing operations. [24]

The forming limits given by the FLD are a useful tool for analysing the cause of failure in both stretching and drawing operations. For more complex stamping operations, the severity of the operation is better judged by shape analysis. A combined stretch-draw chart is set by the correlation between the LDR for a pure drawing and the SL for a pure stretch. Figure 2.3 represents a stretch-draw limit diagram used for evaluate forming viability with deep drawing Al-killed steel, 304 stainless steel and 5052-H24 aluminium alloy. This diagram could be used to evaluate the viability of forming a defined geometry before tool manufacture.

Bending

The simplest method of metal forming consists on bending a sheet in a straight line. Bending operations are mainly held using multiple proposed tools, drastically reducing the initial investment. However, the use of this type of tools strongly harm continuous operation they are labour and time demanding. Special purpose tools may also be used but at a greater cost.

There are several techniques for straightforward bending, depending on part design and production volume. The most common are V-bending and U-bending, folding or wiping, roll bending and roll forming. Figure 2.6 represents basic bending operation processes.

V-bending can be used to bent angles up to 180^{o}, tough bending to 90^{o} is more usual. The process involves a punch pressing a sheet down into a V-shaped die. The bent angle in control by the punch stroke, ending its movement on the air, and the bent radius depends on the width of the die and thickness for thin sheets. Springback is very noticeable in V-bending operation. However, it can be compensated by the punch stroke control or minimised by bottoming. The process creates on straight bent per knock with a restriction of a minimum flange length due to the V die. Two straight bents may be done at once using U-bending.

To form parts with fewer restrictions in what concerns flange size folding or wiping can be used. In these processes the sheet is clamped on one flange and the other is bent be either sliding a wiping die or turning a swing beam. As in V-bending, both angle and radius is influenced by sheet thickness and tools stroke and geometry. A minimum clamping length should also be fulfilled to allow flawless operation.

Both V-bending and wiping are restricted to small radius bents. To manufacture large continuous radius is better performed using roll bending. This process uses rollers, three as a minimum, to form sheet into cylindrical or conical sections. The movement of the roller axis position, changing the wheelbase distance, allows to control the forming radius. Several configurations of roller position can be used to allow working with different thicknesses and rolling the sheet to the leading and trailing edges, avoiding straight ends. In cone bending, breaking latches must be used to avoid or limit the sheet movement, allowing to roll both longer and shorted ends to the same angle [24].

Roll forming is a highly productive continuous production method that allows the forming of several bents at once by rolls placed in tandem. This produces long parts with constant complex cross-sections with good surface finish at high production rates. However, compared to other bending process, it has high tooling costs as rolls must be manufactured for a specific shape. Roll forming commonly includes further operations like welding, cropping, punching and flanging.

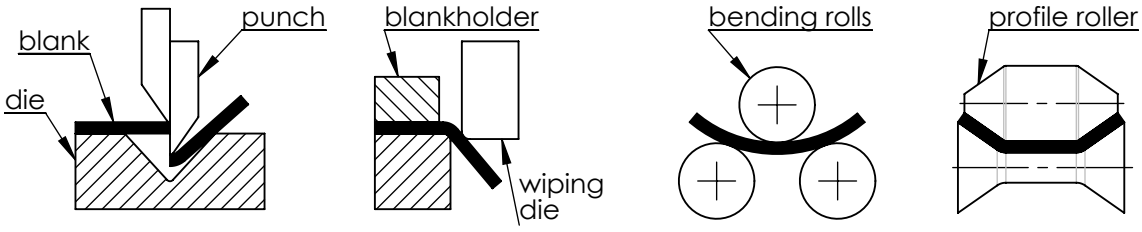

Figure 2.6: Basic bending processes: (a) V-bending or air bending, (b) folding or wiping, (c) roll-bending, (d) roll forming

In bending operations the plastic deformation only occurs in the bent region and the rest of the sheet is only affected by the consequent displacement. This area is under tensile elongation in the outer surface of the sheet and compressive strength in the inner side of the sheet. The tensile and compressive denting strains increase with smaller forming radius. When using small radius, major issues with bending operation involves cracking on the outside bend surface and thinning of the bent area. When using large radius, major difficulty is to control accuracy and repeatability as the process suffers appreciable springback. If the sheet is relatively narrow a contraction in the width may also occur [1].

As many operations principles are used for bending operations, each has specific design guidelines. Summarising, attention should be paid to minimum flange length, distance between bents, withdrawal of cut offs from bent lines, minimum radii and other features related to the blank cut.

2.1.2 Low tooling costs processes

As said, press forming processes allows great possibility of automatic and continuous manufacture at expense of high tool cost. In addition, complexity a size of the parts is limited by process restriction. For low production volume or very large or complex parts, other forming concepts are used.

Flexforming

Flexforming processes allow the manufacture of sheet metal parts with lower tooling costs and more capability to produce complex shapes. The main process that use the concept of flexforming are rubber-pad forming, hydroforming and hydromechanical forming. Figure 2.7 (a) represents the basic rubber-pad forming process and figure 2.7 (b) represents one of many hydroforming concepts.

In rubber-pad forming the specially build steel die is replaced by a rubber die placed inside a die holder container. The metal sheet is placed over the rubber die and a form block punch is pushed against the material. As rubber is incompressible, it deforms elastically and adapts to the punch forming the sheet. Blankholders may be used to help controlling press pressure. The process allows drawing and embossing simple or complex shapes, but with limited depth. Sheet surface is protected by rubber membranes. The process allows a great

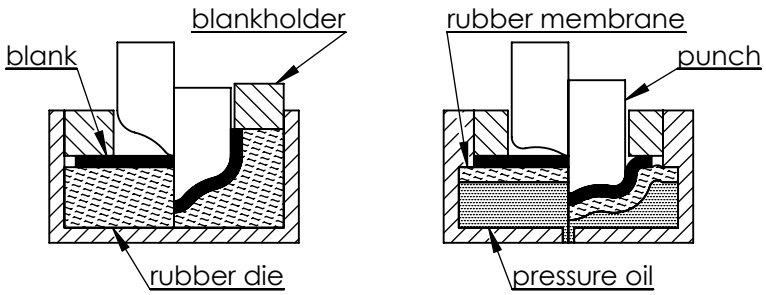

Figure 2.7: Basic forming processes with flexible dies: (a) rubber pad forming, (b) hydroforming

flexibility of operation with low tooling costs, suitable for low batches. However it involves high labor costs and the use of special presses capable of large payloads.

Hydroforming can also be used to the manufacture of high complexity parts. A rubber membrane and a pressurised oil reservoir is used as a die, allowing great flexibility for producing complex parts. The process allows greater depth and complex parts, with the possibility of forming undercuts. Hydroforming processes are also used to produce hollow components with difficult sections.

The deformation process in flexforming processes differs from press forming. The hydrostatic pressure distribution along the surface involves a larger part of the blank, leading to a more evenly distributed strain. This allows the fabrication of complex parts with different sheet thicknesses in fewer stages and better surface finishing than conventional tools [1, 24].

Blast forming

Another process principle that can be used for the manufacture of sheet metal parts is high energy rate forming. This working principle used a single die and the press is replaced by a sudden application of pressure. The source of pressure can be electromagnetic, electrohydraulic or explosive. In explosive forming, represented in figure 2.8 for example, a blast is used to induce a shock wave that pushes the blank to the die. This allows the fabrication of very large sheets with relatively complex shapes, although usually axisymmetric. The process is featured by low tooling costs, but high labor costs and long cycle times, suitable for low-quantity production.

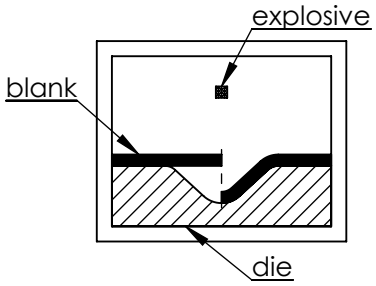

Figure 2.8: Basic explosion forming process.

Superplastic forming

Superplastic forming is one of the few sheet metal hot forming processes. Material is heated to a state in which the Young modulus decreases due to softening. This allows it to be processed with working principles typical of thermoplastics: thermoforming, blow forming, and vacuum forming. It may also be deep drawn or stretched.

The major advantage of this process is that it can form large and complex workpieces with fine detail in one operation. The finished product has close geometrical tolerances and a good surface finish. It also does not suffer from springback or residual stresses. However, parts are not suitable for high-temperature use. Besides, despite low cost tools, forming times are long, and hence production rates are low [25].

Spinning

Spinning is a very old method of producing axisymmetric parts. The process uses a lathe to turn a circular blank while a forming tool pushes the material to a spinning die in a series of sweeping strokes. Operation can either be performed by hand or by a copy or CNC process. Figure 2.9 (a) and (b) represents some forming spinning operations. The final shape is acquired by gradually lay the material against the die. The blank has the same area as the final part so that the wall thickness remains more or less unchanged as is process is roughly an axisymmetric bent. The process allows a good surface finish. Despite low tooling costs, labor costs can be high unless operations are automated. Spinning operation can also be performed with the sheet held by outer frame, operation in the middle.

The spinning process involves low forces but there is a high risk of fracture due to excessive hardening and the parts have high residual stresses. As the blank must be rotated in a lathe, a size and mass limitation must be ensured.

The most common defects in spinning are wrinkling, circumferential cracks and radial cracks. Wrinkling occurs due to high compressive circumferential stresses buckling the flange. To avoid wrinkling, a combination of tensile and compressive stresses in the material needs to be introduced gradually. High tensile radial stress may cause circumferential cracks. Radial cracks may form in two different cases; due to circumferential tensile stresses or a combination of circumferential compressive and bending stresses which occur when existing wrinkles are being worked [26].

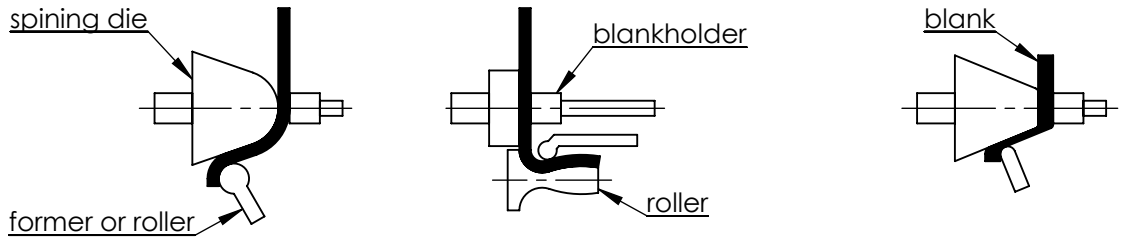

(a) (b) (c)

Figure 2.9: Basic spinning operation: (a) spinning, (b) internal spinning, (c) shear spinning or flow turning.

In the process of shear spinning or flow turning, represented in figure 2.9 (c) the strain is obtained by stretching the material over the die. The blank has thereabout the same diameter as the final shape bu thicker. The shape is achieved as forming tool stretches the material over the die with high thickness reduction, according to the forming angle.

As the deformation only occurs in the point of contact between the forming tool and the sheet, the remaining material remains stress free. This allows a greater degree of deformation to be achieved then in other processes like spinning or drawing, as the flange remains virtually stress-free. Operation forces as much higher then in spinning precluding the hand working.

2.1.3 Adaptive tool processes

Most process described above involve the use of specially built tools. Beyond cost, tool manufacturing strongly influence the time needed to start forming parts. Thus the processes are perfectly suited to the manufacture of prototypes, unique parts or very low volume batches. In recent years, conventional processes have been adapted to the use of adaptive tools in order to fill this gap.

Multi-point forming

Multi-point forming is a novel technology inspired by conventional forming methods that replace the die and punch per reconfigurable new tools composed by a matrix of discrete punches. The punch assembly is done using both fix, passive and active punches which can move along their axis, configuring a multi point die (MDP), as presented in figure 2.10.

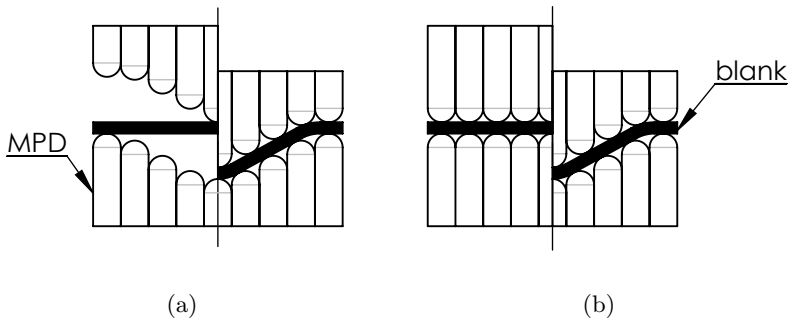

Figure 2.10: Basic multi-point forming operation: (a) multi-point forming, (b) continuous contact multi-point forming

Sub figure (a) represents multi point die forming in which the shape of MPD is constructed according to the final shape and is not varied during the forming process. This operation is much similar to a conventional stamping with pressure distributed over discrete points. The approach represented on sub figure (b) uses real time movement of each punch position. This allows the sheet to be formed along a specific forming path, keeping contact of all punches with the sheet at all times. A correct path designed allows to form the material avoiding defects completely [27]. A single multipoint die can also be used for pure stretch operations.

Multi-point forming is mostly used to fabricate smooth parts, without small radius ore high slope walls. Despite having great potential for forming unique parts, it has a size limitation, mostly due to tool production cost.

Flexible roll bending

Flexible roll bending has been developed as an alternative for multi-point forming. The process is inspired by conventional roll bending, using the concept of continuous forming. Replacing conventional roll with flexible rolls allows the to be repositioned along the axis. The control of the rolls curvature allows to continuously bent a tree dimensional shaped geometry [28].

2.1.4 Dieless forming processes

Conventional forming methods require special proposed built tools. Moreover, a set or many sets of dedicated dies are needed to be used for each different part. In addition, making a die is not cheap and takes a long time. Some processes use multi propose tooling but at the cost of greater geometrical limitations. Reconfigurable tools can be used to avoid dedicated tools but they are very expensive and their use has also limited part design.

Hence, to lower the cost and speed up the process of manufacturing new parts, various kinds of die-less forming methods have been proposed. Today, the dieless forming methods have become important in research as they respond to the increasing demands for low-volume and customer-made products.

Most conventional processes count on one single stroke or continuous movement to perform the forming operation. The great dissemination of automatic motion control techniques has allowed the exploitation of incremental forming techniques where a sheet is gradually deformed to the desired shape [29].

Hammering and english wheel

One of the oldest processes in sheet forming is Hammering. This process was initially done manually using different shapes hammers, dollys and mallets. Since the beginning of the twentieth century the English wheel has been used as wheel to help curving and improve smoothness. Figure 2.11 represents manual hammering and english wheel operation. To improve productivity, power hammers, mechanical or pneumatic, have been used replacing the manual tools. There are two different principles of hammering. On the one hand, deformation is caused by the energy of the moving part and its impact. On the other hand, the predetermined movement directs the forming energy to a specific area [30].

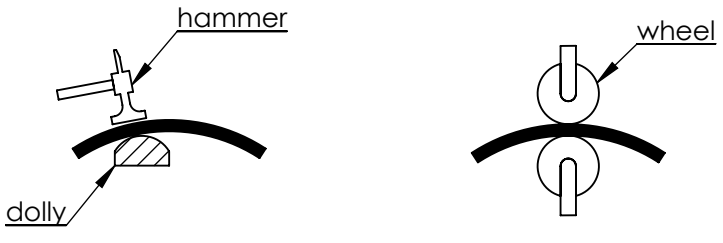

Figure 2.11: Manual metal shaping operation: (a) hammering, (b) english wheel.

Hammering major limitations are related to the operator skills. Additionally the process is very time consuming and repeatability is difficult to achieved.

In recent years hammering has been taking advantage of motion control and uses a robotic arm to handle the hammer tool and form the sheet, which is clamped in a support frame. By moving a hammering tool over a sheet of metal fixed in a frame, a three-dimensional workpiece can be produced without using any special die plate. The use of a common industrial robot is possible because the forces involved in the process are considerable low [31].

Peen forming

Shot Peen forming consists on deforming a metal sheet by shooting small round steel shots to a sheet surface. Every piece of shot impacting the surface acts as a tiny hammer. The impact pressure of the peening shot causes local plastic deformation. The top surface on which the peening has taken place is in a high degree of compression, stretching that surface to cause a change of shape. Figure 2.12 represents a curving operation using shoot peen forming. When shot velocity is fairly low, only a thin layer of the sheet material is deformed, resulting in a convex curvature as shown in figure 2.12. If shot velocity is increased, concave curvatures are produced.

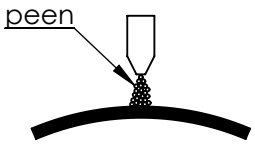

Figure 2.12: Basic shot peen forming curving operation.

Peen forming is used to form shallow contours on large sheets, normally holding the sheet metal stationary while a nozzle-type or centrifugal wheel machine runs along a gantry. This allows a great flexibility of operation but equipment costs can be high [32].

The greatest advantages of peen forming are the possibility of forming very large parts, for example air plane wings, and the possibility of updating the design between parts manufacture. Finally, the use of peening also increased resistance to flexural bending fatigue and stress corrosion. Major disadvantages are related with limitations on sheet thickness, curvature radius and wall angle.

Laser forming

The basic feature of laser forming is the forming by thermal stresses, induced by irradiation of a laser beam. These internal stresses induce plastic strains that bend the material resulting in the local elastic/plastic buckling. For low series one has to rely on applying various pieces of production equipment, each of them being flexible enough to be reprogrammed according to a changing product spectrum. Laser forming allows to use the same production unit for both cutting and forming. As in peen forming, it is possible to form both convex and concave curvatures. However, laser forming is mostly restricted to two dimension bends.

One of the main advantages of laser forming is the ease of forming hard-to-form materials, such as stainless steel. Besides, the process advantages include high accuracy, arising from the progressive nature of the process, and the possibility of doing adjustments of misalignment of a part.

On the other hand, the process is slow and has vast limitations to three dimensional shapes. It also requires extra safety protection equipment because of mulch directional reflection of the laser beam from the metal [29].

Incremental sheet forming

Incremental sheet forming (ISF) is a sheet metal forming technique where a sheet is formed into the final workpiece by a series of small incremental deformations. Forming is controlled entirely by CNC processes, so no die is needed as in traditional sheet metal forming. The removal of the die in the manufacturing process decreases the cost per piece and improves turnaround time for low production runs due to the fact that the need to manufacture a die is removed. In contrast, there is a loss of accuracy with the ISF process. Incremental forming processes can be considered as rapid prototyping as they are well-suited for small-lot production, and rapid production of service parts and may reduce time to market [29].

A large variety of ISF principles have been developed in the past years. Figure 2.13 represents the process of dieless single point incremental forming and two point incremental forming with peripheral support tool. Besides these, several other variants exist, including the use of partial or complete low cost dies, use of multiple tools, use of elastic die and the use of special techniques to improve formability. Incremental sheet forming has been addressed for a long time but only been subject of studies in recent years. As the process needs motion control to perform, is has been accomplished using CNC machining tools, industrial robots and special purposed build machines [6, 33].

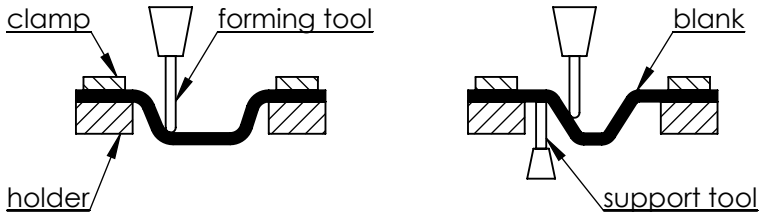

Figure 2.13: Basic incremental sheet forming operation: (a) single point incremental forming, (b) two point incremental forming.

The main advantages of ISF are short time-to-market because parts can be formed by directly generating a CNC program from a 3D CAD model. ISF eliminates partially or totally the need for tooling development and manufacture. The process is cost effective for small sized series. The process provides a high degree of flexibility, and it can be adapted to very different freeform geometries, materials and conditions. Changes in part design can be easily and quickly accommodated and the shape complexity has no major throwback on the manufacture cost. ISF allows to produce parts of any size, with the only limitation related to the available hardware. In addition, the formability of materials under the localised deformation imposed by incremental forming is better than in conventional forming processes [34].

Major issues with incremental forming processes are related with low accuracy and exces-

sive thinning. The process is influenced by the rigidity of used machine and by large amount of springback. However, ISF offers high reproducibility and enables to produce sheet metal parts with good mechanical properties.

Incremental forming principles of operation, particularly single point incremental forming, are explored in the following section.

2.1.5 Common failures in sheet metal forming

As described, several processes may be used in sheet metal forming operations. By submitting a material to stress it is possible to form it by inducing permanent deformation. However, the strain is described in a tree dimensional state with relations between the behaviour of the material in different directions. When imposing any given deformation to convert a blank material to a designed shape along one direction, some sidelong effects happen. The inevitable relation between material behaviour in different direction lead to unwanted outcomes. Furthermore, the existence of a elastic recoverable behaviour before strain hardening and the existence of a ultimate strength of the material also imposes unwanted results.

Some of the most common failures in sheet metal forming operations are the inaccuracy of a deformation due to springback; shearing, cracking, tearing or creasing due to excessive stress or strain; the formation of Luders bands due to yield elongation; thinning and necking due to the conservation of volume when stretching a material and wrinkling due to a compressive minor stress in the sheet. Other common failures in sheet metal forming as earing are due to the anisotropy of the material. As a guideline for metal forming operations, the formability limit defined by the ratio of the membrane strains $\beta = \epsilon_2/\epsilon_1$ for a materialgeometry can be defined, identifying the state of strain where the material can be safely worked. Figure 2.14 represents some of the most common modes of failure [19, 24, 35, 36].

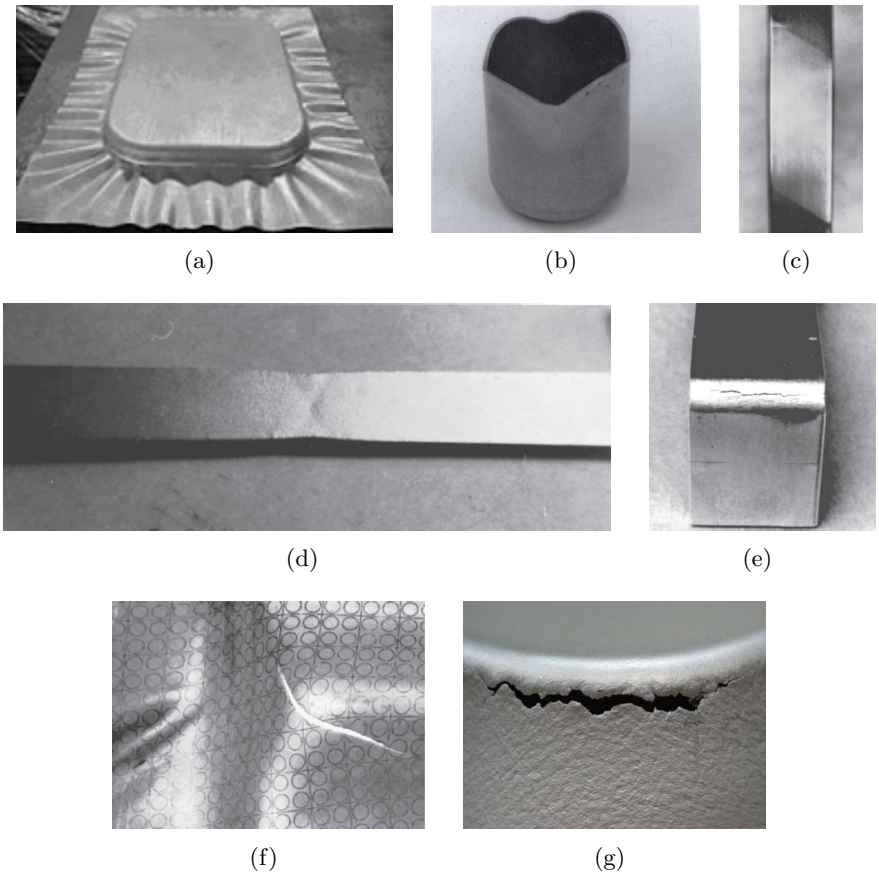

Figure 2.14: Commons failures in sheet metal forming: (a) wrinkling, (b) earing, (c) Lueders band, (d) necking, (e) cracking, (f) tearing , (g) thinning and cracking

2.2 Single Point Incremental Forming

As referred, Single Point Incremental Forming (SPIF) is a increasingly popular forming process due to its potential to produce unique sheet metal parts with very little investment and energy cost. This potential make it a good solution for the manufacture of prototypes, low volume production and rapid tooling applications.

2.2.1 Working principle

Several working principles variations to perform SPIF operations were tested and validated. Most differ with regard to the type of machine used and regard the use of different frames, backing plates and simple support tools. Despite the differences, the basic working principle is common: a ball tipped forming tool controlled by Computer Numerical Control (CNC) follows a programed tool path against a sheet held by its outer limit. The follow of the tool path cause both deformation by strain of some areas of the sheet and rigid body movement of other areas. Incremental sheet forming can provide complex shapes from various materials and scales and produce unique parts or small lot sizes. Figure 2.16 represent the working principle of SPIF, with a metal sheet supported by sheet holder and backing plate and clamped in the upper side. The black shaded area represents and intermediate stage of the process. Both blank and final geometry are represented with dashed lines. The forming tool with a diameter of $\varnothing_t$ deform a t_0 thickness sheet to the desired angle λ. As a consequence of material stretching, sheet thickness reduces to t_f, roughly approximated by the sine-law (equation 2.1) [4, 34, 37].

$$t_f = t_0.sin(\lambda) = t_0.cos(\alpha) \tag{2.1}$$

A simplified tool path and sheet deformation behaviour is represented on figure 2.15 [38]. The first approach consists on moving the forming tool to a position over the sheet. The following movement leads the tool to the entrance point in a plunge or ramp path. The tool path then continues to deform the sheet, deepening the tool tip along the process according to a predefined pitch. Subfigure (d) represents the final design shaded with the tool in the final position and some exemplification intermediate states in white. When the final shape is achieved the tool retracts and moves away form the sheet.

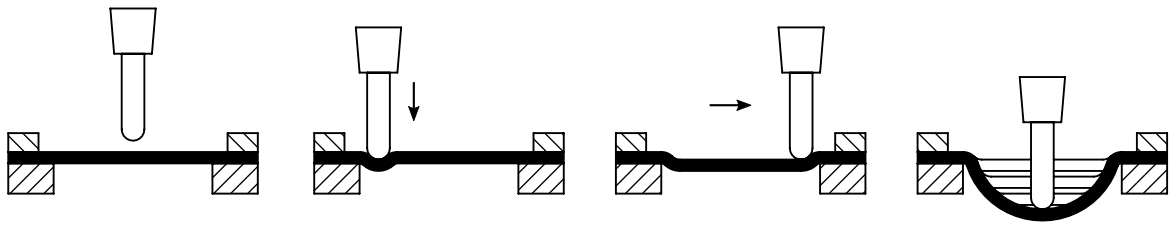

(a) (b) (c) (d)

Figure 2.15: Schematic diagram of the incremental sheet metal forming process

Although the concept of ISF dates back to the decade of sixty has patented by Leszak [2], only in the end of the past century technology allowed major developments. Incremental sheet forming is being studied with much more interest since 2000's. Experimental tests are being carried out extensively searching for reasonable explanations for the particular

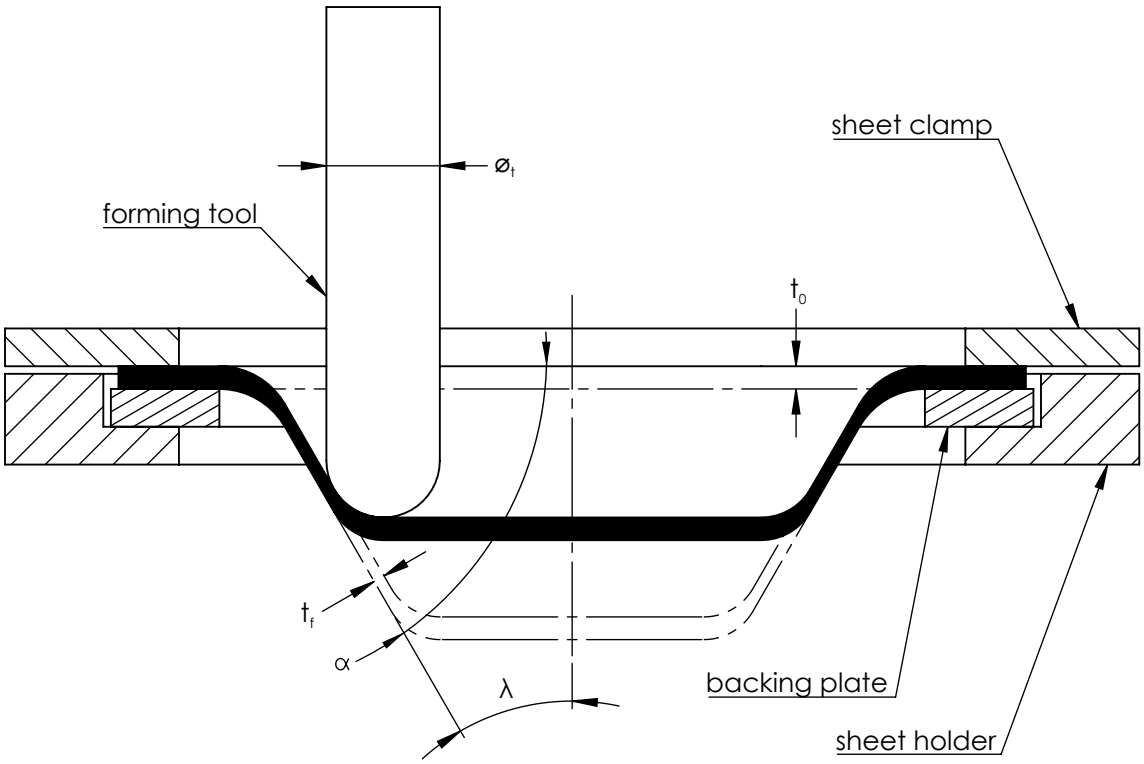

Figure 2.16: Section view of SPIF process

mechanical response of material during the process and pursuing the evaluation and validation of industrial applicability for the process. Figure 2.17 shows the forming process of a cone using a 15mm tool in the SPIF-A machine developed at University of Aveiro [6, 11, 12].

The process allows the fabrication of complex three-dimensional free forms, but there are few limitations with it, depending on the sheet thickness and the equipment used. The tool size defines the minimum inner rounding radius, which is half of the tool diameter. Minimum tool size depends on the sheet thickness, because small and thus thin tools are not strong enough for required forming forces with thick sheets. The wall angle is limited by the sheet thickness and by material properties. The more the sheet is sheared the more it thins, according to the sine law, as shown in figure 2.16. Minimum wall angle for steel is approximately 25°, for pure aluminium 20° and for heat-treated aluminium 30-35°. Various parameters like tool diameter, forming speed, lubrication and other influence the formability in SPIF: spifability. Multi stage tool paths allow the form parts over the refereed limits [4, 34, 39, 40].

The maximum product size and sheet thickness is defined by the used machine. The critical factor is the force needed for forming. As the yield strength varies according to the material used, the forming force increase and thus the maximum sheet thickness also depends on the material. Typical maximum thickness is 2mm for steel and 4mm for aluminium, depending on the hardware. SPIF can also be applied in polymeric materials with sheet thickness greater than 10mm.

Surface quality of the SPIF parts is influenced by the used tool and toolpath. The tool leaves marks on the formed surface on each forming round. Those marks can be decreased by

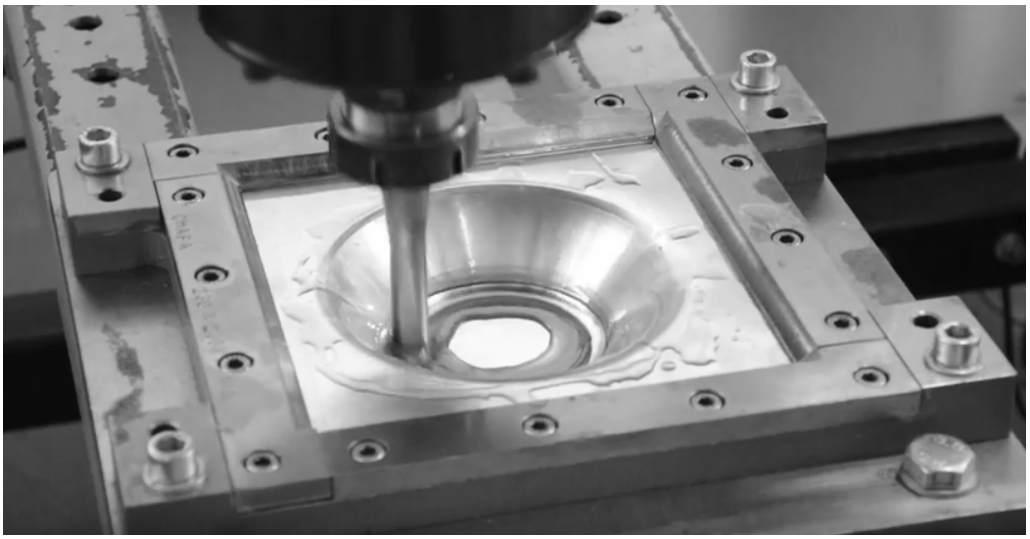

Figure 2.17: SPIF process at University of Aveiro

using large diameter tools and by decreasing the forming pitch. However, smaller pitch leads to longer forming time and if it gets to small, the material is formed several times on the same spot, leading to greater strain hardening. These results may cause tearing of the sheet. Strain hardening also increases the residual stress in the sheet, causing the part to twisted when removed from the frame. Surface quality can be improved by correct lubrication along the process [15].

Forming speeds on SPIF vary from very low speeds as 100mm/min to high speed SPIF over 12000mm/min. Vertical step used typically varies from 0,1 to 2mm, according to material thickness and strength and the accuracy and surface finishing pursuit. Table 2.1 resumes some typical parameters of incremental forming operations [2, 4, 6, 11, 12, 15, 33, 34, 37, 38, 41–43].

Table 2.1: Typical parameters for ISF

blank size		100x100mm to 2000x1500mm
sheet thickness	t_0	0,5 to 4mm
sheet material		steel, aluminium or polymers
forming tool diameter	$\varnothing_t$	5 to 20mm
vertical step size	Δz	0,1 to 2mm
minimum single stage ISF wall angle	λ	10^o to 30^o
maximum single stage ISF drawing angle	α	60^o to 80^o
maximum forming depth		500mm
minimum inner radius		3mm to 6mm
forming speed		500 to 3000mm/min
spindle speed		free or up to 4000rpm
forming time (great dependence on the size and depth)		10 to 60min
geometric tolerance		0,5 to 2mm
equivalent strain	$\bar{\epsilon}$	0 to 2,5
forming forces		300 to 7500N (vertical)
		100 to 2500N (horizontal)

ISF variations

Despite this section being dedicated to the specific process of single point incremental forming, it is important to understand other ISF variations. All of them are based on the described method, forming a blank sheet secured all around to a container type shape.

The simplest procedure method for ISF limits to follow the concept description above. A universal forming tool is used to form a blank secured in a blank holder. This process is called asymmetric incremental sheet forming (AISF) . It is a very simple and efficient method, but it causes inaccuracies and deviations from the desired geometry due in large part to the springback of the sheet and the expansion of the strain along the flat area of the blank. SPIF itself is characterised by adding a backing plate with the outlines of the desired geometry fixed to the sheet on the opposite side of the forming tool. The backingplate provides leverage at the initial bent of the form, reducing some of the deviations caused by springback. Despite the need of cutting a part for the manufacture of a specific part, adding cost and time spent, this method increases accuracy mostly at the periphery of the shape. Figure 2.18 represents both AISF and SPIF, showing the peripheral differences between approaches [33, 34].

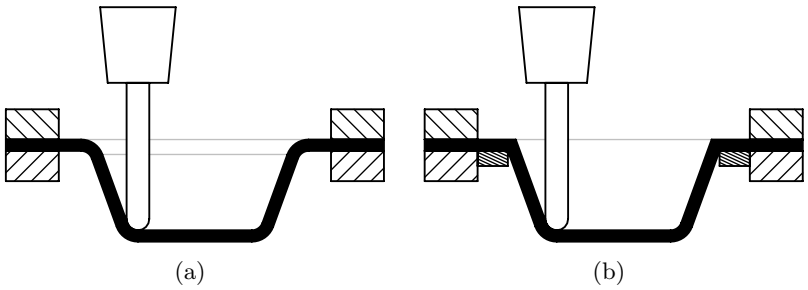

Figure 2.18: ISF variations: single point incremental forming (a) without and (b) with backing plate.

The added support accomplished in SPIF can be extended to a wider area, replacing the backing plate by a simple die. The two point incremental forming (TPIF) has been proposed by adding either a partial or complete male or complete female die as shown in figures 2.19 and 2.20.

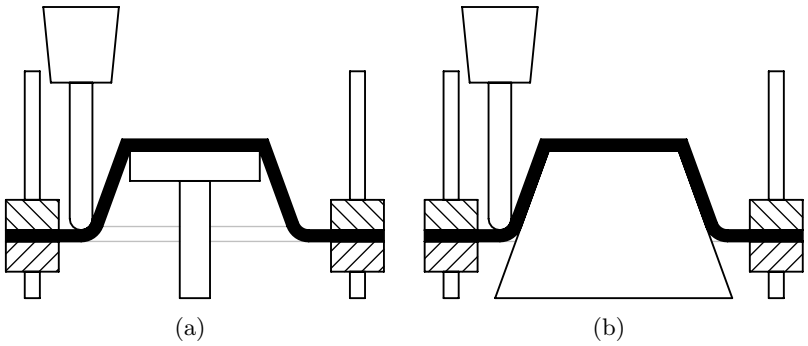

Figure 2.19: ISF variations: two point incremental forming with (a) partial male die, (b) complete male die.

In the male die approaches the blank holder is mounted on a movable table, stepping down the flat area of the blank while the incremental forming happen. Despite the extra cost of the ISF equipment and the need to fabricate special tools for any given shape, this process has increased accuracy. Partial die operation offers special benefits on the apex of the form, inversely from SPIF. Complete dies enables higher geometric accuracy but at a higher cost and longer manufacture time for each part [33, 44, 45]. Further advantage is the possibility of combining ISF the conventional processes like stretch forming [46].

In the female die approach a similar advantage is achieved with the benefit of using the same simple equipment needed for AISF or SPIF operation. Although DPIF offers great benefits on the formed accuracy, it increases the complexity of the process. Besides demanding the manufacture of a die, which is time ans cost consuming, it demands a precise calibration of the die position thus adding extra cost and duration to the process.

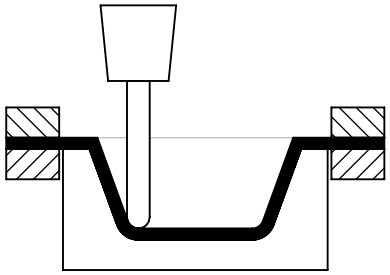

Figure 2.20: ISF variations: two point incremental forming with complete female die.

To provide the advantage of the added support in ISF without the need for dies manufacture, dual point incremental forming (DPIF) can be used. This method uses two independent actuators with two forming tools to deform the sheet to the desired shape. Figure 2.21 represent two possible approaches for DPIF, using either peripheral or local support tools. In the peripheral support method the forming tool pushes incrementally on the sheet, forming it to the shape of the tool path while the support tool follows along the boundary, replacing the need of a backing plate. In the local support approach two universal forming tools are used to follow complementary tool paths, creating a forming gap between them. Beyond helping improving accuracy, this method allows the fabrication of both concave and convex forms [33].

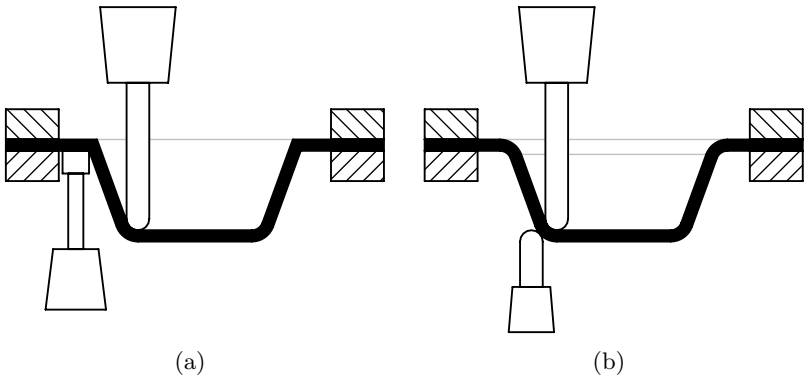

Figure 2.21: ISF variations: dual point incremental forming with (a) peripheral supporting tool, (b) locally supporting tool.

Even though there are benefits on using DPIF, the equipment design and control is much complex. A simplified method has been proposed, using a single actuator to accomplish the tool path. A c type frame is used to connect both tools, reducing investment costs and operating costs in an outstanding way, but allowing only small-scale forming of sheets. Figure 2.22 shows a schematic representation of the c-frame variation of DPIF. In this design the lower tool is mounted on a linear actuator, allowing the adjustments in sheet thickness [47].

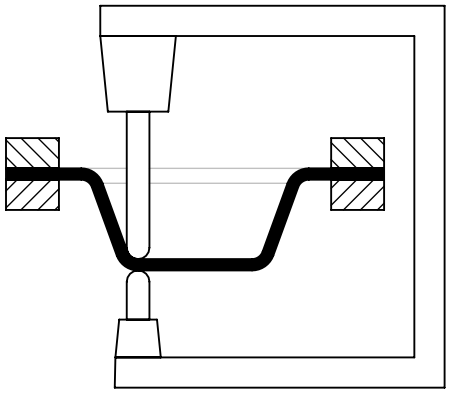

Figure 2.22: ISF variations: dual point incremental forming with locally supporting tool controlled in parallel with the forming tool.

SPIF machines

There is no effective restriction on the type of machine that should be used for SPIF operations. In theory, any machine capable of performing position control in 3 or more axis could be used for forming operation. However, the strength needed for forming operation restricts and influence the machine architecture. Several machines have been developed or adapted with the goal of performing SPIF operations [12, 48].

The different equipment avaiable to perform SPIF nowadays are: CNC milling machines, industrial robot with serial or parallel kinematics and purpose build machines like the one developed by Amino Corporation [45], by Allwood's group at Cambridge University [48] and the SPIF-A machine developed at the University of Aveiro [6].

CNC milling machines are designed for machining, a process in which forces applied at the tool tip are smaller than those obtained in the ISF. Therefore, the process is limited to the conformation of milder materials. The use of a CNC machine tool becomes attractive due to low additional costs involved in adapting a CNC milling machine to SPIF process. On the other hand, serial robots are able to deliver high volumes of work, high accelerations and very fast and flexible positioning, which makes an advantage in incremental forming, but both stiffness and allowable loads are very low, not meeting ISF requirements of forming harder and thicker materials as the non-rigidity of these robots induces extra dimensional errors and dynamic effects. Parallel kinematic robots have a more limited working area as compared to serial robotic manipulators. However, has they are much stiffer and still have a flexible workspace, they present as a viable solution able of performance above average. This allows to overcome limitations from other machines, either with new materials or with more complex geometries and larger thicknesses [12].

Finally, an important aspect of a SPIF machine is the frame used for both supporting

and clamping the blank. The most common approaches is the use of a metal frame bolted all around the blank or the use of a toggle clamps based system [49].

The SPIF-A, presented on figure 2.23, is a vertical specially purposed build machine for SPIF operations. The machine core hardware has a footprint of 1400 mm by 1400 mm with 2400 mm height. The machine is composed by a metal structure, an hydraulic motion system, a free rotation spindle and a forming table. In addiction to the main hardware, the machine is composed by an hydraulic power unit, an electric cabinet and an industrial computer controller.

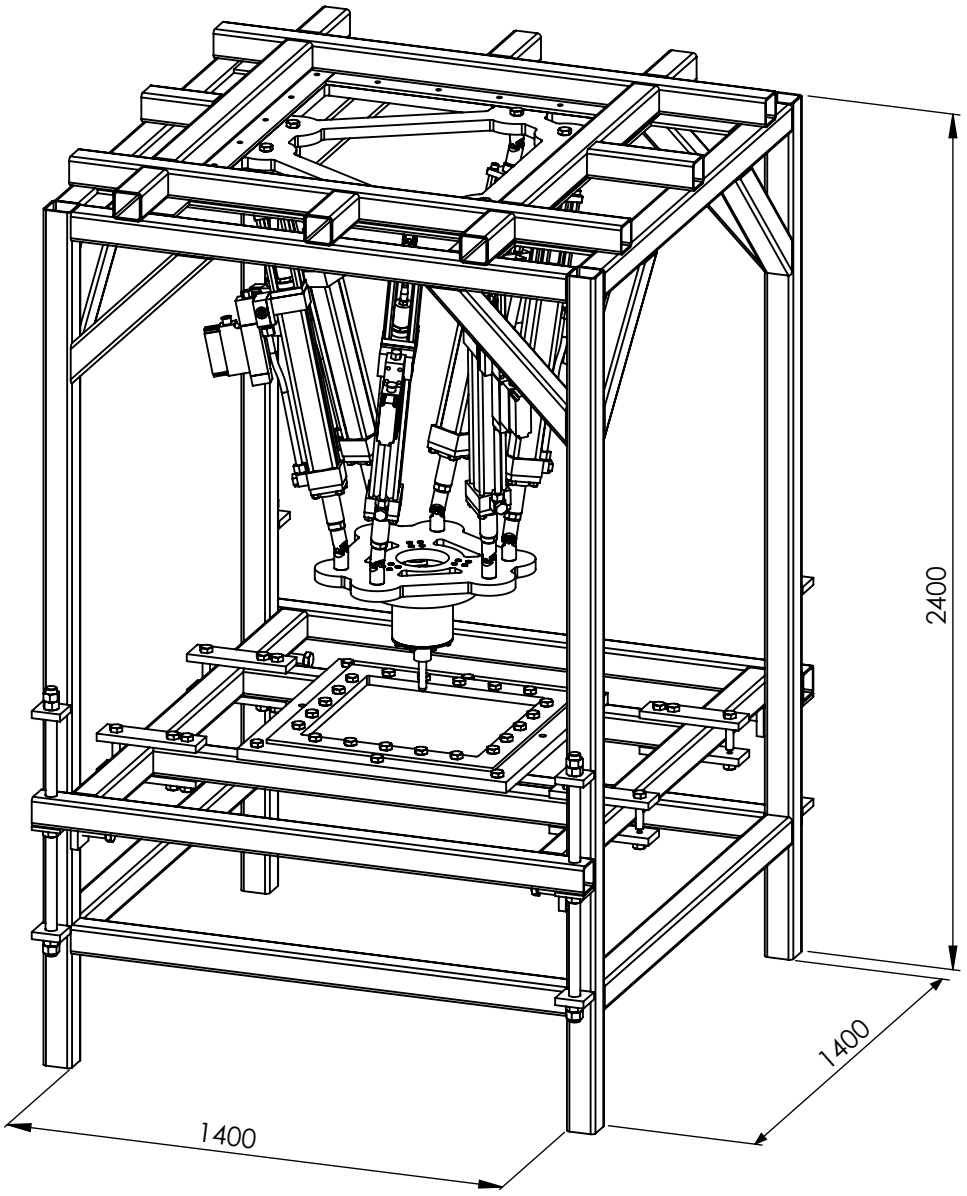

Figure 2.23: SPIF-A machine.

The motion system of the SPIF-A machine is based on a Gough/Stewart parallel platform with six degrees of freedom. Figure 2.24 (a) illustrates the parallel platform design for the SPIF-A. Each leg consist on a linear hydraulic actuator mounted on two universal joints. The platform assembly uses a 6-6 configuration with coplanar semi regular hexagon geometry platforms of 600 mm by 200 mm on the fixed side and 300 mm by 150 mm on the moving platform. Each leg has a retract length of 942 mm with a 400 mm stroke, resulting on a 1080 mm to 1489 mm assembly height. The workspace varies along the height, with an average radius of 400 mm.

The used actuators are Parker®- TCHMIXRPFS27M - M114 cylinders, equipped with Parker®- D1FP*S - Dfplus valves and Temposonics®- RH 550646 C magnetostrictive linear transducer absolute encoders. The cylinders have a 63 mm bore diameter and a 45 mm rod diameter, producing a 50 kN pushing force and a 25 kN pulling force at 160 bar. The valves allow a response time smaller the 3.5 ms and the encoders have a resolution of 0.002 mm with a repeatability of 0.0045 mm. The universal joints used are Rotar®- AL110 with a maximum rotation angle of 45° in either direction. Each actuator assembly has a total of 6 degrees of freedom: two times two passive rotation on the universal joints, one passive rotation of the cylinders rods and one controlled linear motion of the cylinder. Depending on the position and on the pitch and yaw angles, the motion system allows to apply a vertical load from 50 kN to 300 kN and an horizontal force from 30 kN to 100 kN. The actuators are mounted with such an angle that potential collision between near cylinders or valves are prevented.

The hydraulic system is driven by a PVQ40 hydraulic pump powered up by a 15 kW three phase electric motor. The pump has a displacement of 40 cc/rev and was set to supply a pressure of 160 bar at 1500 rpm. The power supply has a 200 L oil reservoir and provides a flow rate of 42 L/min. It is equipped with a oil recirculating valve for a safer motor start up without powering up the cylinders. The machine uses a hexagonal hydraulic distributor, enabling an even distribution of pressure at the six cylinders with re recirculating valve closed. The flow rate enables a maximum downward movement continuous speed of 2250 mm/min. This speed can only be seen as a reference. Horizontal speed is much faster has it results from a combination of small retract and extend movements of each cylinder's stroke, minimising the flow rate consumption. Continuous combined motion can run up to an average continuous speed over 15000 mm/min.

The spindle developed for the SPIF-A machine uses DIN 2080 collet chuck SK50-3/26-63 ER40 tool holder, allowing the use of tools with 3 mm to 26 mm shank. The tool holder is mounted on the spindle shaft with a drawbar. The shaft assembly rotates freely inside the spindle's outer case, supported by an axial, a radial and a combined bearing. The tool change in accomplish with two manual clamping tools, holding the drawbar spinning while contra-rotating the tool holder. The top of the assembly allows the addition of a motor for operation with tool rotation. Figure 2.25 represents a cut view of the spindle assembly. The spindle is linked to the kinematic system moving platform by three load cells. The load cells are equally positioned around the spindle axis, measuring both the axial and horizontal force.

The forming table is mounted on the structure by four threaded axis, allowing the regulation of the table height, as represented in figure 2.23. The table itself, represented on figure 2.26, uses four clamping bars to fix the sheet metal with CHC M6 screws. Different forming tables have been designed and built, to achieved forming areas of 100 mm, 200 mm, 500 mm and 1000 mm squares. The forming tables base frame (sheet holder) has 6 mm deep edge slot around the border, allowing the use of backing plates. The clamping bars allow the use of up to $6mm$ sheets.

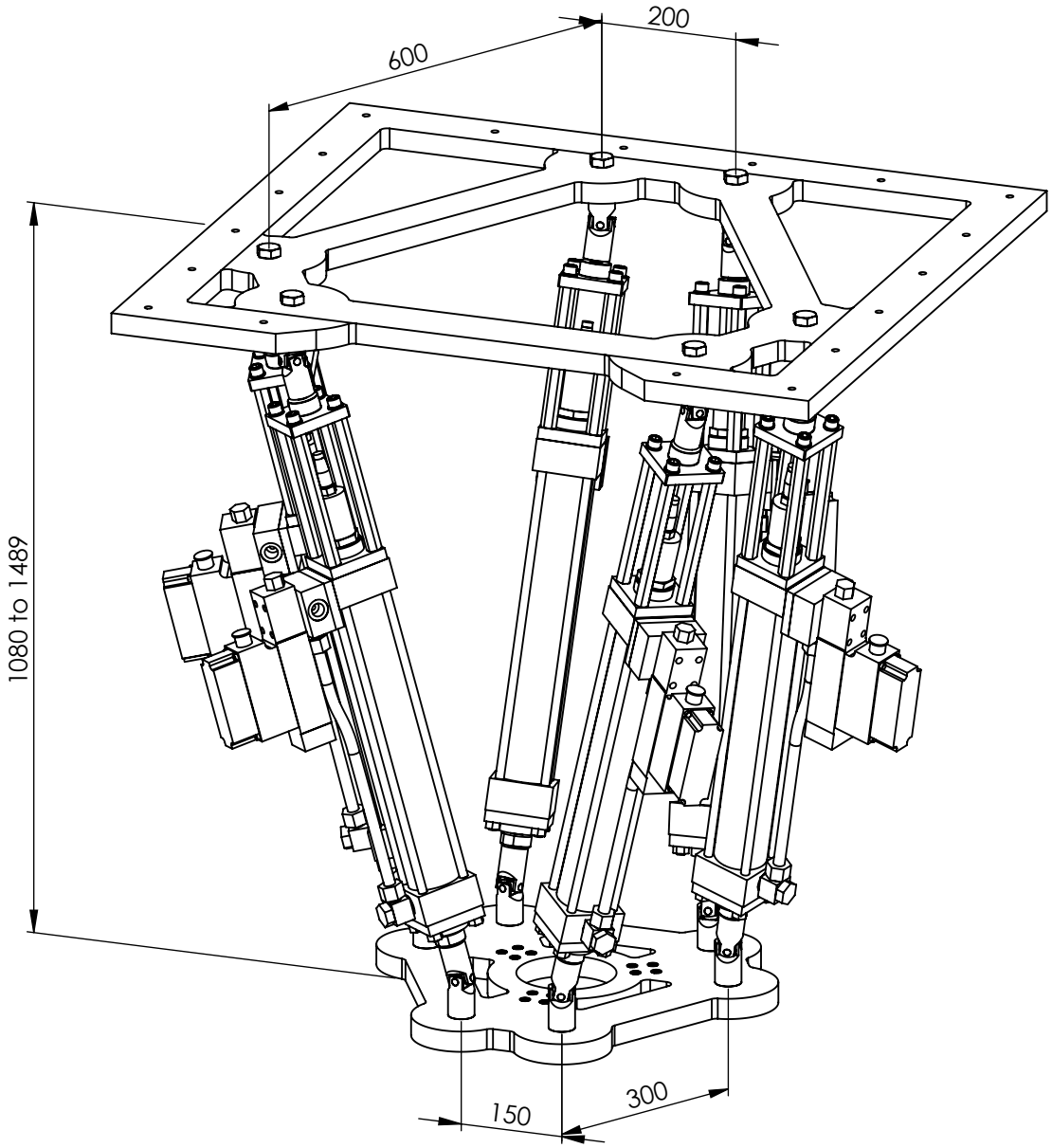

(a)

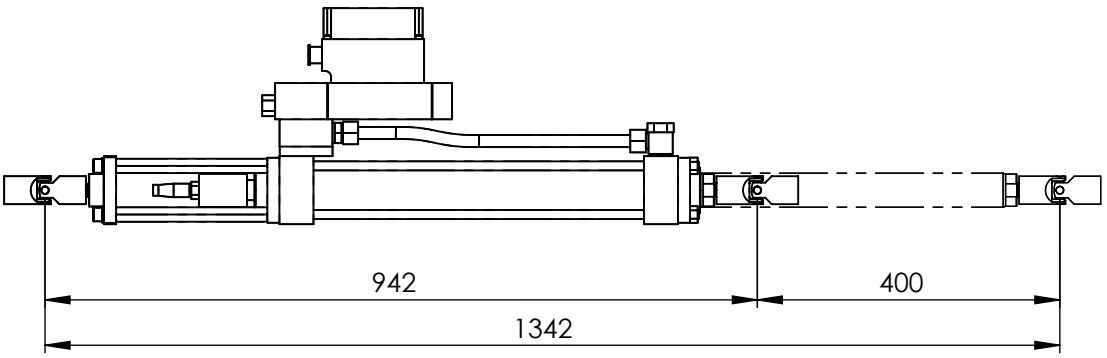

(b)

Figure 2.24: SPIF-A motion system: (a) parallel platform, (b) actuators.

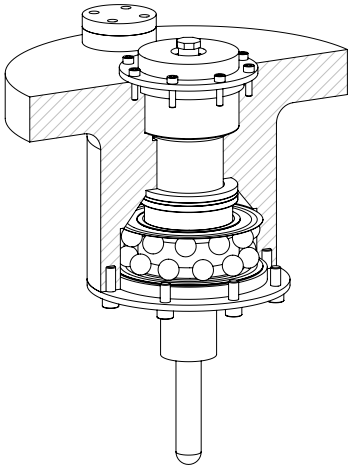

Figure 2.25: SPIF-A spindle.

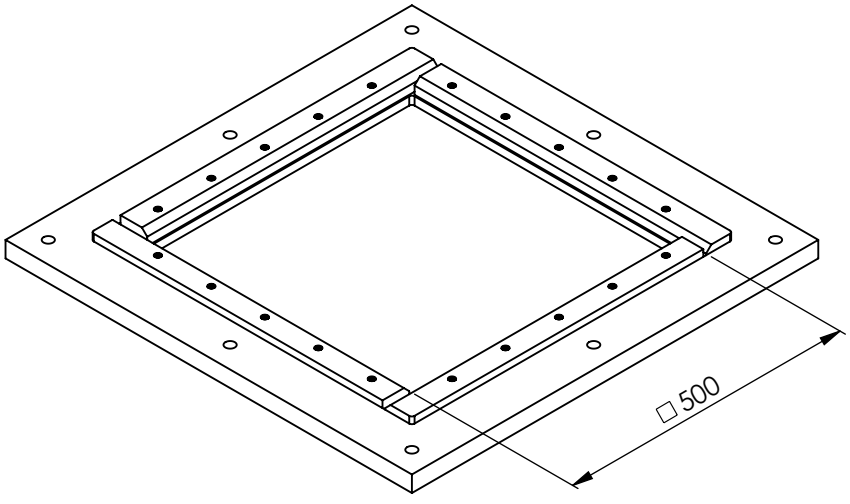

Figure 2.26: SPIF-A forming table.

The machine controls is garoted by Speedgoat^{TM}SN1584 real time target machine, running with Simulink^{TM}and Matlab^{TM}software via xPC Target^{TM}toolbox. The machine operates with a host computer running Matlab^{TM}and Simulink^{TM}Model. The host communicates with the xPC Real-Time controller which with Simulink^{TM}Run. The xPC target controller reads and writes information on the machine by I/O modules installed on SPIF-A's electrical cabinet. These models acquire data from the position transducers, load cells and control buttons and transmit signal to the servo-hydraulic actuators and indicator lamps [6, 11, 12, 50, 51].

Forming tool

For most SPIF applications, the forming tool or forming punch is a rod with a spherical end. Principal parameter of a SPIF tool is its diameter and length. Furthermore, several tool shapes exist as shown on figure 2.27 (a) to (d).

At first approach, tool diameter and length are chosen according to the part geometry. The maximum tool radius to be used in a SPIF operation equals the minimum part radius. The tool length must grand clearance between the tool holder and the part. Being under high compressive and shear stress, the tool must avoid excessive displacement of the tip due to elastic bending and excessive deformation of the hemispherical surface. Hardened steel (55 HRC) is usually used and the tool diameter and shape is chosen according to the forming forces. Tapered and tipped punch allow the use of a small radii notwithstanding the stiffness [33].

Beyond geometry related issues, the chose of tool size, with respect to sheet thickness employed, influences the spifability of the material. For a given material and for a particular sheet thickness, there is only one $\varnothing_t/t_0$ value at which the spifability can be maximized under a given set of conditions. Furthermore, if a tool radius lesser than a particular value is used ($\varnothing_t/t_0$) the material squeezes out from the toolsheet interface. Such a condition adversely affects the material formability and surface finishing [52].

In most machines used for SPIF operations, the forming tool is mounted on a standard tool holder or a custom design tool holder. For most applications, the tool holder is mounted on a spindle. The SPIF operation can either be done by allowing free passive rotation, minimising friction, or by imposing a given spindle speed. Some SPIF operations performed in adapted CNC machines take advantage of the spindle rotation to increase formability. However, as spindle rotation has no noticeable influence on surface quality (if any, negative), most operations performed with industrial robots or purposed machines use a passive interaction mechanism for the forming punch, where it rotates freely as a response to any in-plane loads [6, 12].

As an alternative to a rigid tool, a water jet can be used as a incremental forming tool. A water jet with about 2 mm diameter, 25 MPa and 50 l/min can be used as a forming tool. Figure 2.27 (e) represents a water jet tool for forming operations. Major advantages are more flexibility and better surface integrity. However, Water Jet Forming is less accurate, consumes more energy and takes more time than the other incremental metal forming processes. The water jet incremental sheet metal forming uses lower water pressure and higher water flows then abrasive or pure water cutting machines. This prevents the use of a standard cutting machine to be adapted for forming operations. However, a water jet forming head is much less complicated then a water jet cutting head, allowing to develop a cost effective machine [53].

In addition to the forming tool itself, SPIF operation can be achieved with the help of

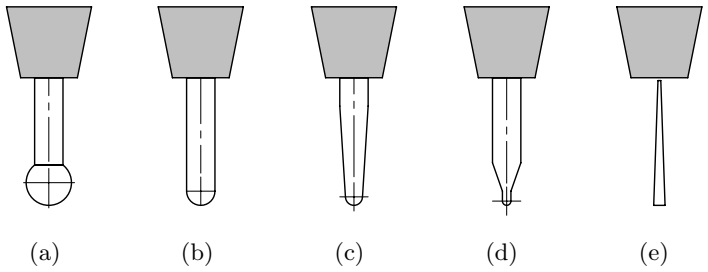

Figure 2.27: ISF forming tools: (a) dapper punch, (b) straight forming tool, (c) tapered forming tool, (d) tipped forming tool, (e) water jet.

complementary tools. Mostly, this secondary tools are used to improve either formability, surface quality or accuracy of the formed part.

A possible secondary tool is used as a heat source for improving both formability and accuracy of the SPIF operation. The heat source used can be a heat gun or a laser. Heat gun assisted incremental forming is applied in polymers [54]. Laser-assisted principles are mainly used to improve the geometrical accuracy of parts made from titanium alloys or high strength steels. Since forming in ISF is localized, localised heating of the forming zone is provided. As heating must occur in front of the moving forming tool, the laser spot has to be able to rotate around the forming tool for the production of complex geometries [55].

A DC current pulse can also be used for improving performance of the SPIF process, as high density electric pulse aide plastic deformation through electron-dislocation interaction. This phenomenon is termed as electro-plasticity [56].

Another possible secondary tool for SPIF operation is the use of a dummy sheet. Two sheets are formed at the same time instead of one. The top sheet is just a dummy and protects the bottom sheet from the sliding of the forming tool. The use of a dummy sheet setup eliminates wear, decreases surface roughness, improves visual appearance and only causes a small reduction in formability. This setup also allows forming of soft aluminium sheets without damage to the sheet surface [57].

2.2.2 Process strategies and tool paths

Whereby SPIF works in an incremental way, where the tool follows a pre-programed path, the definition of the process strategies strongly influence the result. Simplest SPIF operations are fulfilled in a single stage 3 axis strategy. More complex forms are accomplished with multi stage and up to 5 axis approaches.

Most operations performed in SPIF starts the process from the part boundary and progressively deforms the sheet through trajectories drawn. The tool tip follows the contours of the geometry, increasing the forming depth along the way. This increase is performed according to a defined vertical step size (Δz) with typical values from 0,1 to 2mm.

Figure 2.28 represents some variations of constant z step tool path types for SPIF. While the tool follows the outer contour of the piece at each forming step for every path-type, the transition between levels differs. In both contoured or alternating types paths, the tool moves from one level on the z axis to the next diagonally in the xz axes. This creates a line where the tool moved from level to level. The difference between the strategies is a change in the movement direction between levels. In the stepped type strategy the forming contours are

defined in the same way, but when the tool steps to the next level, it moves in the xy and then z axes. In alternative, the tool can step aside of the surface in a perpendicular direction to the surface. This can be performed with either a single or alternative direction movement at each level. The distance from the tool tip to the surface created by the horizontal deviation on the step transition helps removing the line created by the tool as it moves from level to level. As a final alternative, in a helical or spiral type tool path the tool-head follows a continuous path outlining the shape of the geometry. The tool is always moving in the x, y, and z axes, creating a helix pattern in the formed part. Besides resulting on better surface quality, this tool path type leads to better geometrical accuracy [33, 58, 59].

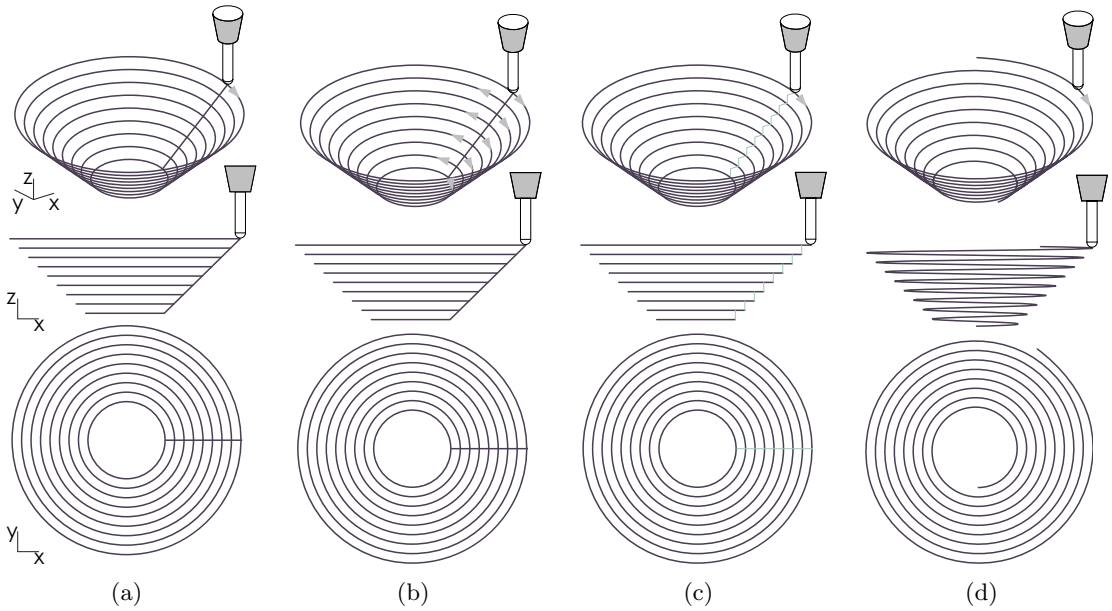

Figure 2.28: Constant z step tool path types for SPIF: (a) contoured, (b) alternating, (c) stepped, (d) helical.

Constant z step offer good results for the manufacture of simple parts with constant slope walls. In fact, this step down path from the top to the bottom of the pocket, in which the tool follows a series of consecutive contours with fixed step depth, is the simplest one but presents two disadvantages. In particular the sheet is marked at the transition point between consecutive layers, except in helical approach, and the quality of flat or near to flat surfaces is poor, specially when high step depth or pitch (more than 0.5mm) are used.

If the surface finishing of the part is an important aspect of the process, mainly in variable slope walls or free form shapes, the path conducted as a pocketing with constant step depth needs to be modified. In this case, to conduct pocketing with constant "scallop height" can give better results. This is a step down path from the top to the bottom of the pocket, in which the tool follows a series of consecutive contours with variable step depth (the maximum of which must be defined) in order to keep constant the value of the scallop height. The scallop height (Δh) is the maximum perpendicular distance from the formed surface and the tool. Equation 2.2 relates the scallop height to the vertical step, as illustrated in figure 2.29. This kind of path reduces the disadvantages of the first type and, in particular, the flat or shallow surfaces show a better quality. Figure 2.30 represents the difference between a constant Δz

and a constant Δh when forming a variable slope container type part [60].

$$\Delta z = 2.\sin(\alpha).\sqrt{\Delta h.(\varnothing_t - \Delta h)} \tag{2.2}$$

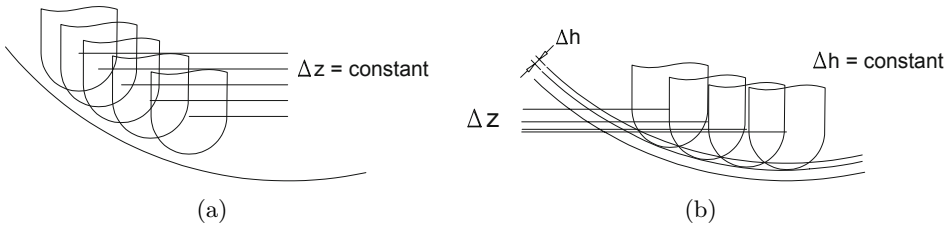

Figure 2.29: Incremental forming increments: (a) constant z steps, (b) constant scallop height.

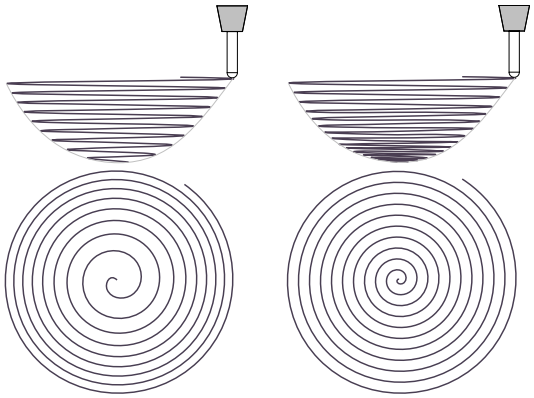

Figure 2.30: Spiral tool path for variable slope parts: (a) fixed z step, (b) fixed scallop height.

The presented option define the tool path of the spherical tool tip. Most machines operate in 3 axes only, so that the tool tip follows the defined tool path with its axis allows alight to z direction. As an alternative, 5 axes strategies can be used to perform SPIF operations. This solution becomes attractive due to its high flexibility, allowing the most convenient punch positioning at the surface sheet metal. At one point, the possibility to alight to tool with the forming force allows to use thinner tools, as bending will be minimised. This allows to fabricate parts with greater detail, for example, smaller radii. Besides, the tool inclination promote lower friction coefficients and improve formability, allowing to achieved steeper wall angles [13, 61].

The use of the different types of tool path presented is widely spread as they are simple to generate using commercial CAD/CAM software and produce very acceptable results in a time effective operation. However, these single stage strategies demand a geometrical complexity limitation. In order to expand the flexibility of the SPIF process, multi stage forming can be used.

There are two major different mottos for the use of a multi stage forming. On the one hand, this strategy can be used to help improving spifability, allowing greater draw angles. On the other and, multi stage can be used to improve accuracy and detailing in some complex shape parts.

On the first, the main goal is to enable the fabrication of parts with draw angles above the single stage forming limit. With these multi stage strategies it is possible to fabricate parts with vertical walls and even with negative draft. Figure 2.31 (a) and (b) represents a schematic of 2 and a 5 stages approach to increase the draw angle to high slope or vertical wall. The strategy extends deformation to all the material available in SPIF. The first stage stretches the blank into a 45° cone. The following stages gradually move the middle of this section towards the corner. All stages except the first can be performed with either downwards or upwards moving tool [62–64].

The first stage can only be performed by downward tool movement. The cone has a constant drawing angle close to 45° and this result in evenly distributed strains, except close to the backing plate and the lowest part of the cone. The following stages can either be performed in a up-down or in a down-up movement. However, despite the option, a residual cone is present after the second stage and it is still present along the sequence of the fourth stages. Besides, there is also an influence on both thickness and the ability to form without fracture given by the direction of the 2^{nd} to 4^{th} stages. The direction of forming has a huge effect on thickness distribution and position of strain [62].

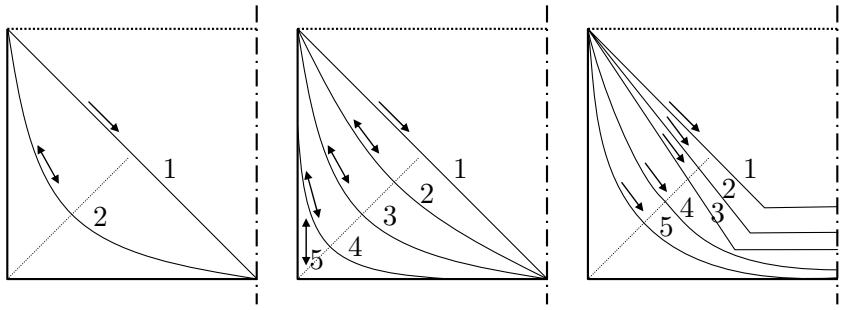

Figure 2.31: Multi stage forming strategies to increase draw angle.

It is found that sheet metal formability is dependent on the slope along the depth of the fabricated part. If the slope changes along the depth, then shell thickness is reduced at a faster rate than in a case with a fixed slope. Figure 2.31 (c) represents a different method for multi stage forming where the first stages are performed with a fixed slope and curvature is only accomplished in the final two. Thus, such mechanism can enhance the dimensional accuracy and delay the fracture. Consequently, this gives the chance to form the sheet in a high forming angle such as 90° [63].

On the second badge to use multi stage, the goal is to seek for better accuracy and greater detail. This approach works in the same way as a finishing milling operation does, with the possibility of using different tools for forming different features of the part [49]. Figure 2.32 represents a concept example of the use of a multi stage strategy to improve the detail by forming one feature of the part at a time.

Strategies in addition to the multi stage are used also to improve accuracy of wall angle. By measuring a SPIF prototype, it is possible to identify the deviations from the desired surface. By mirroring the obtain part through the target contour (original CAD surface) one can obtain a new surface. This virtual surface can be used to generate a new tool path and reproduce the part at better accuracy [4].

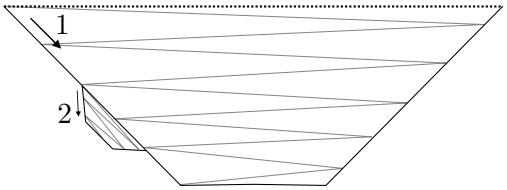

Figure 2.32: Multi stage forming strategies to increase detail.

If a part is impossible or difficult to fabricate due to a steep angle on one wall only, it is possible to tilt the tool axis and regenerate the tool path redistributing the draw angle by creating angled tool paths. This allows local forming of a region with a wall angle higher than the failure wall angle by rotating the plane of the workpiece in an optimised way. Without changing the geometry of the work piece, this strategy virtually lowers the wall angle in the targeted region while increasing the wall angle in other regions [65].

2.2.3 Incremental forming mechanics

Incremental forming is a continuous process where the material is shaped by localised deformation. This huge difference when comparing to the conventional forming processes make the theoretical foundations of conventional processes not valid for ISF.

Another major difference between the conventional processes and ISF is related to the type of strain and the formability limit. The formability of incremental forming is higher than that of conventional forming processes such as stamping. The forming limits can be characterised by the maximum wall angle before failure occurs. This maximum angle is dependent on the material type, sheet thickness and process parameters such as tool radius, step down, feed rate, local temperature of the sheet. Increasing sheet thickness, decreasing tool size and decreasing vertical step size all tend to increase formability.

Although there aren't certainties on how the deformation works, it is consensual that the formability limit is defined by a Forming Fracture Line (FFL), being a straight line with negative slope. Figure 2.33 represents the formability limit configuration on a FLD where the slope of the FFL is given by equation 2.3, usually varying from $-0,7$ to $-1,3$. While the FLC is determined concerning local necking failure, the FFL outcome from fracture. This is because necking phenomena is suppressed in ISF. As the plastic deformation only occurs in a small zone surrounded by rigid material or at least only deformed elastically, a potential neck is unable to grow. In this way it can be regarded that SPIF is limited by fracture only with uniform thinning until fracture [37, 66–70].

$$\frac{\epsilon_1}{\epsilon_2} = -\frac{5.\frac{\varnothing_t}{2.t_0} + 2}{3.\frac{\varnothing_t}{2.t_0} + 6} \tag{2.3}$$

Aside from the FFL, the maximum drawing angle α_{max} that a material can undertake as function of the initial thickness of the sheet is commonly used for assessing the forming limits in SPIF. Table 2.2 summarises some maximum draw angles for a single stage forming operation determined by experimental methods [14,71–73]. The determination of these values is accomplished through the production of truncated cones and pyramids at the varying of the slope of the walls up to fracture occurrence. Although there is no quantifiable relationship between the sheet thickness, material properties and maximum angle, it can be qualify that

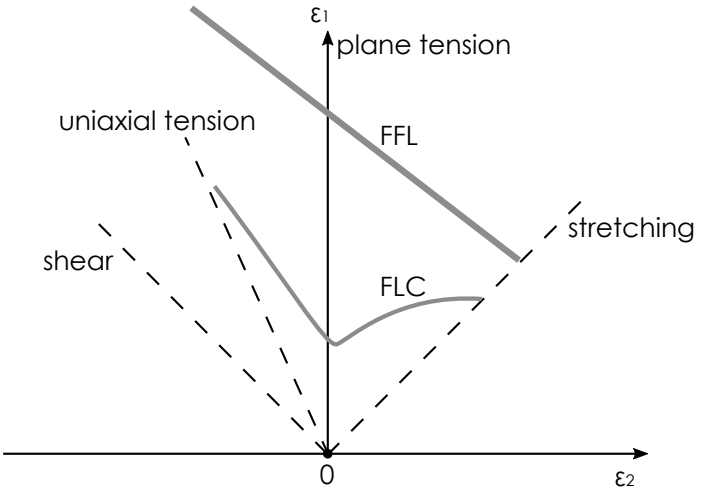

Figure 2.33: FLD with a typical FLC for conventional and ISF operation.

the highest the strain hardening coefficient and the percentage elongation, the largest material formability in SPIF, and, the thicker the sheet, the highest the maximum drawing angle as well [73]. The presented values are references and may vary as they are also influenced by the forming parameters. Furthermore, the anisotropy of some materials in a sheet form lead to differences on these values according to the sheet forming direction.

Table 2.2: Maximum draw angle for SPIF operation as function of material and thickness.

Material	Thickness (t_0)	Maximum draw angle (α_{max})
65Cr2 steel	0,5mm	57°
DP600 steel	1mm	68°
DP1000 steel	1mm	39°
AA 2024-T3	1mm	42°
AA 3003-O	0,85mm	70°
AA 3003-O	1,2mm	71°
AA 3003-O	2mm	76°
Brass	1mm	40°
Copper	1mm	65°
HSS	1mm	65°
Polyamide	3mm	75,4°
Polyethylene	3mm	81°

While there is no certainties on the state of strain in ISF, it is accepted that neither pure stretch or pure shear happen. Authors have considered that the mechanics of deformation in SPIF include plane stretching in the contact area of the tool and an association of stretching, bending and shearing on the surrounding area, partly the reason for the improved formability. During SPIF, stretching along the component wall is also observed [66–69, 74, 75]. The dominant forming mechanism in a SPIF part depends not only on the part geometry but also on the forming tool and parameters. Bending dominates when using large tools and large forming steps while shear dominates when forming thick thicknesses [76].

Local stretching and bending of the sheet around the hemi-spherical end of the tool cause higher plastic strain on the outer side of the sheet, which increases damage on the outer side as compared to the inner side of the sheet. Greater through-the-thickness shear on the inner side of the sheet also has a similar effect on damage accumulation. The combined effect of these two phenomena is the initiation of the crack on the outer side of the sheet which then propagates towards the inner side of the sheet. Shear is greater in SPIF than in conventional forming, however, local bending in SPIF is so much higher that it overwhelms the effect of increased shear. The local nature of deformation is the primary reason for increased formability in SPIF as compared to conventional forming [75].

Forming force and energy

The forming force in ISF is very small in comparison to the deep drawing or stamping processes. Besides, the force intensity does not depend on the part size. That is why the production of very large products is absolutely appropriate for SPIF. Major studies on the ISF forming forces have been done by experimental and numerical methods. The force can be decomposed in a vertical (F_z) and horizontal (F_{xy}) components. The horizontal component can decomposed in a tangential (F_t) and perpendicular (F_r) component, as illustrated in figure 2.34. Experimentally it has been determined that the force, namely its vertical component, is influenced by sheet thickness and material properties, tool diameter, wall angle and vertical step size or scallop height. The forming force increases when forming stiffer materials and with the increase of the sheet thickness. The forming force also increases with bigger forming steps and using bigger tools. Lubrication and tool rotation have no influence on F_z, affecting only the horizontal component of the force [77, 78].

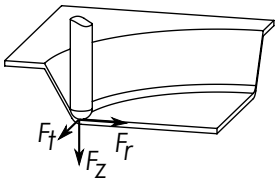

Figure 2.34: Forming forces in ISF operations.

The forming force increases when forming stiffer materials and with the increase of the sheet thickness. Besides, it appears that there are linear relations between the logarithms of the force and the sheet thickness. There is also an increase of the forming force with the increase of the draw angle. However, F_t is not influenced by the wall angle and F_z has a maximum value differs depending on the material. F_z is proportional to the function $\alpha cos\alpha$, physically, it means that the F_z is proportional to the draw angle and to the resulting wall thickness as approximated by the sine-law. F_r also increases with the angle, being negative for small angles. In what concerns the tool diameter, there is also an increase of the forming forces components F_z and F_r when using larger tools. F_t in virtually unaffected. The forming force also increases when using larger vertical steps. A generalised formula which allows to predict the axial force F_z for any material based on the tensile strength only has been developed [77, 78].

Equation 2.4 has been experimentally determined to predict the generalised steady-state value of vertical forming force, where σ_u is the ultimate tensile strength and Δh is the scallop height. Some peak values of the vertical forming force are achieved, mainly when forming

higher wall angles, thicker sheets and using bigger tools. A reference value for the vertical forming force can be obtain by the second member of equation 2.4. Equation 2.5 has been determined to approximate the radial forming force, where c depends on the forming material (e.g.: 2.54 for aluminium alloys). The scallop height relates to the vertical step down according to equation 2.2. All the equation use linear dimensions in millimetre, angles in degree, stress in megaPascal and determine forces in Newton [78]. Equation 2.6 has been estimated to relate the tangential force to the radial force.

$$F_z = 0.0716.\sigma_u.t_0^{1.57}.\varnothing_t^{0.41}.\Delta h^{0.09}.\alpha.cos(\alpha), \qquad F_{z_{\text{ref}}} \approx 3.8.\sigma_u \tag{2.4}$$

$$F_r = F_z.\tan\left(\frac{\alpha+\beta-17.2^{\text{o}}.(\varnothing_t/10)^{-c}}{2}\right), \qquad \beta = \arccos(1-2.\Delta h/\varnothing_t) \tag{2.5}$$

$$F_t \approx F_r.\left(360.\alpha^{-1.23}.\varnothing_t^{-0.62}\right) \tag{2.6}$$

It is reasonably assumed that the rate of plastic work due to the tangential force acting on the forming tool is the product of the tangential forming force and the horizontal component of the feed rate speed [79]. Analogously, one can assumed that the plastic work due to the vertical force is the product of the vertical forming force and the vertical component of the feed rate speed and the perpendicular component of the forming force produces no work. Thus, the forming power can be calculated by equation 2.7, where v_t is the tangential component of the feed rate speed and v_z is the vertical component of the feed rate speed:

$$\dot{W}_{\text{forming}} = \vec{F}.\vec{v} = F_t v_t + F_z v_z \tag{2.7}$$

2.2.4 Design and operation guidelines for SPIF

Since the milestone paper on SPIF in 2005 [4], considerable experience has been gained. Based on the experience of the last decade, a simple guide was introduced with the aim to have an introductory set of instructions to enable designers to fully exploit the advantages of SPIF. The process of taking a design to a final produced shape can be broken down to the following three main areas: model generation,tool path generation,and production.

Creating a design that is suitable for production using SPIF begins with the following general rules:

- The part must fit the forming area. The blank holder must have space to accommodate the blank sheet needed to the new part.
- The parts must be designed in a way such that it consists of one concave surface, bounded by a flange of undeformed sheet. This allows the part to be clamped. Despite the fabrication being almost exclusive for container type shape, after trimming the final part as a virtually free surface and shape.
- Walls must be drafted at some angle α from the sheet plane. Forming is the easiest and fastest when wall angles are kept below maximum draw angle of the material. Steeper walls can be formed using multi-stage methods but at greatly increased cost and time. Besides, inwards bulging of the bottom is a typically geometric inaccuracy in shallow sloped SPIF parts. Improvements can be achieved by, for example, using laser assisted ISF [80–82].

In order to support the part design and choose adequate forming strategies according to the intended part, several authors have studied and proposed different techniques.

Duflou et al. (2007) [83] and Ham and Jeswiet (2008) [84] studied the dimensional accuracy of the SPIF process on aluminium alloys. Depending on sheet thickness, tool size, step size and part shape, accuracy varies from ±1 mm to ±4 mm. Mean deviation is close to zero and the worst accuracy occurs at the part frame. Behera et al. (2011) [85] proposed techniques to improve SPIF accuracy. Mohammadi et al. (2013) [86] studied the particularly inaccuracy of shallow slope parts.

Several authors have tested maximum forming angles for different materials and thicknesses, with different working parameters. Allwood et al. (2005) [48] have summarised some of the achievements. Typical ϕ_{max} angles for aluminium alloys vary around 70°, for steel alloys around 60° and for some thermoplastics around 80°. This value increases with thicker sheets and is also influenced by the forming parameters.

Skjødt et al. (2010) [87] and Liu et al. (2013) [88] proposed tool path strategies for multistage SPIF able to achieve vertical walls and improving thickness distribution. Sá de Farias et al. (2015) [13] proposed 5 axis strategies to increase maximum formability angle.

Vanhove et al. (2011) [89] have proposed an optimisation of the part orientation in order to increase the maximum slope angle of one side and improve the part accuracy.

Thyssen et al. (2016) [90] have used stiffening elements not only to reinforce the part but also to increase the part accuracy.

Do *et al.* [91] tested the incremental formability of structured sheets. This approach adds a blank geometry factor to the material and thickness selection. Although this method leads to great surface differences between formed walls and part top, it allows achieving higher maximum forming angles due to the flatted area in the slopped walls.

2.2.5 Time and energetic cost

In the latest years many researchers focused their attention on evaluating and modeling the environmental impact of some production processes, nevertheless many processes are still poorly documented in terms of environmental footprint. In order to start to fill this knowledge gap, the CO2PE!-Initiative [92] has been launched. In particular, this initiative aims at coordinate international efforts aiming to document and analyze the overall environmental impact for a wide range of available and emerging manufacturing processes and to provide guidelines to improve them. More in particular, the objective of the CO2PE! initiative is to cluster forces in different continents, involving machine builders as well as academics, to analyze existing and emerging manufacturing processes for their ecological impact in terms of direct and indirect emissions. In the case of SPIF, studies have evaluated the environment impact of the process, considering the energy consumption, lubricants use and material. General conclusion state that faster processes benefit the energy consumption and consequently the environment impact [93, 94].

The energy consumption of SPIF processes of various different setups has been analysed and quantified. As the forming time is the dominant factor in energy consumption for SPIF processes, the energy saving potentiality of an innovative high speed set up was analyzed and quantified. In particular, the high cycle time characterizing the SPIF processes has limited the industrial applicability of this promising forming technology [95–97].

The power demand for air forming and sheet forming conditions has been measured for both a CNC milling machine and the six-axes robot adapted to perform SPIF operations.

For the CNC machine tools no difference in power demand was observed. In consequence, it can be stated that the considered material does not affect the power demand. As the six-axes robot is regarded, this machine configuration proved to be sensitive to the material being formed Three different materials, characterized by different strength grades, were formed by SPIF and the energy demand was analyzed. It was observed that as a function of the material strength the power/energy demand monotonously increases. The so-called material contribution share on the total energy demand accounts for up to 22% for the material with the highest tensile strength in the considered material set [96].

2.3 SPIF applications examples

As previously stated, the SPIF process allows manufacturing unique or low volume series. In general, ISF is typically cost effective up to 300-600 pieces. From that level onwards investing in dies becomes feasible. The process enables to produce parts of any size. The size is only limited by available hardware. When compared with conventional processes, the breakeven point have slight dependence on the size of the part produced. For relatively large parts there is an increase in the breakeven point as compared to smaller part in ISF [98, 99]. Graphic on figure 2.35 counters part size and number of parts serviceable by SPIF with typical industrial applications. The better suited identified fields are the manufacturing of prototypes, the manufacture of design and architecture components, the fabrication of spares for obsolete parts and the fabrication of components for small volume industries such as aeronautics [100]. Other identified application fields is the customisation of parts, making them unique for increased value products. Lastly, the fabrication of custom-made products of various shapes and dimensions is also a great potentiality of the SPIF process [14].

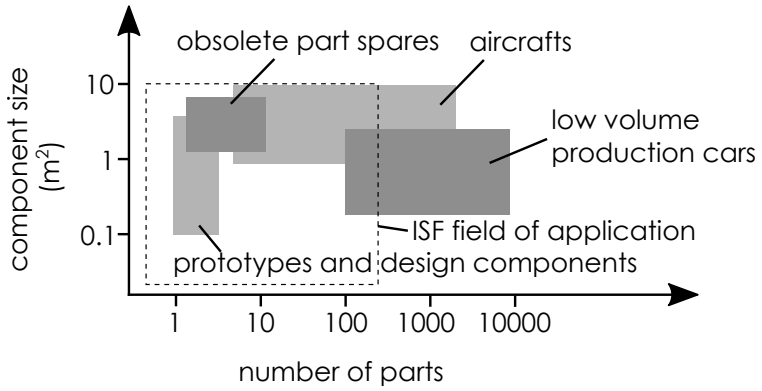

Figure 2.35: Current and potential fields of application of ISF

2.3.1 Benchmark parts

A diversity of benchmarking parts have been design and developed by several research groups. The aim of these parts is to study the geometric accuracy, formability, geometric complexity limit, finishing quality, among other features.

Figure 2.36 represents a simple benchmark cone with a square grid [101]. The use of circles and square grids allow to better observe the deformation on the parts, measure deformations and better evaluate the process. Figure 2.37 shows several benchmarking parts with various shapes, heights and slopes [4].

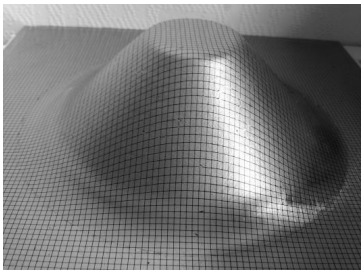

Figure 2.36: Simple benchmarking cone.

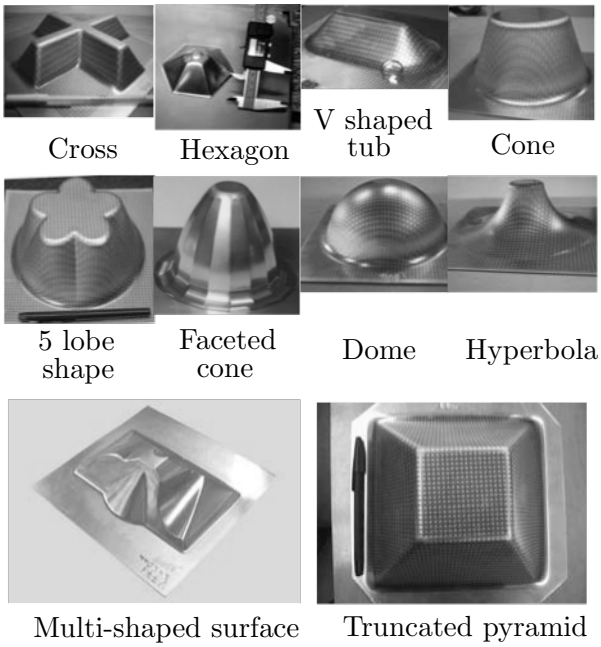

Figure 2.37: Benchmarking parts for SPIF operation.

2.3.2 Automotive and transportation applications

One of the strong fields of SPIF is its application in the automotive industry. Despite this being a mass production industry with lots of sheet metal parts produced by conventional processes, SPIF has a great potential to be used as a tool for prototyping new parts, as a way of customising parts for added value to the product or to fabricate obsolete parts for antique automobile restoration.

Figure 2.38 shows the hood of a Honda S800 manufactured as limited series of replacement parts for the S800 sports car. To do this an existing part was measured with a 3D measuring machine, and the co-ordinates used for producing the part. A series of twenty replacement parts have been produced actually [3, 45, 102].

Figure 2.38: Inner and outer side of a personalised hood from a Honda S800.

Figure 2.39 shows some examples of incremental forming evaluation testes performed by Ford and Toyota [103, 104].

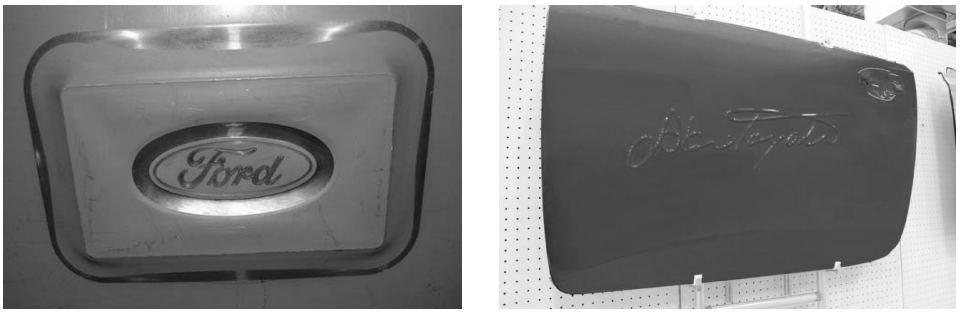

(a) (b)

Figure 2.39: Incremental forming proposals by car manufacturers: (a) Ford badge, (b) Toyota personalised door.

Figure 2.40 shows a scaled model of the front section of a Japanese Shinkansen bullet train model built by Amino [45].

Figure 2.40: 1:8 scaled model of a Shinkansen bullet train.

2.3.3 Medical applications

SPIF has potential possible application in the medical field to develop personalised prosthesis or other equipments. Medical implants have been one of the most researched applications of SPIF due to the need for customization to the shape of the human body. Specific applications have included ankle support, cranial plate, knee prosthesis, backseat prosthesis, dentistry products and facial implants. Titanium has been one of the key materials formed in these studies.

One of the possible application fields is the manufacturing of cranial plates used in reconstructive skull surgery. These plates are quite expensive and take a long time to produce using the conventional means. A case study done in cooperation with Unident Nv. shows the industrial applicability of the SPIF process in this field. Figure 2.41 shows two examples of this application [105, 106].

In the field of dentistry, there is a natural need for personalised devices that are custom made for the patient, area in which SPIF is highly promising. SPIF technology was applied for manufacturing of a denture base (framework) of a complete denture. Figure 2.42 illustrates the denture bases made from two different materials (carbon and stainless steel).

In both cases surface quality as well as dimensional accuracy were satisfied with dimensional discrepancies less than 1mm. SPIF enabled the manufacture of a denture with additional mass reduction of the base by using thinner sheets, which is highly desirable from viewpoint of patient and wear comfort [107].

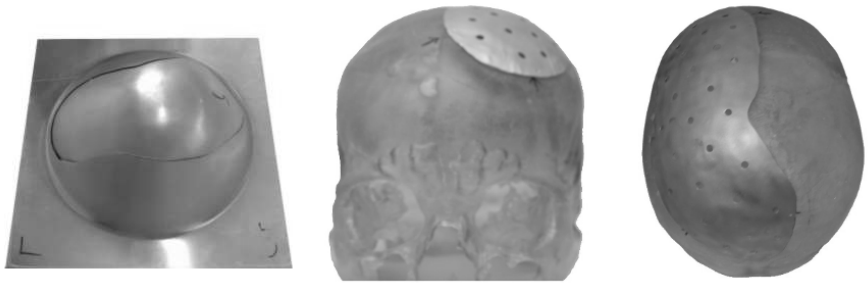

(a)

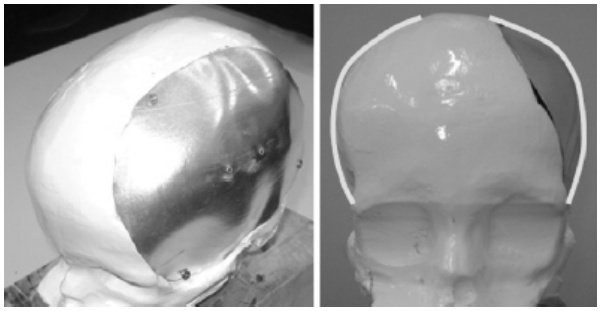

(b)

Figure 2.41: Prototypes of cranial plates.

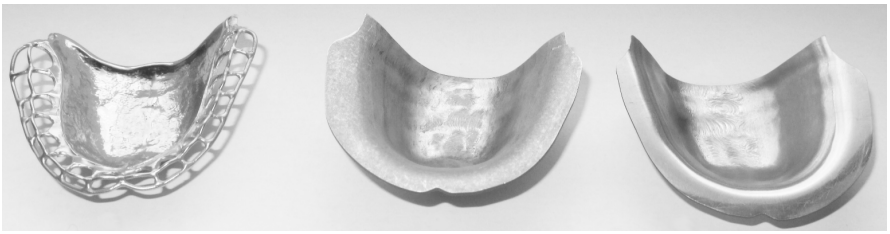

Figure 2.42: Original and two SPIF replicas of a denture base.

2.3.4 Prototypes and Custom-made products

A major field of application for the SPIF process is the development of prototypes to help the industrial product design and development process. As mechanical properties of SPIF parts are similar to the ones produced by mass production processes, it is possible to develop final functional prototypes for both evaluation and presenting a product. Besides, in the industrial design field, SPIF offers a great possibility of designing free form metal shapes for unique or low volume production series, otherwise impossible or very expensive.

A solar cooker (or solar oven) was the manufacturing at KULeuven as one of the first case studies of SPIF. This is a device that is used in third world countries to cook food using the power of the sun. The most expensive component to manufacture was the container for the food, the actual oven. The manufacture of this piece was done by SPIF at a reduced cost and within the needed accuracy. Figure 2.43 shows a picture of the solar oven [4, 83, 108].

A custom design hand washer was produced and is used as an application example by Amino. Figure 2.44 shows the underside of the formed part, still mounted on the frame and

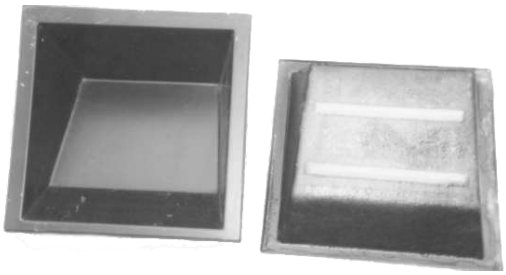

Figure 2.43: Prototype of the container of a solar oven.

the final assembled prototype [45].

Figure 2.44: Hand wash stand.

ISF has been announced among product designers as an reliable alternative for low production sheet metal. Figure 2.45 shows a free form metal bowl fabricated by SPIF as an example of a potentiality of ISF for industrial craft [109].

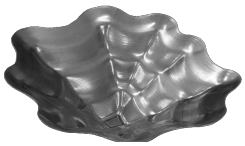

Figure 2.45: Metal bowl as an example of industrial craft.

2.3.5 Architecture products

Several freeform self-supporting metal structure have been design and developed by ISF processes. The structures, mainly organic roof structures have been developed, consisting on a large assembly of formed panels. ISF is used alone or combining with conventional stretch forming operation. Figure 2.46 shows a 1,5m x 0,8m prototype of a roof structure consisting on 8 panels (4 different panel shapes) with 9 to 11 incrementally formed cones each [46]. Figure 2.47 shows a plain panel and 3 configurations of geometrical improvements with the ribbing system performed by SPIF and a collection of other ISF design parts [33, 110].

Figure 2.46: Prototype of a roof structure.

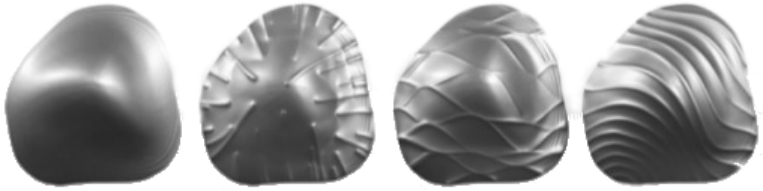

(a)

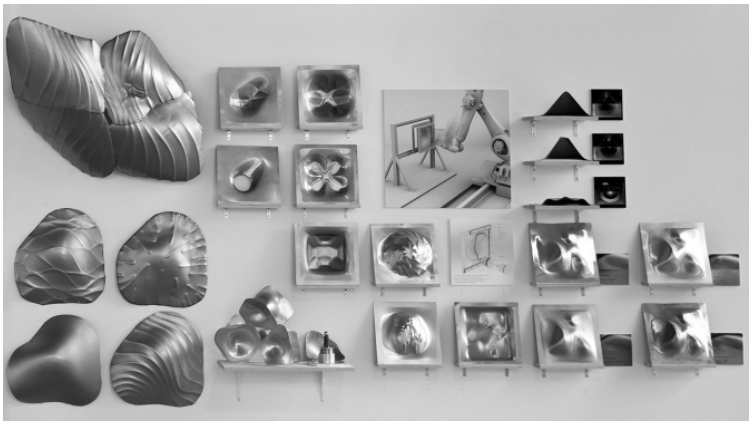

(b)

Figure 2.47: Architecture and interior design parts: (a) ribbing on some architecture panels, (b) a collection of designed parts.

2.3.6 Rapid tooling applications

The capability of producing relatively high strength parts allows SPIF to be used as a rapid tooling process. The use of sheet metal molds for thermoforming operations has been studied. Figure 2.48 shows an example of a simple mold fabricated by ISF [49, 111].

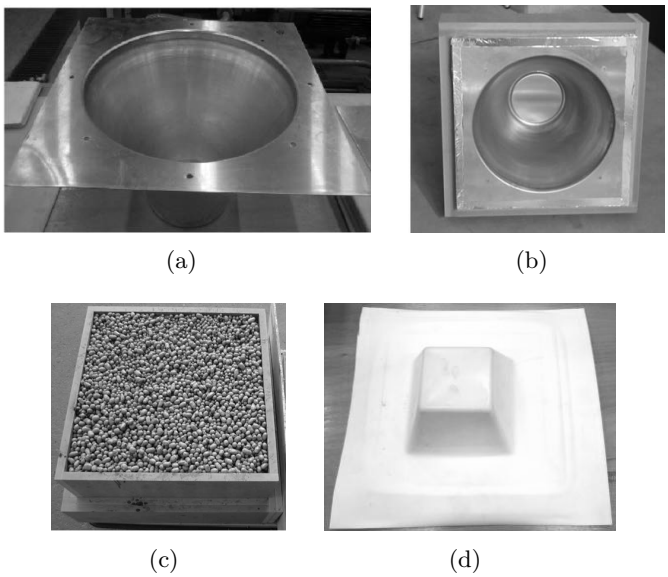

(a) (b)

(c) (d)

Figure 2.48: Thermoforming mold created by SPIF: (a) ISF sheet part, (b) mold inside a MDF box, (c) box filled with a porous mixture casted to provide support, (d) plastic part fabricated in the mold

Chapter 3

Objectives and Methodology

The present PhD aims to contribute to enhancing the SPIF process and analyse possible industrial applications. Within this global objective a three stage working plan with specif research methodology for each stage is defined. In addition, test methods, particularly for measuring operations are defined and developed.

3.1 PhD objectives and working plan

The main goal of the working programme is to analyse the SPIF process in both functional and energy consumption levels in order to leverage its use in industrial product production. At an early stage, it is intended to explore the limits of geometrical complexity and its influence on production time, cost and environmental impact. In a next step, the goal is to search for industrial applicability of the SPIF process through a direct application in product development projects, both as a prototyping and production technology. In addition, the workplan aims to search for new applicability for SPIF as a rapid tooling process.

Summarising, the objectives are:

- Analyse SPIF process:
  - explore and define the geometrical complexity limits;
  - define a production cost and time/energy consumption model;
  - define operation and design guidelines;
  - benchmark with complex industrial parts.
- Test the use of SPIF process for sheet metal parts:
  - prototype future high volume production parts;
  - manufacture of unique or low volume production parts.
- Test SPIF as a rapid tooling process:
  - for the use of thermoplastic, thermosets and composites materials;
  - exploit farfetched applications.

The workplan is organised in three major tasks, with a direct relationship to the main objectives. The sub tasks are organised in such a way to lead to concrete results with scientific relevance, allowing the publication of articles or conference proceedings, disseminating SPIF as a viable manufacture process in both academic and industrial point of view. The three major tasks are complemented with a depth understanding of the state of the art and dissemination phase. The tasks are not necessarily carried out sequentially. Tasks are carried out using SPIF-A machine from the Mechanical Engineering Department of University of Aveiro [6,11] and other industrial and laboratory equipment from The School of Design, Management and Production Technologies Northern Aveiro of University of Aveiro.

State of the art and theoretical analysis

The PhD workplane starts with the review on the state of the art and an insight on theoretical concepts behind sheet forming. The first stage is the review of the of the mechanical principles on strain and stress and the understand of the mechanics in sheet material forming. For a more extensive analysis, the state of the art include the study of different industrial sheet metal forming processes: operation, applications and limitations. The formability concept is considered and related to diverse methods of sheet forming. The state of the art analysis is concluded with the understand of the incremental sheet forming processes and variant principles of operation. The single point incremental forming is studied, understanding the working principle, forming parameters, forming mechanics and applications. The results are presented mainly in chapter 1 and 2, being also used for the definition of the methodologies presented in chapter 3.

Characterisation of the SPIF process

The first task relates with the study of different aspects of the SPIF manufacture process and establish a link between the theoretical and state of the art analysis and the practical stadium of the PhD program. During this stage the use of SPIF for the manufacture of sheet metal parts is tested, mainly using the SPIF-A machine developed at the Mechanical Engineering Department of University of Aveiro [6,11]. A variety of materials are evaluated under different forming parameters in experimental tests while analysing both the process itself and the result part. This task aims to balance with the latest developments and contribute to the advance of the state of the art. The results of this first research task are presented in chapter 4 of the thesis. Among other activities that may result from significant opportunities, the task one includes:

- Establish well defined design guidelines for SPIF of freeform parts. Define geometric part typology and topology for SPIF and explore the geometric features possibilities and limits. Explore the manufacture of new part configuration using semi-constrain blanks and the combination of SPIF and other forming processes.

- Evaluate the energetic efficiency and consumption of the SPIF process, in particular the SPIF-A machine. Relate the energy response to different forming parameters. Determine the influence of the forming force and process time to the energetic efficiency, not neglecting the part quality.

- Define a process based cost model for SPIF: production, energy, material, tooling, manufacture time, preparation time, environmental impact. Explore possibilities for the implementation of a SPIF based business. Define breakeven chart for SPIF against press forming concerning the batch size for benchmark parts.

Manufacture of sheet metal parts by SPIF

The second task aims to contribute to the validation of the SPIF process original purpose. With the cooperation of industrial partners, use SPIF to produce sheet metal prototypes or small batches. The task results are presented in chapter 5, organised in case studies, contributing to the evaluation of the proposed forming parameters and strategies, while spreading the use of ISF in the industrial sector and evaluating its applicability in real scenarios. Despite being very dependent on the partnerships to identify case study candidates, the task intended activities are:

- Use SPIF for prototyping parts for domestic appliances, helping achieving photo realist or functional prototypes. Test the possibility of using ISF for the manufacture of custom products or small batches for niche markets.
- Test SPIF for the manufacture of automotive parts, both for prototyping new concepts or to replicate out-of-the-market parts for restoration jobs.
- Collaborate with designers to explore the product development of SPIF purpose designed parts.

Managing other materials, SPIF as a rapid tooling technology

The third major task of the working plan is to study the use of SPIF as a rapid tooling process. It is intended to design, manufacture and test rapid sheet metal moulds for processing different materials. The results of the experimental research and discussion are presented in chapter 6. For each process tooling in analysis, the task three activities enclose:

- Analyse the manufacture tooling requirements and design proposal for sheet metal moulds. Evaluate the expected sheet metal mould behaviour under the process conditions: loading, temperature, wear. Use of analytical, analog comparison and numerical methods for the evaluation.
- Design of a benchmark part and sheet metal rapid tools. Fabricate the moulds while performing cost and energy analysis.
- Test and validate the use of the sheet metal moulds. Compare with conventional alternatives. Evaluate the produced parts using the sheet metal tools.

Conclusions

The thesis final chapter (chapter 7) presents conclusions regarding the research results. A summary is presented and the findings are discussed and interpreted, analysing its contributions to the main goal of the PhD workplan.

3.2 Methodology

The PhD workplan involves a variety of experimental and applied work. The activities presented in chapter 4 require a systematic approach to generate experimental data and analyse it in an overall point of view, using factorial experiments to maximise the outputs for each activity conclusions [112, 113]. In the chapter 5, problem orientated case studies are used to take real life examples and reach conclusions to be used in other problems and issues [114]. The activities presented in chapter 6 use generation and validation methods to evaluate possible comprehensive systems hypothesis through the scientific method [115, 116]. Despite the different methodology defined in each chapter, a common frame is followed in each test, based on the same three phase method: planning, implementing and analysis.

The planning included a theoretical analysis of the testing elements or may include simulation works. In this stage, design of experiments its use to determined the parameters to be evaluated and plan the series of tests. A specific methodology is defined per each individual test, all including the fabrication of parts, the instrumentation method of the SPIF process and the evaluation of the results. Thus, planning include the identification of data to be collected and all hardware and software required. The planning stage is completed with the definitions of the experiment layout, managing the best way of performing them.

During the implementation stage, the experiments follows according to the planning phase. The implementation stage starts by testing the procedure. All parts are formed under careful observation while monitoring the process conditions. The result parts are also evaluated for the relevant features. All collected data is saved and organised for further analysis.

In the third stage, the acquired data is analysed. The performance of individual tests is taken into account and used for a general experiment comparison. An overall analysis leads to the identification of conclusions. All results are judiciously examined and compared to the forecasts, validating the conclusions and preparing the results for publishing.

The design of experiments for the chapter 4 activities is done considering a combination of fundamental research and developmental research, both with open results [112]. The experiments seek the achievement of output results that underlie the use of case studies to generally describe the incremental forming process. For that, the design of experiments considers a sequence of small tests. Between each individual test a major number of variables remains unaffected, only changing the studied parameter in question.

Due to the number of possible analysis parameters, p^k factorial experiments design is used, where each experience studies k factors each on p levels, usually a prime number. For the experimental work on different topics, changes in forming parameters are tested: vertical step, forming feed rate speed, sheet thickness, material, geometry, tool diameter, tool path strategy, lubrication and others. The parameters in analysis are chosen to have major influence on the experiment topic under evaluation. Between each individual test only one parameter varies while the others remain unchanged. Excluding exceptional cases, each factor is tested for three different levels: a standard value from previous experimental work or from literature, a lower value and a higher value. If possible, a factor independent reference test is performed. Test may either be completed in blocks or individually [113, 117].

For each experimental work a table is written, summarising the values for each factor in analysis and all the p^k combinations to perform. The testing values in table are used to, every time possible, algebraically or numerically determine a prediction for the results to be used both for validating the parameters in analysis and the experiment results.

When the number of variables to consider is too high, it leads to an untenable number of

combinations. Thus, a multiphase approach is better suited for these cases, using one-factor-at-a-time on the first stages and factorial design in the last. Since the one-factor-at-a-time can not ascertain the correlation between different parameters, the factors that can be assumed the most independent are tested in isolation on a first phase, maintaining all remaining parameters unchanged at reference values. After getting conclusion on the influence of those quasi-independent variables on the forming operation, they are fixed at the best value and the remaining parameters are tested using factorial design of experiments. In these cases, beyond the referred chart with the testing parameters, a set of testing phases is defined with an individual table per phase [118].

As an alternative or complement to the first stages, data triangulation may be used to determine the values for the fixed parameters. In addiction to the results of one-factor-at-a-time experiments, results from previous experimental results and values from literature may be used to set values for design of experiments.

During the tests, both the power consumption, forming force, forming time, punch tool path and feed rate speed are measured and recorded. The measurement methods are described further in this section and uncertainty analysis is performed when applicable. The formed part quality is also quantitatively evaluated for accuracy and surface finishing. Each different set up is photographed and a described report of the forming process is written. The formed parts are also qualitatively evaluated according to their purpose. Accuracy is measured for the cavity side of the part and, if relevant, the bottom side. Thickness is measured to determine thinning. Surface finishing is also measured or visually evaluated. Whenever possible, the part quality is compared with other manufacturing alternatives, using the same or different materials. The results of each experiment are used to get conclusion that may be used in future work, improving the process performance.

For each experiment, the data in treated using descriptive statistics. Tables are written with the response to the analysis factors and the information is plotted in graphical form. The data analysis explore not only the relation between the analysis factors and the results but also the influence of dependent factors and the results. If determined, the experimental results are also compared to the prediction. Conclusions and recommendations are the drawn from the experiment results. Bar plots, pie plots and scatter plots are used to illustrate and support the conclusions. When applicable, regression may be used to define empirical model that relate the response and the most important analysis factors or dependent factors.

The case studies developed and analysed in chapter 5 activities have a slight different approach. Being an applied work, the core research is not the study of the forming operation itself but the SPIF technology usage validation. Each case study identifies all the stakeholders that relate to the project and clearly defines the part development needs. All assignments needed to achieve the final piece are described, including all operation done before and after sheet forming. An analysis and assessment of each case study is performed, exploring both the project result validation and defining recommendations for further projects [114]. The design of each study case is accomplished according to protocols specifically developed for Case Study Planning [119, 120].

As referred in the task planning, partnerships with industrial companies and with designers are sought and used to identify candidate parts to be manufactured by SPIF. The identified parts are used to test and validate the initial purpose of ISF of fabricating prototypes and small batches in real life scenarios. Thus, the selected cases must be robust enough to provide conclusions about the manufacturing process and its practical application. For that, the knowledge on forming operation acquired from literature, past experiences and the results

from the first activities are used to prepare and set up the part's manufacture strategy. All manufacturing work is developed while acquiring data about the process and describing the operations. Result is quantitatively evaluated for part quality, exploring accuracy and surface finishing, and qualitatively valued in characteristics as reliability, conformance, aesthetics and performance.

Each case study should include information for a full understanding of its purpose and conclusions. For that, the background is defined, specifying the particular research goals. The object of study is described identifying the criteria used for the case selection. The followed procedure is described and all data presented. The analysis presents and interprets the findings, identifying the range of possible outcomes and alternative explanations of the outcomes. It is performed as the case study task progresses. The case study validity is justified, in parallel to the limitations. Finally, the replicability for similar problems is discussed, defining the validity and exploring recommendations for all of the major steps.

The chapter 6 activities explores new applications for the SPIF processes proposing and validating rapid tooling solutions to process different materials. For that, innovative thinking and the scientific method is used to propose a research question from the observation of material processing technologies, define an hypothesis, execute experiments and evaluate the result, leading to conclusions about the feasibility of the new proposed applications and effectively communicate and justify conclusions whilst taking risks in accordance with predictions and confidence level. The Applied Scientific Method (ASM) : Observation - hypothesis - testing - conclusions method may be cyclical, resulting on multiple experiments formulation [115,116]. The applied experimental process can also be referred to as the CSSC methodology: Case identification, Solution identification, Solution implementation and Case review [121].

The observation phase searches for manufacturing process that require the use of purpose build tools. The identification of a candidate process is defined by the viability of using those processes for single part or low batches manufacture strongly depend on the tools cost and development and manufacture time. The benefit of reducing tool cost or production time is analysed and the process requirements are studied, defining tooling specifications and process principle of operation.

After identifying a candidate manufacture process, a research question based on the observation is defined. The process includes the analysis of both hard science and soft science topics that relate to the defined question.

Hypothesis are then proposed to answer the question consistent with existing knowledge, formulating a new technology concept. This definition requires to ground the hypothesis with analytical models, analog comparison or simulation models and to propose conditional hypothesis defining the expected cause and effect in a given circumstance. Finally, the criteria for failure or success of the proposed hypothesis is defined, in response to the identified process requirements.

Before the testing phase, a well designed experiment protocol is defined. All variables in analysis are defined, including the test part geometry, mould design, operation procedure and measurement a evaluation procedures. All materials and equipments needed to perform the experiment are identified. A logical set of steps to complete the experiment is established, giving the procedure directions. Both simple or multiple trial tests may be used, assuring reproducible and verifiable testing results. The data collection method, both describing the experiment and the result analysis is defined, describing the energy and time consumption measurement, calculation of material and manufacture cost and evaluation of the tools operation performance. This step justifies and grounds the new developed technology concept.

The experiments are then rolled according to the proposed protocol. The experiment results are analysed to make sure bias or inadequate procedure did not lead to incorrect conclusions. Qualitative and quantitative analysis is applied, according to the defined hypothesis criteria. When the proposed hypothesis is found true, a generalisation method is proposed for the use of SPIF as a rapid tooling technology. If possible, the first academic approach is revalidated with an industrial applied application or the new tools performance is compared to the one from conventional tools.

For each particular experiment, some complementary methodologies and methods may be used to achieve any specific result which may require additional protocols. In such scenarios, the additional research approach is defined during the experimental work description. Further, the experimental data from each test is globally used, contributing to the conclusions of multiple activities.

3.3 Technology readiness level contribution

The study on industrial applicability of SPIF directly relates to the potential increase of the Technology readiness Level (TRL) , as defined by the European Commission for the Horizon 2020 program [122]. Experimental work during the PhD workplan is developed in laboratorial environment, carefully observing all criteria that influence the manufacture process and the result. Notwithstanding industrial companies are involved in the course of some activities, the laboratory conditions can not truly be considered as an industrially relevant environment as some standards are not met and the process is not industrial orientated, conceptually limiting the maximum achievable TRL index to four. Nevertheless, the proven results are evaluated for validation by the industrial partners and may have direct implementation on industrial companies, leading to fast potential higher TRL indexes.

Being the most verily academic group of activities, the chapter 4 contribution to the TRL is to consolidate and enhance the technology validation in lab: TRL 4. The actual state of the art has achieved a TRL 4 index, with some pilot industrial application leading to higher indexes. However, many issues about the process still exist. Framed on the functional and energetic approach concept of the PhD work program, the goals of the first task aim to contribute to a steadier use of the ISF technologies.

For the activities of chapter 5, partnerships with industrial and services companies are established. The workplan carries a series of case studies, evaluating the SPIF results and performance for different industrial fields. Thus, during the second task, the TRL index is brought from TRL 4 to potential TRL 5/6 in a short period of time.

During the activities of chapter 6, the most innovative section of the PhD program is fulfilled. Disruptive ideas are developed, formulating new technology application concepts and experimentally testing them for proof of concept. This way, new rapid tooling concepts for a variety of material processing processes are generated and studied achieving TRL 3 in chapter 6. Exceptionally, depending on the technology and information access, some concept ideas may only achieve TRL 2 and other may be brought to TRL 4. Table 3.1 summarises the main goal, research methodology and the TRL contribution of the three major tasks.

Table 3.1: Milestones, methodology and TRL contribution

Activity	Main goal	Research methodology	TRL contribution
Chapter 4	Enhance scientific and academic knowledge about SPIF	Factorial Design of Experiments	Cement TRL4
Chapter 5	Prove the industrial applicability of the SPIF process	Problem orientated case studies	Cement TRL4, leading to TRL5/6
Chapter 6	Develop new SPIF applications concepts: rapid tooling	Proof of concept, scientific method	Disruptive concept to TRL 3

3.4 CAD/CAM methods and design guidelines

3.4.1 SPIF CAD modelling

For the manufacturing of a incremental formed part, it is necessary to model the inner surface of the part. However, most applications require a full model with information on sheet thickness. Besides, although the SPIF part must arise from a flat blank, the finished part contour may be cut only from the formed area.

As refereed, the final sheet thickness may be fairly estimated using the sine-law, mainly while using single stage forming strategies, relating the final thickness t_f to the blank thickness t_0 and the formed wall angle α.

For an effective modulation of a CAD model, it is not correct to define a constant thickness, nor is viable to calculate the expected final thickness by the sine-law (equation 2.1). Figure 3.1 represents an easier geometric application of the sine law, where the inner surface is copied and shifted along the initial thickness. Thus, the initial modelling should only look into the inner surface, and the formed part thickness is defined at the end.

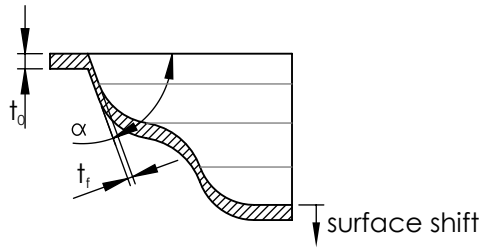

Figure 3.1: Thickness prediction through geometric application of the sine law.

When the part edge is a 3D contour, away from the blank flat surface, the part's inner surface must be extended to intercept the blank surface in one of the possible part configurations. It is important to assure neither the α angle nor the available forming area are exceeded. As the extended surface not only adequate a free contour geometry to flat blank but also serve as a deformation stabilisation mechanism, its use contributes to the part quality improvement, particularly accuracy. For that, a minimum extended wall height should be defined to ensure all part is away from the flat blank. Figure 3.2 represents an example of a part extend with a 45º slope to the flat blank.

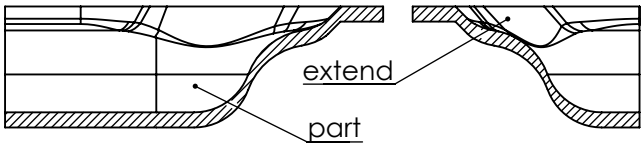

Figure 3.2: Part extend of a SPIF part.

When multistage SPIF is required for a part manufacturing, either because the forming angle outperforms the α_{max} value or the design require the use of multiple tools or part flips, the modelling method should be adapted.

The multistage part model should have information not only about the model but also on the intermediate stages. Figure 3.3 represents an example of the surface modelling for an intermediate stage of a part with a high slope wall angle. The figure illustration is representative of a dual stage strategy, where there are many possible options.

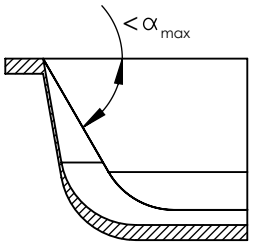

Figure 3.3: Intermediate stage modelling for multistage parts.

Besides, as the sine law does not fit the thickness prediction for multistage parts (e.g. vertical walls would thickness 0 mm according to the sine law and they are achievable using multistage strategies), the thin thickness should be increased. However, there is not yet an accurate method for the prediction of the final thickness that can be applied to a CAD model. A suggestion method for the correct modelling of a part is to perform correction after a part inspection using coordinate measure machines or 3D probing. As an alternative, numerical simulations may be performed although very time consuming.

3.4.2 SPIF CAM

For the generation of tool path strategies for SPIF, commercial computer aided manufacturing software may be used. Although the software are mostly used for the generation of milling operation tool paths, similar strategies may be used for SPIF. For generation of single stage strategies, the CAM software use is straightforward, with a similar method as the milling work preparation, generating tool paths from a CAD model and the geometric definition of the forming tool. As referred, for SPIF operation, the inner surface of the part is required for CAM works. For multistage operations, the geometry of each intermediate state must be imported to the CAM software. Each state surface is used for the generation of a different forming stage.

During the PhD experimental work Delcam® PowerMill is used for the generation of SPIF tool paths. The tool paths are generated using mainly finishing strategies. In PowerMill, constant Z finishing and optimised constant Z finishing strategy are better suited for

generation forming tool paths. The forming strategy can either be defined using constant Z or constant H steps with plunge of spiral down movement.

PowerMill has a more complex principle of operation but with greater customisation, allowing the develop and study of new strategy options for higher complexity parts. The CAM software not only generate the tool path but also predict the forming time and air movement time.

In order to run the CAM work in the forming machine, the trajectories must be post processed for the SPIF-A machine. A new post processor for the SPIF-A machine has been developed for using PowerMill.

SPIF-A post processor

A post processor is responsible for translating the CAM software information to the machine code particularities. A post processor has been developed to generate the numerical control (NC) code for the SPIF-A machine, from CAM performed using Delcam® Powermill software. The NC code for the SPIF-A machine is a simplified version of the G code (RS-274) programming language [50].

The SPIF-A machine language starts its reading in the N111 block. Only linear movements are supported by G1 preparatory command. The movements are defined by the three axis position and two rotation: X, Y, Z, B and C. All rotation is done in the machine head. Feed rate or spin speeds are not read by the machine controller, but manually controlled. Thus, F and S commands are not used. Circular motions are neither supported. The program ends with a M30 block.

A standard post processor was edited and adapted to the SPIF-A machine, using the Delcam® Postprocessor software. The post processor creates a program heading with information about the job, including the program name, the operators name, the date, the units, the tool type and the tool geometry. The first movement is performed in block number N111 first positioning the Z axis and then the X and Y with G1 code. The following movements are then also defined by the G1 code for X, Y and Z for three axis operation and X, Y, Z, B and C for the five axis operation. After the last movement, an M30 function is added. The developed post processor is detailed in appendix A.1.

3.4.3 Efficient CAD/CAM strategies for SPIF using the SPIF-A machine

In order to define methodical tools for the definition of CAD models and the generation of tool path strategies using CAM software, a guidebook has been developed. The document has instruction about CAD modelling and describes the CAM principle for SPIF using Delcam® PowerMill. Further, it describes a post processor adapted for the SPIF-A machine and adds information about how to generate the NC programs. Figure 3.4 shows the printed version of the "SPIF CAD CAM - Manual for preparing SPIF tool paths using PowerMill - Post-processing for the SPIF-A machine" document [123]. The new document adds relevant information to the SPIF-A machine, completing the required manual library for performing SPIF operations. As done for the part configuration and design guidelines, the CAD CAM description has been presented in the Working plan and methodology section.

Figure 3.4: CADCAM for SPIF guidebook.

3.5 Measurements and calculus methods

During the experimental work, different parameters must be instrumented for the better understanding of the forming process. The final parts are also quantitatively evaluated by measuring the geometry and surface, beyond the qualitative assessment.

Different techniques and methods are presented for the measurement of the experimental parameters during the PhD workplan. The following sections describe the methods used for measuring the fundamental parameters. The sections do not complete illustrate the data acquisition as other simpler measuring equipments as rulers, protractors, callipers, bevels and chronometer are used.

3.5.1 Energy consumption measuring

In order to measure the energy consumption on the SPIF process it is needed to determine the power consumption over time. The instant power can be estimated by considering a constant line voltage $V_{power} = 230$ V and measure the consumed current. A LEM HASS 50-S Hall effect current transducer was selected to measure an instant current up to up to 50 A RMS with a maximum response time of 5 μs for a 45 A step on single phase equipments and three LEM HASS 100-S Hall effect current transducer were selected to measure an instant current up to 100 A RMS with a maximum response time of 5 μs for a 90 A step and an accuracy of 1% of the nominal current on tree phase equipments. Figure 3.6 shows a picture of the LEM HASS 100-S transducer [124].

The Hall effect creates a voltage difference on the width of a thin plate of a conductive material when it is under a lenghtwise electric current and a perpendicular magnetic filed. Figure 3.5 (a) represents the basic principle of the Hall effect. The mobile charges of the current I_c are affected by the Lorentz force created by the magnetic field B. The resulting deflection of current causes more charge carriers to be located at one edge of the sheet, creating a potential difference referred to as the Hall voltage, V_H. The Hall voltage can be calculated by equation 3.1 where K is the Hall constant of the conducting material, t is the thickness of the sheet, B is the magnetic field and V_{OH} is an offset voltage of the Hall generator in the absence of an external field [125].

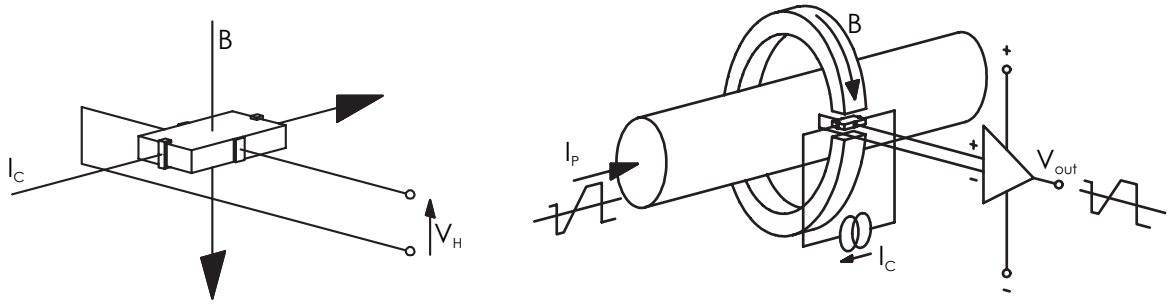

(a) (b)

Figure 3.5: Hall effect principle: (a) electrical parameters of the Hall effect, (b) conversion of the primary current into an output voltage using open loop hall effect transducer

$$V_{\mathrm{H}} = \frac{K.I_{\mathrm{C}}}{t}.B + V_{\mathrm{OH}} \tag{3.1}$$

The current transducers used operate on open loop Hall effect technology, as represented in figure 3.5 (b). A current carrying conductor creates a magnetic field. This field is concentrated around the wire by a magnetic core. The core has a gap cut through it and a hall generator is used to sense the magnetic flux density in the gap. The magnetic field around a wire is given by Ampere's law, where for a infinite straight wire is give by equation 3.2 where μ_0 is a constant of magnetic permeability and r is the distance from the wire. The magnetic field is proportional to the probing current and, with exception of the offset voltage, the Hall voltage is proportional to the magnetic fields. Therefore, the Hall voltage is proportional to the probing current plus the offset voltage [125].

$$B = \frac{\mu_0}{2\pi r}.I_{\mathrm{P}} \tag{3.2}$$

In the LEM HASS transducers used, presented on figure 3.6, the Hall voltage is compensated and amplified to a value of $0.625.I_{\mathrm{P}}/I_{\mathrm{PN}} \pm V_{\mathrm{ref}}$ where I_{PN} is the maximum nominal current of the transducer and V_{ref} is an offset voltage of 2.5 ± 0.025 V. Thus, the instant probing current can be calculated by equation 3.3 [124].

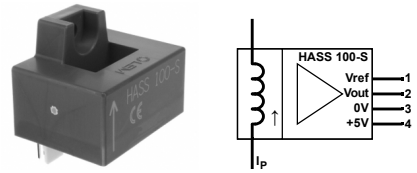

(a) (b)

Figure 3.6: LEM HASS 100-S

$$I_{\mathrm{P}_{(\text{HASS 50-S})}} = \frac{(V_{\mathrm{out}} - V_{\mathrm{ref}}).50}{0.625} \qquad I_{\mathrm{P}_{(\text{HASS 100-S})}} = \frac{(V_{\mathrm{out}} - V_{\mathrm{ref}}).100}{0.625} \tag{3.3}$$

In order to measure the electric consumption on both single phase and three phase equipments, the schematics presented in figure 3.7 was developed and mounted on a cabinet. The

assembly has one HASS 50-S transducer measuring the current of the power line of a single phase cable, connected to a male and a female plug and three HASS 100-S transducers measuring the current of the power lines of a three phase cable, connected to both a male and a female plug and electric terminal blocks. The transducers are powered by a +5 V power supply and the V_{out} is connected to terminal blocks, represented in the schematics by voltmeters [124].

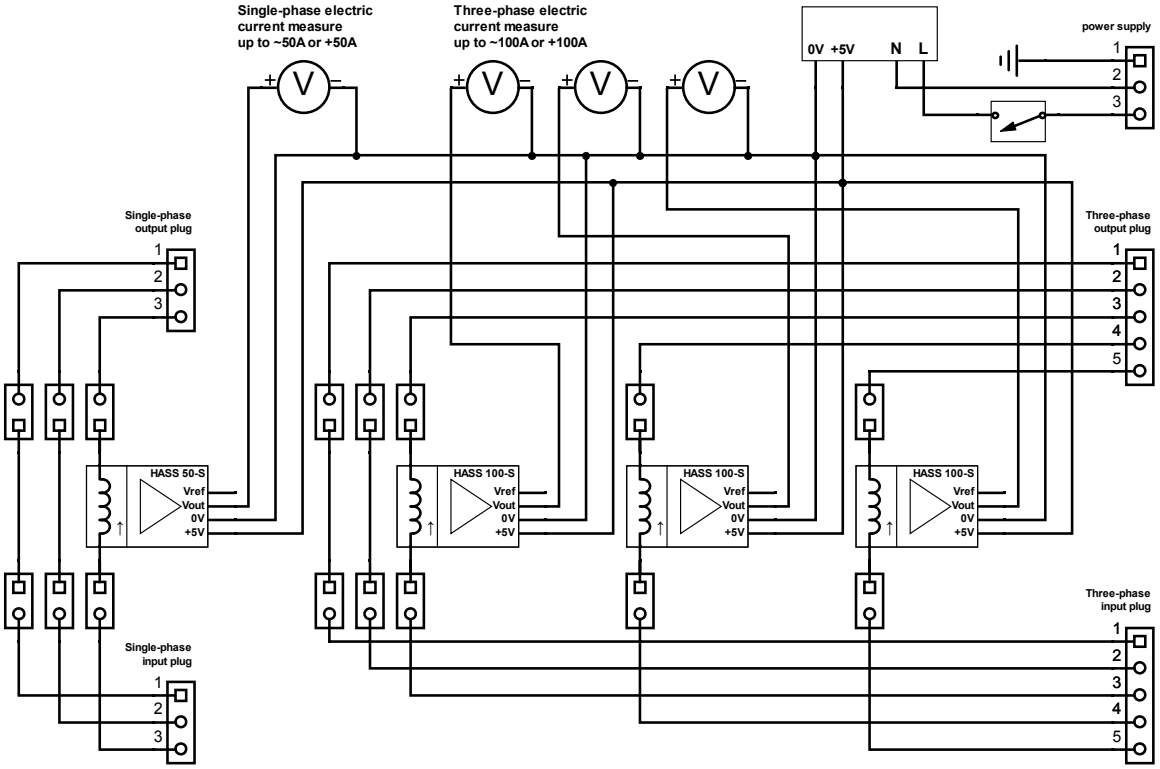

Figure 3.7: Current measurement circuit architecture

As the electrical consumption varies along each stage of the manufacturing process, a data logger was used to register the output voltage of each power line over time. A Fluke Hydra Series III Data Acquisition System was used to register the signals. As all equipment used for the mould fabrication are powered on 50 Hz AC current, the V_{out} signal from the transducers is also alternate. Thus, the signal varies from $V_{\text{ref}} - 0.625.I_{\text{P}}/I_{\text{PN}}$ to $V_{\text{ref}} + 0.625.I_{\text{P}}/I_{\text{PN}}$ at a 50 Hz rate. Thus, the signal can be interpreted as a V_{DC} plus a V_{AC} voltage.

If measuring the instant signal, a voltage of $V_{\text{AC+DC}} = ({V_{\text{AC}}}^2 + {V_{\text{DC}}}^2)^{1/2}$ would be recorded. This would oblige to instrument the V_{ref} signal as well as the output. Besides, the measuring error would sum the error of both measurements. To avoid this, the signal was instrumented using an AC-coupled true-rms measuring method. This method works by first recording the total voltage and then recording the voltage with the low pass filter. The true-rms signal is the calculated by $V_{\text{RMS}} = ({V_{\text{Total}}}^2 - {V_{\text{Low Pass}}}^2)^{1/2}$. By removing the DC component of the signal the value of the V_{ref} can be set aside and the calculus of the measuring current is then given by equation 3.4 [124, 126].

$$I_{\text{P}_{(\text{HASS 50-S})}} = \frac{V_{\text{RMS}}.50}{0.625} \qquad I_{\text{P}_{(\text{HASS 100-S})}} = \frac{V_{\text{RMS}}.100}{0.625} \tag{3.4}$$

The developed apparatus for current measuring is represented in figure 3.8. Subfigure (a) shows the electrical assembly with the power lines passing in the transducers and the signal cables connected to terminal blocks in the top. The presented assembly was then fixed on a electrical cabinet with only the power lines plugs and the signal data cables passing to the outside. Subfigure (b) shows the data logger during measurements of a three phase current.

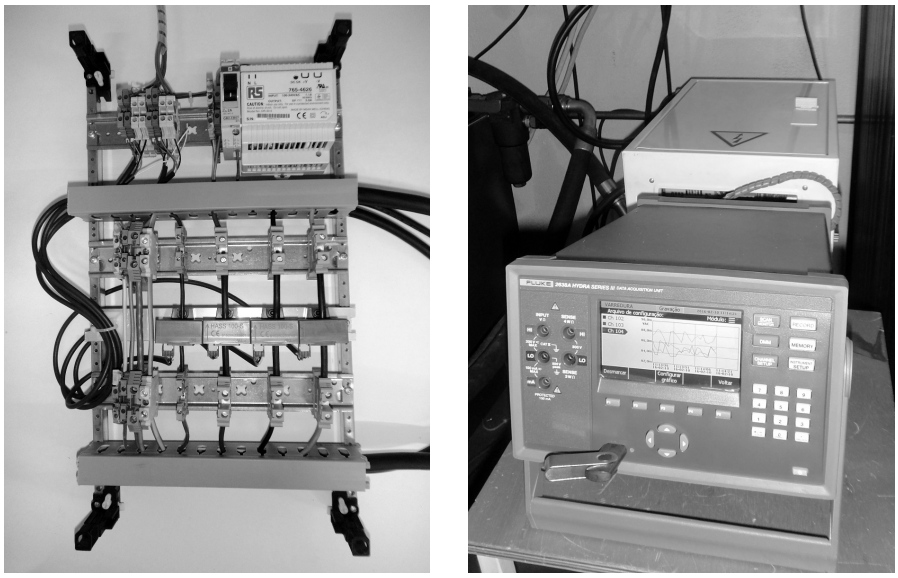

(a) (b)

Figure 3.8: Apparatus for current measurement: (a) electrical assembly with current transducers (b) data logger during measurements

The electrical assembly left space in the top left for a further replacement of the external data logger for an integrated reading system based on micro controllers, replacing the terminal blocks that connect the data lines.

The total error of the current measurement adds the transducers error and the data logger measuring error. The instrumentation error of the transducers is ±1% of the nominal current [124]. Thus, maximum error of measurement is 0.5 A in the HASS 50-S and 1.0 A in the HASS 100-S. The data logger reading error for a signal with a 10 V range at 50 Hz is 0.1% of the measurement plus 0.05% of the range [126]. For both transducers, the maximum V_{RMS} value is 0.625 V. Thus, the maximum error of reading is $\pm(0.1\%0.625 + 0.05\%10) = 0.005625$ V, corresponding to 0.45 A in the HASS 50-S and 0.9 A in the HASS 100-S. By the worst case method, the maximum error of the current measurement in single phase equipments is ±0.95 A and in three phase equipments is $3 \times \pm 1.9$ A. By the propagation of errors theory, considering that measurement and reading errors are independent, the absolute error in the result is the square root of the sum of the squares of the absolute errors of the inputs. Thus, the maximum absolute error of the current measurement is given by equation 3.5, in single phase equipment consumption is ±0.67 A and in three phase equipments is $3 \times \pm 1.35$ A.

$$\begin{cases} e_{I_{\text{P}_{(\text{HASS 50-S})}}} = \pm\sqrt{e^2_{\text{HASS 50}} + e^2_{\text{Hydra}_{HASS50-S}}} = \pm 0.67 \text{ A} \\ e_{I_{\text{P}_{(\text{HASS 100-S})}}} = 3 \times \pm\sqrt{e^2_{\text{HASS 100}} + e^2_{\text{Hydra}_{HASS100-S}}} = 3 \times \pm 1.35 \text{ A} \end{cases} \tag{3.5}$$

The acquired data was analysed using SciLab. The measurement data of each manufacturing stage was imported and the instant current was calculated by multiplying in recorded output voltage by the corresponding factor of equation 3.4. The instant power was calculated by multiplying the instant current by $V_{power} = 230$ V. Instant power plots were made to help interpret the electric consumption of each manufacture stage. Finally, the total electrical consumption of each stage was calculated by integrating instant power over time [127]. Figure 3.9 shows the data recovered during the tests made measuring single and three phase power lines. The graphics show power consumption over time and total test time and consumption is indicated on the top left corner. The instant power measurements were compared with measurements done with a calibrated ISO-TECH ICM20 Clamp Meter and validated. The Scilab script to calculate total consumption and generate instant power over time graphics is in appendix B.1.

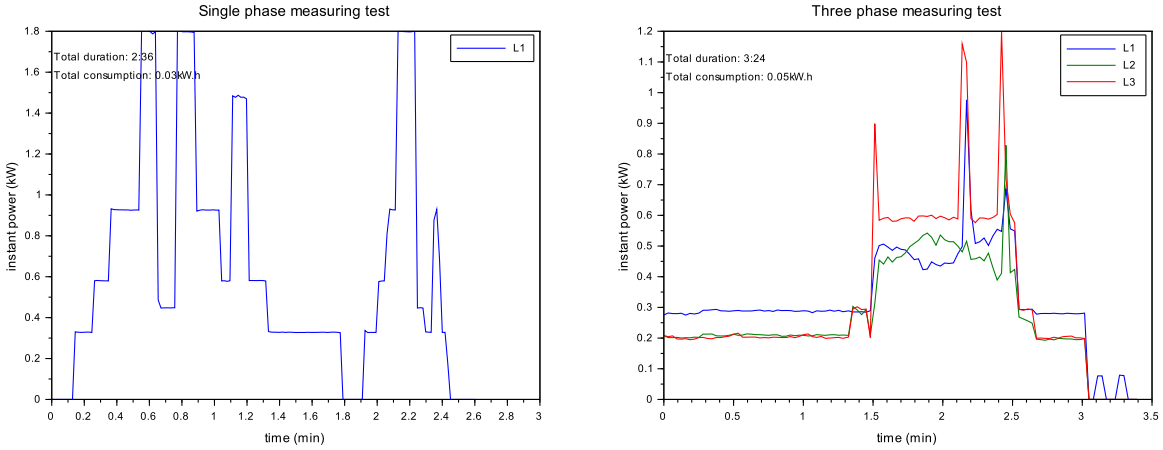

(a) (b)

Figure 3.9: Energy consumption measure tests: (a) Single phase, (b) Three phase.

3.5.2 Force measuring

The forming force results from the interaction between the punch and the sheet. As mentioned, the forming force can be decomposed in a axial compressive force, a tangential (lateral) force and a radial force. In order to measure this force, the tool holder was mounted on three tri-axial load cells, equally spaced around its axis, as described in [6]. Figure 3.11 represents the assembly arrangement used to measure the force, where: F_{1x}, F_{1y} and F_{1z} are the forces measured in the first load cell, mounted at and angle $\alpha_1 = 90^o$ and $r = 110$ mm; F_{2x}, F_{2y} and F_{2z} are the forces measured in the second load cell, mounted at and angle $\alpha_2 = 210^o$ and the same $r = 110$ mm; F_{3x}, F_{3y} and F_{3z} are the forces measured in the third load cell, mounted at and angle $\alpha_3 = 330^o$ and the same $r = 110$ mm; and F_x, F_y and F_z are the forming force components at a vertical distance $L = L_{\text{tool}} + 182$ mm from the load cells centre.

As the tool is mounted on a free spinning system, the in-plane contribution of each load cell can be considered equivalent, and the vertical ones can assume different values. Thus, $F_{1x} = F_{2x} = F_{3x}$ and $F_{1y} = F_{2y} = F_{3y}$. By the equilibrium of forces, it is possible to relate the forming forces to the measured forces by equation 3.6.

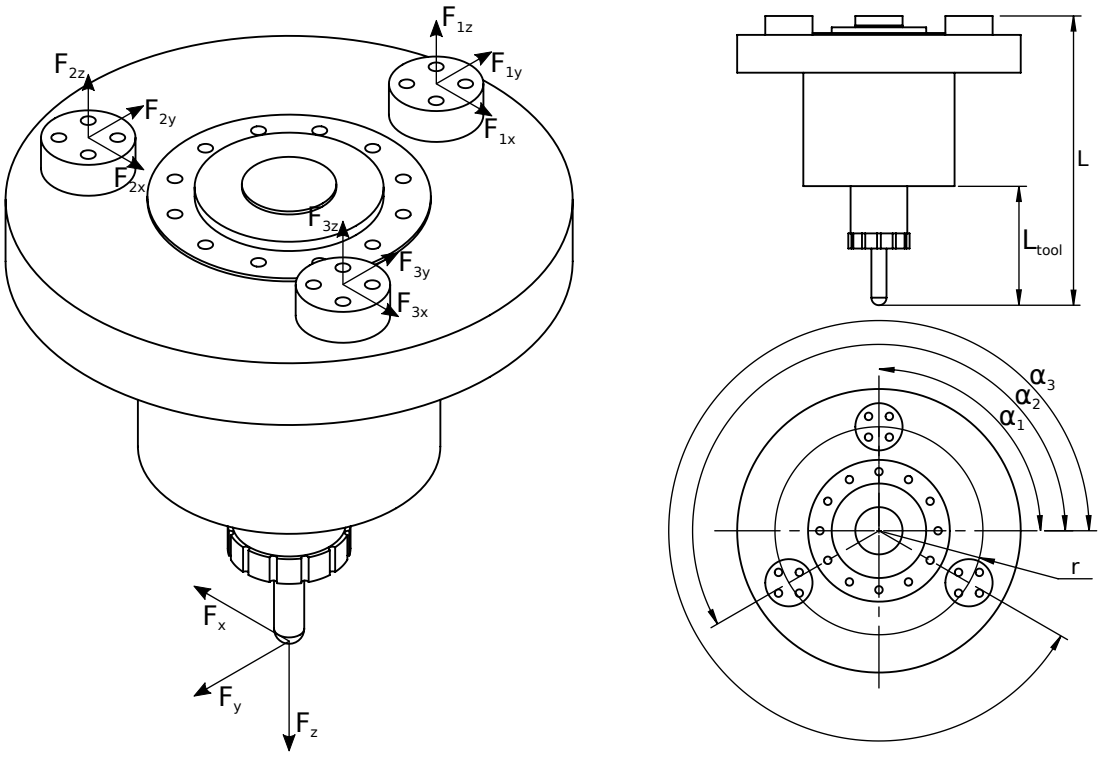

(a) (b)

Figure 3.10: Load cells arrangement for force measurement: (a) force representation, (b) dimensions.

$$\sum F = 0 \Leftrightarrow \begin{cases} \sum F_{\mathrm{x}} = 0 \\ \sum F_{\mathrm{y}} = 0 \\ \sum F_{\mathrm{z}} = 0 \end{cases} \Leftrightarrow \begin{bmatrix} F_x \\ F_y \\ F_z \end{bmatrix} = \begin{bmatrix} F_{1x} \\ F_{1y} \\ F_{1z} \end{bmatrix} + \begin{bmatrix} F_{2x} \\ F_{2y} \\ F_{2z} \end{bmatrix} + \begin{bmatrix} F_{3x} \\ F_{3y} \\ F_{3z} \end{bmatrix} \tag{3.6}$$

As a redundancy, the forming forces can also be calculated by equilibrium of forces and moments by equation 3.7.

$$\begin{cases} \sum M = 0 \\ \sum F = 0 \end{cases} \Leftrightarrow \begin{cases} \sum M_{\mathrm{x}} = 0 \\ \sum M_{\mathrm{y}} = 0 \\ \sum F_{\mathrm{z}} = 0 \end{cases} \Leftrightarrow \begin{bmatrix} F_x \\ F_y \\ F_z \end{bmatrix} = \begin{bmatrix} \frac{r.\sin(\alpha_1)}{L} & \frac{r.\sin(\alpha_2)}{L} & \frac{r.\sin(\alpha_3)}{L} \\ \frac{r.\cos(\alpha_1)}{L} & \frac{r.\cos(\alpha_2)}{L} & \frac{r.\cos(\alpha_3)}{L} \\ 1 & 1 & 1 \end{bmatrix} \times \begin{bmatrix} F_{1z} \\ F_{2z} \\ F_{3z} \end{bmatrix} \tag{3.7}$$

The horizontal forces F_x and F_y can be vectorially added to calculate the total horizontal force: $F_{xy} = \sqrt{F_x^2 + F_y^2}$. The angle between then can be calculated by $\psi = \arctan(F_y/F_x)$. By analysing the punch position and motion direction it is possible to decompose forces F_x and F_y in the tangential and radial direction. This relation depends on the forming geometry, being achieved by equation 3.8 for circular paths, where θ in angle between the punch position and the "x" axis of the machine.

$$\begin{cases} F_t = \mathrm{sign}(F_x).F_{xy}.\sin(\theta + \psi) \\ F_r = -\mathrm{sign}(F_x).F_{xy}.\cos(\theta + \psi) \end{cases} \tag{3.8}$$

Figure 3.11 represents the Michigan Scientific's TR3D-A-5k round three directional load cells used to measure force up to 22500 N in each direction. The load cells measure both tensile/compression and positive/negative shear loads in two perpendicular axis.

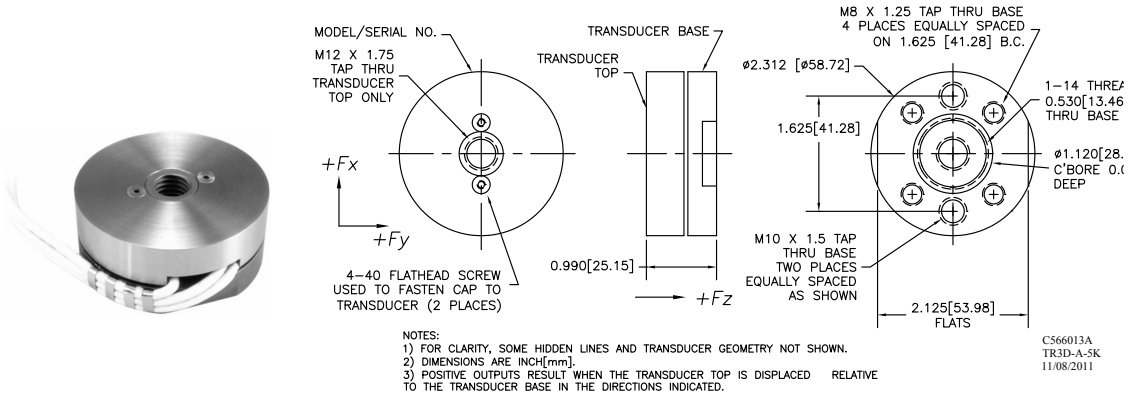

(a) (b)

Figure 3.11: TR3D-A-5k load cells.

The load cells operate with a Wheatstone bridge working principle (figure 3.12) with an excitation voltage of $V_{\mathrm{S}} = 10$ V DC with and output of $V_{\mathrm{G}} = 4.0$ mV/V for the maximum load, resulting on a signal of $562,5$ N/mV with a linearity up to 0.5% of the full scale, an hysteresis of 0.05% of the full scale and a repeatability of 0.05% of the full scale [128].

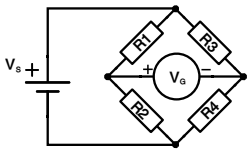

Figure 3.12: Wheatstone bridge operating principle.

As the output voltage is very low, with a maximum $V_{\mathrm{G}} = 40$ mV, the signal must be amplified before being instrumented. LMU 209 amplifiers for strain gauge transducers by Magtrol were chosen to complete the force measuring sensors (FMS), according to the circuit presented on figure 3.13. This way, the output signal is amplified form $V_{\mathrm{G}} = -40$ to 40 mV to $V_{\mathrm{out}} = -10$ to 10 V adding a linearity error up to 0.05% [129].

In order to minimise the force reading error, the loads cells were tested against known loads on a Shimadzu AG-50kNG universal testing machine. The force measuring system calibration curves are presented in table 3.2. The maximum error on force value determinate by the given equation is $0,2\%$, corresponding to a maximum measurement error of ± 45 N [51].

Table 3.2: FMS calibrated curves.

Load cell 1	Load cell 2	Load cell 3
$F_{1\mathrm{x}} = 2391.4V_{\mathrm{out}} - 40.4$	$F_{2\mathrm{x}} = 2456.7V_{\mathrm{out}} + 67.6$	$F_{3\mathrm{x}} = 2497.9V_{\mathrm{out}} - 126.6$
$F_{1\mathrm{y}} = 2376.6V_{\mathrm{out}} + 19.1$	$F_{2\mathrm{y}} = 2441.7V_{\mathrm{out}} + 61.8$	$F_{3\mathrm{y}} = 2401.9V_{\mathrm{out}} - 177.1$
$F_{1\mathrm{z}} = 2302.6V_{\mathrm{out}} + 202.4$	$F_{2\mathrm{z}} = 2298.4V_{\mathrm{out}} - 99.0$	$F_{3\mathrm{z}} = 2218.2V_{\mathrm{out}} - 79.5$

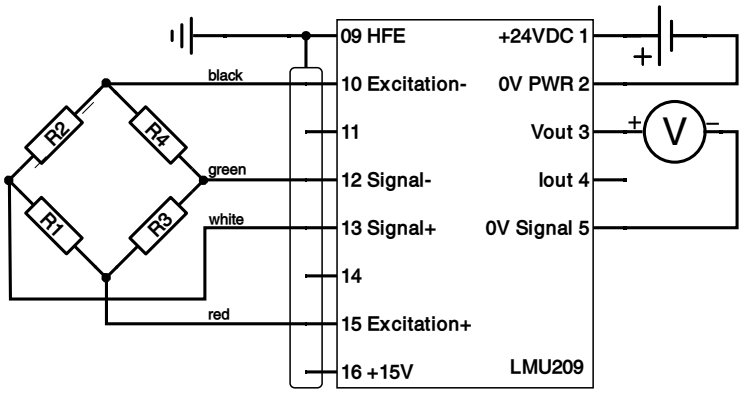

Figure 3.13: FMS circuit architecture.

During the forming process, the load cells signal is read by the Speedgoat$^{\text{TM}}$SN1584 real time target machine with a IO101 module and recorded Matlab$^{\text{TM}}$. Input reading error of the module for a ±10 V signal is 0.007% of the range, ±1.4 mV, corresponding to a force of ±3.5 N. The total error of the $F_{1\text{x}}$ to $F_{3\text{z}}$ forces adds the force measurement system error and the signal measurement error. Thus, by the worst case method, the maximum error of the force measurement is ±48.5 N. By the propagation of errors theory, considering that measurement and reading errors are independent, the absolute error in force reading is ±45.14 N.

The total uncertainty of the F_x, F_y and F_z force measurement depends on the way the calculation is accomplished. The uncertainty may be a consequence of force error, the spindle geometry dimensional errors and the tool length L_{tool} error.

Considering the calculus of F_x, F_y and F_z according to equation 3.6, the uncertainty is given by equation 3.9, where e represents the error, calculated for the maximum possible error.

$$\begin{cases} e_{F_x} = \pm\sqrt{e_{F_{1x}}^2 + e_{F_{2x}}^2 + e_{F_{3x}}^2} = \pm\sqrt{45.14^2 + 45.14^2 + 45.14^2} = \pm 78.2 \text{ N} \\ e_{F_y} = \pm\sqrt{e_{F_{1y}}^2 + e_{F_{2y}}^2 + e_{F_{3y}}^2} = \pm\sqrt{45.14^2 + 45.14^2 + 45.14^2} = \pm 78.2 \text{ N} \\ e_{F_z} = \pm\sqrt{e_{F_{1z}}^2 + e_{F_{2z}}^2 + e_{F_{3z}}^2} = \pm\sqrt{45.14^2 + 45.14^2 + 45.14^2} = \pm 78.2 \text{ N} \end{cases} \tag{3.9}$$

Considering the calculus of the forming forces according to equation 3.7, assuming negligible errors in the spindle geometry $e_r = 0$ mm and $e_\alpha = 0^{\text{o}}$ and a measuring error in the tool length $e_L = 0.5$ mm, the uncertainty is given by equation 3.10, calculated for the maximum possible error with a $L_{\text{tool}} = 100$ mm tool. Although the error is very large, it is substantially lower with smaller loads and using longer tools [112, 130].

$$
\begin{cases}
e_{F_x} = \pm \Bigg[& \left[\frac{r.\sin(\alpha_1)}{L}.F_{1z}\right].\sqrt{\left(\frac{r.\sin(\alpha_1).e_{F_{1z}}}{F_{1z}}\right)^2+\left(\frac{-e_L}{L}\right)^2}\Bigg]^2 \\
& + \left[\frac{r.\sin(\alpha_2)}{L}.F_{2z}\right].\sqrt{\left(\frac{r.\sin(\alpha_2).e_{F_{2z}}}{F_{2z}}\right)^2+\left(\frac{-e_L}{L}\right)^2}\Bigg]^2 \\
& + \left[\frac{r.\sin(\alpha_3)}{L}.F_{3z}\right].\sqrt{\left(\frac{r.\sin(\alpha_3).e_{F_{3z}}}{F_{3z}}\right)^2+\left(\frac{-e_L}{L}\right)^2}\Bigg]^2 \Bigg]^{1/2} = \pm 2054.3 \text{ N} \\
e_{F_y} = \pm \Bigg[& \left[\frac{r.\cos(\alpha_1)}{L}.F_{1z}\right].\sqrt{\left(\frac{r.\cos(\alpha_1).e_{F_{1z}}}{F_{1z}}\right)^2+\left(\frac{-e_L}{L}\right)^2}\Bigg]^2 \\
& + \left[\frac{r.\cos(\alpha_2)}{L}.F_{2z}\right].\sqrt{\left(\frac{r.\cos(\alpha_2).e_{F_{2z}}}{F_{2z}}\right)^2+\left(\frac{-e_L}{L}\right)^2}\Bigg]^2 \\
& + \left[\frac{r.\cos(\alpha_3)}{L}.F_{3z}\right].\sqrt{\left(\frac{r.\cos(\alpha_3).e_{F_{3z}}}{F_{3z}}\right)^2+\left(\frac{-e_L}{L}\right)^2}\Bigg]^2 \Bigg]^{1/2} = \pm 2054.3 \text{ N} \\
e_{F_z} = \pm \Big[& e_{F_{1z}}^2 + e_{F_{2z}}^2 + e_{F_{3z}}^2 \Big]^{1/2} = \pm 78.2 \text{ N}
\end{cases}
\tag{3.10}
$$

The acquired data was analysed using SciLab. Appendix B.2 has the Scilab script to calculate the instant forming power and generate instant forming power over time plots, where the force over time are also plotted. Due to the noise in the data signal, the forces are filtered and offset [127, 131]. Figure 3.14 represents the plot of the force over from a preliminary test where the tool was forced in the three directions, one at a time.

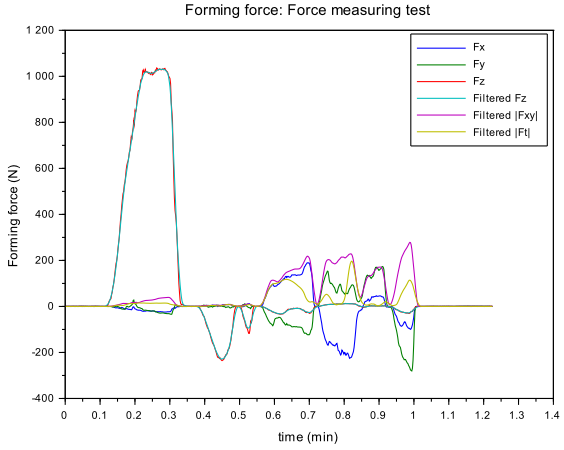

Figure 3.14: Force measure tests.

3.5.3 Position and speed measurement

Aside form the forming force, the instant feed rate speed and punch position is also recorded. The machine kinematics is calculated based on the cylinders stroke position. The position of the cylinders can be read at great precision, thus the error in the position can be neglected when compared to the force reading.

The inverse kinematics is straightforward. The position of the moving platform can be calculated based on the desired position and orientation of the tool tip. As the position of the connection point of the base platform is also known, the stroke of each cylinder can easily be determined by the total leg assembly length. The inverse kinematics is used to define the point by point path tracking at a desired speed. For the machine control, the forward kinematics is also computed to control the movement in a close loop. The forward kinematics is further indirect, as mathematically the same cylinder lengths can lead to different positions. Thus, the real instant position in computed throughout a numerical method.

During the forming process, both the defined feed rate speed and real position are recorded, as well as the running time. As said, the absolute encoders precision grant an accurate calculation of the instant position. In what concerns the speed, it is possible to use a position derivative to confirm the the efficiency in the fulfilment of the feed rate and to acquire its decomposition into the orthogonal axis.

The acquired data was analysed using SciLab to decompose the position and calculate the real feed rate. Appendix B.2 has the script to calculate the feed rate tangential and vertical speeds, as well as the punch position angle used to decompose the horizontal component of the force. Figure 3.15 shows the plot generated within a movement test, with the tool path as followed and the vertical and horizontal components of the feed rate. Slight overshoots are noticeable at sharp corners at higher speeds.

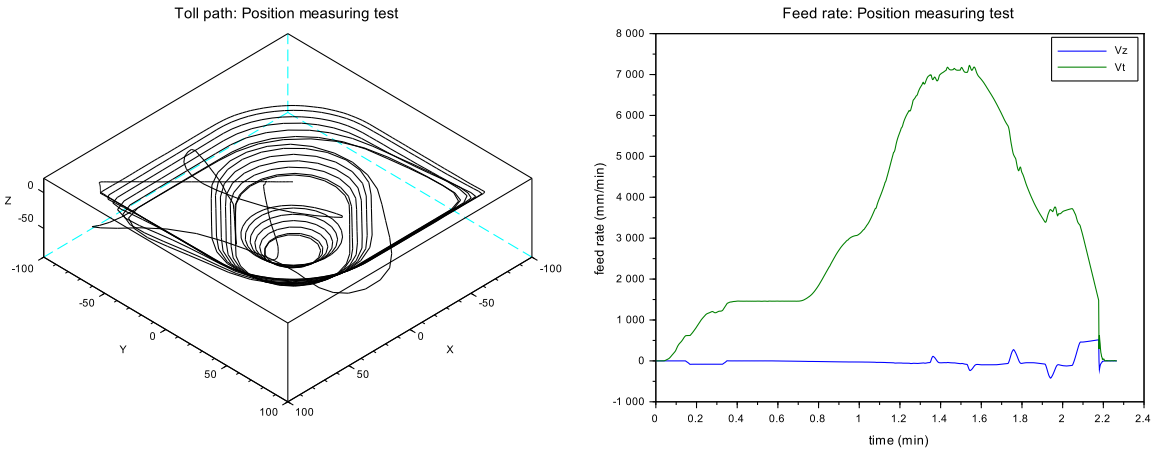

(a) (b)

Figure 3.15: Position and feed rate measure tests: (a) Tool path, (b) Feed rate.

3.5.4 Forming energy calculation

The instant forming power is calculated from the computed forces and feed rates according to equation 2.7. The forming energy is calculated by numerical integration [127] using the results of equation 2.7 over time. Figure 3.16 represents the computed energy for the movement test performed while manually applying a load on the punch using a lever. The forming time is also calculated from the force data. The script for the power and energy calculus is presented in appendix B.2.

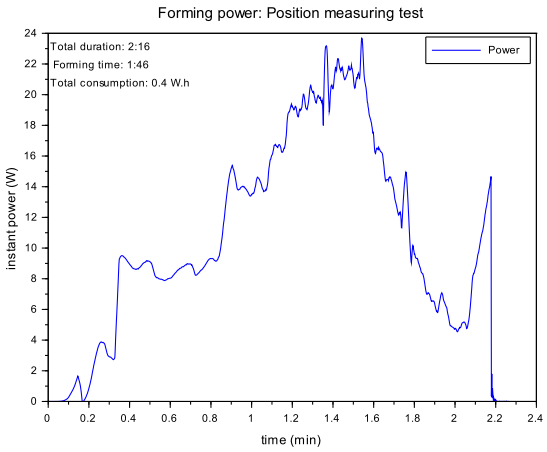

Figure 3.16: Energy measure tests.

3.5.5 Part quality measurement

After the parts manufacture, a quality measurement procedure is performed for evaluating both accuracy, final thickness and surface finishing. The testing methods use only non destructive techniques, causing the less possible damage to the finished part.

For the accuracy evaluation, a coordinate measure machine (CMM) Renishaw®Cyclone 2 with a ruby ball tip touch probe styli with a maximum diameter of half the forming tool. The measurement is accomplished by contact with a repeatability of 5 μm [132]. Parts are measured in the cavity side, except in the cases where the cavity is defined to control the boss side the dimensions. Parts are measured before being trimmed, held by the frame using step blocks and clamps. The measured is automatically performed using a x-y aligned grid with a spacing limited by a third of the minimum feature of the part or 5% of the total part area. The acquired data is compared with the CAD file using SolidWorks®ScanTo3D add-in module deviation analysis function. The comparison computes the maximum inner and outer deviation, as well as the average deviation and standard deviation. The percent of points in bound of the average SPIF accuracy is also computed, for values of $\pm$2 mm and $\pm$4 mm [84].

The formed part sheet thickness is either determined using a double measurement on the CMM machine or by acquiring points from both part sides with a serial arm 3D digitising system MicroScribe®G2X. The digitising system allows a flexible solution for measure, with an accuracy up to 0.23 mm [133]. With the formed part held in a vertical position, the digitising arm allows to trace over both sides of the part. The data acquisition is fast and

uses the same position referential, minimising the error, despite the lack of accuracy of the system. Besides, to minimise the error, the measure procedure follows a minimum of five lines per part feature, acquires points with a spacing equal or less then the initial sheet thickness. The digitise contours are then used to analyse the thinness distribution along the part. If tighter accuracy is needed for a given analysis, the thickness is indirectly computed from two different measurements using the CMM machine. Although each measure is consistently more accurate, the measuring process e much slower and the result may be influenced by error in the relative positioning of the two data sets.

The surface quality of the formed parts is evaluated in a two phase procedure. In a first approach, a visual inspection search for surface irregularities, crests and troughs or any other visual defects is performed. Parts are evaluated under the light at various angles and parts are photographed for record. In a second stage, the roughness is evaluated using rugosimeter for both average roughness (Ra) and mean roughness depth (Rz). Both the formed surface and the blank unformed frame are evaluated to analyse the effect of the forming process in the surface finishing.

3.5.6 Process efficiency calculation

Different approaches can be accomplished in what concerns efficiency calculation. In a pure energetic point of view, the efficiency can be described by the ratio between the forming energy and the energetic consumption. The energetic efficiency of the SPIF-A machine is calculated by equation 3.11. However, for a complete process evaluation the part quality and the process time must be also directly considered. The geometric forming efficiency may be calculated according to one of the options in equation 3.12, where $\Delta_{99\%}$ is the symmetric accuracy limit of 99% of the part area and $\bar{\Delta}_{\text{SPIF}}$ is the reference accuracy for the material and thickness for the SPIF process. The time efficiency is calculated by equation 3.13, where t_{forming} is the forming time and $\bar{t}_{\text{SPIF}}$ is the reference forming time.

$$\eta_{\text{energy}} = \frac{W_{\text{forming}}}{W_{\text{consumed}}} \tag{3.11}$$

$$\eta_{\text{forming}} = \frac{\bar{\Delta}_{\text{SPIF}}}{\Delta_{99\%}} \times \frac{\text{Rz}_{\text{sheet}}}{\text{Rz}_{\text{formed part}}} \qquad \eta_{\text{forming}} = \frac{\bar{\Delta}_{\text{SPIF}}}{\Delta_{99\%}} \tag{3.12}$$

$$\eta_{\text{time}} = \frac{t_{\text{forming}}}{\bar{t}_{\text{SPIF}}} \tag{3.13}$$

Chapter 4

Developing SPIF

Within the general goal of contribute to ISF technologies advance, studies were developed both regarding energetic and functional approaches. Tests were performed using the SPIF-A machine, namely the energetic consumption analysis. Nevertheless, the results can be extrapolated to the use of other SPIF apparatus and the research procedure can be used for the reproduction of the experiments in other manufacturing systems.

4.1 Energetic analysis of the SPIF-A machine

The necessary energy to form a sheet part strongly depend on the forming force, feed rate speed and process time. The experiment intends to study the variations of the forming energy with different forming parameters and conditions, and its relations to the total energy consumption at the SPIF-A machine. The part accuracy and surface finishing are also analysed to validate the used parameters.

For the experimental work on energy analysis, a 3^3 factorial experiment is proposed with changes in three different forming parameters tested: vertical step, forming feed rate speed and sheet thickness. The variation of these parameters allows the testing of different forming powers and lead to different part qualities. Other parameters like material, geometry, tool diameter, tool path strategy and lubrication remain unchanged during tests. The parameters in analysis are chosen because it is expected that they have major influence on the forming energy, as well as part quality. Differences in material thickness lead to high variations on the forming force and consequently forming work, as well as variation on part accuracy and surface quality. Changes in the forming feed rate have major influence on the process time, directly affecting the forming time thus influencing the forming energy. Forming feed rate also affects part quality. Differences in the vertical step down during incremental forming also affect substantially the process time, forming force and part accuracy and surface finishing. Table 4.1 summarises the expected relationship between the forming parameters and the evaluated aspects the affect energy consumption and the process performance acceptance.

For this work, a simple cone geometry is proposed, being manufactured using different combinations of the presented parameters. Figure 4.1 represents the top surface of the designed part for tests, with nine 48 mm, 45°, 20 mm deep cones. The circular geometry of the test parts is chosen to favor maintaining a constant speed during the process. During the tests, each row is formed at a different feeding speed and each column uses different vertical steps. Figure 4.2 represents the geometry of one cone at different material thickness.

Table 4.1: Relationship between forming parameters and evaluation aspects for strain rate independent materials

Forming parameter	Forging force	Process time	Part quality
Vertical step	×	×	×
Feed rate		×	×
Sheet thickness	×		×

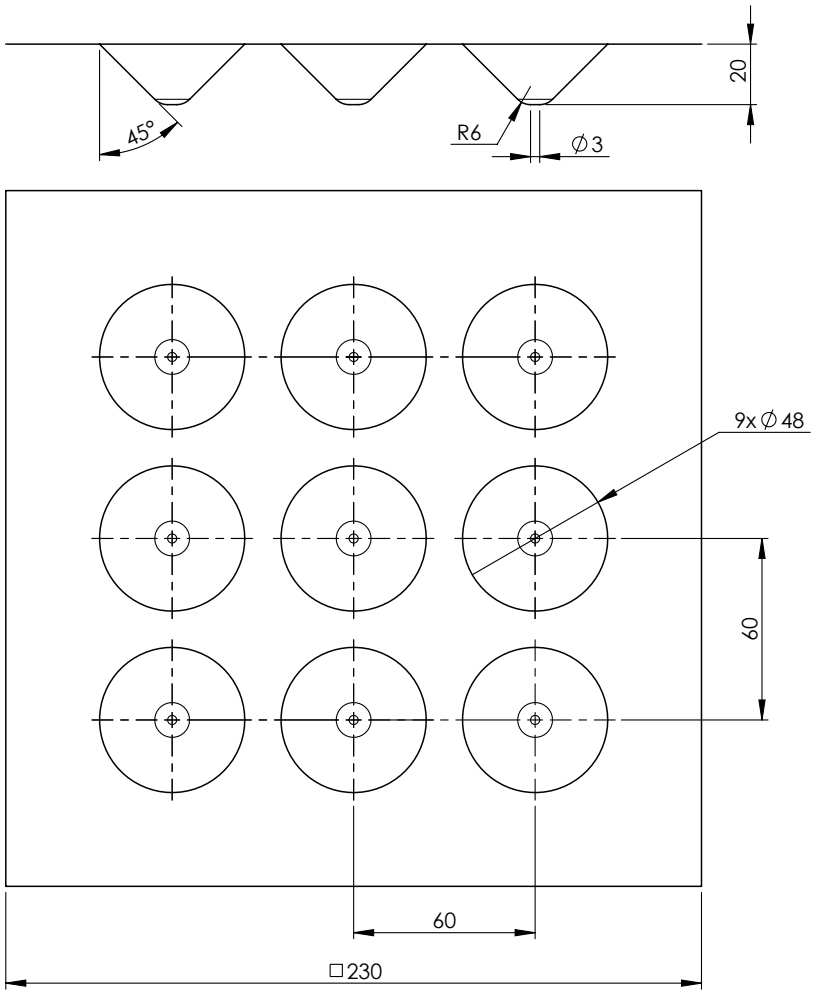

Figure 4.1: Top surface of the experiment geometry with nine 48 mm, 45°, 20 mm deep cones

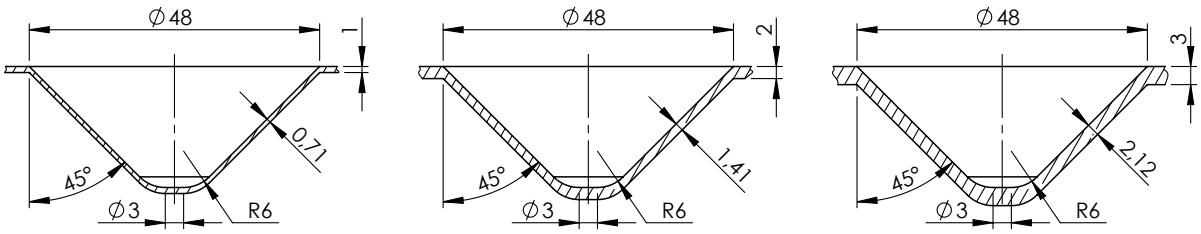

Figure 4.2: Drawing of the test cones at different initial thicknesses with final thickness foresee by the sine law

During the tests, both the power consumption, forming force and feed rate speed were measured and recorded. The total energy consumption was calculated by the integration of the instant power consumption over time. The instant forming power was calculated according to equation 2.7 and the total forming energy is determined by the integration of instant forming power over time. After manufacture, parts were measured for evaluation accuracy and surface quality.

All forming tests were done using at the same condition and using the same parameters, apart form the vertical increment, forming speed and sheet thickness.

The experiments were accomplished using a 12 mm ball tip punch following a helical tool path. Figure 4.3 represents the tool path generated to form the cones where the step down differences are noticeable. The material in study is an aluminium alloy 1050 H111 and the forming process uses a 10W40 oil as a lubricant.

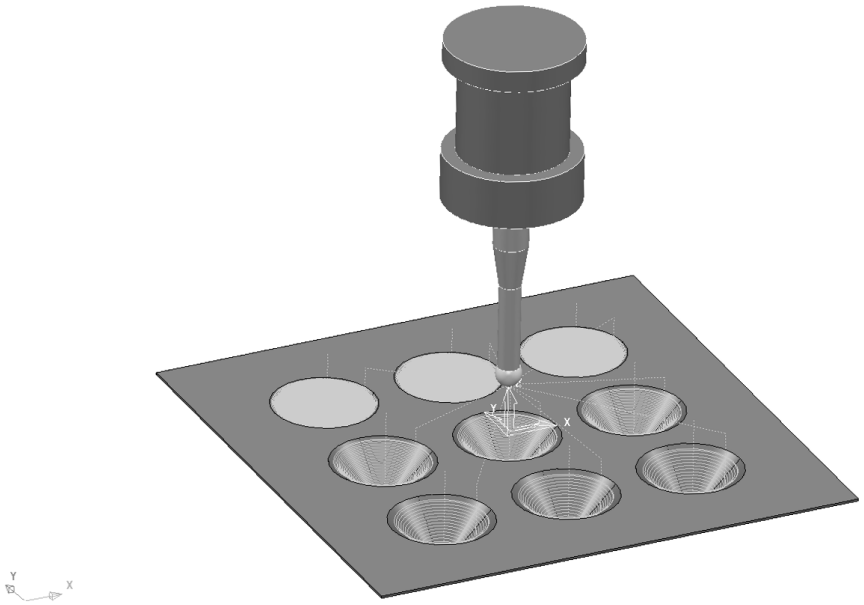

Figure 4.3: Helical tool path used on experimental tests

Considering the variable parameters, vertical step downs of 0.1 mm, 0.5 mm and 1 mm were tested along the y direction and feed rates of 1000 mm/min, 3000 mm/min and 5000 mm/min are used along the x direction. Four different sets of tests were done. A reference experiment follows the nine tool paths in the air. The other tests repeat the tool path while forming 1 mm, 2 mm and 3 mm sheets.

Before testing, the measuring data was predicted. The forming force was calculated according to equations 2.4, 2.5 and 2.6. The force prediction for the 36 tests is presented on table 4.3. The time prediction is determined by the computer aided manufacturing software used to generate the tool paths. The time prediction of the three sets of feed rates and three sets of vertical steps is presented in table 4.2.

The forming power and consumption were also estimated before testing. The forming power was estimated by equation 2.7. The speed component v_t is assumed with feed rate speed and the average v_z is calculated by the ratio between the cone depth and the forming time: $20/time$. The forming power and consumption is presented in table 4.4. The machine consumption is also estimated by an operation at 70% of the available power along the operation time, as the power unit uses a constant displacement pump with oil recirculation. The energy consumption estimation is presented in table 4.5. The energetic efficiency is predicted to vary from 0‰ to 10‰, with values shown on table 4.6. The script calculus is presented in the appendix B.3.

Table 4.2: Time prediction for experimental tests

	$\Delta_z = 0.1$ mm	$\Delta_z = 0.5$ mm	$\Delta_z = 1.0$ mm
$F1000$	14 : 37	3 : 02	1 : 37
$F3000$	4 : 51	1 : 00	0 : 32
$F5000$	2 : 55	0 : 36	0 : 19

Table 4.3: Force prediction for experimental tests

	$\Delta_z = 0.1$ mm	$\Delta_z = 0.5$ mm	$\Delta_z = 1.0$ mm
air		$F = 0$ N	
$t_0 = 1$ mm	$F_z = 329$ N $F_r = 177$ N $F_t = 126$ N	$F_z = 439$ N $F_r = 250$ N $F_t = 178$ N	$F_z = 498$ N $F_r = 303$ N $F_t = 216$ N
$t_0 = 2$ mm	$F_z = 976$ N $F_r = 525$ N $F_t = 375$ N	$F_z = 1305$ N $F_r = 741$ N $F_t = 529$ N	$F_z = 1478$ N $F_r = 899$ N $F_t = 642$ N
$t_0 = 3$ mm	$F_z = 1846$ N $F_r = 992$ N $F_t = 708$ N	$F_z = 2466$ N $F_r = 1401$ N $F_t = 1000$ N	$F_z = 2794$ N $F_r = 1699$ N $F_t = 1213$ N

Table 4.4: Forming power prediction for experimental tests

		$\Delta_z = 0.1$ mm	$\Delta_z = 0.5$ mm	$\Delta_z = 1.0$ mm
air			$\dot{W} = 0$ W, $W = 0$ W.h	
t_0	$F1000$	2.11 W, 0.53 W.h	2.99 W, 0.35 W.h	3.64 W, 0.24 W.h
=	$F3000$	6.33 W, 0.53 W.h	8.99 W, 0.30 W.h	10.97 W, 0.18 W.h
1 mm	$F5000$	10.57 W, 0.35 W.h	15.00 W, 0.25 W.h	18.35 W, 0.15 W.h
t_0	$F1000$	6.27 W, 1.57 W.h	8.88 W, 1.04 W.h	10.82 W, 0.72 W.h
=	$F3000$	18.80 W, 1.57 W.h	26.68 W, 0.89 W.h	32.58 W, 0.54 W.h
2 mm	$F5000$	31.39 W, 1.05 W.h	44.54 W, 0.74 W.h	54.47 W, 0.45 W.h
t_0	$F1000$	11.53 W, 2.96 W.h	16.79 W, 1.96 W.h	20.45 W, 1.36 W.h
=	$F3000$	35.53 W, 2.96 W.h	50.43 W, 1.68 W.h	61.58 W, 1.03 W.h
3 mm	$F5000$	59.32 W, 1.98 W.h	84.19 W, 1.40 W.h	102.95 W,0.86 W.h

Table 4.5: Consumption prediction for experimental tests

	$\Delta_z = 0.1$ mm	$\Delta_z = 0.5$ mm	$\Delta_z = 1.0$ mm
$F1000$	$C = 2.63$ kW.h	$C = 1.23$ kW.h	$C = 0.70$ kW.h
$F3000$	$C = 0.88$ kW.h	$C = 0.35$ kW.h	$C = 0.18$ kW.h
$F5000$	$C = 0.35$ kW.h	$C = 0.18$ kW.h	$C = 0.09$ kW.h

Table 4.6: Energetic efficiency prediction for experimental tests

		$\Delta_z = 0.1$ mm	$\Delta_z = 0.5$ mm	$\Delta_z = 1.0$ mm
air			$\eta = 0‰$	
	$F1000$	$\eta = 0.2‰$	$\eta = 0.3‰$	$\eta = 0.4‰$
$t_0 = 1$ mm	$F3000$	$\eta = 0.6‰$	$\eta = 0.9‰$	$\eta = 1.1‰$
	$F5000$	$\eta = 1.0‰$	$\eta = 1.4‰$	$\eta = 1.8‰$
	$F1000$	$\eta = 0.6‰$	$\eta = 0.9‰$	$\eta = 1.0‰$
$t_0 = 2$ mm	$F3000$	$\eta = 1.8‰$	$\eta = 2.5‰$	$\eta = 3.1‰$
	$F5000$	$\eta = 3.0‰$	$\eta = 4.3‰$	$\eta = 5.2‰$
	$F1000$	$\eta = 1.1‰$	$\eta = 1.6‰$	$\eta = 2.0‰$
$t_0 = 3$ mm	$F3000$	$\eta = 3.4‰$	$\eta = 4.8‰$	$\eta = 5.9‰$
	$F5000$	$\eta = 5.7‰$	$\eta = 8.0‰$	$\eta = 9.8‰$

4.1.1 Experimental data analysis

During the experimental work, four different testing sets are performed, according to the design of experiments. PowerMill® is used to program the tool paths of the nine cones for three series of 0.1 mm, 0.5 mm and 1.0 mm. The feed rate is directly controlled in the SPIF-A machine. As intended, all tests are done while recording the energy consumption, the forming force, the punch position and the process time. The cones are formed one at a time, allowing individual records of the measurements.

The first experiment run the tool in the air (forces = 0), acquiring values for a reference comparison. The other tests are performed with the sheets clamped in the forming table and oiled for a better operation. The experiments two and three formed the nine cones in the aluminium alloy 1050 H111 sheet with 1 mm and 2 mm respectively. The fourth test used a 3 mm sheet, forming only the three cones with 0.1 mm step down and one failed cone with 0.5 mm step down, as the forces in the remaining are too large. Table 4.7 show the experiment conditions for the four experiment sets. Figure 4.4 shows the forming process of the cone 7 on the 1 mm sheet on the SPIF-A machine.

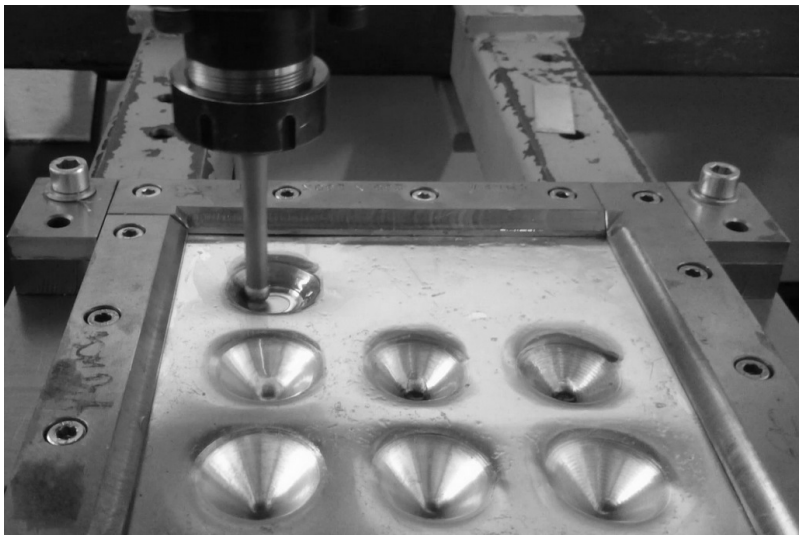

Figure 4.4: Forming process of cone 7, 1mm thickness.

The acquired data is treated and analysed using SciLab, using the scripts presented in appendix B.1 and B.2. The measurement data from the energy consumption of each manufactured cone is imported and the electrical consumption is calculated by integrating instant power over time. Instant power plots are made to help interpreting the electric consumption and forming power of each manufacture stage. The recorded forces and position are used to calculate the instant forming power, which is integrated to calculate the forming energy. The calculus results are presented in tables 4.8 to 4.13.

Table 4.7: Experiment 1 conditions

test	step down (mm)	feed rate (mm/min)			
		air	AA1050 (1mm)	AA1050 (2mm)	AA1050 (3mm)
cone 1	0.1	1060	980	1040	1020
cone 2	0.5	1020	990	1000	970
cone 3	1.0	990	1000	980	n.d.
cone 4	0.1	2970	3003	2990	3010
cone 5	0.5	2990	3020	3000	n.d.
cone 6	1.0	3000	2980	3030	n.d.
cone 7	0.1	5050	4980	5030	4970
cone 8	0.5	5000	4990	5010	n.d.
cone 9	1.0	5020	5050	4980	n.d.

Table 4.8: Experimental tests feed rates

		$\Delta_z = 0.1$ mm	$\Delta_z = 0.5$ mm	$\Delta_z = 1.0$ mm
	$F1000$	1046 mm/min	983 mm/min	959 mm/min
air	$F3000$	2689 mm/min	2658 mm/min	2720 mm/min
	$F5000$	4550 mm/min	4057 mm/min	4370 mm/min
t_0	$F1000$	956 mm/min	952 mm/min	956 mm/min
=	$F3000$	2897 mm/min	2701 mm/min	2651 mm/min
1 mm	$F5000$	4555 mm/min	3825 mm/min	3499 mm/min
t_0	$F1000$	1022 mm/min	969 mm/min	868 mm/min
=	$F3000$	2255 mm/min	2567 mm/min	2321 mm/min
2 mm	$F5000$	4502 mm/min	3880 mm/min	3226 mm/min
t_0	$F1000$	969 mm/min	935 mm/min	-
=	$F3000$	2828 mm/min	-	-
3 mm	$F5000$	4062 mm/min	-	-

Table 4.9: Experimental tests measured forces

		$\Delta_z = 0.1$ mm	$\Delta_z = 0.5$ mm	$\Delta_z = 1.0$ mm
air			$F_z = 0$ N, $F_t = 0$ N	
t_0	$F1000$	$F_z = 338$ N, $F_t = 59$ N	$F_z = 428$ N, $F_t = 80$ N	$F_z = 620$ N, $F_t = 116$ N
=	$F3000$	$F_z = 341$ N, $F_t = 54$ N	$F_z = 429$ N, $F_t = 74$ N	$F_z = 484$ N, $F_t = 105$ N
1 mm	$F5000$	$F_z = 339$ N, $F_t = 50$ N	$F_z = 424$ N, $F_t = 66$ N	$F_z = 477$ N, $F_t = 97$ N
t_0	$F1000$	$F_z = 877$ N, $F_t = 121$ N	$F_z = 1992$ N, $F_t = 259$ N	$F_z = 2748$ N, $F_t = 506$ N
=	$F3000$	$F_z = 1090$ N, $F_t = 118$ N	$F_z = 1864$ N, $F_t = 284$ N	$F_z = 2417$ N, $F_t = 456$ N
2 mm	$F5000$	$F_z = 1046$ N, $F_t = 105$ N	$F_z = 1798$ N, $F_t = 271$ N	$F_z = 2257$ N, $F_t = 362$ N
t_0	$F1000$	$F_z = 5610$ N, $F_t = 561$ N	$F_z = 7954$ N, $F_t = 990$ N	-
=	$F3000$	$F_z = 4783$ N, $F_t = 449$ N	-	-
3 mm	$F5000$	$F_z = 5378$ N, $F_t = 416$ N	-	-

Table 4.10: Experimental tests forming times

		$\Delta_z = 0.1$ mm	$\Delta_z = 0.5$ mm	$\Delta_z = 1.0$ mm
air			0:00	
t_0	$F1000$	15 : 16	3 : 06	2 : 13
=	$F3000$	4 : 59	1 : 08	0 : 32
1 mm	$F5000$	3 : 11	0 : 44	0 : 22
t_0	$F1000$	14 : 16	3 : 46	1 : 55
=	$F3000$	5 : 06	1 : 04	0 : 37
2 mm	$F5000$	3 : 07	0 : 35	0 : 21
t_0	$F1000$	15 : 12	3 : 13	-
=	$F3000$	5 : 12	-	-
3 mm	$F5000$	3 : 37	-	-

Table 4.11: Experimental tests forming powers

		$\Delta_z = 0.1$ mm	$\Delta_z = 0.5$ mm	$\Delta_z = 1.0$ mm
air			$\dot{W} = 0$ W, $W = 0$ W.h	
t_0	$F1000$	1.04 W, 0.19 W.h	1.36 W, 0.06 W.h	2.03 W, 0.04 W.h
=	$F3000$	2.39 W, 0.15 W.h	3.14 W, 0.04 W.h	4.64 W, 0.03 W.h
1 mm	$F5000$	3.29 W, 0.14 W.h	4.31 W, 0.04 W.h	7.05 W, 0.03 W.h
t_0	$F1000$	2.10 W, 0.5 W.h	4.75 W, 0.23 W.h	7.14 W, 0.18 W.h
=	$F3000$	4.96 W, 0.41 W.h	11.80 W,0.18 W.h	15.99 W,0.14 W.h
2 mm	$F5000$	7.27 W, 0.36 W.h	16.01 W,0.17 W.h	18.11 W,0.11 W.h
t_0	$F1000$	6.57 W, 1.64 W.h	10.83 W, 0.48 W.h	-
=	$F3000$	13.68 W, 1.15 W.h	-	-
3 mm	$F5000$	22.52 W, 1.31 W.h	-	-

Table 4.12: Experimental tests consumptions

		$\Delta_z = 0.1$ mm	$\Delta_z = 0.5$ mm	$\Delta_z = 1.0$ mm
	$F1000$	2.43 kW.h	0.74 kW.h	0.47 kW.h
air	$F3000$	1.00 kW.h	0.41 kW.h	0.34 kW.h
	$F5000$	0.76 kW.h	0.36 kW.h	0.29 kW.h
t_0	$F1000$	2.59 kW.h	0.76 kW.h	0.53 kW.h
=	$F3000$	1.07 kW.h	0.42 kW.h	0.35 kW.h
1 mm	$F5000$	0.79 kW.h	0.38 kW.h	0.33 kW.h
t_0	$F1000$	2.58 kW.h	0.76 kW.h	0.55 kW.h
=	$F3000$	1.09 kW.h	0.42 kW.h	0.33 kW.h
2 mm	$F5000$	0.78 kW.h	0.33 kW.h	0.30 kW.h
t_0	$F1000$	2.74 kW.h	0.75 kW.h	-
=	$F3000$	1.10 kW.h	-	-
3 mm	$F5000$	0.86 kW.h	-	-

Table 4.13: Experimental tests energetic efficiency

		$\Delta_z = 0.1$ mm	$\Delta_z = 0.5$ mm	$\Delta_z = 1.0$ mm
air			$\eta = 0‰$	
$t_0 = 1$ mm	$F1000$	$\eta = 0.07‰$	$\eta = 0.07‰$	$\eta = 0.07‰$
	$F3000$	$\eta = 0.14‰$	$\eta = 0.10‰$	$\eta = 0.09‰$
	$F5000$	$\eta = 0.18‰$	$\eta = 0.10‰$	$\eta = 0.09‰$
$t_0 = 2$ mm	$F1000$	$\eta = 0.19‰$	$\eta = 0.30‰$	$\eta = 0.33‰$
	$F3000$	$\eta = 0.37‰$	$\eta = 0.44‰$	$\eta = 0.43‰$
	$F5000$	$\eta = 0.47‰$	$\eta = 0.52‰$	$\eta = 0.38‰$
$t_0 = 3$ mm	$F1000$	$\eta = 0.60‰$	$\eta = 0.64‰$	-
	$F3000$	$\eta = 1.05‰$	-	-
	$F5000$	$\eta = 1.52‰$	-	-

The plots of energy consumption over time, tool path, feed rate speed, forming force and forming energy are analysed to understand the process behaviour. All readings and calculations are plotted in appendix D of the internal report "SPIF Energy Consumption - Experimental evaluation of Single Point Incremental Forming consumption on the SPIF-A machine" [134]. All the graphics are discussed. The cone 5 of the 2 mm sheet analysis is described, among some considerations related to all experiments.

Figure 4.5 shows the tool path and the feed rate speed of the experiment. In the tool path graphic it is clearly defined the approximation and plunge movement, the defined cone along the forming movement and exit movement. In the forming tool path recording, mainly at the cone tip, it is visible a discrete angle change instead of a continuous curvature due to the sampling rate. In some experiments, mainly the ones with the fastest feed rate, a slight overshoot is spotted in the beginning and end of the forming movement.

In the feed rate plot, the downward and upward movements are also noticeable. In addiction, a slight increase of the vertical component of the feed rate is observed as each layer circle gets smaller and takes less time to complete. The gradual increase of the feed rate responds to the manual control used by the SPIF-A machine. In some feed rate graphics a speed decrease in the higher feed rate experiments is observed. That feed rate reduction is needed to avoid excessive vibration of the machine in short direction changing moves.

The force measured during the experiment is represented on figure 4.6 (a). The graph shows the vertical and horizontal (x and y) components of the forming force. The vertical force is filtered for a smother further calculus. The radial and tangential forces are calculated and also filtered. In the force graphic, the forming time can be split in two periods. The first period matches the forming of the cone's edge, with the tool contact in smaller than the wall slope. During this period the forming force gradually increases. The second period has a constant forming force and corresponds to the continuous forming of the 45º wall. The x and y components of the forming force have a sinusoidal behaviour due to the circle movement of each forming step. The calculated horizontal force (radial and tangential) have a similar behaviour to the vertical force, being almost four times smaller.

The calculated forces and the determined feed rate are used to draw the forming power, illustrated on figure 4.6 (b). The same two distinctive periods, relative to the edge and wall forming, are noticeable. One peek in the end also appears, due to the increase of the vertical feed rate in the cone tip forming. A slight delay in the force reading may also influence the

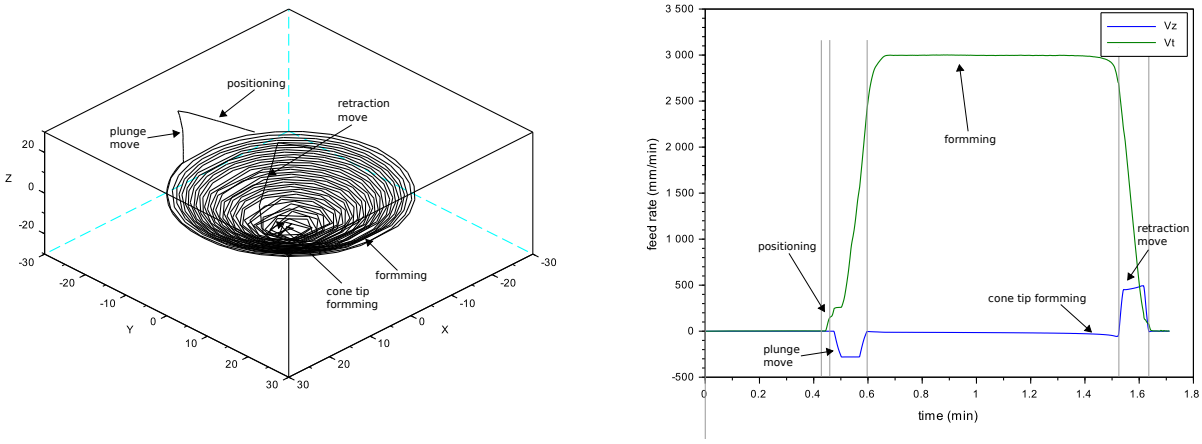

(a) (b)

Figure 4.5: Tool path (a) and feed rate (b) of the cone 5 of the 2 mm sheet

apparent power peek as a force value still exists during the extraction movement. However, an additional error at the end of the power plot has a minor influence on the forming energy integrations as it takes very little time.

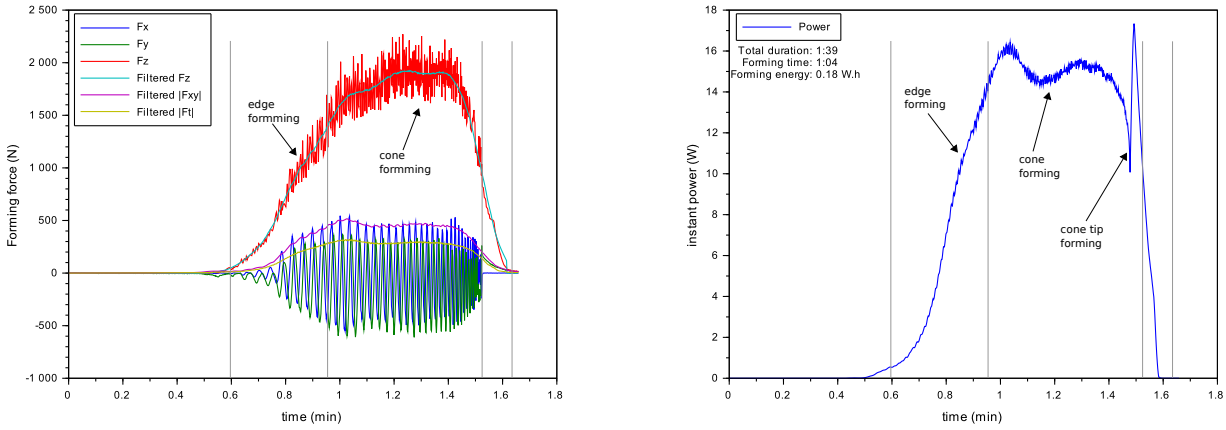

(a) (b)

Figure 4.6: Force (a) and forming power (b) of the cone 5 of the 2 mm sheet

During the experiment, the energy consumption is measured and plotted on figure 4.7. The time axis differs form the other graphics as the reading are accomplished by a different equipment. The recording starts with a little lag. However, the energy consumption lasts longer until the hydraulic power supply is turned off.

The energy consumption has two well-defined peaks, corresponding to the hydraulic power supply valve opening and closing. During the valve position shift, the oil flow is occluded,

leading to a motor power consumption increase. It is also noticeable that the power consumption is higher with the valve open. In that state, despite the pressure forwarded to the machine kinematics system being lower, the oil flow is bigger, due to recirculation, leading to the higher power value. Although the higher power consumption with the open valve, it is required to allow a safe start up of the power supply.

During the time when the recirculation valve is close, two power levels are also present, separated by power peeks. The lower value corresponds to the stopped machine and the higher value to the forming operation. The power peeks are due to an increase in oil intake in the cylinders during the vertical movements, thus they identify the plunge and retraction of the punch. The power variation between the stop machine and the forming operation is only $\Delta\dot{W} = 0.2$ kW for the cone 5 of the 2 mm sheet, and result mainly from the increase of oil intake due to the platform movement and also from the increase in the applied force.

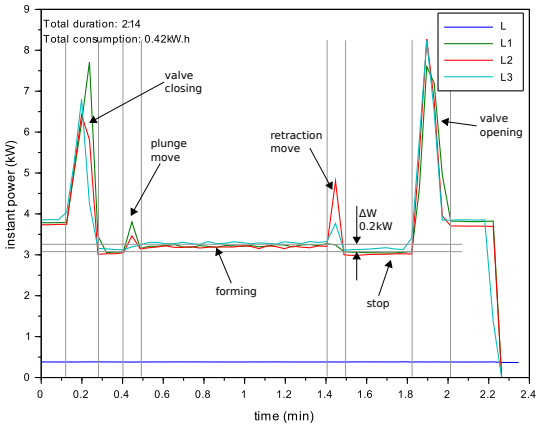

Figure 4.7: Energy consumption of the cone 5 of the 2 mm sheet

Given the 0.18 W.h used for the sheet forming and the 420 W.h overall consumption, the overall energetic efficiency of the cone 5 of the 2 mm sheet is $\eta_{\text{energy}} = 0.44‰$. Considering exclusively the power supply during the forming operation, the energy consumption is 183 W.h, resulting on an operation energetic efficiency of $\eta_{\text{energy}} = 0.98‰$.

As the total process duration took 2 : 14 minutes and the forming operation took 1 : 04 minutes, the time efficiency is $\eta_{\text{time}} = 0.48\%$.

After manufacture, parts are visually analysed and measured using the CCM machine. Figure 4.8 shows the measurement procedure of the cones formed on the 2 mm aluminium sheet. All cones and the comparison between the measurement data and the CAD model is presented in appendix E of [134]. The accuracy reference values for maximum deviation an point in bound are summarised in tables 4.15 and 4.14.

Figure 4.8: Measurement process for the 2 mm sheet part

Table 4.14: Experimental tests accuracy: maximum deviation

		$\Delta_z = 0.1$ mm	$\Delta_z = 0.5$ mm	$\Delta_z = 1.0$ mm
$t_0 = 1$ mm	$F1000$	± 2.6 mm	± 3.2 mm	± 3.2 mm
	$F3000$	± 3.0 mm	± 3.5 mm	± 3.7 mm
	$F5000$	± 2.6 mm	± 3.5 mm	± 3.2 mm
$t_0 = 2$ mm	$F1000$	± 2.9 mm	± 4.0 mm	± 4.3 mm
	$F3000$	± 3.9 mm	± 5.1 mm	± 5.2 mm
	$F5000$	± 3.4 mm	± 4.9 mm	± 4.9 mm
$t_0 = 3$ mm	$F1000$	± 8.3 mm	± 8.5 mm	-
	$F3000$	± 8.6 mm	-	-
	$F5000$	± 7.8 mm	-	-

Table 4.15: Experimental tests accuracy: percentage of points in a -2 to 2 mm bound

		$\Delta_z = 0.1$ mm	$\Delta_z = 0.5$ mm	$\Delta_z = 1.0$ mm
$t_0 = 1$ mm	$F1000$	78.6%	51.8%	65.7%
	$F3000$	65.1%	42.4%	46.4%
	$F5000$	84.3%	49.8%	66.4%
$t_0 = 2$ mm	$F1000$	68.1%	47.7%	52.2%
	$F3000$	44.1%	41.5%	46.4%
	$F5000$	48.6%	39.8%	48.7%
$t_0 = 3$ mm	$F1000$	42.2%	27.1%	-
	$F3000$	44.2%	-	-
	$F5000$	55.9%	-	-

As previously done for the energy analysis, the geometric evaluation of the cone 5 of the 2 mm sheet is described. Figure 4.9 shows a photo of the cone 5 of the 2 mm sheet for visual surface evaluation. Some punch marks are visible, mainly on the cone edge when the forming in accomplished by the punch tip instead of an angular contact. Overall surface quality is acceptable and uniformity of the surface finishing is good. On the bottom side, a slight mark of the backing plate is noticeable.

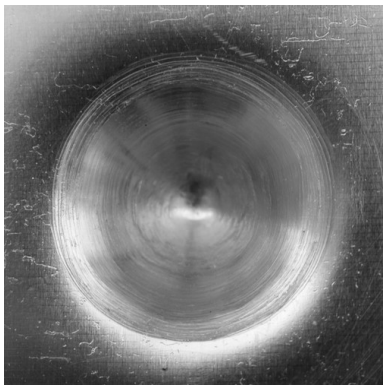

Figure 4.9: Surface aspect of the cone 5 of the 2 mm sheet

Regarding precision, a maximum deviation of ±5.1 mm is observed, with and average error of 2.4 mm. The accuracy for the best 99% of the part is ±4.9 mm. Figure 4.10 (a) shows the accuracy distribution. By analysing the dimensional distribution, 99.4% of the points are in a −5 to 5 mm bound, 68.5% of the points are in a −4 to 4 mm bound and 41.5% of the points are in a −2 to 2 mm bound.

Figure 4.10 (b) adds information on curvature to a geometric comparison between the measured part and the CAD model. The cone curvature uniformity is acceptable. The average curvature values of the formed cone, one over the radius of curvature, is 0.05 mm^{-1} in the walls and 0.25 mm^{-1} in the bottom, compared to 0.06 mm^{-1} and 0.17 mm^{-1} of the CAD model. However, the flat area in the bottom does not exist in the formed part. The flat area in the top of the cone is formed to an average curvature of 0.01 mm^{-1}.

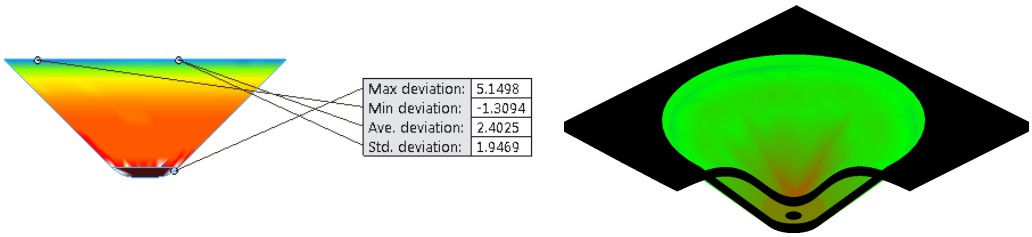

(a) (b)

Figure 4.10: Part quality analysis of the cone 5 of the 2 mm sheet: (a) accuracy, (b) curvature distribution

Considering the part deviation and a standard error of ±2 mm for a SPIF part, the geometric forming efficiency is $\eta_{\text{forming}} = 40.8\%$.

4.1.2 Conclusions

The experimental work tested the energetic behaviour of the SPIF-A machine while forming a simple part, under different forming parameters. In addiction, it tested the parameters influence not only on the energetic efficiency of the machine but also in the quality of the formed part.

The experimental tests confirmed the low energetic efficiency of the SPIF-A machine, obtaining values in the same order of magnitude as the theoretical calculus. The graphic on figure 4.11 compares the efficiency of the different experimental tests, and the difference from the experimental results and the prediction. The shaded bars represent the experimental results and the lightened the prediction values.

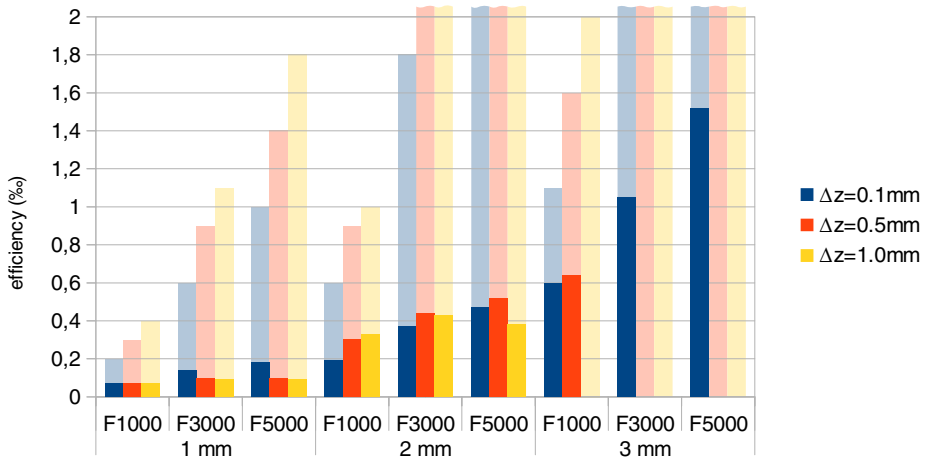

Figure 4.11: Efficiency comparison

The main divergence dues to the fact that the prediction only considered the electric consumption during the forming operation and the experimental work took an holistic approach, considering the all process from beginning to the power supply shutdown. This aspect is mostly noticeable at higher feed rates, where the forming process is faster, giving more weight to the preparatory and finishing phases.

Giving the low efficiency value, the total power consumption is more relevant to the process parameters selection. The graphic on figure 4.12 illustrates energetic consumption of the different forming tests in the shaded bar, and the reference value for air forming in the lightened bars. In all sheet thicknesses, the energy consumption is smaller for higher feed rates and for larger step downs.

The energy consumption strongly decreases for the fastest operations. The small increase in the energy consumption due to the forming force is far compensated by the decrease achieved by the lower time consumption. This fact is supported not only by the comparison between different forming parameters, but also by the comparison between the air movement and the forming itself. This near independence between the energy consumption and the forming force dues to the high strength of the SPIF system and the hydraulic operation. It is expected that other ISF systems, particularly with electric actuation may have a much higher energetic efficiency, despite the operational restraints.

For the development of an energetic consumption model of the SPIF-A machine, it is reasonable to perform an exclusive evaluation of energy consumption over the forming time, neglecting the influence on the forming parameters. The energy consumption variation is only noticeable at the vertical movements due to a high oil flow in the cylinders. Nevertheless, as these movements have little significance during the forming process, this slight increase can be neglected. Figure 4.13 represents the relation between the forming time and the energy consumption, approximated by a linear equation. There is a fixed consumption of 0.25 kW.h corresponding to the forming process set up and machine shutdown and an additional average consumption of 0.16 kW.h/min of forming.

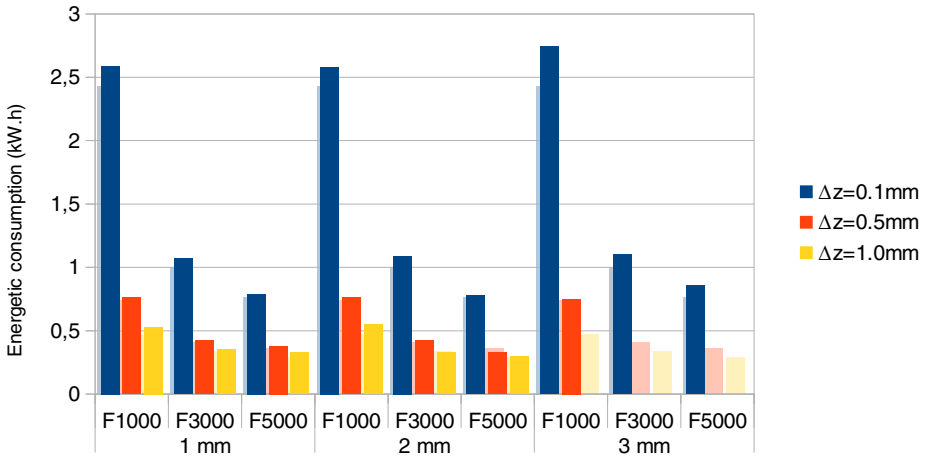

Figure 4.12: Energetic consumption comparison

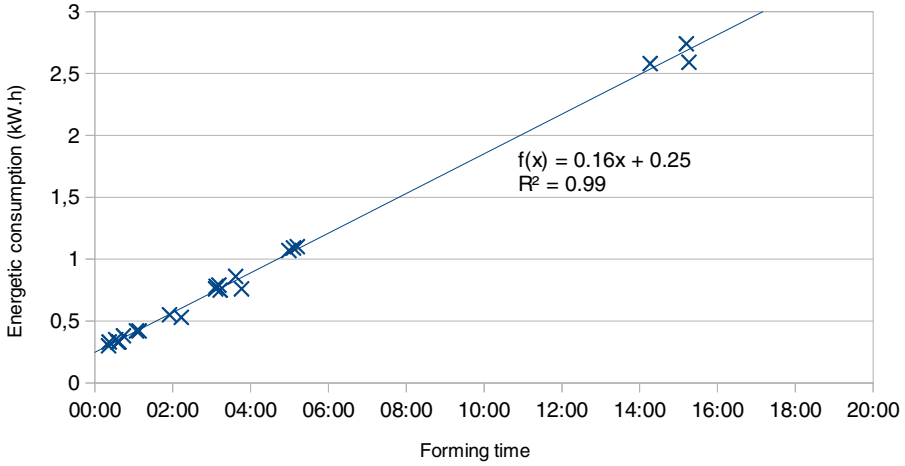

Figure 4.13: Energetic consumption over forming time

On the other hand, the part quality benefits most from small forming increments, thus a compromise has to be made. The forming speed has no significant influence on the part accuracy when forming aluminium, as long as it does not causes considerable machine vibration. Despite it hasn't been measured, higher feed rates lead to a better surface quality when using small vertical increments.

Better part quality is verified for the thinner sheets. The better accuracy results mostly from a smaller effect of the spring back effect. The better surface finishing dues to the lower forming force, leading to smaller friction and lower material removal by scratching.

Summarising, the experimental work conclusions are:

- A energetic consumption prediction for the SPIF-A operation can be estimated based on the forming time by equation 4.1, where t is the forming time in minutes.

$$C = 0.16 \times t + 0.25 \tag{4.1}$$

- Higher feed rates benefits energy savings by reducing forming time.
- Higher vertical step downs benefits energy savings by reducing forming time.
- Vertical movements lead to a slight increase of the instant consumption.
- Changes in the forming forces have little influence on the energy consumption of the SPIF-A machine.
- Part accuracy and surface finishing are better when forming with smaller vertical steps on AA1050 H111.
- Part accuracy and surface finishing are better for thinner sheets on AA1050 H111.
- Surface finishing seems to be better when forming with fastest feed rates on AA1050 H111.

4.2 Incremental forming of tunnel and semi-tunnel type parts

SPIF is commonly referred as a freeform forming process, only limited by a few geometric features as the wall angle, material thickness, part size, feature size and radius and changes in curvature. However, studied application generally use a full constrained blank, leading to container type parts. The most common academic shapes are full or truncated pyramids and cones.

The better suited identified fields are the manufacturing of prototypes, the manufacture of design and architecture components, the fabrication of spares for obsolete parts and the fabrication of components for small volume industries such as aeronautics. Other identified application fields are the customization of parts and manufacture of unique increased value products, as for example medical applications [135].

4.2.1 Preliminary evaluation of tunnel type parts

As referred, parts formed by ISF have typically a container type configuration. This geometry often requires effort post processing cutting operations and lead to a substantial iste of material when some geometries are intended. Besides, the need of extending the part's edge to the blank plane at an angle bellow $\phi_{\max}$ to create a container also reduces the useful available forming area. The goal of the study is to explore the possibility of incrementally form a semi constrained flat blank to a tunnel configuration. The use of tunnel or semi-tunnel part configuration benefits the useful area of the part, reducing the amount of scrap and allowing the fabrication of bigger parts. Thus, within the goal of explore and define the geometrical complexity limits for SPIF, experimental work on this configuration are performed.

The new proposed principle is based on using partially constrain blank for ISF operations instead of a fully clamped sheet. As no publications are found on semi constrain incremental forming, the experimental work started with preliminary tests as proof of concept. A straight geometry is design with a frustum profile to validate the possibility of forming tunnels and find preliminary data about forming angle.

The frustum part is a 180 mm wide tunnel, with two symmetric side walls with a 75 mm radius, leaving the horizontal plane at 30º. The frustum wall for a slope angle from 30º to 90º, during 65 mm depth. The geometry continues with parallel vertical walls until 80 mm. Figure 4.14 represents the drawing of the frustum tunnel.

The forming operation of the part is perform until failure. By measuring the part depth at failure one can determine an estimation for the maximum forming angle $\phi_{max,t}$ by equation 4.2, where d is the part depth at any given time and d_{max} is the part depth at failure [14]. For a 2 mm thickness Aluminium Alloy 1050-H111 sheet, by analogy of the container type part, it is expected to reach a $\phi_{max,t} = 70^{\circ}$ to $\phi_{max,t} = 75^{\circ}$, corresponding to a forming depth between $d \approx 40$ mm to $d \approx 45$ mm. This value should vary based on the forming parameters and strategy.

$$\phi = 90 - \arcsin\left(\frac{65-d}{75}\right) \Rightarrow \phi_{max,t} = 90 - \arcsin\left(\frac{65-d_{max}}{75}\right) \tag{4.2}$$

For the forming operation, new tool path strategies are proposed. The strategies derive from the ones used in container type parts, defined from the final intended geometry and adapted and dealing with the geometric discontinuity of the tunnel ends. For the initial evaluation, a 12 mm ball tip punch is used, forming with 0.5 mm constant Z steps down.

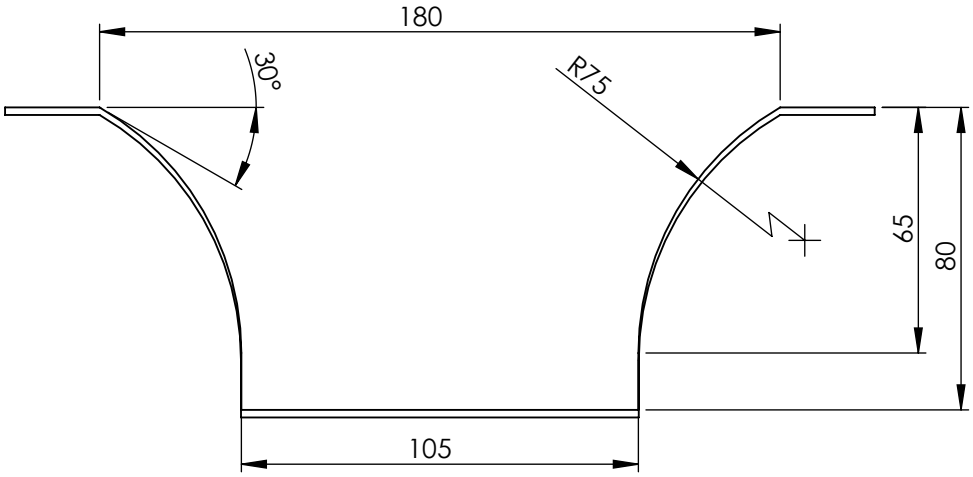

Figure 4.14: Frustum tunnel part drawing with thickness approximated by the sine law

To minimise the twisting and air movements, the forming strategy proposed for the frustum tunnel used two ways forming movement. Figure 4.15 represents the proposed strategy. The first forming movement is performed on one tunnel side. An air movement changes side and a second forming movement is performed on the opposite side in the opposite direction. The step down movement is performed in contact with the sheet and the third movement returns in the same direction as the first. A second air movement changes back side and the process continues. The last movement is done in the same side as the first, in the opposite direction.

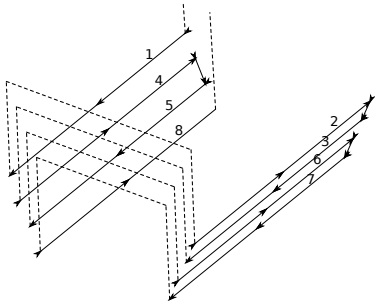

Figure 4.15: Forming strategy for tunnel type parts with air transition movements

The forming process proceeded according to expected, forming the part up to failure at 42 mm depth, corresponding to a $\phi_{max,t} = 72^{o}$. At the side walls, forming occurred is a similar way as in the container type parts. However, some excessive thinning on the side edges lead to a premature failure by tearing. Besides, the changes in the forming side lead to a noticeable free form movement of the part, shifting position alternately. By analysing the formed part, it is noticeable that an excessive thinning an a strong lack of accuracy occur after 30 mm deep, corresponding to $\phi = 62^{o}$. Thus, one can presume that a lower maximum angle is applied in tunnel type configuration when comparing with more common container type parts.

The test results validated the tunnel type part concept and lead to the need to improve the working strategy. Before following a more systematic approach on the tool path strategy

definition and evaluation, new strategies are proposed, replacing the air movement by sheet contact transition along the edge. It is intended to develop more knowledge about tunnel part forming to better define the major experiments. Figure 4.16 represents the initial option for tunnel part forming without lose of contact. The option in subfigure (a) keeps the bi directional forming operation and the one in subfigure (b) uses close loop movements in a single direction.

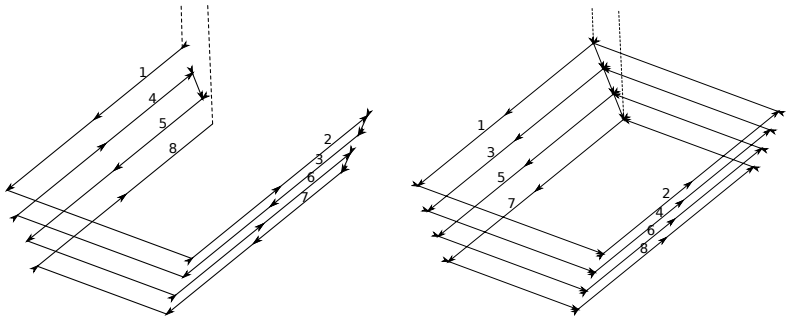

(a) (b)

Figure 4.16: Forming strategy for tunnel type parts with edge contact transition movements

When using the new proposed strategies, the constant contact with the sheet lead to better results when forming the tunnel features, minimising the position shifting resulting from the regain of contact. However, despite the improvement in part quality, no effect is found within the formability. The excessive thinning on the edge still accoutred, mainly on downward movements. As the tool performs a downward movement, it also leads to a localised thinning that may lead to tearing. In the tool path with alternating movement direction, the damage on the edge is most noticeable at the tool entrance side. As the tool enters the sheet moving from the edge it pulls material inward, contributing to the localised thinning. The outward movement has minor issues about local defaults. However, in continuous direction movement, the failure always occur at tool exit. The twisting effect cause a premature tearing when moving along the part's bottom.

The forming operations with three different tool path strategies validated the concept of using SPIF for the manufacturing of tunnel type parts. With this, the larger available useful workspace is confirmed, as well as the potential for a fastest build of large parts. The forming along the tunnel sides mimics the standard behaviour of SPIF, leading to an expectation that ISF is compatible with tunnel configuration. A lower formability limit is observed in the tunnel ends. Premature tearing occurs when forming with angles bellow the ϕ_{max} value of container type parts, thus, leading to a lower maximum slope angle for tunnel ends defined as $\phi_{max,t}$. This seams to occur both due to excessive thinning in tunnel edges, lost and regain of tool contact and twisting phenomena.

The preliminary results base the definition of a systematic study on tunnel and semi tunnel part manufacturing using SPIF.

4.2.2 Tool path performance study

Design of experiment

The capability of forming tunnel like parts using SPIF is proposed and validated. To better develop the study on tunnel parts forming, a systematic approach to generate experimental data and analyse it in an overall point of view is performed using factorial experiments. The design of experiments (DOE) considers a sequence of small tests. Between each individual test a major number of factors remains unaffected, only changing the studied parameter in question [112,113]. For the fulfilment of the studies on tunnel and semi tunnel configurations, an initial 3^2 factorial experiment is proposed, followed by two single factor experiments.

The proposed tests are performed in a simple straight tunnel with a frustum based geometry, as illustrated on the lower half of the drawing in figure 4.17. The geometry has a constant 60^o slope during 20 mm deep followed by a 40 mm radius up to vertical walls. The geometry used for the factorial test uses a full tunnel, $l = \infty$, with a width of $w = 50$ mm. The factors in analysis for the factorial experiment are the strategy type and the side changing position at the tunnel ends. All remaining forming factors are established. Experimental tests are performed using 2mm thick 1050-H111 aluminium sheet. A 10mm spherical tip punch is used, with a 0.5 mm constant step down and a 1500 mm/min feed rate. Each test is performed until part failure. The effect of the different experiment factors is measured after each test. Results ate evaluated for accuracy and maximum forming angle. The formed tunnels profiles are measured using a coordinate measuring machine (CMM) [132]. Accuracy is determined by comparing data to the CAD model and measuring the maximum deviation. The maximum forming angle $\phi_{max,t}$ is determined by equation 4.3, where d_{max} is the forming deep at failure [14]. In addition, the total process time during the constant slope feature is measured and the forming efficiency is determined by the effective forming time over the total process time.

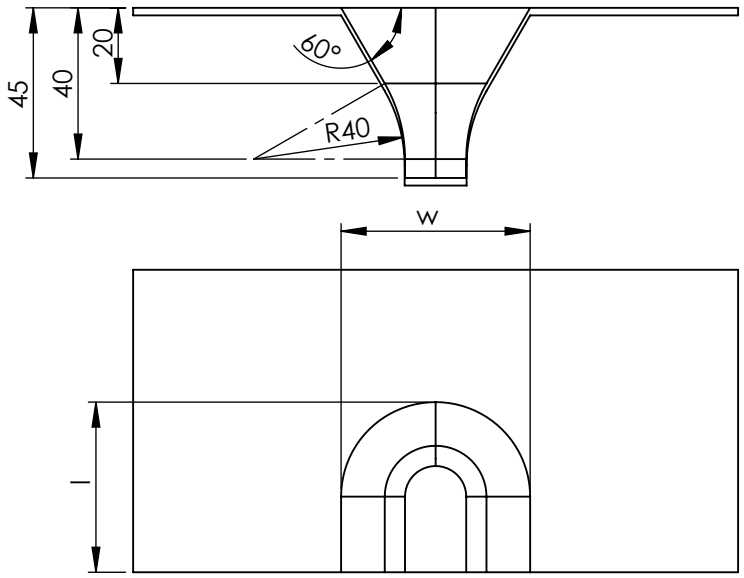

Figure 4.17: Frustum tunnel/semi tunnel for factorial experiment

$$\phi = 90 - \arcsin\left(\frac{40-d}{40}\right) \Rightarrow \phi_{max,t} = 90 - \arcsin\left(\frac{40-d_{max}}{40}\right) \tag{4.3}$$

In what regards the forming strategy, a continuous downward movement in a helical tool path strategy is used as the standard value, as illustrated on figure 4.18 (a). Note that due to a necessary final loop at constant Z, this strategy uses one extra loop when comparing with the ones used in preliminary tests. By using the helical strategy, it is expected to benefit from the absence of a located vertical movement. Besides, moving the downward movement away from the part edge should reduce the excessive thinning and premature tearing. This tool path strategy is very similar to the ones used on container type parts, with the difference of maintaining the X or Y position along the tunnel end during the side changing movement. As the failure occurred at the tunnel ends, the other proposed tool paths are based on ward the downward movement from the part ends. A simpler approach uses a alternating direction forming tool path with a step down increment at the geometry centre. It is indented not only to perform the vertical movement at the centre but also in alternate the entrance side, reducing twisting, as illustrated on figure 4.18 (b). Despite the disadvantage of a localised down increment, the strategy should relief the ends tearing by lowering the higher stress and avoiding half the entrance movements. As a third value for the strategy factor, a more complex tool path is also proposed, maintaining the localised step down at the geometry centre but performing every movement in an inside-out strategy, as illustrated on figure 4.18 (c). Is is expected to achieve better results at the cost of a longer forming time.

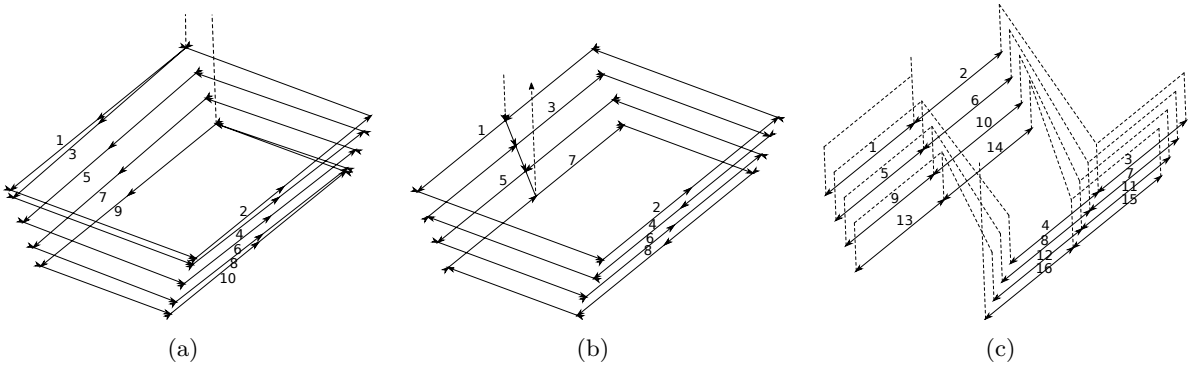

Figure 4.18: Forming strategy for tunnel type parts without edge downward movements: (a) helical, (b) alternating, (c) inside-out

The second factor in test is the position of side change movement. This also indents to explore the best options for tunnel forming. As a standard reference, the transition is performed over the end edge. Two other values with the change in position shifted half tool diameter inward or outward of the edge are tested. Figure 4.19 represents the three options for the side changing position. The figure only represents the forming path. Surface links or air movements are added according to the applied strategy.

After the 3^2 factorial experiment, the best reached strategy combination is used for the following single factor tests. The single factors in the following experiments are the tunnel width in full tunnels or length/width ratio in semi tunnels. For the single factor tests, the same simple geometry are used, forming a straight tunnel and semi tunnel according to figure 4.29. The tunnels width is represented by w and the semi tunnels length by l in figure 4.29. With

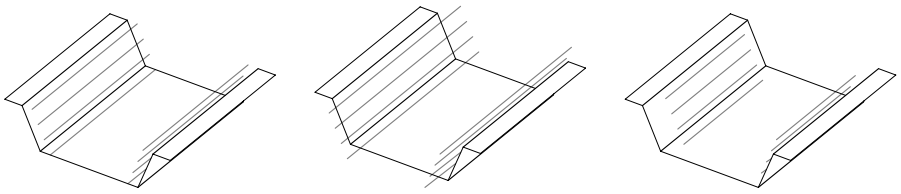

(a) (b) (c)

Figure 4.19: Side changing position on tunnel forming: (a)on edge, (b) outside edge, (c) inside edge

these tests it is intended to not only evaluate the influence of the strategies on the forming process but also to define new geometric guidelines for tunnel and semi tunnel configuration parts.

The experiment diverges in two branches, analysing the tunnel and the semi tunnel geometry for the influence of the width or length/width ratio on the formed parts. For the tunnel part, a thin, a medium and a large width geometry is tested with values of 50 mm, 75 mm and 100 mm. It is also intended to study not only the maximum wall angle but the part accuracy as well. For the semi tunnel geometry, the width is constant and fixed at 50 mm and the length is set to a length/width ratio of 0.5, 1.0 and 1.5. It is also intended to study the forming limit and the accuracy. Besides, it is expected to define influence of the lenght/width ratio influence on the achievable depth.

From a general viewpoint for the DOE, table 4.16 resumes the values used in the fix factors for all experimental tests. Table 4.17 resumes the factors in values used in the 2^3 factorial analysis and tables 4.18 and 4.19 resume the factors and values in single factor analysis.

Table 4.16: Fix factors and values

tool shape	spherical
tool size	10 mm
step down (ΔZ)	0.5 mm
feed rate	1500 mm/min
material	AA1050-H111
sheet thickness (t_0)	2 mm

Table 4.17: Tunnel 2^3 factorial test resume

		tool path	
	helical on edge	alternating on edge	inside-out on edge
side changing position	helical outside edge	alternating outside edge	inside-out outside edge
	helical inside edge	alternating inside edge	inside-out inside edge

Table 4.18: Tunnel width single factor test resume

	thin	medium	large
width	50 mm	75 mm	100 mm

Table 4.19: Semi-tunnel lenght/width single factor test resume

	short	medium	long
lenght/width ratio	0.5	1.0	1.5
width	50 mm	50 mm	50 mm
lenght	25 mm	50 mm	75 mm

To avoid the need for a unique backing plate for each different tunnel size, a new adaptive backing plate concept is detailed. The concept uses bridge parts and spacers that are assembled to allow a backing plate geometry with different tunnel widths. Figure 4.20 shows the working principle of the modular backing plate. The backing plate provides full support for the tunnel parts and leaves the semi tunnel central end unsupported.

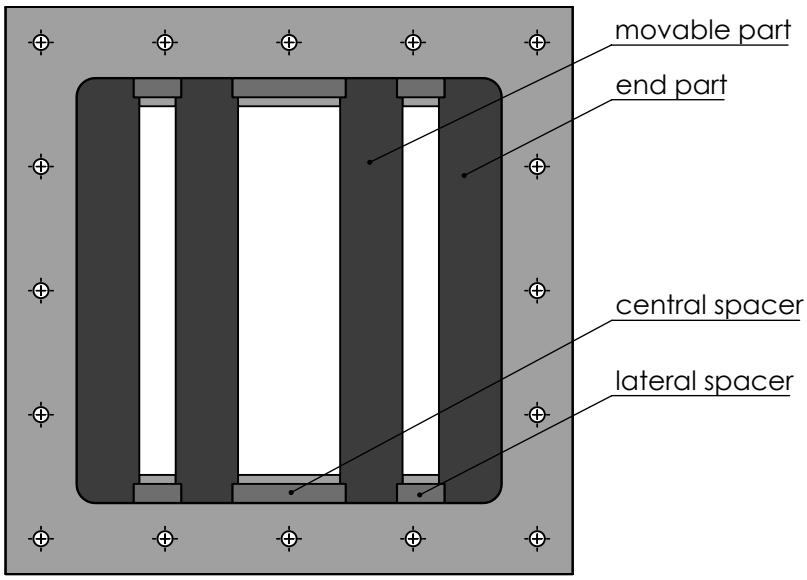

Figure 4.20: Modular backing plate designed for the tunnel and semi tunnel tests

Each baking plate assembly uses two movable bridge parts and two end bridge parts, each one 30 mm wide. The bridges position is restricted by central and lateral spacers. The backing plate is design to form with a 2 mm nominal gap between part perimeter and support. For the 50 mm tunnel tests, a 54 mm slot is assembled, using 60 mm central spacers and 31 mm lateral spacers. The 75 mm tunnel is formed in a 79 mm slot using 85 mm central spacers and 18.5 mm lateral spacers. The 100 mm tunnel is formed in a 104 mm slot using 110 mm central spacers and no lateral spacers. Tolerance is defined to ensure the assembly and lead to nominal gap of 1 mm parcelled out by all interfaces. A minimum gap of 0.3 mm and a maximum gap of 2.3 mm may be noticeable. The parts drawings are presented on the appendix C.1 to be manufactured using water jet cutting and milling operations.

Experimental work and results

Experimental tests are performed using the SPIF-A machine with 230 × 120 mm blanks clamped only along the shorter edge. One test is performed per blank, recording the forming process time and the instant forming depth. Figure 4.21 represents the forming process of the helical tool path with on edge side changing position. Small chocks are used to help to lock the backing plate in position.

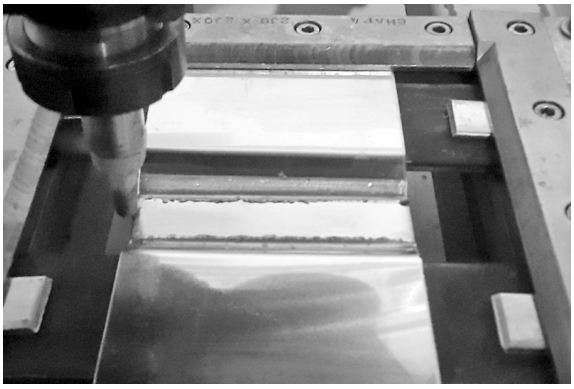

Figure 4.21: SPIF tunnel part forming

Apart from the DOE tests, a conventional container type part with a geometry similar to the tunnels has also been formed as a reference benchmark achieving a maximum forming angle of $\phi_{max} = 75.5^{o}$. Failure in the container part happen by initial cracking at the slot ends and tearing propagation along its length. Figure 4.22 shows the formed container part.

Figure 4.22: Container type part formed as a benchmark

The measuring results and online recordings are used to determine the maximum wall angle, accuracy and forming efficiency. The maximum wall angle is determined by equation 4.3 using the forming depth recorded from the machine controller at failure. The accuracy is determined by CMM measurements. The forming time is measured through online recordings since the process start to the end of the 20 mm loop. The forming time efficiency is determined by the effective forming time over the total process time by the CAM software used to calculate the tool paths. Table 4.20 summarizes the maximum wall angle and the accuracy achieved with the factors in analysis combinations. Table 4.21 presents the total process time for the first 20mm depth of each analysis and the time efficiency.

Table 4.20: Maximum wall angle and accuracy on tunnel parts

side changing position / tool path	alternating	helical	inside-out
inside edge	82.1° ±3.4 mm	63.1° ±3.5 mm	67.2° ±3.5 mm
on edge	68.8° ±3.6 mm	62.5° ±3.1 mm	70.3° ±3.3 mm
outside edge	69.5° ±3.4 mm	66.9° ±3.5 mm	65.6° ±3.7 mm

Table 4.21: Process time and time efficiency on tunnel parts

side changing position / tool path	alternating	helical	inside-out
inside edge	07:36min 73%	07:31min 73%	17:42min 28%
on edge	08:03min 75%	08:02min 75%	18:11min 31%
outside edge	08:38min 70%	08:35min 70%	18:40min 30%

Figure 4.23 shows pictures and the measured profiles of the nine experimental tests. The tunnels in each picture are grouped with the three tool path strategies for each side changing position per picture, according to the lines of table 4.20. The profiles are grouped the same way.

The inside edge side changing position strategies fail mostly by cracking, as a container like configuration is formed along the depth. Both the on edge and the outside edge side changing positions strategies failure occurs mainly by tearing. The on edge side changing position strategies show an additional thinning on the edge.

After the factorial tests, the single factor tests where performed to study the influence of the tunnel width on the forming process and the possibility of forming a semi tunnel configuration and its lenght/width ratio. Tests used an alternating tool path strategy with outside shifting position. Despite not being the strategy with the highest $\phi_{max,t}$, the overall results are considered the better. Notwithstanding they achieve higher formability, inside edge side shifting position requires post cutting operation, which is intended to avoid or minimise. Inside-out tool path reach good results but at higher process time and with lower surface quality due to the continuous lost and gain of contact.

Table 4.22 presents the maximum wall angle and accuracy of the tunnel width test. Figure 4.24 shows the three different width tunnels and their profiles. Tunnel width has little influence on the forming process. However, larger tunnels cause a raising movement of the tunnel walls requiring the sheet clamping to be placed near the tunnel top. The absence of this close clamping may lead part failure by tool collision with the tunnel edge due to the raising movement before failure happen by tearing.

Table 4.23 presents the values of the semi-tunnel test. Figure 4.25 shows a photo of the formed semi tunnels and the comparison between their profiles. The semi tunnel with the smaller length/width ratio failure occurs by leading to a quasi flange feature, replacing the semi tunnel bottom. Semi tunnels are possible and allow greater formability at the cost of accuracy loss. A noticeable side movement of the semi tunnel lead to a deeper part. Higher length/width ratio allow better results. It is expected that higher ratios lead to a behaviour in the end edge similar to the one found in the full tunnel configuration.

(a)

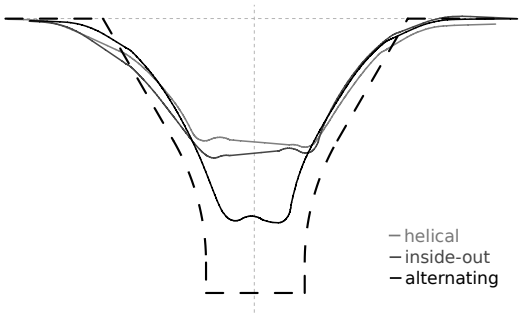

(b)

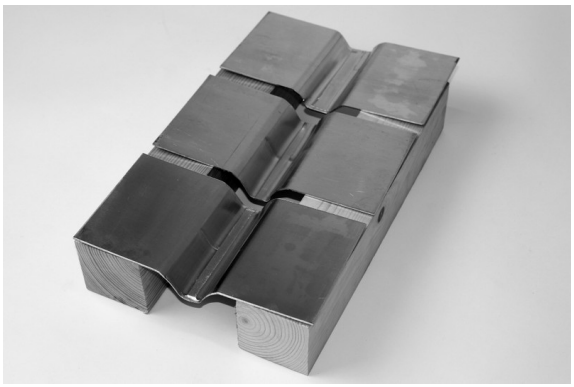

(c)

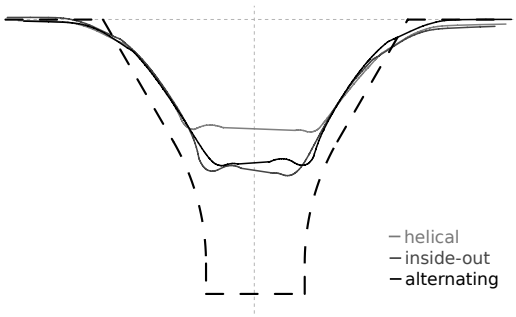

(d)

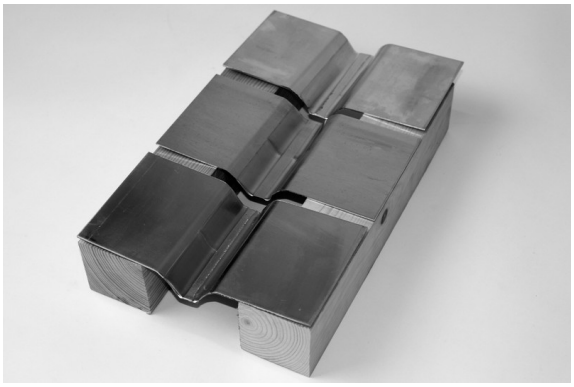

(e)

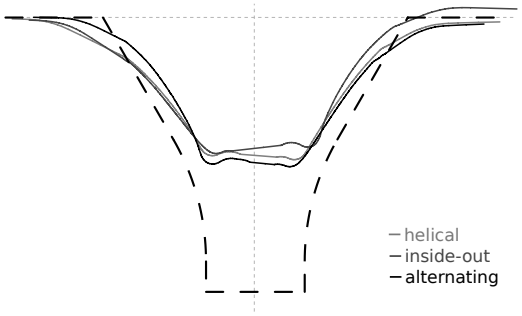

(f)

Figure 4.23: Tunnel parts formed and profile comparison: (a) and (b) Inside edge side changing position, (c) and (d) on edge side changing positions, (e) and (f) outside edge side changing position

Table 4.22: Maximum wall angle and accuracy on different width tunnel parts

tunnel width	50 mm	75 mm	100 mm
	69.5^{o} ± 3.4 mm	69.5^{o} ± 3.3 mm	68.0^{o} ± 4.8 mm

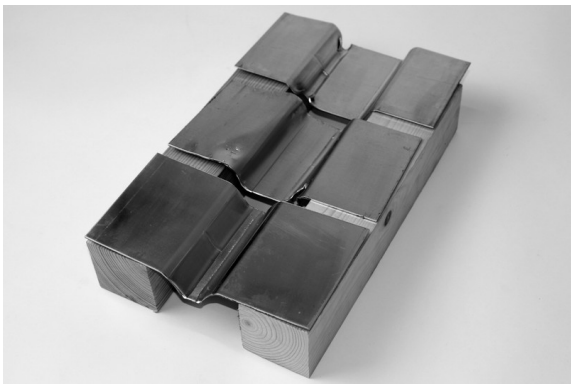

(a)

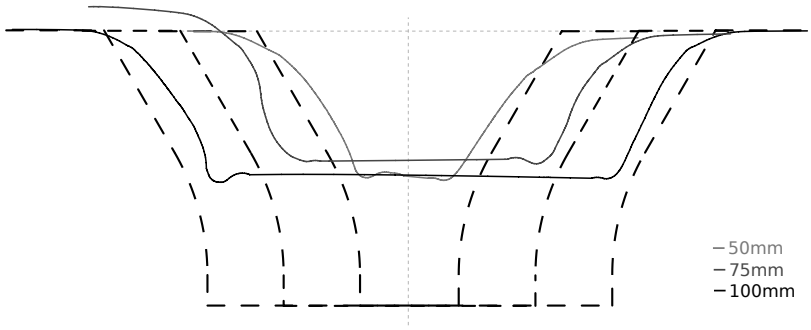

(b)

Figure 4.24: Different width tunnel parts formed and profile comparison

Table 4.23: Maximum wall angle and accuracy on semi tunnel parts

semi tunnel lenght/width	0.5 ratio	1.0 ratio	1.5 ratio
	60.8° ±6.3 mm	86.4° ±4.5 mm	82.1° ±4.3 mm

(a)

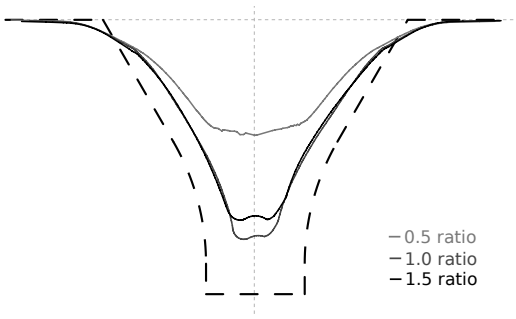

(b)

Figure 4.25: Semi tunnel parts formed and profile comparison

Tunnel forming failure modes

The failure modes in semi constrained incremental forming differ from the ones in conventional full constrained parts. Typical incremental forming failures like cracking and skinning are also possible in tunnel type parts. However, the free edge tends leads to other failure modes. This premature failure is responsible for the $\phi_{max,t}$ angle lower then the typical ϕ_{max}. The most common failure modes in tunnel type parts are tearing, excessive thinning on the tunnel edge, cracking and tool collision with the part's edge.

Tearing happens with all tool path strategies, mainly with on edge and outside edge side changing position. Tears are usually created with length less or equal the sheet thickness. However, a fast propagation is observed if the process is continued per each vertical increment. Figure 4.26 (a) shows a tearing failure propagated along four vertical increments on a outside edge side changing position.

Excessive thinning on the tunnel edge happens with contoured tool path strategies, either alternating or helical, with on edge side changing position. Figure 4.26 (b) shows the edge thinning resulted from the tool compression force against the sheet. The illustrated excessive thinning is mainly formed and noticeable at the tunnel bottom but it is shifted to the tunnel walls along the process. This phenomena leads to the premature tearing of the on edge side changing position when compared with the outside edge.

The inside edge side changing position lead to quasi container type configuration at the tunnel bottom. This result on a part failure by cracking, similar to the one found in conventional incremental forming processes. Figure 4.26 (c) shows the cracking failure and propagated tearing on the alternating inside edge side changing position tool path.

Tool collision with the part edge may also lead to failure, mainly when forming large tunnels with outside edge side changing position. Figure 4.26 (d) shows the failure in the 100 mm tunnel. This failure mode happens due to raising movement of the tunnel walls and can be minimised by locating the sheet clamping near the tunnel top.

Semi tunnel parts may have the same failure modes that the full tunnel experience. Nonetheless, failure may also happen by forming a quasi flange geometry when dealing the small length/width ratios. When dealing with these geometric features, the semi tunnel bottom tends to move towards the part centre and shifted to the end wall, causing the bottom to recede and form a bottomless flange.

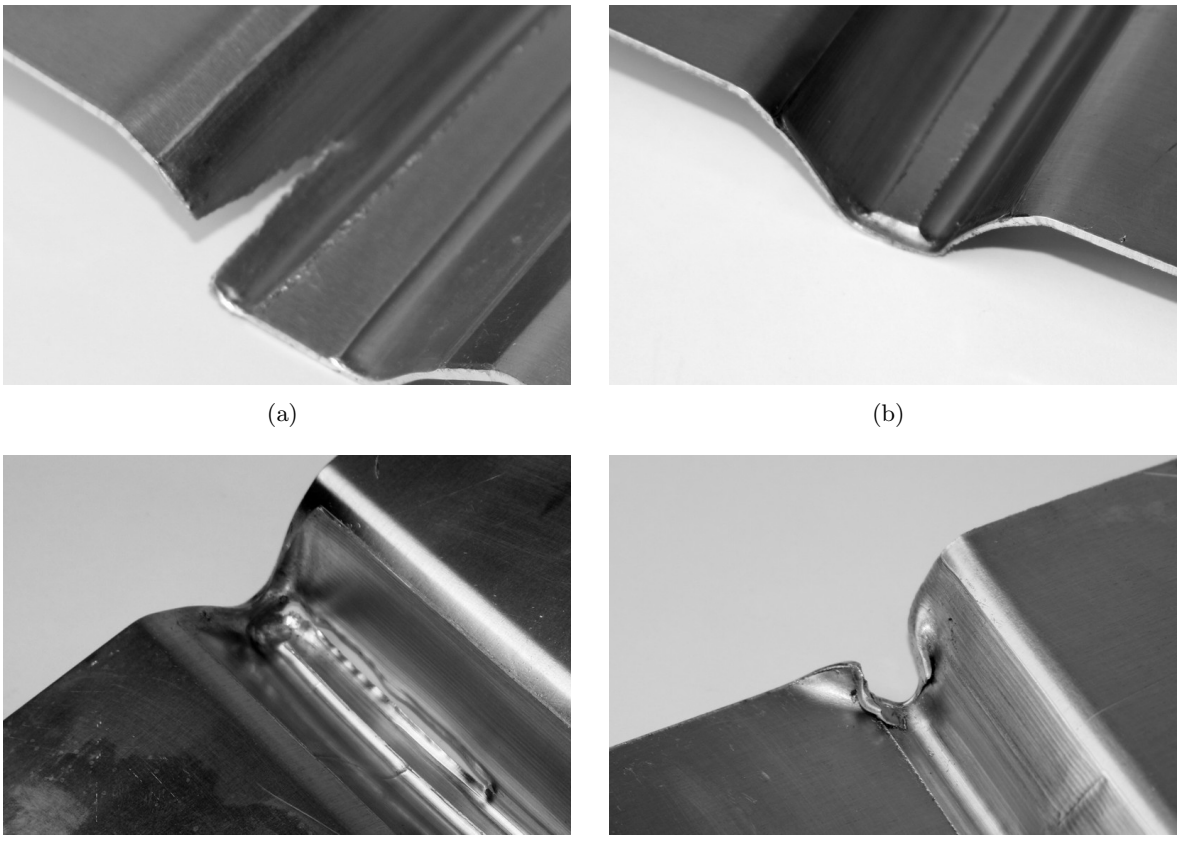

(a) (b)

(c) (d)

Figure 4.26: Tunnel parts failure modes: (a) tearing, (b) edge thinning, (c) cracking, (d) tool collision

4.2.3 Forming freeform tunnels

The achieved results on incremental forming of tunnel type parts where tested on more complex parts. To test and validate the possibility of forming free form tunnels, four different tunnels are designed. Design parts used an S shaped, T shaped, L shaped and P shaped geometry and feature 60mm width and 35 mm deep tunnels with 60° constant slope walls. All parts are drawn from a 230 mm by 140 mm, 2 mm thick reference sheet. No bottom radius is added to the part design, making the formed parts bottom radii depend on the used tool. The tunnel configurations where defined not only to study different forming behaviours but also as benchmark geometries form industrial parts.

A S shaped tunnel is design to analyse changes in curvature. The part is complement with two undersized length/width ratio semi tunnel circles. Figure 4.27 present the drawing of the S shaped part with two 60° turns with and middle radius of 60 mm. The part is complemented with two semi circles semi tunnel type configuration. The change in curvature is intended to evaluate higher complexity geometry forming behaviour.

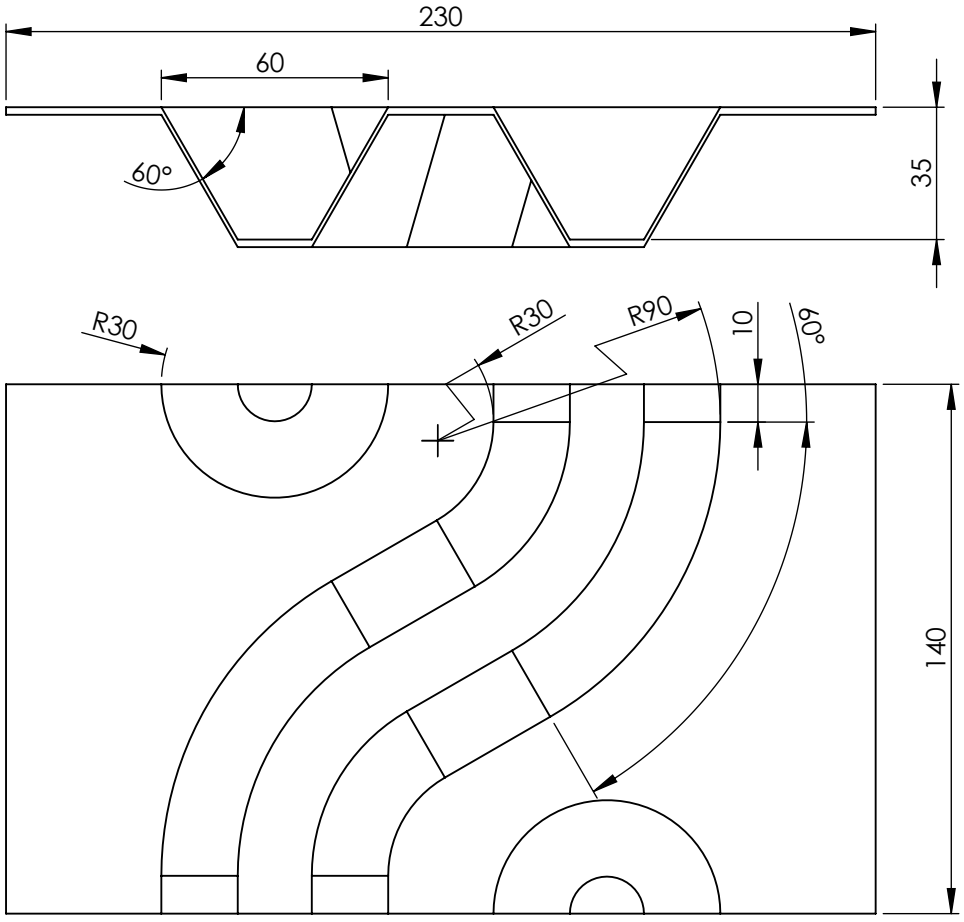

Figure 4.27: S shaped part drawing

A T shaped tunnel is design to forecast asymmetric lateral faces behaviour. Figure 4.28 present the drawing of the T shaped part. The T shaped part has a primary straight tunnel. At the middle of the part, one side is perpendicularly diverted 103.5 mm away from the main feature. The side tunnel element end with a continuous fillet.

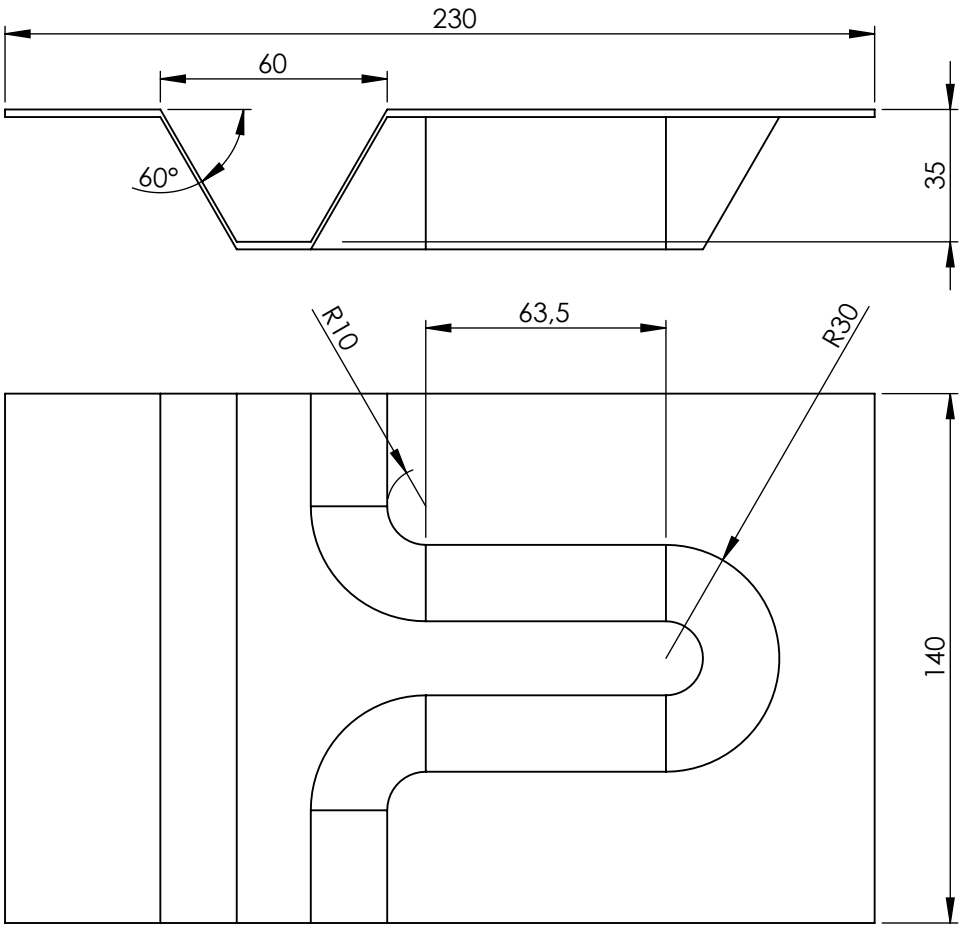

Figure 4.28: T shaped part drawing

A L shaped part is design to study the result of a smaller constraining area and the behaviour of a perpendicular geometry. Figure 4.29 shows the drawing of the L shaped part. The flat sheet is reduced to a 140 by 140 mm area and the tunnel performs a 90° turn with a middle radius of 60 mm. The part constraining area is reduced from the two opposite sheet sides to two adjacent sides and a small area at the centre.

A P shaped tunnel is design to analyse the behaviour of width changes along the tunnel. Figure 4.30 present the drawing of the P shaped part. The tunnel starts with a 60 mm width and extends to a 93 mm width. The enlargement is done on only one side of the tunnel, along two turns with 130 mm at the meddle of the sheet.

For all parts, backing plates are design with 1 mm clearance from the top border. The backing plates are cut in 5 mm steel and used specifically for the tests.

The designed parts are formed using an helical tool path with on edge side shifting position, using a 12 mm punch and 0.5 mm vertical step down with a feed rate of 1500 mm/min. Despite being the strategy which allows the smaller formability, it allows the 60° slope walls and leads to better accuracy.

Figure 4.31 shows photos of the four formed tunnels. All tunnel features are acceptable in the four parts. As expected, semi tunnel features fail on having the flat bottom area due to the undersized length/width ratio.

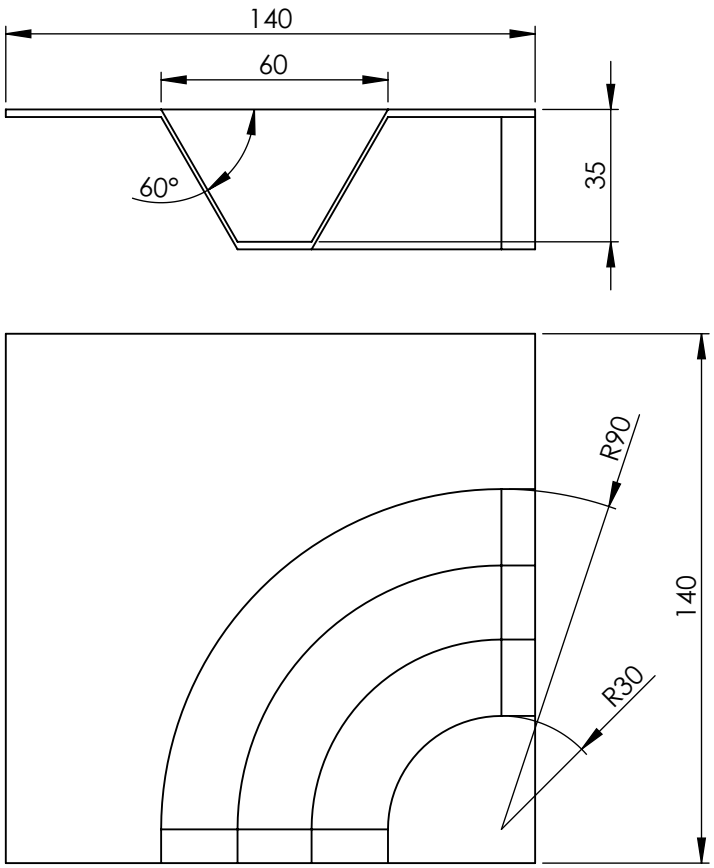

Figure 4.29: L shaped part drawing

The S shaped part led to great results along the double curvature tunnel. The free form capability for dealing with changes in curvature on tunnel parts is confirmed. The opposite constrained sides are enough to support the part under manufacture and no issue is observed. In what concerns the semi tunnels, as expected, a quasi flange configuration is formed due to the small ratio. However, the process showed that this smaller ratio is possible if the forming depth is limited to a shallow value, 15 mm for this part.

The T shaped part also gave good results. The manufacture of the part required the use of tool holders near the tunnel top where the formed geometry is parallel to the blank edge to avoid it raising movement. Nevertheless, the possibility of forming asymmetric shapes in tunnel parts is confirmed. The additional clamping is easily executable and remains the tunnel ends loose to allow a free movement. This achievement give greater support to the possibility enlarging the available workspace by leaving only the formed area unrestrained.

The L shaped part is also formed with the support of additional clamping in the centre. The perpendicular feature had no negative effect on the forming process. The reduced clamping area led a harder application of the clamping device result on little sliding of the material, harming accuracy. General appreciation of the part is still acceptable.

The P shaped part led to great results, with a similar behaviour as the S shaped part. The width variation has no effect on the process behaviour. In addition, this part showed that variable geometry walls produce better results than straight wall.

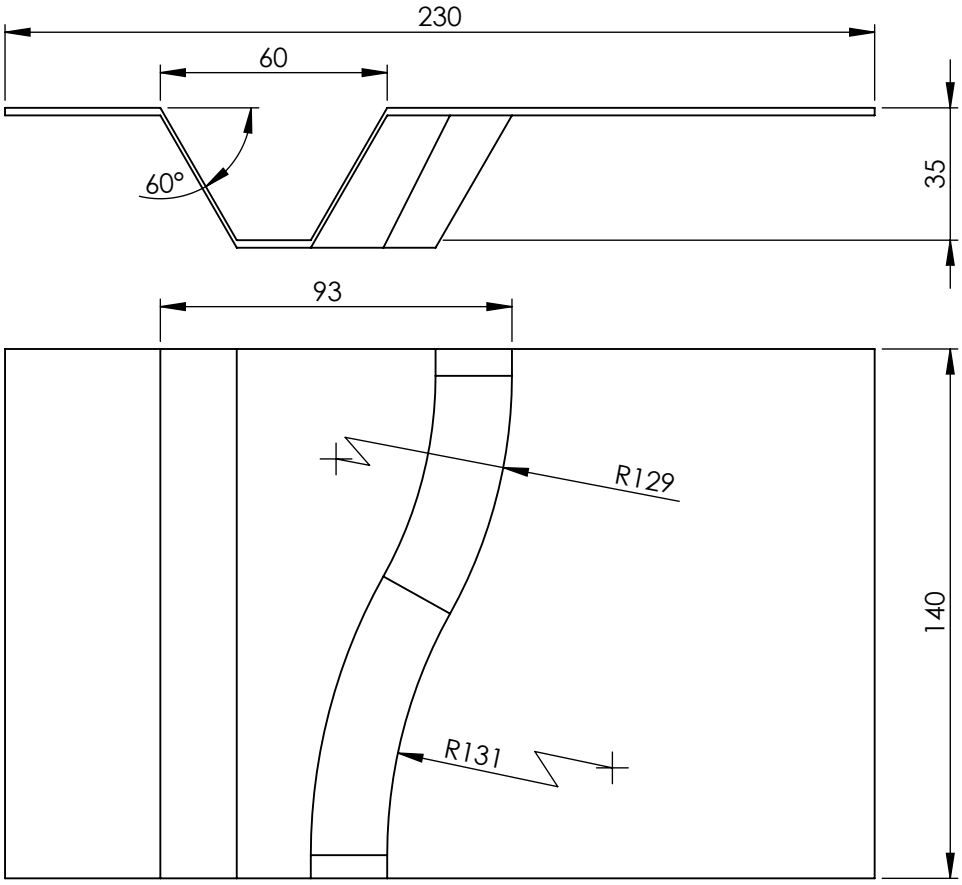

Figure 4.30: P shaped part drawing

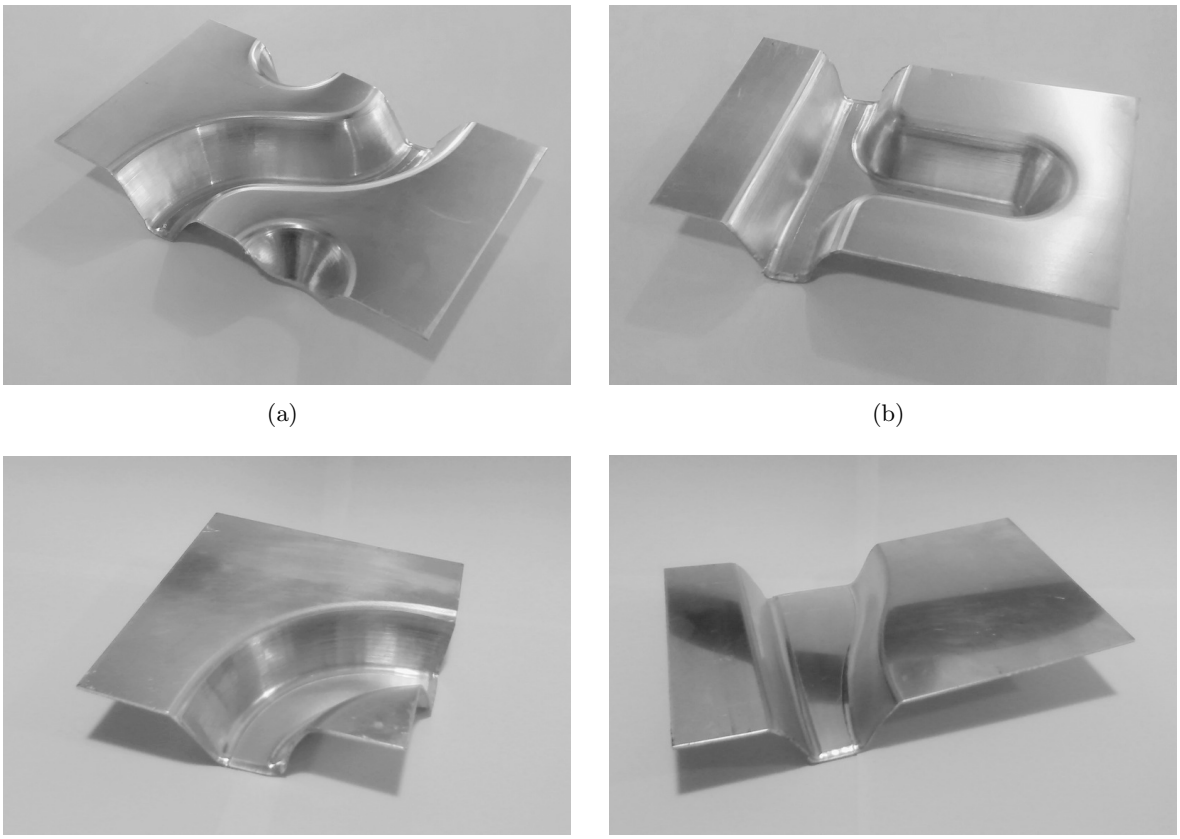

(a) (b)

(c) (d)

Figure 4.31: Tunnel type parts formed: (a) S shaped part, (b) T shaped part, (c) L shaped part, (d) P shaped part

4.2.4 Conclusion

The study concludes that, although the forming limit is reduced and the accuracy is lower than the container parts, it is possible to form tunnel and semi tunnel type parts using SPIF. This possibility increases the capability to adapt to different part geometry, allowing some saves in material and eliminating or reducing some post processing processes and allowing large parts manufacture.

A maximum tunnel forming angle defined by $\phi_{max,t}$ limits the wall angle of the tunnels, particularly near the loose ends. It is doable 68º walls with an accuracy bellow ± 5 mm when forming 2mm 1050-H111 aluminium sheet with a 10mm ball tip punch. An alternating tool path with the side changing position from one tunnel wall to the other outside the parts edge allows the better compromise between formability, accuracy and process time. An helical tool path with on edge side changing position is consider the most reliable when dealing with lower slopes. The tunnel geometry doesn't seem to affect the formability limits, being only restricted to the generic design guidelines as the container type parts. The possibility of forming up to ϕ_{max} in the centre of the tunnel is yet to be confirmed. Multi stage forming must be tested to explore getting higher slopes.

Tunnels are possible to form with different widths although larger features requires to place the sheet holder near the tunnel top. A free form geometry of the tunnel has little effect on the process, despite may require some additional clamping device and leaving only the forming area unrestricted. Contrariwise, the use of a free form wall with variable geometry may benefit the part quality when compared with a straight wall.

Semi tunnels are possible to form with length/width ratio greater than 1 as the bottom flanges when using smaller values. The depth of the semi tunnels may also affect its feasibility, being possible to form shallow semi-tunnels with smaller length/width ratios.

Major differences between incremental forming of conventional container type parts and tunnel parts relate with the failure modes. While in container parts failure happens by cracking due to excessive thinning, in tunnel type parts other damage can happen, particularly on the parts edge. The most common failure happens by tearing before cracking, limiting the $\phi_{max,t}$ to a lower angle. In addition, supplementary thinning on the tunnel ends may be noticeable due to tool contact, mainly when using on the edge side shifting position. Finally, forming strategies with outside side changing position can also face tool collision as the spring back effect exceeds the tool radius and avoids a smooth entrance.

In what concerns accuracy, current values are coarser than the typical SPIF reference. Forming strategies with plunge movements in the part center inflict a defect that affects local accuracy and part aesthetics. In addition, a lateral movement of the tunnel bottom due to the lack of rigidity adds to the spring back effect, leading to minor accuracy. Nevertheless, results are acceptable, mainly away from the edges and on freeform parts, where the forming behavior mimics the most the conventional forming process.

4.3 Design Guidelines for SPIF

4.3.1 SPIF Part Configuration

As mentioned, ISF process incrementally forms a blank sheet to the desired shape. Several confirmations types for a SPIF part are illustrated on figure 4.32. The configuration influence both the design and the processing of the part, influencing both the suitable sheet thickness, geometrical features and process tool path and parameters.

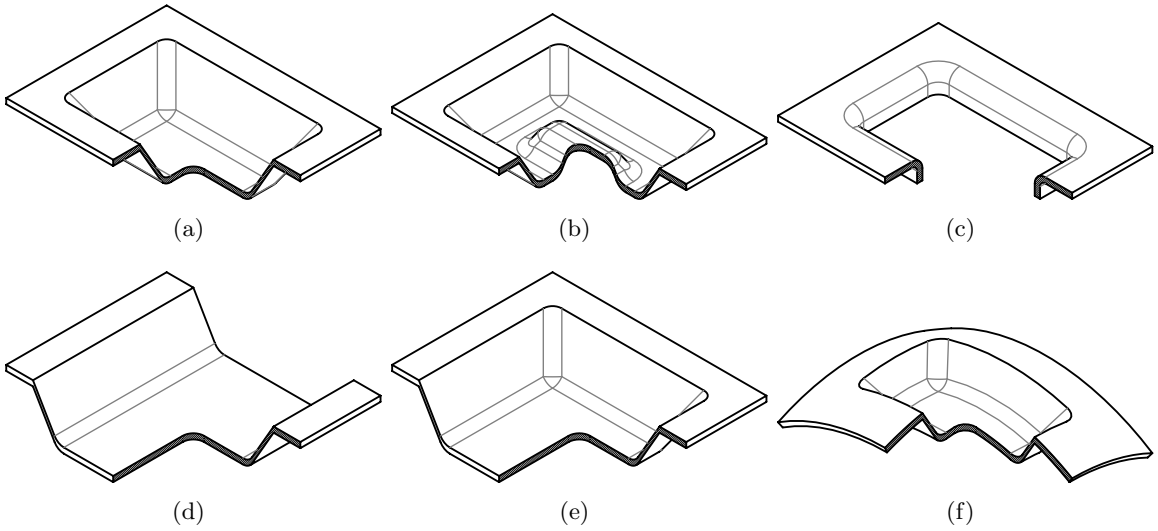

Figure 4.32: Possible SPIF part configuration: (a) container part, (b) "island" type part, (c) flanged part, (d) tunnel part, (e) semi-tunnel part, (f) pre-formed part

In addition to the shape configuration used during forming operation, the final part results from further trimming and finishing operations. Thus, the end piece may appear different from any of the presented shapes (e.g. trimming operation can completely remove the flat area of the initial blank, succeeding on a full curved part).

Single curvature container type parts

Most parts manufactured by SPIF consist on a single or multiple container type shapes. The part geometry comes out of a flat plate with a wall angle between 0 and ϕ_{max} from the edge to the center. Figure 4.32 (a) represents the basic configuration of a single curvature container part with one quarter cut. Inside the container, the part shape is virtually free-form, requiring its extension to the blank plane. The container type part configuration is the most common configuration of SPIF parts and allow the most versatile part design possible. A container shape can either define a full desired shape or can be the result of the surface extension up to the flat blank plane. The container type part configuration lead to the most cost affective compromise between part quality and process time and afford in most instances.

Figure 4.33 represents an example of 230×230 mm 1 mm thickness aluminium container type part of a 45^{o} 30 mm deep cone over a 30 mm twisted pyramid with a variable slope between 20^{o} and 40^{o}, formed with 0.25 mm vertical increments using a 10 mm punch.

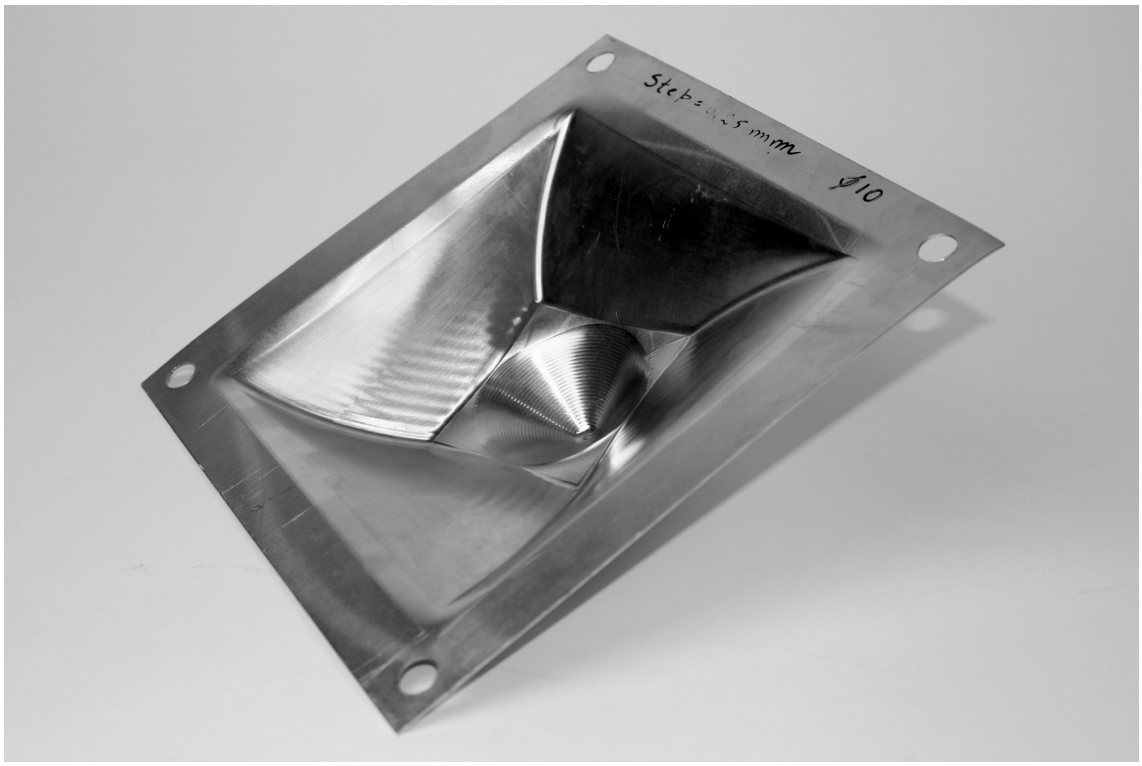

Figure 4.33: Container part example.

"Island" type parts

Despite the recommendation to design parts without changes in curvature, the SPIF process allows to attain higher complex parts, with two or more shifts in curvature. Nevertheless, it is important to understand that while using SPIF, each change in curvature direction requires a flip of the blank and the continue of the forming process in a new set up. Figure 4.32 (b) represents an island type part where a flip of the formed part is needed during the SPIF process. Simpler island configurations may only decrease the wall slope and be formed without a blank flip, but may lead to worst accuracy.

Other variations of ISF process like TPIF or DPIF may be better suited for this part configuration. The use of simple additional support to a SPIF procedure, in between SPIF and TPIF, could improve the decreased accuracy or avoid blank flips.

Flange type parts

Another option of SPIF process is to form free form flanges along parts. Figure 4.32 (c) represents a simple flange type part. Both inner and outer flanges can be formed and the forming limits are typically higher then in container type parts. As in the tunnel part configuration, ISF is proper suited for curve flanges, as other conventional processes are better suited for straight line flanges.

Tunnel and semi-tunnel parts

It is possible to perform ISF operations without a full clamp of the blank sheet, as proposed in section 4.2. By leaving one or two free sides, it is possible to obtain tunnel and semi-tunnel type parts. Figures 4.32 (d) and (e) represent the tunnel and semi-tunnel part configuration. The figure illustrates a simple straight line bent but the process allows to produce free-form parts. Figure 4.34 represents an example of 140×230 mm aluminium S shaped 65^{o} wall angle tunnel part, formed with 0.5 mm vertical increments using a 12 mm punch. It is noticeable a thickness reduction from 1.95 mm to 0.90 mm on the punch exit and to 0.80 mm on the entrance.

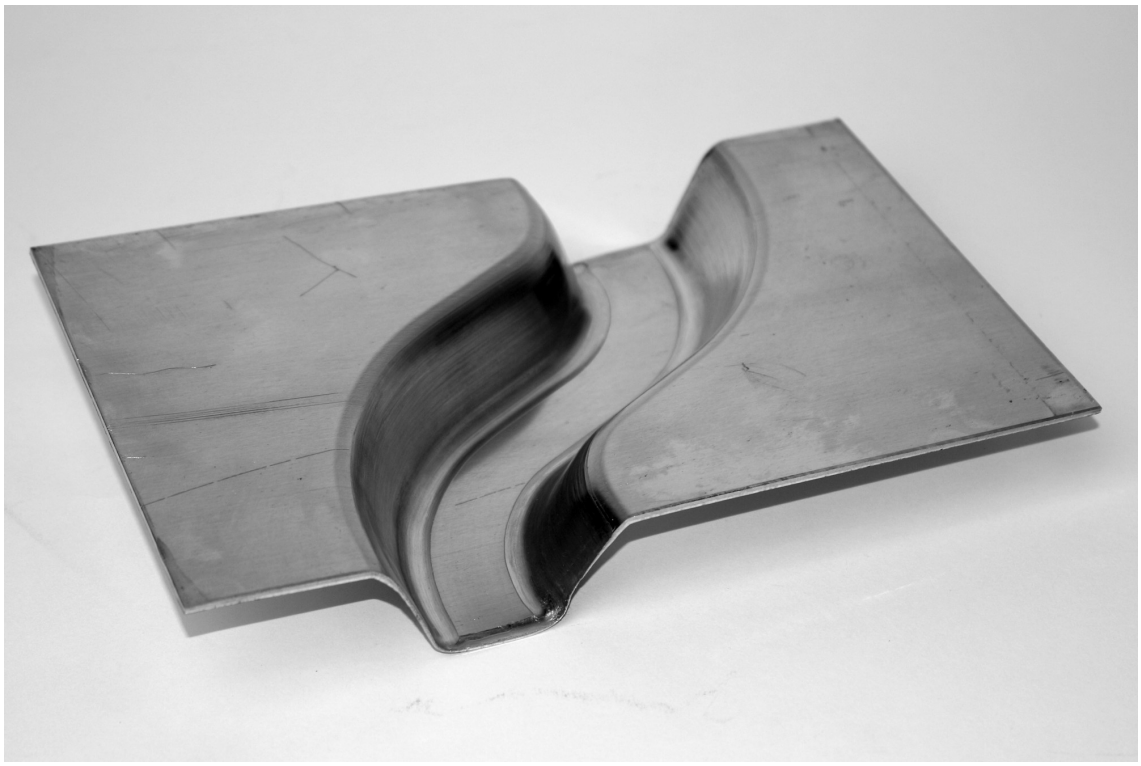

Figure 4.34: Tunnel part example.

Tunnel and semi-tunnel parts are widely used in different products and applications. The use of tunnel or semi-tunnel part configuration benefits the useful area of the part, reducing the amount of scrap and allowing the fabrication of bigger parts. In large parts, this configuration also benefits process time. A setback on forming tunnel like parts is the reduced maximum forming angle due to premature failure by tearing.

Pre-formed parts

A distinct option of SPIF process implies the use of other forming processes in an initial phase. ISF can be used to complement and surpass the limitation of other forming processes in the fabrication of prototypes, unique parts or small batches or for part customization of mass production frames. Figure 4.32 (f) illustrates a pre-formed part configuration, forming

a container type configuration on a pre spherical sheet.

A pre-formed part configuration replaces the flat blank by a stretch formed, deep drawing or bent part. Any type of the presented configurations can be used in a pre-formed part. Major restrictions result from an increased difficulty on clamping the part and higher complexity on the tool path generation.

A derivative part configuration is the post-formed part. After initial operations of ISF process, the part can be finished by complementary forming operations like bending or coinage. Welding operations are also often use in post-forming stage.

Tracing type parts

SPIF is finally a suitable process to form marks and low reliefs in sheet parts. A single or a few passage tool path strategy can be used to simply locally trace a sheet instead of producing a deep 3D shape (e.g. adding texture or lettering). Tracing operation can either be accomplished in flat sheets, incrementally formed parts or pre-formed parts. Figure 4.35 represents an example of a 170×170 mm 2 mm thickness aluminium traced part, post-formed by bending operations. Forming operation used a 6mm punch and a simpler 1mm vertical increment.

Figure 4.35: Trace part example.

4.3.2 SPIF Design Guidelines

A good part design starts with the right selection of the material and thickness. It is important to note that the SPIF parts are completed with other accessory processes as trimming, surface finishing, welding and others. Thus, the proposed guidelines for incremental forming should be considered attached to accessories processes restrictions. A good part project should look to the part feasibility and develop a detailed and accurate CAD model.

Materials and thickness

Although ISF processes are better suited for high formability materials, SPIF works with both metals and plastics sheet materials. Table 4.24 summarises some of the most used materials and thicknesses. A more extensive list of possible materials and thicknesses has been presented in the state of the art chapter.

Table 4.24: Materials and thickness suitable for SPIF.

Material	Alloy	Thickness
Aluminium	1xxx	0.5 to 3.0 mm
	3xxx	0.5 to 3.0 mm
	5xxx	0.5 to 3.0 mm
Steel	low carbon	0.5 to 2.0 mm
	DPxxxx	0.5 to 1.5 mm
Brass	—	0.5 to 1.5 mm
Cooper	—	0.5 to 1.5 mm
Titanium	grade 2	0.5 to 1.5 mm
PE	—	1.0 to 5.0 mm
PA	—	1.0 to 5.0 mm

The selection of material and thickness should take into account the required mechanical behaviour for the formed part as well as the consequent restrictions regarding the geometric features limitations.

Geometric features

The most important feature when designing a SPIF part is the wall angle ϕ. Furthermore, as specified by Adams and Jeswiet [82], limiting the part size to the available area and minimising the number of curvature variation is also relevant.

In addition to the defined orientation lines, generic extended guidelines for a SPIF part design are proposed. Figure 4.36 illustrates some of the most relevant guidelines:

- Avoid exceed the reference α_{max} angle, available on literature and table 4.25 for different materials and thickness (figure 4.36 (a)). Better results occur if the slope angle is kept away from the maximum value.
- Larger slope angles are possible at the cost of larger forming time and higher process complexity and risk of failure using multistage strategies (figure 4.36 (b)).
- Undercuts are possible at even more difficult and failure risk.

- Minimize changes in curvature between convex and concave shapes (islands). Smooth curvature changes that don't create islands are possible (figures 4.36 (c) and (d)).
- Avoid the definition of peninsula type geometries, mainly when the part is to be formed without a backing plate.
- Avoid abrupt gains of forming angle in a sloped wall.
- Parts may include more than one design feature, combining different shape configuration (e.g. multiple containers or combination of tunnels and containers).
- Limit the part area and depth to the machine workspace.
- Adequate the part size to the available sheet clamping system, considering both the part and the addendum surface.
- Avoid large flat sloped areas, unless accuracy for that region is not an issue.
- Avoid shallow sloped walls, unless accuracy is not an issue (usually bellow 20^{o}).
- Add reinforcement indents to large areas to improve accuracy and stiffness.
- Avoid large radii between the slope walls and the bottom or the top, unless accuracy for that region is not an issue (figure 4.36 (e)).
- Evenly distribute the depth of the part.
- Minimum feature should be greater than twice the sheet thickness (figure 4.36 (f)).
- Minimum top radius is zero, better results with small radius (figure 4.36 (g)).
- Minimum bottom radius equals the sheet initial thickness, better result using a value two to ten times the sheet thickness (figures 4.36 (g) and (h)).
- Minimum concave side radius should equal the bottom radius, better results if larger radii are used (figures 4.36 (g) and (h)).
- Minimum convex side radius equals the sheet thickness, better results if larger radii are used.
- Tunnel parts should be narrow, wide tunnels are possible at higher risk of failure.
- Semi-tunnel parts length/width ratio should be greater than 1.
- Special care should be taken with the blank cut to form flanges, mainly on small radius corners.
- Pre-formed parts should avoid changes of the curvature direction, mainly on small bending radii (change from convex to concave or vice verse).
- Pre-formed parts should consider features to ensure the part fixation and referral.

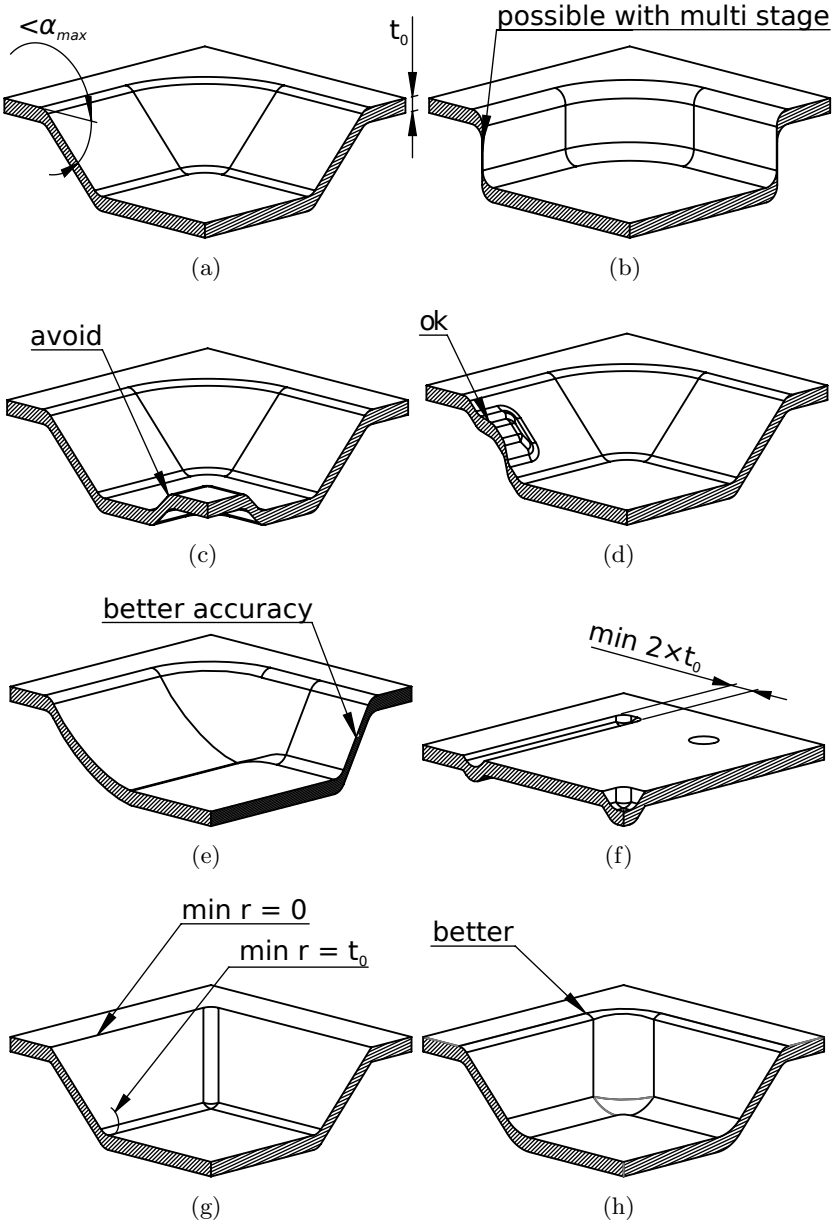

Figure 4.36: ISF part design guidelines.

Table 4.25: Maximum reference wall angle for single passage SPIF of container type parts.

Alloy	Thickness	α_{max} angle
AA 1050-O	1.5 mm	76°
AA 3003-O	0.85 mm	70°
AA 3003-O	1.2 mm	71°
AA 3003-O	2.1 mm	78°
DP600 steel	1.0 mm	68°
DP780 steel	1.0 mm	42°
DP1000 steel	1.0 mm	39°
HSS	1.0 mm	65°
brass	1.0 mm	40°
cooper	1.0 mm	65°
Polyethylene	3.0 mm	81°
smaller angle for tunnel type parts		
larger angle for flange type parts		

Following of the purposed guidelines helps ensuring it is possible to form a designed part without tearing or any other major failure. However, experimental testing may be required for some complex designs. Further, the desired accuracy or surface finishing required for the part may influence or limit the choice of the process.

It is also important to keep in mind that thinning occurs during SPIF and it affects the final shape. When the design requires the use of the bottom surface, final thickness should be considered. If the part has structural functions, it is recommended to analyse the mechanical behaviour of the formed part.

4.4 SPIF Cost Model

The definition of a process based cost model is defined under three steps. At the first step, a process model is defined. At the second step, an operation model is defined, taking consideration from the operation conditions. Finally, a financial model is defined based on the price factors and the first two models. A conceptual presentation of a process based cost model is presented on figure 4.37. A SPIF based cost model is developed based on these three stage model [136].

The SPIF process model uses the part design properties as inputs. Based on these properties, both related with geometry, material and part intended quality, the model aims to develop an algorithm to select and determine the best working parameters to manufacture a given part. This includes the forming tools selection and the definition of forming parameters. The operation model takes advantages of the determined forming parameters to determine the resource requirements, based on defined operation conditions. The model includes the definition of the setup operation and the production operations, determining operation time, material and energy consumption. The cost model determines an estimated cost per part for a given batch size. This model uses the processing requirements and resource requirements as inputs, and determine the process cost based on factor prices. The model cost elements are the used material, including scrap, energy consumption, labour, tooling cost and forming equipment.

Due to the SPIF process being mainly suitable for unique parts or very small batches, where other manufacturing processes coexist, other cost elements are not considered. Cost elements regarding logistics, overheads or taxes should be considered in a complete analysis for a product manufacturing, where the SPIF cost model and other manufacturing cost models are included [137].

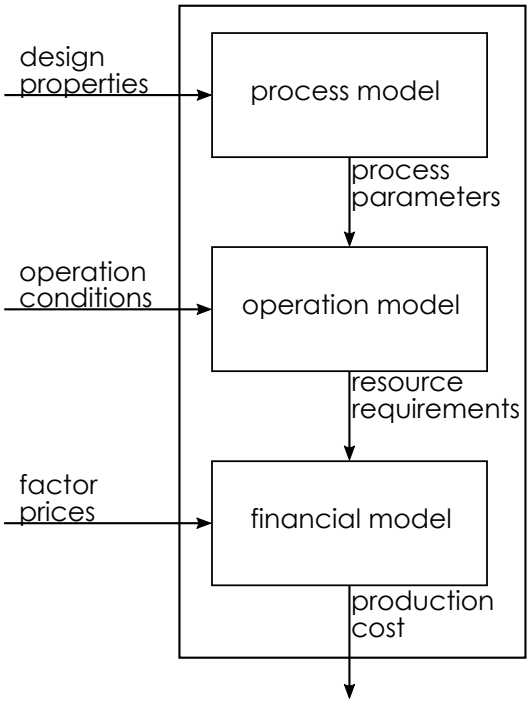

Figure 4.37: Process based cost model

4.4.1 Process model

The SPIF process model aims to select suitable forming tools and strategies for the manufacture of a given part, determining the preferable forming parameters. This algorithm is based on a set of geometric features of the part that are used to compute the most relevant processing requirements.

The input includes a product description organised by the geometric properties, the material properties and the intended part quality. Table 4.26 summarises the input parameters for the process model, including both intrinsic and resultant design properties. In what concerns the geometric definition, the model requires information on the part size, wall angle, and minimum design feature size. The geometry definition is completed by selecting the most adequate part configuration. The sheet material definition is set by defining both the material and the initial thickness. The input ends with the definition of the intended accuracy and surface finishing, considering three different quality levels for each parameter.

Table 4.26: Input parameters for the process model

Process stage	Input parameters	Units
Part geometric properties	Part length	mm
	Part width	mm
	Maximum depth	mm
	Formed area	mm^2
	Maximum wall angle	degrees
	Top perimeter	mm
	Minimum side radius	mm
	Minimum bottom radius	mm
	Part configuration	list
Material	Material	list
	Thickness	mm
Intended part quality	Accuracy	list
	Surface finishing	list

Concerning the outputs, the model targets the forming tool selection and the process parameters. Table 4.27 presents the output factors of the process model. The forming tool selection includes the determination of the need for the use of a backing plate and the settlement of the number of punches to use and their size and tip geometry. Regarding the forming operation, the model test the part for the need of multistage forming and selects adequate forming parameters. Those parameters, as well as the input data are used to estimate the tool path length and forming time.

The forming strategy definition is first determined by selecting the number of forming stages, considering the maximum wall angle and the desired accuracy and surface finishing. When the maximum angle of the part is lower then the maximum forming angle approximated by the material and thickness, the forming strategy uses a single forming strategy with an additional finishing strategy if high accuracy or good surface finishing is intended. When the part's angle is greater, one additional stage is suggested per every 5 additional degrees.

The intended accuracy and surface finishing are also used to determine the recommended step down. At first instance, for a good or fair surface finishing a 0.5 mm is selected and for a rough surface a 1.0 mm is selected. For a high part accuracy, a finishing pass is used with

Table 4.27: Output parameters from the process model

Process stage	Output parameters	Units
Forming tools	Need of backing plate	binary
	Number of forming tools	number
	Tool(s) diameter	mm
	Tool(s) tip radius	mm
Forming parameters	Number of stages	number
	Step down increment	mm
	Tool path length	mm
	Feed rate	mm/min
	Forming time	minutes

the same step down. For a good surface finishing a 0.1 mm finishing pass is used. A course accuracy part dispense the use of a backing plate.

If the sheet material ultimate strength is greater then 400 MPa, the vertical step down is limited to 0.5 mm. If the ultimate strength is greater then 800 MPa, the vertical step down is limited to 0.1 mm.

The first definition for the tool diameter consider a spherical tip tool sized by the part side radius. The tool diameter is first calculated by decreasing 1 mm to the minimum side radius, avoiding sharp turns when contouring radii. The closest smaller tool from the available list is then pre-selected. The selected tool is compared to the bottom radius. If too large, the tool diameter is reselected to be smaller or equal than that radius. If the bottom radius requires a tool too small, a second forming stage is required using a toroidal tool with the bottom radius defined by that radius.

A recommended minimum tool diameter is calculated by keeping the stress under 35 MPa considering the force estimation given by equation 2.4. Tool sizing considers this reference value and suggest to increase part radius if the tool integrity not assured.

The limitation of the vertical step down and the recommendation of larger part radius helps ensuring a feasible forming operation, without significant punch flexure or yielding rick. The tool length is not considered as tapered forming tools can safely be used due to the part angle.

The tool path feed rate speed is determined from the difference between the minimum side radius and the selected forming tool radius. A minimum feed rate of 750 mm/min is intended if sharp turns exist during the forming operation. A maximum feed rate of 9000 mm/min is defined for tool path countering equal or superior to 30 mm.

The tool path length is approximated considering the area to be formed, the part height and the defined step down. This approximation is considered both valid form constant slopes and variable slopes.

An average perimeter of the sloped walls is calculated by dividing the formed area by the part depth. Since the tool diameter is sized to always contour the side radii, avoiding sharp turns, each tool path loop length equals the part perimeter at the given z minus $\pi \times \varnothing_t$. The tool path full length is calculated by multiplying the average perimeter by the number of loops, which is determined by dividing the part depth by the forming step down.

Since the determined length is an approximation, the same value is used for different stages of a multistage operation with the exception of finishing passages. Thus, if the forming

strategy uses no finishing strategy, the total forming length is calculated by multiplying each stage length by the number of stages. If the strategy uses a finishing forming stage, the last stage length is calculated using the finishing step down. The forming time is calculated by dividing the tool path total length by the feed rate speed.

The blank is sized based on the part length and width, considering the defined material thickness. For container, island or traced type parts, the blank area is rounded up from the part size to the closer multiple of 100 and, if needed, increased to the machine minimum value. For tunnel or semi-tunnel configurations the blank length is dimensioned by the same method. The blank width equals the part width on tunnel parts and is rounded up to the closer multiple of 50 on semi-tunnel parts.

4.4.2 Operations Model

The operation model is developed considering the common steps to incrementally form a part. The model aims to defined the operation times in order to be used in the cost model. This considers both the operations performed for beginning the manufacture process and the operation time per formed part. In addition to the operation time, the model determines energetic consumption and environment footprint. The model is loaded with data measured from the use of the SPIF-A machine. These measurements include average operation times and the developed energy consumption model. Nevertheless, it can be updated with time and energy consuming information from other forming systems.

The new input parameters considered for the operation model are summarised is table 4.28. These parameters include information about the forming operation in a functional, energetic and environment impact approach. The criterion include data do model the complete forming operation, from the job preparation to the material handling e machine operation. This allows to determine and estimation for the preparation work and the manufacture time per part. Apart from these specifications, the model considers the output parameters from the process model, presented in table 4.27, as well as some of the design inputs, presented on table 4.26.

Table 4.28: Input parameters for the operation model

Process stage	Input parameters	Units
Starting Labour time	CAM programing average time	min/forming stage
	Machine table setup time	min
	Tool changing time	min
Forming Labour time	Standard table sheet clamping time	min/clamping side
(per part)	Additional time for larger tables	min/50mm additional length
	Machine power up time	min
	Part referral time	min
	Forming operation following up time	minutes
	Part release time	min/clamping side
Forming operation	Power up energy consumption	kW.h
energy consumption	Part referral energy consumption	kW.h
(per part)	Forming operation energy consumption	kW.h/min
	electric consumption CO2 emission	kg CO_2/kW.h
	oil consumption CO2 emission	kg CO_2/cc
	material consumption CO2 emission	kg CO_2/kg

The operation model determines the most relevant procedure stages. The model outputs are summarised in table 4.29 in two groups, considering labour alone time and forming machine operation time and energy consumption.

Table 4.29: Output parameters from the operation model

Process stage	Output parameters	Units
Labour time	Start and finishing time	min
	Handling time	min/part
	Forming following up time	min/part
Machine operation	Power up time	min/part
	Forming time	min/part
	Energy consumption	kW.h
	CO2 emission	kg CO_2

In a first stage, it is considered the labour time to start the manufacturing process. This start time considers the strategy definition time and the machine set up. It is considered the time for the tool path programing. The model considers an average time for a tool path stage CAM programming as an input and multiplies it by the number of forming stages. In addition, the start time includes the machine set up for starting the forming process of a given part. This set up includes a tool change time as an input, needed for every part. If the blank size differs from the forming machine default table size, the start time adds the reconfiguration of this table. In this case, a process end time is also considered to reset the forming table to the default size.

On a second stage, the operation time per part is considered. This includes the blank handling, the machine initialisation, the forming process and the part release and cleaning. To simplify the model, all handling operation are included in the same index despite occur before or after forming. Thus, four different times are determined: handling time, machine power up time, forming operation time and forming operation follow up time.

The handling time includes the blank clamping before the forming operation and the part release and cleaning after forming. The total handling time is determined based on the part configuration and the blank size. The operation includes clamping two, three or four sheet sides depending on the part configuration. The clamping considers a base time per side of the standard table size and an additional time for larger blanks. Whenever the tool path strategy includes the use of more than one tool, the handling time includes a proportional tool changing time. Besides, the camping and releasing time is doubled when dealing with "island" configuration parts, where a blank flip is needed.

The power up time is calculated by adding the machine power up time and the sheet metal referral. This value is also increased proportionally according to the number of different tools to use and doubled when dealing with "island" configuration parts.

The forming operation time is equal to the forming time, determined by the tool path length and the feed rate speed. The forming operation follow up time equals this value while limited to a maximum input value.

The operation model presents the handling time, power up time and forming operation time graphically for a comprehensive reading.

The energy consumption is determined according to equation 4.1, determined in the energetic analysis of the SPIF-A machine. However, form a more detailed and feasible approxima-

tion, the fix term of the equation is affected by the number of machine power ups and sheet referral needed to complete the part. The time depended term of the equation is calculated by the forming operation time.

Finally, the CO_2 equivalent emissions are calculated considering the machine operation and the forming process. Regarding the machine operation, the environment impact considers the electric consumption and the useful life of the hydraulic system oil. For the forming process, the CO_2 equivalent emissions considering the portions related to the lubrication oil consumption and to the material consumption.

4.4.3 Financial Model

At the final stage of the SPIF based cost model, a financial model is developed. This considers all the outputs from the process and operation models as well as price factors to estimate the part SPIF process cost. Thus, the completed process based cost model provides various resources requirements in cost and time for the development of SPIF parts or its inclusion along with other manufacturing processes.

Apart from the previous outputs, the cost model several fix and variable costs, as presented on table 4.30. These inputs include material and energy cost, labour and machine operation. Besides, the input parameters adds information on the intended batch size to frame the cost evaluation.

Table 4.30: Input parameters for the cost model

Process stage	Input parameters	Units
Tools	Backing plate material cost	€/m^2
	Backing plate cut cost	€/m
	Punch wear cost	€/(m^2.N)
Forming operation	Material cost	list of €/m^3
	Labour cost	€/hour
	Machine operation cost	€/hour
	Batch size	Number of parts
Energy	Energy cost	€/kW.h
	CO2 emission cost	€/kg CO_2

The cost model outputs the expected cost per part, considering a certain production lot. For this, the model considers the tooling develop and wearing cost, the labour, the forming machine use, the material cost and the energy cost, as presented on table 4.31. These parameters allow an financial evaluation of the use of the SPIF process according to the number of parts to produce.

As in the operation model, in a first stage the cost model determines the cost associated to the manufacturing process beginning. Despite very low when comparing to conventional forming processes, this cost includes the job preparation and, if needed, the tool path fabrication.

A start and finishing cost is calculated by product of the start and finishing time and the labour cost. A backing plate cost is determined considering the backing plate material cost and a cutting process based cost model with a cut with the length of the part perimeter.

In a second stage, the model determines the production cost per part. The material cost considers the blank area and thickness. Thus the blank material cost is calculated

Table 4.31: Output parameters from the cost model

Process stage	Output parameters	Units
Work preparation	Start and finishing cost	€
Tooling	Backing plate cost	€
	Punch wear cost	€/part
Material	Blank cost	€/part
Forming operation	Handling cost	€/part
	Power up cost (machine and labour)	€/part
	Forming cost (machine and follow up labour)	€/part
	Energy cost	€/part
	Environment cost	€/part

based volumetric price of the selected material. The total labour cost is calculated from the handling time, machine power up time and forming operation follow up time. The machine operation cost is calculated from the machine power up time and forming operation time. The energy cost is determined based on the energy consumption. A forming tool wear cost is estimated considering the tool size, tool path length and forming force. The environment cost is determined based on the equivalent CO_2 emissions.

The number of parts to produce is used to determine the estimated cost per part, considering the starting and the manufacturing cost. The cost per part is presented graphically in function of the number of parts to produce.

4.4.4 Process based cost model validation

A SPIF based cost model is developed and implemented using scilab, including the definition of a graphic user interface. The developed script is presented in appendix D.

The input values for the process model and the operation model are set based on the experience of the SPIF-A machine operation. The input values for the financial model are based on multiple online reference, considering the portuguese reference values. For a more convenient use of the developed SPIF cost model, a graphic user interface is developed. Figure 4.38 present the output result from the default example.

For the cost model validation, it is used to calculate the cost estimation for the case study parts, presented in chapter 5. Table 4.32 presents the cost estimation determined by the cost model against the determined cost, calculated from the measurements during the part manufacture. When applied, the cost of finishing processes is subtracted to the calculated value. Except for the larger part, the cost model succeed to predict the part manufacture cost within a $\pm 20\%$ error.

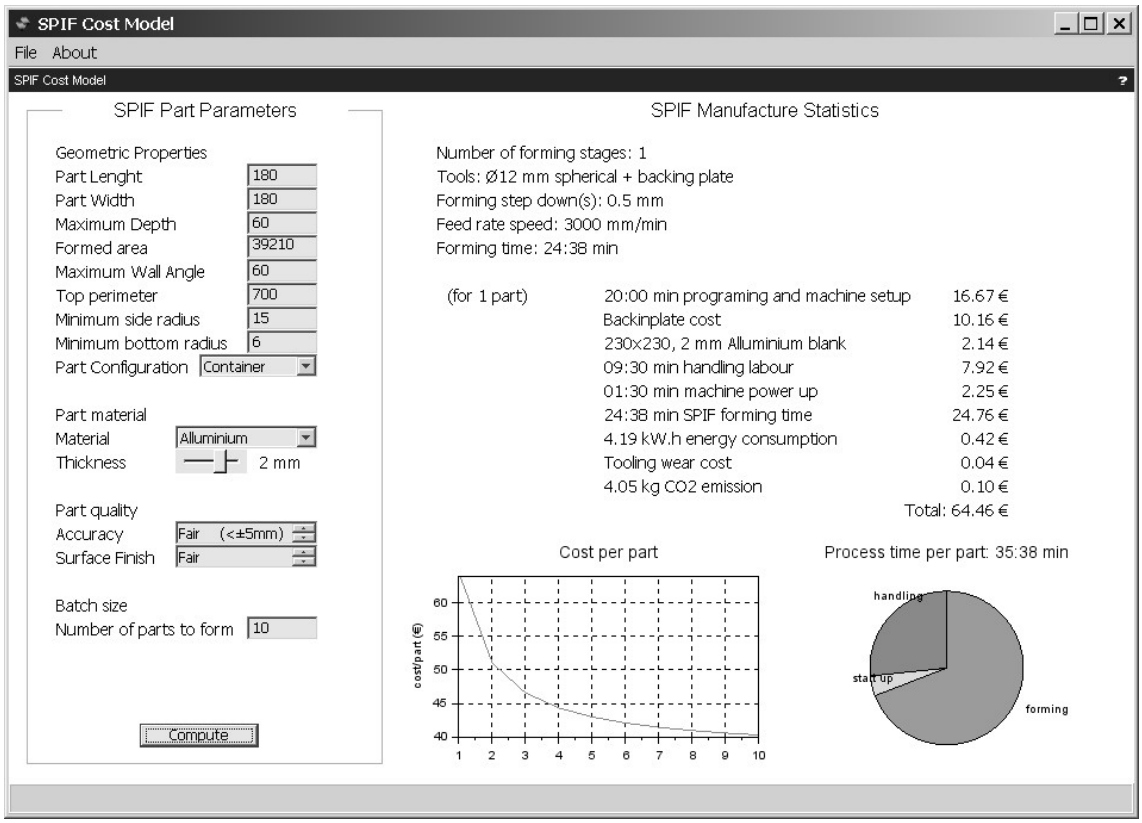

Figure 4.38: SPIF cost model graphic user interface result output

Table 4.32: Comparison between cost model calculation and case studies

Case study part	Cost model cost estimation	Case study average cost	error
Pan (considered as a container)	169.14€	206€	-17.9%
Car fender support	85.50€	97.5€	-12.3%
Seat panel mould	271.25€	178€	+52.4%
Bike tank	90.58€	78€	+16.1%
Hopper	47.64€	43€	+10.8%
Stool	149.21€	182€	-18.0%
Facade panels	69.80€	65€	+7.4%

Chapter 5

Fabrication of Sheet Metal Parts

For the validation of the initial purpose of the SPIF process, specific industrial applications are tested and analysed as problem orientated case studies. The formed parts are representative from different fields of application. The case studies test the use of SPIF for the manufacture of prototypes, pre-series, obsolete part replacements, unique parts and custom parts.

In the course of the case studies, different part configurations are used and the SPIF operation is performed using multiple strategies. The part manufacture not only validates the possibility of using SPIF to help solving industrial problems but also deliver study outcomes that can be used in future operations. As the presented examples are performed alongside the SPIF development study, some of the conclusion contribute to its improvement, particularly to the definition of the design guidelines presented in section 4.3 and to the definition of the process based cost model presented in section 4.4.

For the definition of the case studies, different approaches are taken. On the one hand, partnerships with industrial companies are established in order to work on real industrial problems. In these cases, SPIF is evaluated against other manufacturing alternatives, particularly conventional forming processes. On the other hand, the availability of companies interested in the collaboration with the PhD workplan is limited. Thus, two different paths are taken. Partnerships are established with other entities interested in developing projects that involve the manufacture of sheet metal parts. This includes designers, other scientific research groups and sport teams, each presenting different challenges and enabling experiments in various fields. Finally, some case studies are performed in in-house projects, using SPIF for the development of parts for very specific applications.

During the case studies development and analysis the process elaboration and results evaluation is adapt depending on the main goals for the developed part. All examples include the presentation of the goal geometry through the CAD model and drawings, the description of the forming operation and the presentation of the formed part. In what concerns the forming operation, various strategies are tested for the best results. The operation time is measured, including the development of backing plates or other support tools, the machine set up and the forming process. The energy consumption is measured and taken into consideration, mainly when multiple parts are to be formed. The forming operation is photographed and described to state guidelines for future parts. After forming operation, the parts are finished before quality evaluation, including post-forming operations, trimming, drilling and joining. The part final geometry is measured and validated against the design requirements. A qualitative evaluation is also performed considering the part performance and aesthetics.

5.1 Prototyping domestic appliances parts

A partnership is made with Silampos® S.A., regarding the fabrication of metal tableware prototypes. The goal is to develop prototypes for the presentation of final products before the mass production. Due to confidentiality agreement, the indented geometry an product application can not be fully presented. The formed part should be accurate enough to coexist with other parts of the assembled product and the surface finishing should be as similar as possible to a finished market part.

The proposed case study involves the fabrication of a prototype of a dedicated container for a domestic appliance. The part consists on a 210 mm diameter with 190 mm height pan with a circular indent on the bottom of the part and two slot features on the part's side, as shown on figure 5.1.

The prototype uses a pre-formed configuration SPIF part. A primary geometry is obtain through deep drawing by using reused tools in a 0.9 mm stainless steel sheet. This pre-form is then fixed in various set ups in the camping table and subjected to a multistage SPIF operation, forming different geometric features. The pre-form is fixed upside down to form the circular indent at the pan bottom and sideways to form the two slot indents on the side.

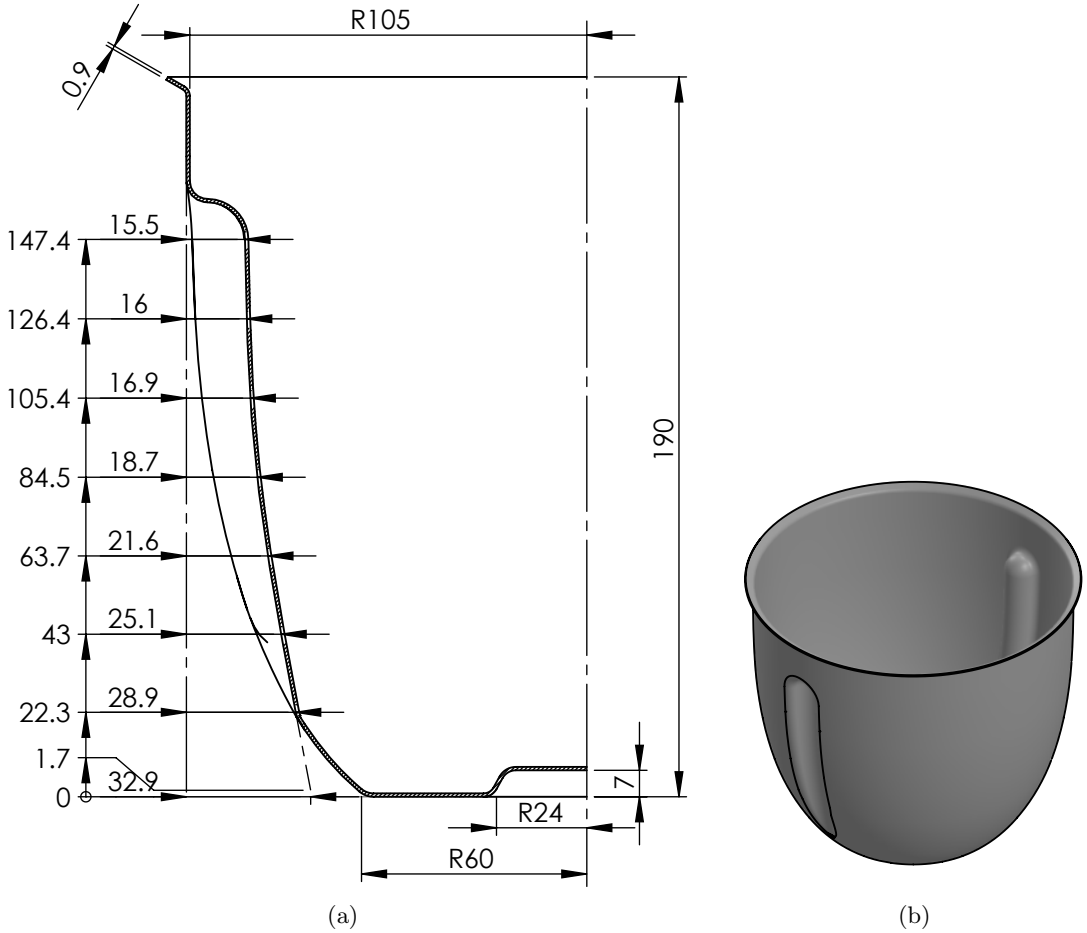

Figure 5.1: Dedicated pan for a domestic appliance: (a) drawing, scale 1:2, (b) CAD model, scale 1:5

The forming operation with the pre formed part requires a change in the SPIF-A machine set up due to the increased part height when compared to a conventional flat blank. This machine set up takes longer due to the need of adjusting the table height. The ribs are formed with the part positioned sideways. As the part has a 210 mm diameter, the table position needs to be lower by 180 mm. This makes the Z zero to be defined close to machine minimum position but since the tool path is close the xy origin, and the Z decreases as Y increases, it leads to no workspace restriction issue. This decrease of the table position is also compatible with the forming operation at the part bottom. The machine set up is reset at the end of the operation, considering it for the complete process analysis. The change in the table height not only has to deal with the position variation but also ensure the forming table level.

On the first test operation, the forming strategy uses a helical tool path strategy, forming the indents outside-in from the pre-formed geometry, in a straight forward adaptation from single container parts to pre-formed parts. Due to the parts curvature, the side elements requires the motion of X, Y and Z axis at once, adapting the horizontal flat step by step strategy to a curved surface. The tool path is parametrised to use a 0.1 mm constant step down in a helical path, forming with a 20 mm ball tip punch. The tool was chosen based on the part geometry and the material stiffness. Due to the great material stiffness and the sharp turns on the tool path ends, the forming operation is performed at 1000 mm/min.

For the side indent, the pan is positioned sideways and fixed from the inside using clamping blocks style sheet holder. The bottom is positioned vertically and used to reference the height direction. The radial direction is referenced at the centre of parts top. The forming operation of the bottom side is much easy since it is similar to a simple container configuration. Figure 5.2 presents the forming operation of a circular indent on the bottom of the part (a) and a slot indenting feature on the part's side (b).

(a) (b)

Figure 5.2: SPIF forming operation of a pre-formed pan: (a) bottom indent, (b) side slot indent

Due to the lack on stiffness of the pre-formed part, it is not possible to obtain an accurate part. The forming load causes the part to make the circular part oval under elastic deformation, causing a great spring back effect. The large scale deformation absorbs almost all the tool vertical movement, resulting on a very under formed part. Over forming operation fail to compensate for this phenomena since they lead to a permanent deformation of the pan radius instead of forming the indent. The operation on the part bottom is again much simpler.

To minimise this occurrence, a reinforcing structure is developed and built. The structure consists on a central part with six threaded rods that are tight to the part inside. This structure helps avoiding the ovalisation of the pan while adapting to radius differences between preformed parts. This structure uses six M8 screws and nuts as rods and the centre part is milled from standard M30 nut, taking advantage from the predefined hexagonal shape. The structure manufacture and assembly takes close to one hour.

The forming operation is repeated using the same tool path strategy. Figure 5.3 presents the new forming operation, where the reinforcing structure is visible at 5.3 (a). The use of the developed support avoids the global deformation of the part, benefiting the forming operation of the indents. The process starts forming from the outside, defining the feature footprint as seen in figure 5.3 (a). The forming operation is performed in 20:48 minutes, including machine startup, part position referencing and forming operation, with a total energy consumption of 3.4 kW.h. As the forming operation continues, the concave surface is pushed to the centre, resulting on compression forces along the sheet. This occurs due to the attempt of changing the curvature direction from concave to convex inside the indent. On the tangential direction parallel to the bottom, an arc with an average radius of 100 mm and length of 31.4 mm is transformed into a cavity, passing trough a flat state 31.2 mm wide. On the perpendicular direction, an approximated arc of 365 mm radius with a 149 mm length is forced trough a 148 mm long flat state. This result on a two direction plane compression stress during the forming operation. This state of stress, in addition to the spring back effect, causes the formation of wrinkles as seen in figure 5.3 (b), dues to the inability of compressing the sheet.

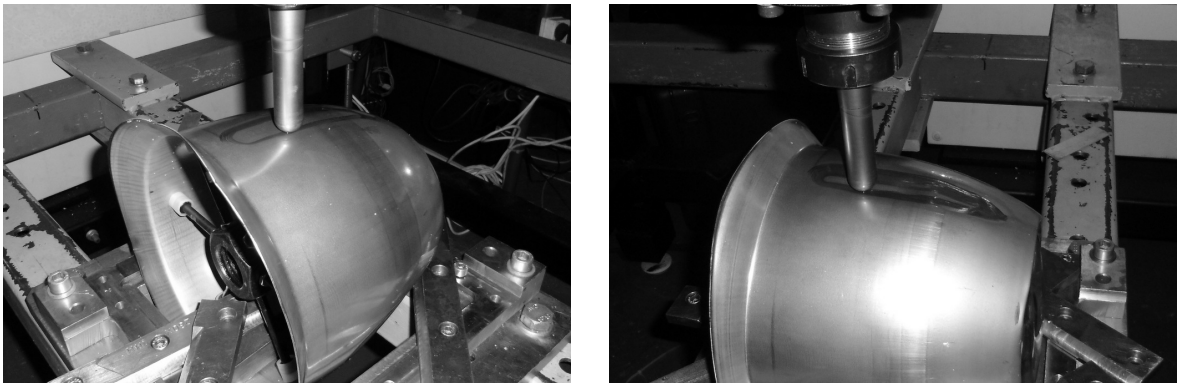

(a) (b)

Figure 5.3: SPIF forming operation of a pre-formed pan with a reinforcing structure: (a) first forming steps, (b) deeper forming steps with wrinkles starting to develop

The forming tool path is reprogramed to work with an 2 mm vertical over forming to attempt to minimise the defects. The new operation is performed in 26:38 minutes with a total energy consumption of 4.1 kW.h. Although the result is slight better, wrinkles are still formed and the new process lead to instability in the part positioning.

The creation of the wrinkles is particularly increased as the material is pushed alternatively from the top to bottom and from the bottom to the top due to the helical tool path. The wrinkles position is shifted downward and upward the indent, propagating damage along the part. Besides, the cyclic change in the tangential forming force direction during the forming operation harms the camping system. Since the part is support near the part rims but

clamped only from the inside, no issues occur when the tool is moving to the bottom but the part tends to rise when the tool is moving back in the opposite direction. This rise movement can lead to a small change of the part position, compromising the results.

Since the wrinkle is caused on the metal sheet partly by the change of forming direction, a simplified alternative tool path strategy is tested. The new tool path is based on the rib bottom geometry centre line, defining all the forming strategy based on the final step. Apart form trying to improve the rib geometry, the new strategy aims to avoid forming forces in a upward direction, benefiting the part fixation.

In the new forming strategy, the punch plunges at the top of the rib, close to the upper rim of the pan. The plunge movement defines the slot upper end. The tool follows a movement down the rib and going out at the part bottom, propagating the deformation along the indent feature. All forming steps are performed parallel to the final one, aiming for the final rib geometry without requiring contour changes. All tool path is performed along the YZ plan, avoiding X movements by using a 20 mm tool equal to the rib width. The new strategy uses a 0.5 mm vertical increment and the tool path is prolonged beyond the indent geometry, leading to an over forming operation up to -2 mm. Since the sharp turn between the plunge movement and the quasi horizontal forming movement, the feed rate is kept at 1000 mm/min. Figure 5.4 present the forming operation with the new strategy. The tool scratch marks reflect the tool motion along a line instead of contouring. Figure 5.4 (a) shows particularly the increased deformation under the punch recovered by the spring back, with forming forces up to 2000N. The use of the new tool path strategy benefits the part clamping, being able to run until the end without any part movement. The new forming strategy is performed in 15:10 minutes, including machine startup, part position referencing and forming operation, with a total energy consumption of 2.4 kW.h.

(a) (b)

Figure 5.4: SPIF forming operation of a pre-formed pan with a simplified tool path

The use of the new tool path strategy benefits the forming results. The tool path rise to achieve an indent with acceptable geometry, anticipating its validation. During the forming operation, a wrinkle is still formed due to the change in curvature direction. However, the defect first appear near the part top and is shifted downward until it disappears, as presented in figure 5.4 (b). The bending phenomena caused by the forming operation leads to a continuous formed geometry despite the use of a single plunge direction movement. The first formed rib is used as an aid to repositioning the part to form the second feature.

The completed part is measured for and quantitative evaluation. The part is positioned sideways in the CMM and the rib indent profiled is measured using a 6 mm touch trigger probe. Figure 5.5 presents the measuring results of the slot profile. Despite the maximum deviation of +9.2 mm between the formed slots and the CAD model, the formed part can manage to fulfil the prototype requirements. The biggest deviation is found at the top of the indent, failing to achieve a spherical end. Besides, significant deviations are found along the tangential direction, due to the inability of forming well defined bends because of the absence of a backing plate, reaching values of −4.6 mm. In what concerns the slot indent depth, the accuracy improves towards the part bottom, by veer from the indent end. The average deviation of the indent deep along all the lenght is +3.2 mm. After the first 30 mm of the indent top end, an accuracy of ±5.0 mm is found. Despite being too high for a production part, this error is compatible with the prototype development.

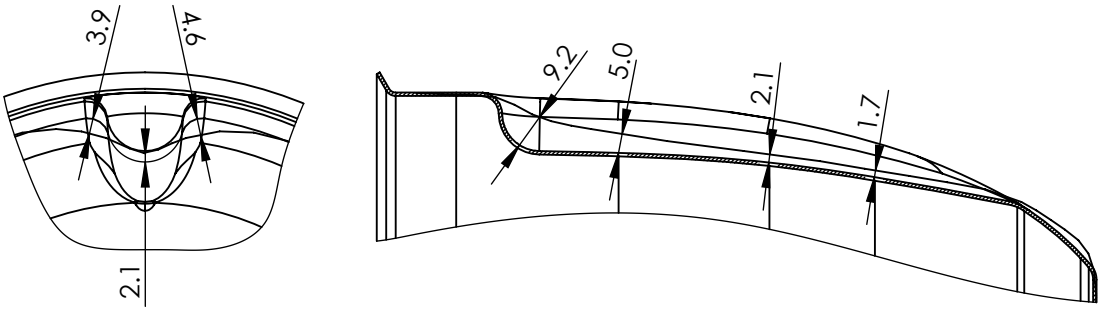

Figure 5.5: Dedicated pan for a domestic appliance prototype measurement

The formed prototype of the dedicated pan for a domestic appliance is presented in figure 5.6. It is visible both the inside and outside of the slot ribs as well as in inside of the circular indent. The part finishing process is missing the preformed flange trimming and surface finishing operations, since those operations are not relevant to the incremental forming case study.

Figure 5.6: Dedicated pan for a domestic appliance prototype manufactured by SPIF

With regard to the full process analysis, the prototype development from the preformed part takes close to four hours, with a total energy consumption of 5.8 kW.h and a total manufacture cost of 206€. Table 5.1 summarises the considered operation for the full process analysis. Despite the high cost value, only 30% relate to the part handling and forming operation, while the remaining cost due the set up of the machine and job preparation. Thus could drastically reduce manufacturing cost per part if more than one is to be produced, even if all different, as parts could share the machine setup and the reinforcement structure.

Table 5.1: Pre-formed pan full process analysis

Operation	Time	Energy	Cost
Preformed pan fabrication	n.a.	n.a.	n.a.
Reinforcement structure fabrication	1:00	$\lesssim$ 0.2 kW.h	55€
CAM programing	0:10	n.a.	8€
SPIF machine table setup	0:45	n.a.	38€
Tool change	0:05	n.a.	4€
Part fix	0:10	n.a.	8€
Slot indent forming	0:15	2.4 kW.h	14€
Part reposition	0:05	n.a.	4€
Slot indent forming	0:15	2.4 kW.h	14€
Part reposition	0:10	n.a.	8€
Circular indent forming	0:05	0.8 kW.h	7€
Part release and cleaning	0:10	n.a.	8€
Restore SPIF machine table setup	0:45	n.a.	38€
Complete process	3:55	5.8 kW.h	206€

The development of the dedicated pan for a domestic appliance prototype case study contributed with relevant information to the study of the SPIF process, particularly to the used of preformed parts. The ability to form over preform parts is one of the ISF biggest advantage when comparing to conventional forming processes, making possible a mass customisation on industrial parts. However, special care must be taken with the reconfiguration design. Changes in the curvature direction impose compression forces on the sheet that harm the part quality. Besides, it is important to grant the possibility of clamping or fixing the preformed part, and ensure it is stiff enough to support the forming loads.

Relatively to the possibility of using SPIF for the development of prototypes, it is validated the feasibility of using SPIF to support the product design and development process, including product presentation. The case study deals with a hard to form material using a lesser studied part configuration, still achieving acceptable results. Thus, it is acceptable to assume that simpler situations can be fulfilled in a much straightforward way and reaching great results. The case study contributed to the validation of the use of ISF process for models and prototypes development.

5.2 Prototyping automotive parts

For a case study on the use of the SPIF on the automotive field, a partnership is made with General Motors Corporation. The goal is to test the integration of SPIF not only for rapid-prototyping of complete parts but also to make details and final forming operation in press formed big panels, like doors, hoods and other.

For the case study, a part is chosen from Opel. The goal is to define the fixture details in the front end of a car fender. The large panels prototyping is achievable by using conventional stamping tools and hand craft metal work. However, detailed areas like the fixtures are hard to obtain. Thus, the part is selected as a test for the SPIF potential analysis. Figure 5.7 shows the drawing of the car fender with a detail on the fixture selected as a case study example.

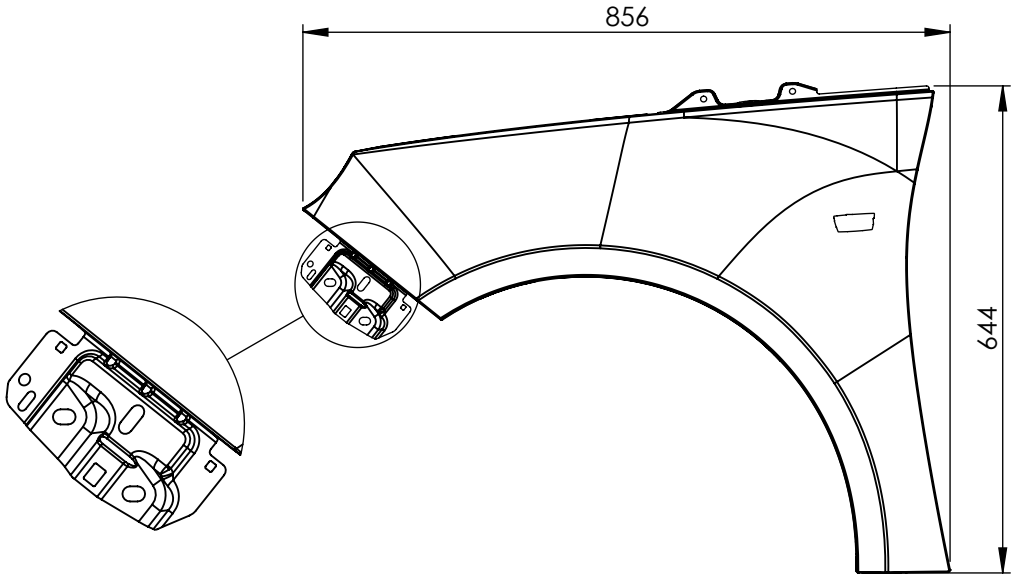

Figure 5.7: Car fender with fixture detail

As the goal is to define the fender fixture alone, a smaller blank is used to form this structural element alone. For that, a 1 mm aluminium sheet is used. For the fender fixture prototype manufacture, a part is designed with based on the presented geometry, being extended to a flat blank. Figure 5.8 presents the defined part drawing. The fender fixture fits in a 82.5×168 mm area, with a maximum depth of 13.4 mm and maximum wall angle of 38^{o}. The part as a T shaped flat area at the top plane and a second flat plane at 4.6 mm deep. The extended part hold an area of 150×178 mm, being extended to the flat blank through a 50^{o} wall.

For the development of the fender fixture prototype, a backing plate is cut. As the part include a small island type feature, the backing plate is cut from multiple thin sheets and assembled. This allows to support the centre T shaped area while forming all around without the need for a part flip. For the backing plate fabrication, four identical parts are cut from 2 mm steel sheet using a punching machine. The three parts are assembled in layers. The top part is cut and the centre piece is attached to the middle one, creating a gap to define the part island. The assembled backing plate is presented on figure 5.9. Despite the possibility to support the island configuration, these backing plate concept a reduced stiffness.

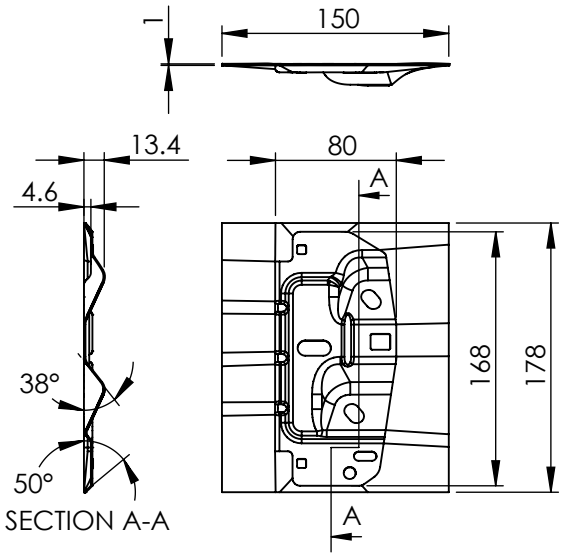

Figure 5.8: Car fender with fixture prototype drawing, scale 1:5

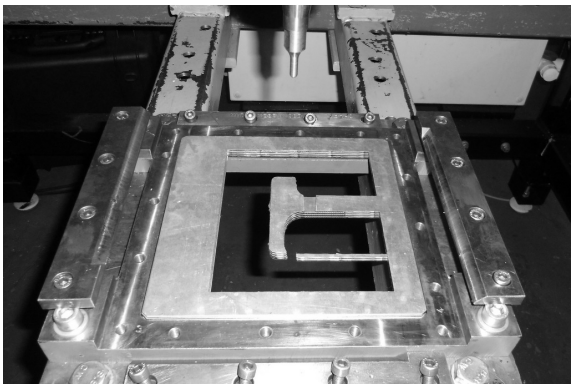

Figure 5.9: Car fender prototype backing plate

Two manufacturing options are used for the forming operation. Both option use a 6 mm spherical punch following a helical tool path strategy at 1750 mm/min. The forming feed rate is decreased to form the smaller features of the part. Due to necessary air movements to form in different areas, ramp lead in and lead out is used to avoid abrupt tool contact to the surface.

The first forming approach uses a constant step down strategy with a vertical increment of 0.3 mm for the first forming stage. As it leads to a rough part surface, mainly on the lower slopes, a second forming stage is used, following the same strategy with constant overforming of 1 mm. This finishing operation leads to improvements in both accuracy and surface finishing.

On the second approach, a single stage strategy is applied using constant crisp height, leading to vertical increments from 0.1 mm to 0.3 mm. Besides, to improve the geometry definition, an over forming of 40% of the depth, limited at 2 mm is used. Although being slower due to the shorter vertical steps, this strategy leads to a better surface and geometry definition.

Figure 5.10 presents the comparison between the first forming stage using the constant step down strategy and the constant crisp height strategy. The punch marks on the sheet are notorious from the different operation and denote an unequal part quality.

Despite the two different approaches, where the first uses two forming stages and the second a single one, the overall forming time and energy consumption are similar. The dismiss of the finishing passage compensates for the extra time due to the smaller vertical increments in the lower slope walls on the second manufacture approach, which leads to better surface results.

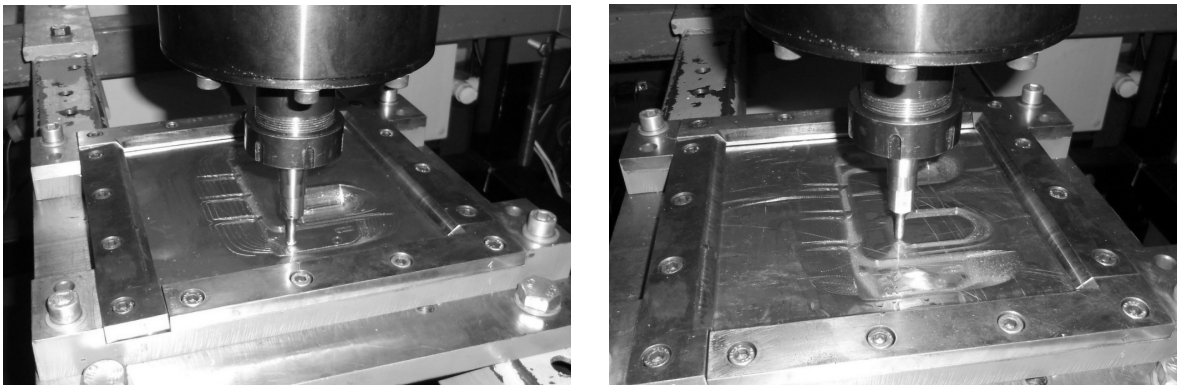

(a) (b)

Figure 5.10: Car fender fixture prototype forming operation: (a) manufacture option 1 - constant step down, (b) manufacture option 2 - constant crisp height

The part accuracy is measured using a CMM. The part formed with the constant step down has dimensional deviation of ± 3.4 mm for the 99% most accurate bound, with an average deviation of 0.4 mm. The part formed with the constant crisp height has the same ± 3.4 mm dimensional error with an average value of 0.1 mm. Figure 5.11 presents the accuracy distribution of the part manufactured by the two options. Although the dimensional error boundary is similar in both manufacturing option, the dimensional distribution is better at the part formed with the constant crisp.

The main lack of accuracy is found at the part top flat area. A flexure of the backing plate leads to an insufficient support of the formed part resulting both on a position deviation on the top plane and miss definition of the boundary walls.

Regarding the surface finishing, the part manufactured with the constant crisp height has a higher density of punch scratches, although shallower. This results on a smoother surface where the forming increments are less noticeable.

The part formed with the second forming strategy is cut and drilled. Figure 5.12 presents the part after finishing operation. Despite the considerable lack of accuracy, the overall appearance is fairly good, legitimising the use of SPIF for first prototype development.

The development of the car fender fixture prototype take close to two hours, including the backing plate cut, with a manufacturing cost around 100€. Table 5.2 summarises the part development steps with the respective time and energy consumption and estimated cost. The manufacturing time and cost is compatible with prototyping work.

The case study contributes to the validation of the SPIF technology for prototyping automotive parts, mainly in what concerns complex non visible parts. However it anticipates

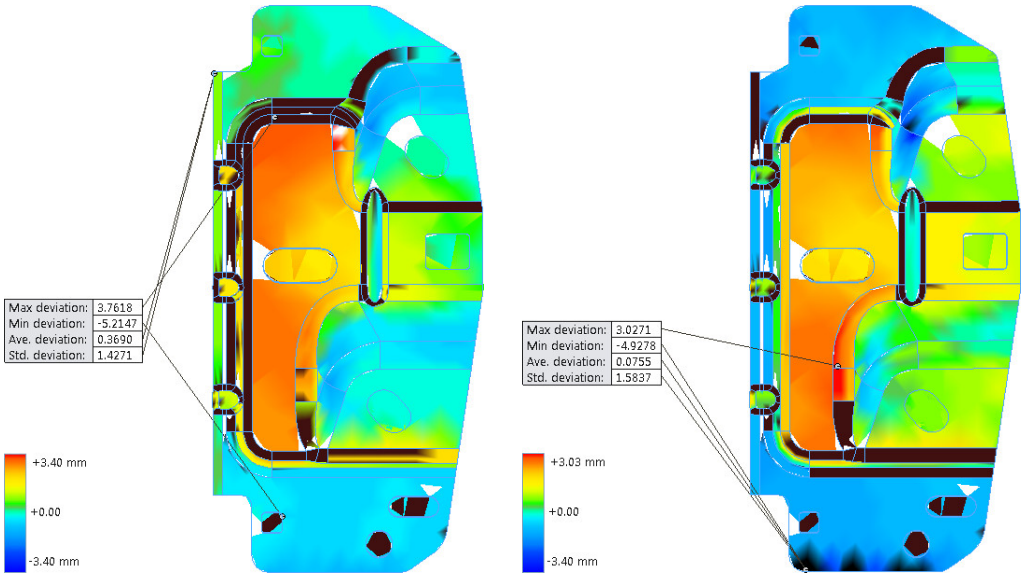

(a) (b)

Figure 5.11: Car fender fixture prototype dimensional measurement: (a) manufacture option 1 - constant step down, (b) manufacture option 2 - constant crisp height

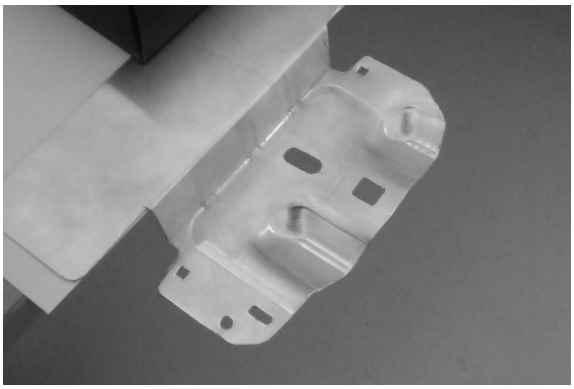

Figure 5.12: Car fender fixture prototype

Table 5.2: Car fender fixture prototype process analysis

(a) manufacture option 1 - constant step down

Operation	Time	Energy	Cost
CAM programing	0:15	n.a.	13€
Backing plate develop	0:45	$\lesssim 2.0$	40€
Tool change	0:05	n.a.	4€
Part fix	0:10	n.a.	8€
Forming operation	0:18	3.1 kW.h	16€
Finishing operation	0:17	1.9 kW.h	15€
Part release and cleaning	0:05	n.a.	4€
Complete process	1:55	7.0 kW.h	100€

(b) manufacture option 2 - constant crisp height

Operation	Time	Energy	Cost
CAM programing	0:15	n.a.	13€
Backing plate develop	0:45	$\lesssim 2.0$	40€
Tool change	0:05	n.a.	4€
Part fix	0:10	n.a.	8€
Forming operation	0:33	5.2 kW.h	26€
Part release and cleaning	0:05	n.a.	4€
Complete process	1:53	7.2 kW.h	95€

that the process is still not accurate enough for end part manufacturing.

In what concerns contributions to the SPIF operation analysis, a comparative analysis between the use of constant vertical step and constant crisp height in low slope parts is perform. The use of constant vertical steps lead to weaker results, often requiring the use of a second forming stage for finishing. The use of the constant crisp height allows to achieve better results at the first stage. The total forming time and energy consumption in both option is similar as the additional time due to the lower vertical steps can be related to the finishing passage when using double stage operation with higher increments.

For the part support, a multi layer backing plate is used. This approach offers advantages both from the backing plate manufacture and the operation point of view. The use of thinner sheets allows the use of a punching machine for the backing plate cut, reducing the energy consumption when comparing with other cutting processes. The assembly of the multi layer backing plate allows the creation of additional support for shallow features, even when the part includes changes in curvature direction. On the other hand, the mechanical behaviour of the backing plate is inferior to the use of a single thick sheet and leads to a lower accuracy of the peninsula and island type features.

During the forming operation, a vertical overforming is used to improve the part accuracy, mainly on the deeper areas of the part. A vertical over forming of 2 mm leads to the best result at the higher slope walls and deeper features. However, the over forming can not be defined from the top surface. A growth rate of 40% of the part depth leads both to a fair definition of the part geometry and improved accuracy.

5.3 Fabrication of tools

The possibility of manufacturing unique parts give SPIF possible application in tool making. The chapter 6 is dedicated to research work on the definition and fabrication of tools for different technologies. In order to test the development and manufacture of a sheet metal mould in a real industrial scenario, a partnership is made with Sunviauto, S.A.. The goal is to develop sheet metal parts to be used as tools for composite open contact moulding.

The case study is based on a part from a train seat, namely the back rest rear panel. The part, presented in figure 5.13 is to be manufactured in fibre glass reinforced plastics, through spray up and hand layup processes. The part follows a free form shape inside an 630×600 mm area. Along the geometry, the minimum radius is 19 mm at two indents along the part height direction. Given the part size and detail, a conventional milled mould could reach values close to 5000 €, mainly due to the cost of milling operations and mould finishing. Due to the small series production, the initial cost for a mould is too high and doesn't pay off. Thus, the goal of using SPIF is to produce a cheap alternative to the conventional moulds by forming a moulding surface from flat metal sheet.

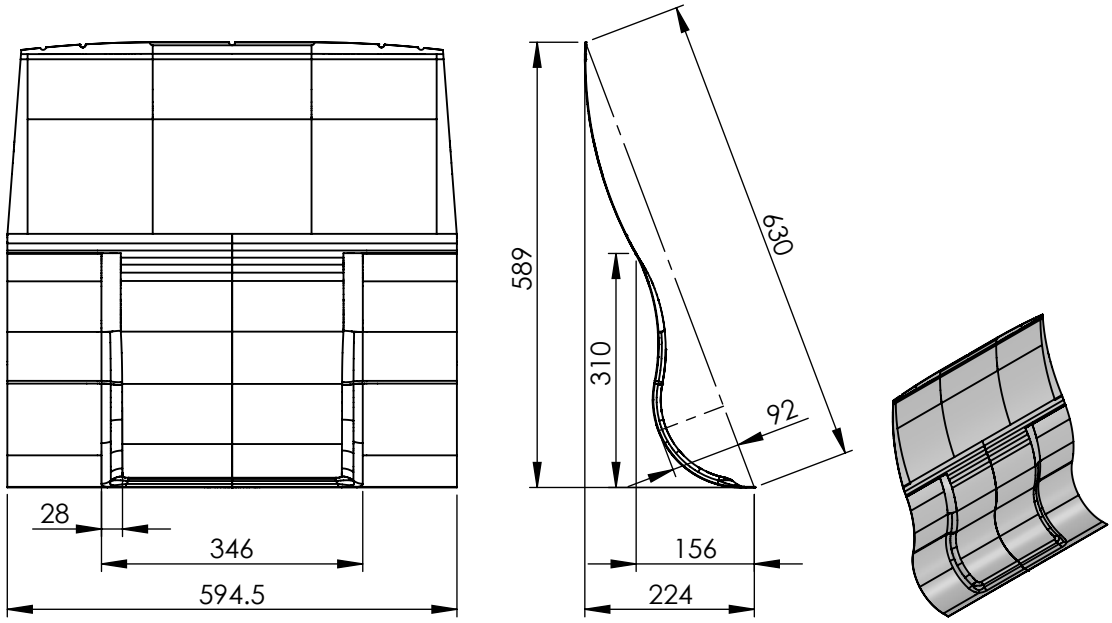

Figure 5.13: Train seat back rest rear panel: (a) drawing, scale 1:10, (b) CAD model, scale 1:20

The mould geometry is shaped as a container like cavity by extending the part surface to a flat plan. The mould flat plane is defined along the 630 mm diagonal of the part. Thus, along the vertical direction of the part no extended surface is needed. On the perpendicular direction, the edge distance 92 mm from the flat plane, hense needing a surface extension. The near 600 mm width part is extended by 50 mm in each direction to allow an easier part trimming after moulding operation. The new edge is extended to the flat plane through an average 45º, ending on a 700 mm wide frame. The blank is sized by adding a 25 mm flat clamping area all around the part, ending on a 680×750 mm.

The maximum wall angle in the mould cavity is 69º, only happening locally. By analysing the draft distribution, only the first 18 mm deep section in the bottom edge face that wall angle. Figure 5.14 represent the draft angle analysis of mould cavity, with the area with wall angle greater then 60º identified in light grey. It is noticeable that the largest area of the part faces wall angles bellow 60º, thus expecting a final thickness greater than half the blank thickness in all those areas.

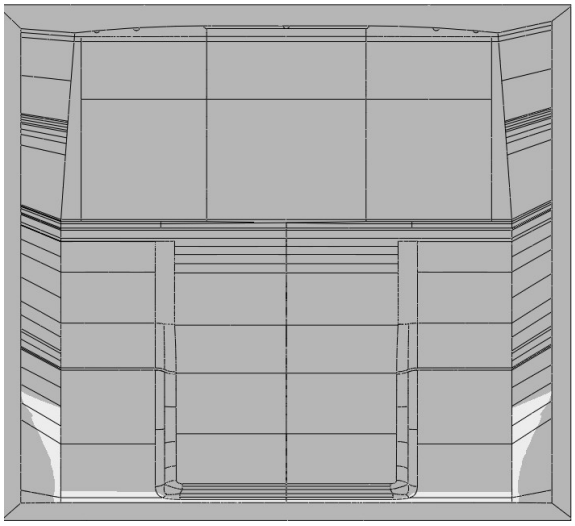

Figure 5.14: Wall angle analysis for the seat back rest rear panel mould for angles greater then 60º

Despite the minimum required blank size, the hand layup moulding surface is manufacture on a 1×1 m 1 mm thickness aluminium sheet, with a total material cost of 40€. The blank is cut using an hydraulic press and positioned on the forming table held by a 40 mm band all around.

The forming operation is performed using a 10 mm spherical punch in a single stage forming strategy along a helical tool path with a 0.5 mm step down. Due to the sharp corners, the feed rate must be kept at a low speed. However, the large area would lead to a very time consuming forming operation. As the sharp edges are locates on the surface extensions, the accuracy is those areas is not an issue, thus, allowing to increase the feed rate. The forming operation is performed at 5000 mm/min. As the tool path requires some air movements for repositioning the punch, the feed rate is decreased for these movements to avoid overshoot movements to cause local deformities on the part. Figure 5.14 presents the forming operation of the back rest mould. The overall forming operation is performed in 76 minutes with an energy consumption of 13.2 kW.h.

Due to the distance from the formed cavity to the sheet support and to the absence of a backing plate, the top geometry as a strong inaccuracy. However, since the useful area of the part is away from the top bends, this flexure does not harm the mould performance.

After forming operation, the part is unclamp and clean. Figure 5.16 presents the finished back rest mould. As the used sheet is relatively thin, despite some minor differences due to the part thickness, the mould can be used both as a cavity or as a core. Before hand layup operation, the part is finished by sanding operations and the blank boundary is fix on a support box.

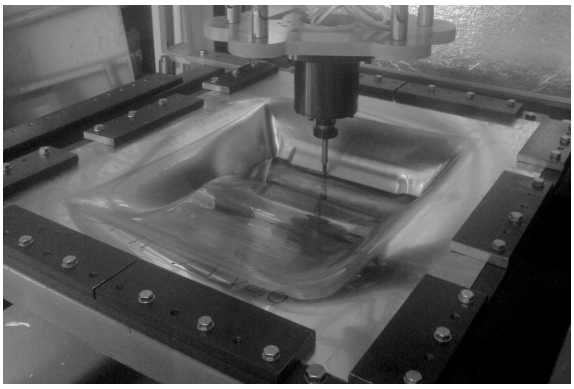

Figure 5.15: Train seat back rest rear panel mould forming operation

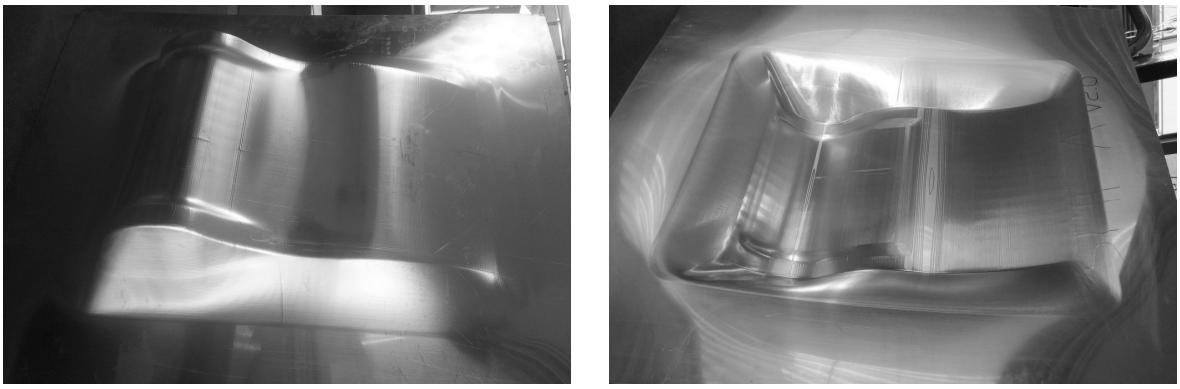

(a) (b)

Figure 5.16: Train seat back rest rear panel SPIF mould: (a) outer side, (b) inner side

The overall mould sheet metal surface manufacture process analysis is described in table 5.3. The complete forming operation takes three hours to complete, with an energy consumption of 13.2 kW.h and a total cost bellow 200€. The mould development adds the surface finishing operations and the construction of a simple support box. Given those additional works, the estimated cost for the hand layup mould is kept under 400€, much lower then the reference value from conventional tools.

Table 5.3: Train seat back rest rear panel SPIF mould process analysis

Operation	Time	Energy	Cost
CAM programing	0:15	n.a.	13€
Machine table set up	0:30	n.a.	25€
Tool change	0:05	n.a.	4€
Blank cut	0:05	n.a.	40€
Part fix	0:10	n.a.	8€
Forming operation	1:16	13.2 kW.h	55€
Part release and cleaning and setup restore	0:40	n.a.	33€
Complete process	3:01	13.2 kW.h	178€

5.4 Manufacture old parts replacements

For a second application of the SPIF process to the automotive sector, and both validating the use of the process for the production of out-of-the-market parts, a partnership is made with a classical racing bikes team called Team Clássico Racing who run on the Portuguese National Speed Championship - Classic Bikes. A Yamaha TZ350G racing bike from 1980 has been acquired by the racing team. The bike's tank has been adapted to run the Isle of Man Tourist Trophy, extending it in its width to get a larger volume. However, it is intended to restore the bike to its original shape, requiring the need to fabricate an original tank replica.

The enlarged tank is measured to define a CAD model using reverse engineering techniques. Figure 5.17 shows a photo of the scanning process of the bike's tank. Since the modified tank has the same side geometry as the original one, the CAD model, together with the bike's frame model, can be used to remodel the original tank. The part is 630 mm long and should be fabricated on 1.2 to 2.0 mm aluminium sheet.

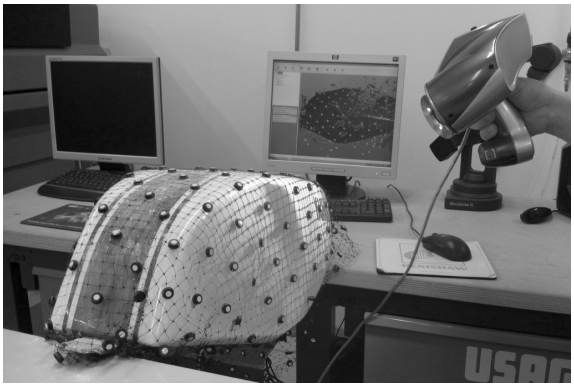

Figure 5.17: 3D scanning of the bike tank part

Due to the part's geometry, for a practical forming operation is was divided in four sections: two symmetrical side faces, a top section and a bottom section. The bottom section is composed by flat sheets, thus do not require forming operation. Both the side faces and the top face are achieved through sheet forming. To enable the fabrication of those section by SPIF, they are isolated and extended at a 45^{o} wall angle to a flat blank. Figure 5.18 represents two intersecting extended sections of the tank. To obtain the complete tank, the formed part are then trimmed and welded in position. Is is important to note that the cutting and welding operation order may influence the part result, since the formed parts are under accumulated stress.

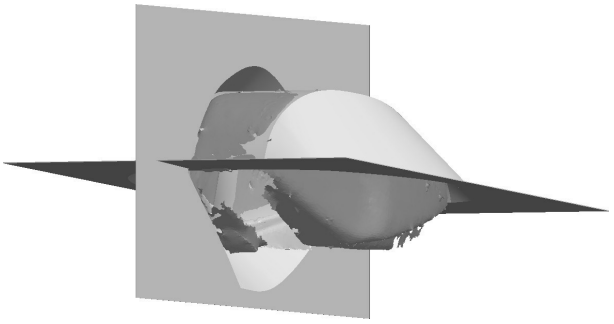

Figure 5.18: CAD model for the bike tank part manufacture

For the manufacture of an original tank replacement, the side sections can be formed from a 700 mm by 465 mm blank and the top section can be formed form a 700 mm by 600 mm flat sheet. The maximum wall angle in the top part is 75º, only happening locally. By analysing the draft distribution, only a 7 mm deep section in the top of the part has a wall angle greater then 65º. Figure 5.19 (a) represent the draft angle analysis of the top section of the tank, with the area with wall angle greater then 65º identified in light grey. The lateral section of the tank have a low slope, resulting on a maximum wall angle of 45º in the extended surfaces. Figure 5.19 (b) represents the draft angle analysis of the side section. In both subfigure (a) and (b), the section intended for the tank and the extended surfaces are clearly identifiable.

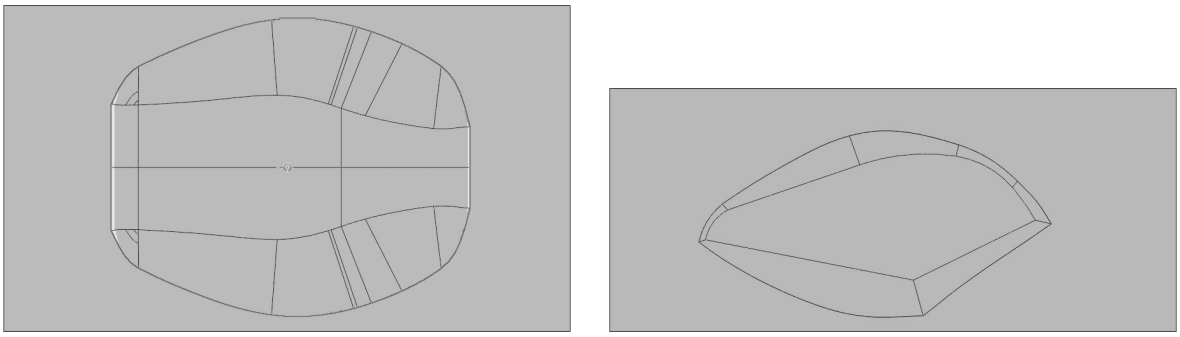

(a) (b)

Figure 5.19: Wall angle analysis for the bike tank sections for angles greater then 65º

Due to the part dimension, before the manufacture of the bike's tank, it is proposed to develop a scaled prototype. In order to use the available holding table for small parts, a 1:4 scale was proposed, resulting on top section formed from a 175 mm by 150 mm blank and a side section formed from a 175 mm by 110 mm blank. Since the three parts are extended to the flat blank by a constant slope wall, the part forming can dismiss the use of a backing plate since those walls absorb the inaccuracy of the top bend.

The manufacture of the scaled prototype is performed using 1 mm 1050 Aluminium sheet. Both the top and the side parts are formed using a helical tool path strategies with a 0.5 mm vertical step using a 12 mm spherical punch. To take advantage of the available sheet clamping tables, the blanks are resided to 230 mm by 230 mm. Two blanks are used with the top part being formed in one and the two mirrored side parts formed on the other.

Since the top part is a quasi "island" type part, the forming operation is performed in two stages, requiring a part flip between them. The first stage works on the tank inside to form the major cavity. The forming operation is performed at 3000 mm/min, taking 13 minutes to complete, including the machine start up and sheet referencing, with a total energy consumption of 1.9 kW.h. The second stage is performed after a part flip to form the gas cover indent. Due to the short movements, the forming operation is performed at 1000 mm/min to avoid machine vibration. The second stage is completed in 5 minutes, consuming 0.7 kW.h, where most of the time corresponds to the part referral. Figure 5.20 presents the forming operation of the top part with the first stage shown in 5.20 (a) and the second in 5.20 (b).

The two side parts are formed in the same blank with a thin steel bar splitting the two forming areas as a backing plate. Despite the vertical force applied to the sheet holder and support bar, no differences are noticeable between the two mirrored parts and no permanent

deformation is enforced to the sheel bar. The forming operation is performed at 2000 mm/min and reduced to 1000 mm/min in the final z steps because of the sharp turns and small movements. Figure 5.21 presents the manufacture of the two side parts manufacture seen from the top and bottom views. The total forming time to shape the two parts is 15 minutes with an energy consumption of 2.2 kW.h. The sheet referral in much faster since it uses the same tool and position as the first part.

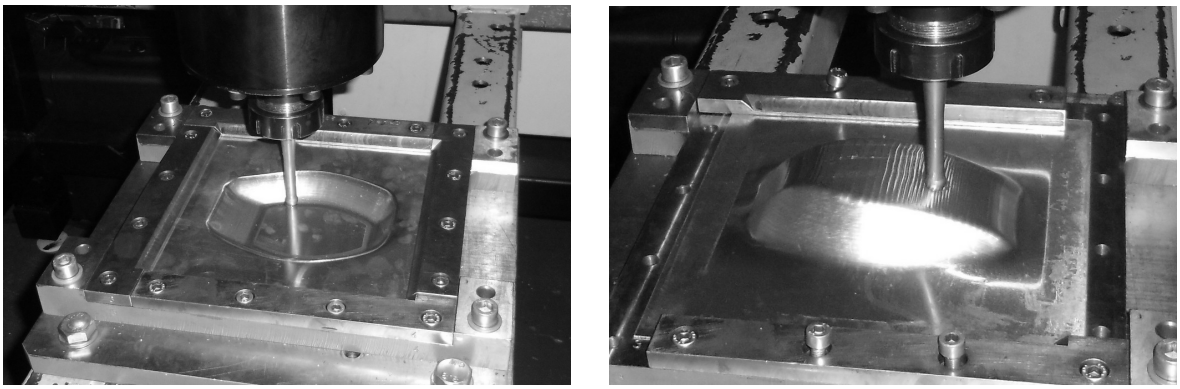

(a) (b)

Figure 5.20: Scaled bike tank prototype top part manufacture: (a) container forming, (b) gas cover indent forming after part flip

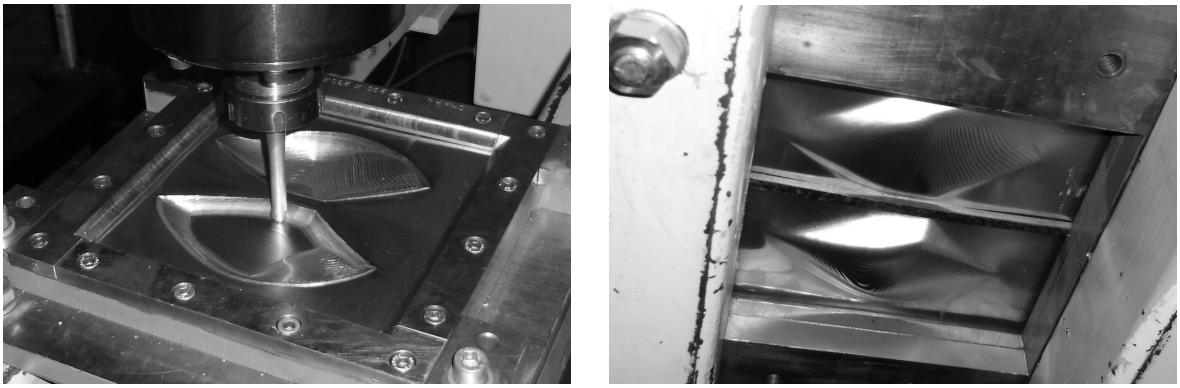

(a) (b)

Figure 5.21: Scaled bike tank prototype side parts manufacture: (a) forming of the second side part, (b) bottom view of the forming operation

After forming operation, the parts are cleaned and prepared for mounting. The edge between the part area of the container and the extended surfaces helps trimming the pieces. Figure 5.22 presents the cutting and pre assembly operation. Apart from the use of the edges, the parts are placed in position to help marking the cutting line. The trimming operation is performed manually using a rotary tool with cutting disk. The same rotary tool is used to sand the trimmed edges to allow the better possible fit between pieces. The side parts are finished in parallel to benefit symmetry.

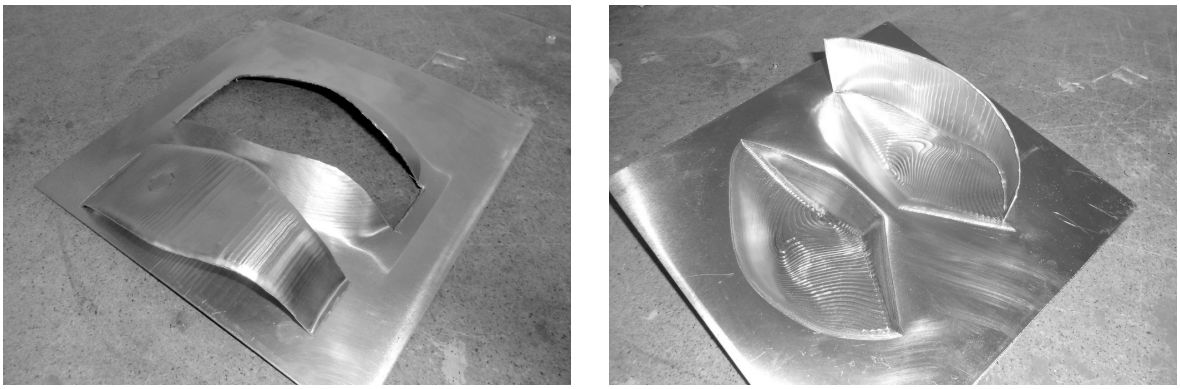

(a) (b)

Figure 5.22: Scaled bike tank prototype cut and assembly operations: (a) top part cut, (b) relative position between parts

The three formed pieced are assembled together using epoxy cold welding mass. In a first stage, modelling clay is used to temporally join the parts at specific points. The epoxy mass is applied from the inside, adding a material fillet. The tank model bottom is added from a bent sheet. Figure 5.23 show the assembled model. No finishing operation is performed on the part surface since the sliced appearance caused by the forming step down is compelling to the part aesthetics.

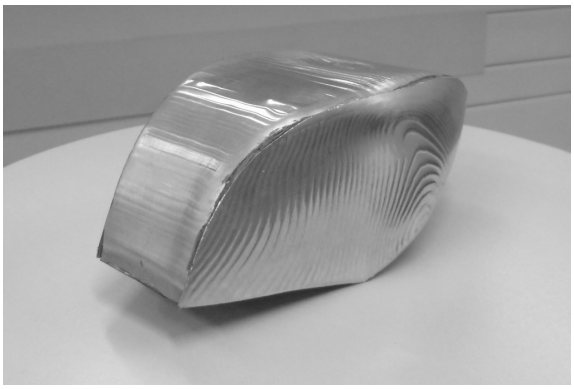

Figure 5.23: Scaled bike tank prototype

The overall analysis of the scaled model development is presented in table 5.4. The prototype development takes close to three hours, with a total energy consumption of 5 kW.h and a total manufacture cost just over 150€.

At the moment, the full scale tank replacement hasn't been developed. Nevertheless, the analysis of the scaled prototype grounds the possibility of achieving a functional replacement for the bike tank. The possibility of manufacturing a unique part by multiple panels using SPIF is validated. The approach adds labour time to the process, and presumably decreasing accuracy, but allows the execution of higher complexity shapes in fewer thickness differences. In the case study, cold welding mass is used for convenience while arc welding processes could allow to attain better performance results.

Table 5.4: Bike tank scaled prototype full process analysis

Operation	Time	Energy	Cost
CAM programming	0:25	n.a.	21€
Blank cut	0:05	n.a.	5€
Tool change	0:05	n.a.	4€
Blank clamping	0:05	n.a.	4€
Top part forming	0:13	1.9 kW.h	13€
Reverse top part	0:05	n.a.	4€
Top part reverse forming	0:05	0.7 kW.h	7€
Top part release and cleaning	0:02	n.a.	2€
Blank clamping	0:05	n.a.	4€
Double side part forming	0:15	2.2 kW.h	14€
Side part release and cleaning	0:05	n.a.	5€
Top part cut from formed part	0:15	$\lesssim$ 0.1 kW.h	13€
Side parts cut from formed part	0:25	$\lesssim$ 0.1 kW.h	25€
Bottom part cut and bending	0:15	$\lesssim$ 0.1 kW.h	13€
Assembly and fitting	0:15	n.a.	13€
Cold mass welding	0:05	n.a.	9€
Complete process	2:45	5.1 kW.h	151€

5.5 Manufacture of custom parts

A case study for the test of the fabrication of custom parts is performed in a partnership with the research group of the project SIM T-RTM, in development at the School of Design, Management and Production Technologies Northern Aveiro. The aim of the project is to research into in use of reaction injection moulding technologies. Within the work plan, a room temperature vulcanization (RTV) vacuum machine is adapted to a resin transfer molding (RTM) machine to be able to work with thermoplastic resins. Figure 5.24 presents the original RTV vacuum machine. In addition to other changes, a new material hopper is built to allow a material supply through a 10 mm hose.

Figure 5.24: RTV vacuum machine with original hopper

The hopper is placed inside the machine in a 200×145 mm window. The original hopper is 90 mm tall with an additional 30 mm diameter 20 mm long tube at the bottom. The goal of the new custom part is to allow the use of larger moulds in the inferior part of the machine and supplying the material to the mould through a smaller hose. For that, the new hopper design is shorter and uses a thinner tube at the bottom. Figure 5.25 presents the drawing of the new part. The hopper surface is a shaped from a 200×145 mm with 20 mm fillet to a 10 *textmm* diameter over 60mm deep. An additional 10 mm diameter and minimum 10 mm long cylinder is intended.

The original part is manufactured by welding flat sheets to each other and to a cylindrical tube. Apart from being a time consuming process, it involves the cut of the parts and the need to place them in position for welding. Besides, the welding process is a very skilled depended operation and requires exhaustive part finishing. SPIF is an effective alternative for the fabrication of the new part, forming the hopper from a flat blank.

The part is essentially shaped in a container configuration, with a maximum wall angle of 60^{o} near the part top and 50^{o} in the remaining part. The material output tube follows a flange like configuration. However, the diameterdeep ratio is to low be formed by flanging the sheet metal alone. Considering the limit hypothetical scenario where a flange is created without an initial hole, the material volume inside a 10 mm circle is 78.5 mm^3. Due to the volume conservation during the forming operation, as specified by equation 5.1, in order to achieve a 10 mm outside diameter flange with 10 mm height, the thickness must reduce to 0.26 mm, too thin to obtain. As a initial hole is essential for a flanged operation without significant edge damage, the limit minimum thickness is even lower.

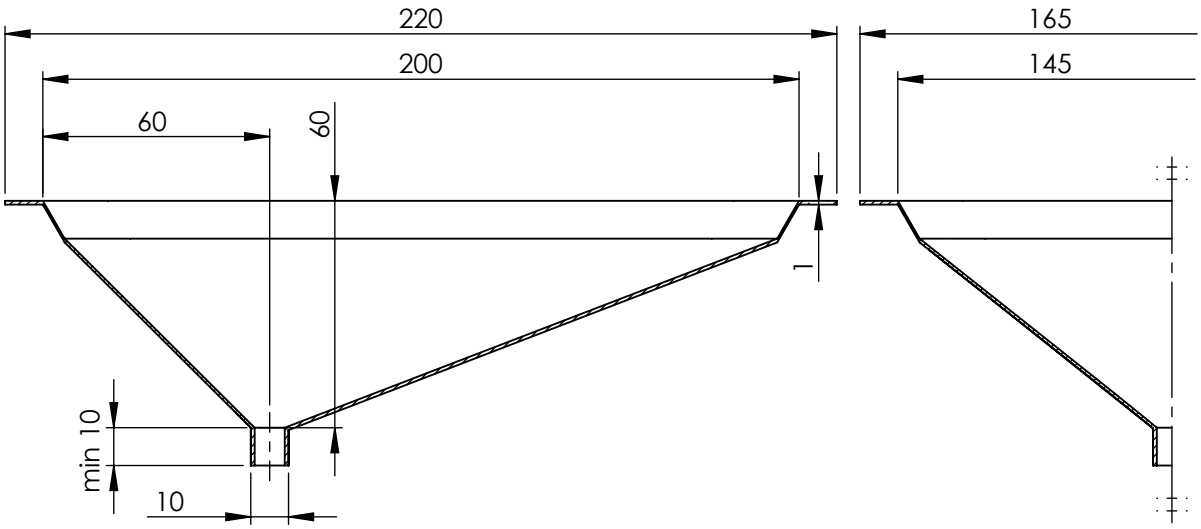

Figure 5.25: RTM machine custom hopper drawing, scale 1:2

$$\pi.r^2.t_i = \left(\pi.r^2 - \pi.(r - t_f)^2\right).h \Leftrightarrow t_f = r - \sqrt{\frac{r^2.(h - t_i)}{h}} \tag{5.1}$$

In order to achieve the intended design, the new hopper uses a two part assembly. The container is form from a 1 mm thickness flat blank. The material output is created by cramping a 10 mm diameter with 2 mm wall thickness tube. The cramping link is reinforced to improve the part strength. The part in manufactured with a longer material exit tube to be cut in the most adequate length before first use.

The forming operation is perform using the modular backing plate developed for the tunnel research. The hopper forming operation uses a 12 mm spherical punch in a helical tool path with a vertical increment of 0.5 mm and a feed rate of 4000 mm/min, reducing up to 2500 mm/min at the final step downs. Figure 5.26 presents the forming operation of the hopper from a top and a bottom point of view.

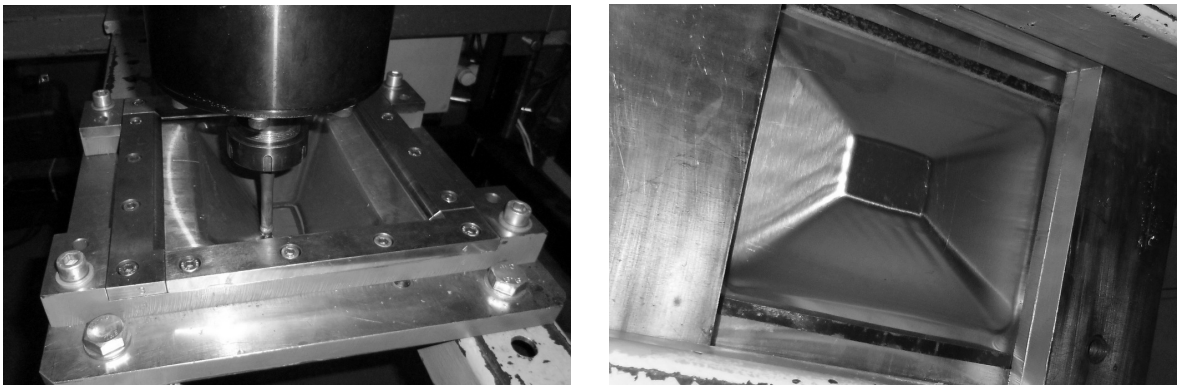

(a) (b)

Figure 5.26: RTM machine custom hopper forming operation

After the forming operation, the container part is drilled with a 1 mm hole at the bottom centre. A 40 mm piece of tube is cut and one end in shear formed to create a inner flange. Figure 5.27 shows the drilled container part and the flanged tube. The tube is positioned on the bottom of the hopper and a tapered punch is used to enlarge the hole and cramp the tube. The punch has a 30° tapered tip up to a 3 mm diameter and a second 30° tapered neck to a 6 mm. The cramping is perform on a manual press.

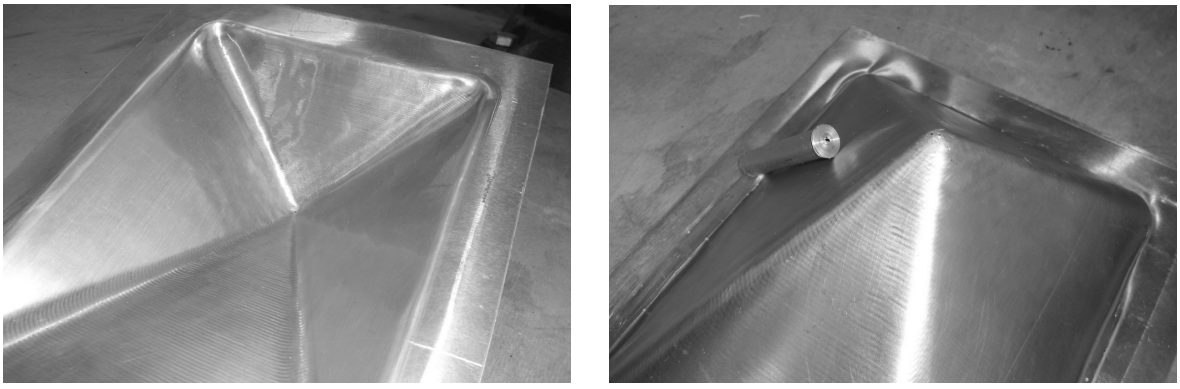

(a) (b)

Figure 5.27: RTM machine custom hopper tube cramping preparation

After cramped, the tube connection to the hopper sheet metal part is reinforced. Due to the unavailability of a welding process compatible with the thin thickness, high temperature cold welding epoxy mass is used. The part is finished by trimming and deburing the top plane. Figure 5.28 (a) presents the finished part with the still untrimmed tube and the 6 mm material exit visible.

The new hopper fits right in the RTV vacuum machine, allowing the placement of taller moulds. Along with other modifications, the new sheet metal part allow the success of the retrofit of the machine, making it able to be used for RTM operation. Figure 5.28 (b) presents the reconfigured RTM machine with a 10 mm hose connected to the new hopper.

(a) (b)

Figure 5.28: RTM machine custom hopper

The new hopper manufacture is perform is just over one hour, with a total fabrication cost of 60 €. Table 5.5 summarises the time, energy and cost of the hopper development steps.

Table 5.5: RTM machine custom hopper full process analysis

Operation	Time	Energy	Cost
CAM programing	0:10	n.a.	8 €
Blank cutting	0:05	n.a.	5 €
Blank clamping	0:05	n.a.	4 €
Tool change	0:05	n.a.	4 €
Hopper forming	0:15	2.6 kW.h	14€
Part release and cleaning	0:05	n.a.	4 €
Tube cut, flange and cramp	0:10	n.a.	8 €
Tube reinforcement	0:05	n.a.	9 €
Part trimming and finishing	0:05	n.a.	4€
Complete process	1:05	2.6 kW.h	60€

The case study contributed to the validation of use of SPIF for the development of custom parts. The developed part contributed to the success retrofit of an industrial machine, by manufacturing a part with low developing cost and improved performance. Apart from ensuring the dimensional requirements for the new part, the filleted edges allow and easier clean when operating with the new hopper.

From the operation point of view, the SPIF part is developed with ease for being a single container designed according to the design guidelines. The case study contributed as a additional example of the use of SPIF in association with other forming process for the development of metal parts.

5.6 Manufacture of design parts

For the validation of the feasibility of using SPIF for the manufacture of design parts, a partnership with the designers Rogério Santos & Sérgio Barbosa, team RO·SE. By considering the possible part configuration, part stiffness, freeform possibilities and design guidelines of the SPIF process, the goal is to explore and generate new concepts reinterpretations for iconic objects, thought for SPIF. It is intended to use the case study both as a proof of concept for the development of custom design products using SPIF and as a demonstrative methodology for technology oriented design.

The case study focus on the development of a stool due to its importance as a design object. Several concepts are developed based on the fundamental principles of a SPIF part. The concepts take advantage on the free form capability to develop ergonomic seat for the stool. Further, the high specific strength of 3D shaped sheet metal parts allow to design light and clean proposals. The proposals take advantage not only on the SPIF part development possibilities but also on its association with other materials.

Several drawing proposals have been developed, aiming for a meaningful design. Due to its process oriented design approach, the creation process seek for technological distinctive elements to include in the conception. Figure 5.29 presents the selected proposal for the case study development. The stool is formed by a shaped sheet metal part as a seat and four individual legs. The seat thin geometry plunges from the continuous top surface to create a geometrical continuity along all part. The transition is based on truncated frustum cones, providing to the part a strong influence from the early SPIF tests heritage. A variety of options is refined for the material selection, considering choices from a full metal product to a combination of sheet and wood. The case study is developed under an all aluminium option.

Figure 5.29: Stool concept render for SPIF prototype development

The seat part is isolated for analysis and manufacturing strategy proposal. Figure 5.30 present the drawing of the sheet metal seat with an overall dimension of 291 $\times$ 291.5 mm and a minimum curvature of 6 mm radius. The part is represented with constant thickness while it is known that thinning occurs. Thus, the manufacturing development is performed considering the top surface dimensions. From the part analysis, two distinct geometric features are identified: a continuous free form surface and four variable slope cones. In such a way, the forming strategy definition is also defined considering the two geometric features. Due to the part minimum radius and general geometry, a 12 mm spherical punch is selected for the forming operation.

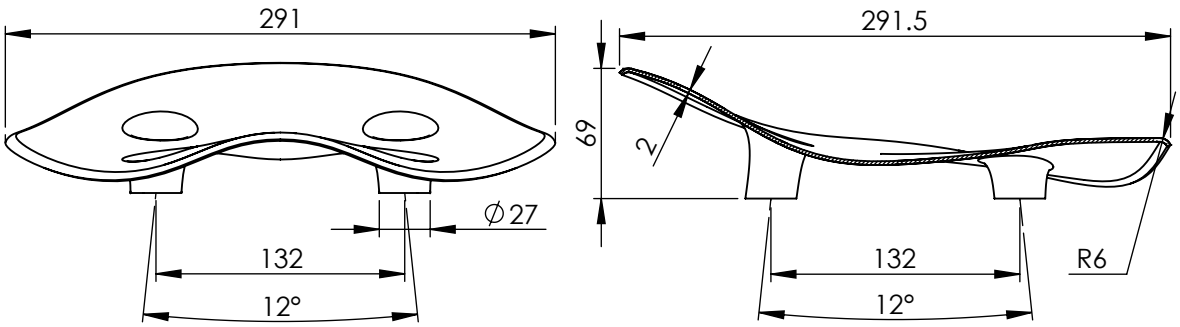

Figure 5.30: Stool seat drawing, scale 1:4

For the forming operation of the seat top surface, two possible approaches are considered. On the one hand, a metal part is designed from the stool seat in a shallow island part configuration. This option leads to an expected thicker part, at the cost of a longer forming period and the need of multiple forming set ups. On the other hand, the part may be tilted to shape a semi-tunnel type configuration SPIF metal part. The configuration may lead to a fast forming operation by dismissing the need for multiple setups and uses less blank material, at the cost of a higher thinning phenomena. Figure 5.31 presents the two possible part configuration.

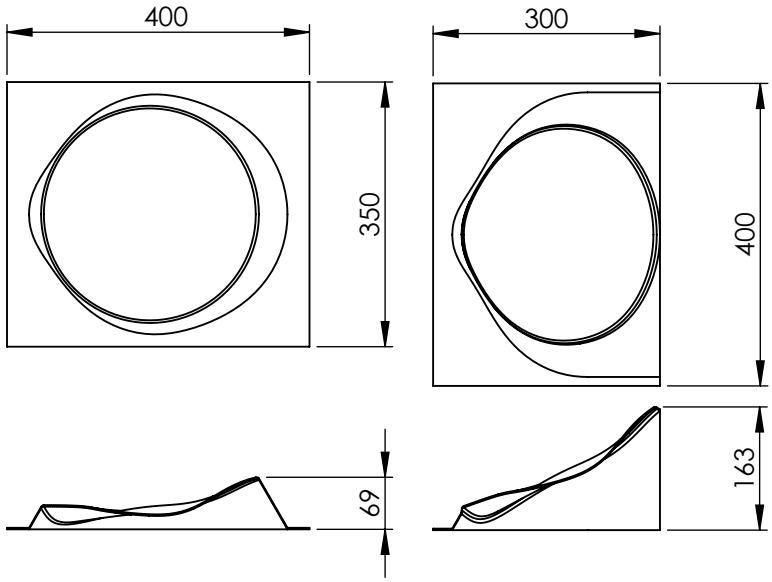

Figure 5.31: Stool seat possible manufacturing configurations: (a) island container, (b) semi tunnel

Since the case study deals with the development of a SPIF oriented design, it is intended to use the punch tool path marks on the part as an enriching design feature. Thus, the island configuration container is selected, both for forming the larger thickness but mainly due to the potential noticeable forming increment pattern marks on the part. In such a way, a 400×350 mm, 2 mm thickness aluminium blank is used for the product manufacturing.

The forming operation is performed in a multistage strategy, all using the same 12 mm tool. The process starts with the underside forming operation. After a part flip a second forming step shapes the stool seat surface and a third operation the legs connection flanges.

Before the stool manufacture, the machine table is set up do accommodate the 350 mm wide blank. For the forming operation a 350 mm wide blank is cut with the full length of the raw sheet. The table support is set with a 320 mm wide opening and the blank is held by 15 mm on the longer edges. The shorter edges are held on one side and only supported on the other. During the clamping procedure, marks are made in both the blank and the support table to allow the part flip.

The underside is formed in a helical tool path with 0.5 *textmm* step down increments and finished by a edge contour passage to define the fillet around the seat. The forming operation starts at 4000 mm/min during the first 6 mm deep. The forming speed is then reduced to 3000 mm/min for the definition of the lower slope areas. The deeper steps are formed at a even lower feed rate due to sharp turn next to the edges. This continue decrease end at 2000 mm/min at the bottom of the part. The edge contour is performed also performed at 2000 mm/min. The overall forming operation takes 45 minutes with an energy consumption of 7 kW.h. Figure 5.32 (a) presents the first forming operation of the underside and figure 5.32 (b) shows the contour fillet defining operation.

After the underside forming operation, the blank is flipped and repositioned and aligned along the X-Y plane by the marks. A machine movement along the X axis is used to check the part position before performing the reverse forming operations.

The seat surface is shaped using a offset tool path strategy in a continuous helical movement from the part boundary to the centre, with a lateral increment of 1 mm. The upper forming operation is performed at 2500 mm/min, with a feed rate reduction up to 1000 mm/min as the forming area becomes smaller than a 50 mm diameter. The feedrate speed is limited due to the alternative up and down movement as the tool follows the seat surface. The forming operation is completed in just over 15 minutes with an energy consumption of 2.6 kW.h. Figure 5.32 (c) presents the forming operation on the upper side of the stool seat. Due to the inaccuracy of the lower side forming operation, the match between the followed tool path and pre shaped surface is not fully achieved. Although this causes no issue in what concerns the shape geometry, it leads to discontinuities in the punch tool path pattern marks. Hence, a finishing operation is performed, running the same tool path in a 2 mm lower reference work plane. This over forming operation strongly improves the surface aesthetics and also contributes to a better definition of the geometry, particularly the transition between the seat perimeter and the inner surface. However, this operation doubles the upper side forming time and energy consumption.

The forming operation is finished by forming the flanged holes for connecting the legs. Four helical tool paths with 0.3 mm step down are used to form the flanged holes for the stool legs. Due to the small size of the flanged holes, the forming operation is performed without pre cut holes. As the hole flagging is performed on a sloped area, the sheet crack occurs at the lower side, with the material being shifted to the upper side and resulting on a near flat, despite irregular, flange end. The tool path runs only at 1000 mm/min due to the small forming area. Figure 5.32 (d) shows the forming operation of the first front leg mounting hole. The operation takes 15 minutes with and energy consumption of 2.4 kW.h. The holes succeed to open despite no achieving the height from the CAD model.

The stool seat part is then released from the forming table and cleaned. The formed area is cut from the blank, resulting on a 20€ material cost in sheet.

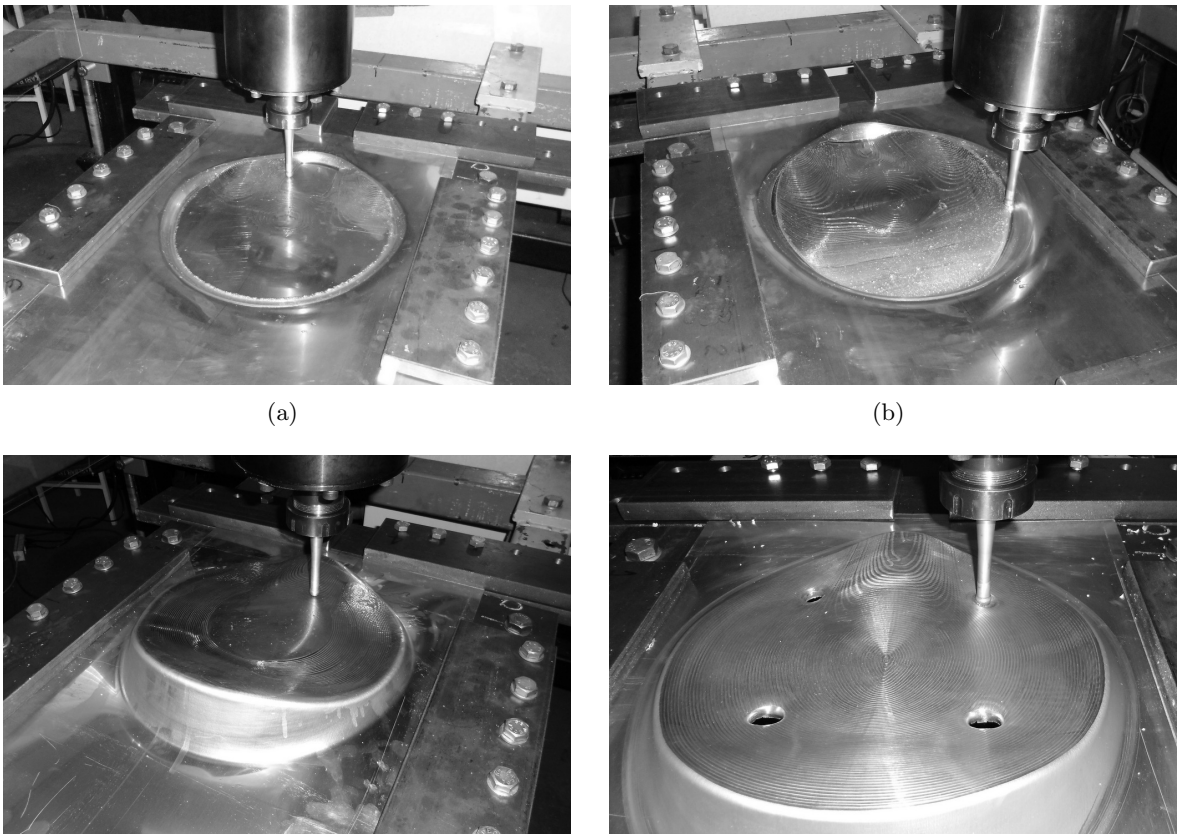

(a) (b)

(c) (d)

Figure 5.32: Stool seat forming: (a) underside forming, (b) fillet definition, (c) seat upper side shaping, (d) legs mounting flanging

The useful area from the formed part is trimmed using a angle grinder. The well defined line caused by the fillet contour passage at the end of the bottom side forming operation helps defining the trimming line. The cut in then sanded and deburred using a hand tool for a better finishing and safer edge. The irregular flanges for the legs mount are also trimmed and finished. Figure 5.33 presents the finishing process of the stool seat.

The stool legs are manufactured by turning pine wood with a total cost of 12€. The legs are cramped in the formed flanges and the link is reinforced using resin. The finished stool is presented in figure 5.34. Table 5.6 summarises the full stool manufacturing process. The overall process takes close to four hours to complete the stool, costing 225€, from which 32€ are spent in materials. The total energy consumption exceed 15 kW.h.

The case study concludes with success one of the first design pieces thought for SPIF, achieving good results with the process restrains in what concerns accuracy and surface finishing. The manufacturing cost for one piece is significantly high. Nevertheless, the job preparation still has 24% weight on the single part manufacturing. The manufacturing cost drops by 20% for a batch of six pieces, ending at a cost of 180€ per part, from which 32€ are spent in material. The cost could also be reduced by shaping the upper side of the seat in a single stage and by creating a positioning jig to speed up the blank positioning both while flat and after flip, lowering the cost up to 150€.

(a) (b)

Figure 5.33: Stool finishing: (a) trimmed part, (b) legs mounting

Figure 5.34: SPIF stool

The dissemination of the SPIF process have the potential for product designer to design and develop objects with the inclusion of 3D shaped sheet metal parts. This way, new projects can benefit majorly in two different fields. Sheet metal could be used to replace other materials with free formed surfaces for a more environmental favourable solutions. Metal parts design freedom is increased by the potential to form beyond strait bends and simple curvatures.

From the operational point of view, the case study contributed to the settlement of strategies to form free boundary parts using SPIF. Different possible part configuration are discussed with the selection being made based on the potential finishing aesthetics and part strength. In what regards the definition of the extended container to place the part on a flat blank, a minimum depth is recommended to improve the part boundary accuracy. Particularly when forming without a backing plate, this depth depends mainly on the distance to the clamping system and the ease of forming the material, namely the thickness. The case study uses a stabilisation container with a 60^{o} wall angle and a minimum depth of 8 mm 80 mm away from

Table 5.6: Stool full process analysis

Operation	Time	Energy	Cost
CAM Programing	0:30	n.a.	25€
SPIF machine table setup	0:30	n.a.	25€
Tool change	0:05	n.a.	4€
Blank cut	0:02	n.a.	20€
Part fix	0:10	n.a.	8€
Underside forming	0:45	7.16 kW.h	34€
Part reposition	0:15	0.25 kW.h	14€
Seat shaping	0:16	2.58 kW.h	15€
Seat finishing	0:16	2.66 kW.h	15€
Legs mount hole flanging	0:15	2.42 kW.h	14€
Part release and cleaning	0:10	n.a.	8€
Part trimming	0:20	0.12 kW.h	17€
Legs mounting	0:12	n.a.	22€
Part finishing	0:05	n.a.	4€
Complete process	3:51	15.3 kW.h	225€

the sheet support on a 2 mm aluminium sheet. The use of a deeper container could have a slight improvement on the part boundary fillet while spending the same material. The use of a more shallow container could harm the part quality.

In what concerns the product design process, SPIF presents a major advantage when comparison with other prototyping processes. Although is the stool design case study the seat geometry is defined and manufactured in one iteration, it is common to use the prototypes to evaluate and evolve the design. In these cases, with a possible geometry evaluation of the part before being trimmed, it is possible to reshape the part to follow design improvements without additional expense of material and with reduced manufacturing time.

5.7 Manufacture of architecture parts

A partnership is made with the Digital Fabrication Laboratory from the Center for Studies in Architecture and Urbanism of the Faculty of Architecture - University of Porto in order to test the use of ISF processes for the development of architecture products. The part possibilities, explicitly described by the possible part configuration and design guidelines are presented as a brief for the development of architecture application using sheet metal parts.

As a result from the interaction, facade panels are designed to be developed in sheet metal using SPIF as a primary manufacturing process. A variety of panels are drafted, exploring the possibilities given by the different conceivable part configuration. Each facade sample installation is established by assembling nine unique panels in a 3×3 matrix. This prototypical proposal allows to anticipate and evaluate the aesthetic effect on a larger scale since in uses both boundary and central panels.

For the case study, a triangulation concept panels installation is selected, presented in figure 5.35. The concept is based on a crumpled paper idea, exploring the definition of multiple directional faces to create a dynamic light effect. Each panel part is pattern as a multi container configuration, defined by a group of fix slope triangular walls. The panels are differentiated by using different container mapping, different wall slopes and different areas. The panel 5 is even more unique by adding an island configuration to the multi container geometry.

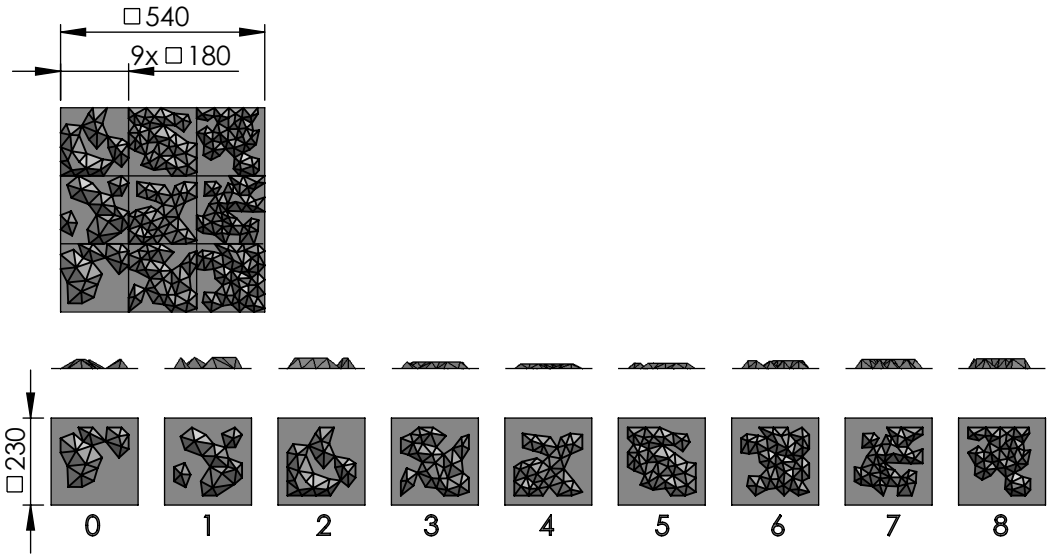

Figure 5.35: Sheet metal architecture facade panels: triangulations concept

Each panel is designed to be manufactured inside a 180×180 mm window without a use of a backing plate. Thus, despite the very geometrical shape, it is expected to achieve a partial organic geometry by the overall warping of the sheet and a mix of smooth and sharp wall transitions. Table 5.7 summarises some information about each individual panel, including the height and number and area of containers. The parts height varies from just 12 mm to 30 mm. In each part, all container have the same height. The containers area varies from under 1000 mm^2 to almost 16000 mm^2 in a 32400 mm^2 panel area. The containers occupied area compared to the overall panel area varies from 50% to 75%.

Table 5.7: Sheet metal architecture facade panels configuration

Panel	Height	Number of containers	Flat area of containers	Shaped fraction
0	24 mm	3	2116, 3564, 10480 mm^2	50%
1	30 mm	5	1870, 1965, 3042, 3978, 6880 mm^2	55%
2	27 mm	3	3107, 4692, 11072 mm^2	58%
3	18 mm	4	1665, 1863, 2856, 15952 mm^2	69%
4	12 mm	3	3620, 3632, 14016 mm^2	66%
5*	15 mm	5+1	1474, 1778, 3359, 3690, 13182 + 2765 mm^2	72% + 9%
6	21 mm	6	1740, 1784, 2054, 3072, 7580, 8010 mm^2	75%
7	24 mm	5	0872, 1334, 2381, 2533, 13698 mm^2	64%
8	26 mm	4	1294, 1392, 3244, 14198 mm^2	62%

* shaped in both directions

For the installation assembly, each panel design is extended by 24 mm perpendicular edge flanges with two 8 mm holes per side. The connection between panels is done using M5 screws and nuts with large flat washers, with the panels separated by 3 mm thickness rubber washer. Figure 5.36 represents a connection and the joint between panels. The gap between the screws and the holes and the ability to control the rubber washers compression allows to compensate for miss accurate parts.

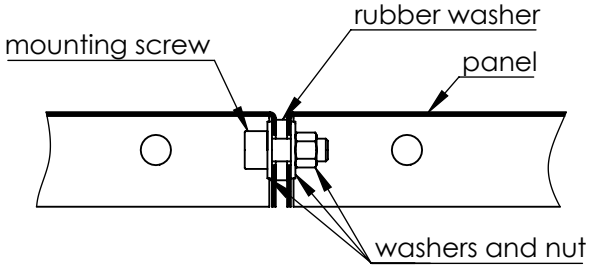

Figure 5.36: Sheet metal architecture facade panels mounting system

The architecture facade panels are manufactured on 1 mm thickness pure aluminium sheet. Given the pre formed or post form configuration, the blank outline is defined not only by the 180 mm square but also by the flanges length. Thus, each panel is manufactured form a 225×225 mm blanks with 24.5×24.5 mm cuts at the four corners and eight holes.

As the case study only intends to developing nine panels, it is not vital to develop specific supports for the parts manufacturing. Thus, the SPIF process is performed on flat blanks which are bent after. In such a way, the machine set up only requires the use of a simple 180×180 mm backing plate.

The first operation of the panels fabrication is the blank cut and the clamping at the forming table. This cut is restrict to the outer line of the blank since the corner trimming is performed after forming.

The forming operation of the panels is performed in a multistage strategy. Besides, each forming stage uses a different tool, forcing two tool changes per part. In a first step, the containers are formed using a 10 mm spherical punch. This forming operation is performed at 2000 mm/min, with a 0.5 mm step down in an helical tool path. The sharp edges of

the parts inhibits the forming operation to be formed at a higher rate to prevent vibration related issues positioning control overshoot. In a second step, a smaller 6 mm punch is used to better defined the containers edges. This operation follows a corner finishing tool path, countering around the edges with a 0.5 mm lateral step until a final central passage along the edge. This second stage helps creasing the parts edges for a better geometry definition. Due to the alternate up and down movements, the edge finishing operation is performed at only 1000 mm/min. The panel 5 has complementary forming strategy for being the only part with an island type configuration. After the two steps operation, the part is flip and a 10 mm spherical punch is used for the reverse forming operation. As this operation is being performed in the front side of the panel, the edge creasing is not performed to avoid visible tool marks. Figure 5.37 present the complete forming operation of the panel 5, for being the most complete one. The result of the two stage forming, particularly the detail of the edge creasing is also presented in figure 5.39. The average container forming operation takes 25:38 minutes with an energy consumption of 3.84 kW.h. The edge creasing process add an average 14:00 minutes and 2.28 kW.h to the forming process. Although the second stage adds significant time to the forming process, it allows to achieve distinctive results. Besides, the first stage forming operation using the thinner punch would also take longer since it requires smaller vertical increments.

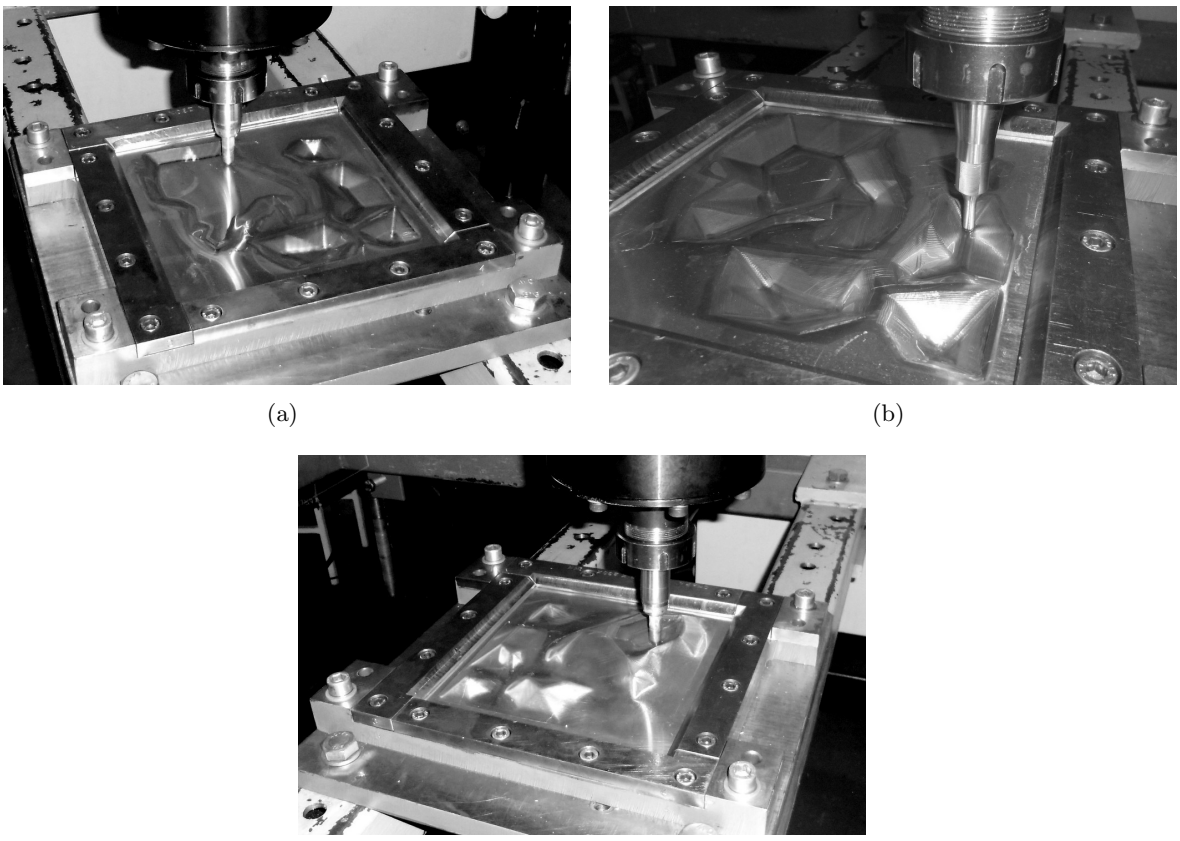

(a) (b)

(c)

Figure 5.37: Forming operation of the architecture panels: (a) containers forming, (b) edge creasing, (c) reverse forming

During the manufacturing of the panels, the geometry accuracy is highly influence by the order that each container is formed. Due to the absence of a backing plate, the forming operation on the part centre creates a bending effect along the flat blank. This deformation not only affects the definition of the feature being formed but also has influence on the nearby containers. To maximise the part quality, special care must be taken when selecting the order in which the multiple features are formed.

There are two factor for the selection of the order of the forming operation. Preferably, the multi containers are formed from to edge of the blank to the centre. While the peripheral features are mainly supported by the backing plate, the containers at the centre are in a much bendable area. By forming the peripheral indents first, the moment of inertia of the blank increases, benefiting the blank stiffness and thus the achieve better accuracy at the centre indents. When a panel include large containers, the priority is given to the smaller ones. The forming of the largest areas induce more curvature in the unformed flat blank, thus harming the definition of neighbour elements. Besides, the shape of the smaller container also have a moment of inertia increase effect, benefiting the forming operation of the largest ones.

After forming operation, the parts are identified and the upward position is marked. The panels are hole punched and the corners are cut out. The corner relief allows the bent of the side flanges, using a manual folding process. Due to the three dimensional formed shape up to the bending edge, special care must be taken during the folding operation. A split tool is used both on the sheet clamp and on the table. A PVC foam strip is used on the table to protect the sheet surface and distribute the folding force along all the bent while the table only true supports the flat areas. Figure 5.38 present the finishing cut and bending operation on the panel 0.

Despite not increasing the energy consumption, the finishing operation add significant time to the panels development. The measurement, marking a cut operation takes on average five minutes per panel, considering all holes punch in a row and corners cut after to require only one tool change. The bending operation is a much slower process since the table must be repositioned for every bend, taking on average ten minutes per part. Each part is finished by deburring the sheet edges both from the guillotine cut and the punch holes. The panels are finally cleaned and prepared for assembly.

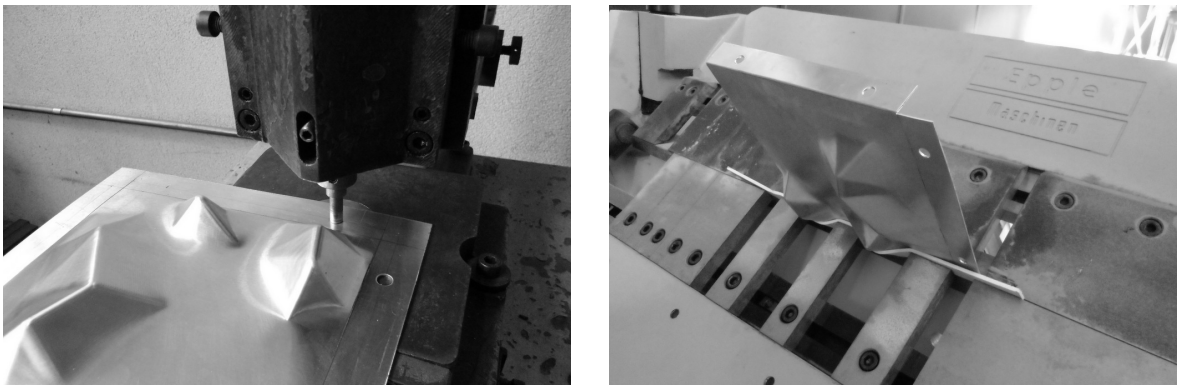

(a) (b)

Figure 5.38: Finishing operation of the architecture panels: (a) punch holing, (b) flange bend folding operation

The finished panels are assembled using the fastening connection with the rubber washer in the joints. The panels are first linked along the matrix lines which are then put together to help alignment. The panel connection not only allows to compensate for differences in the panel size, but also to align the front plane.

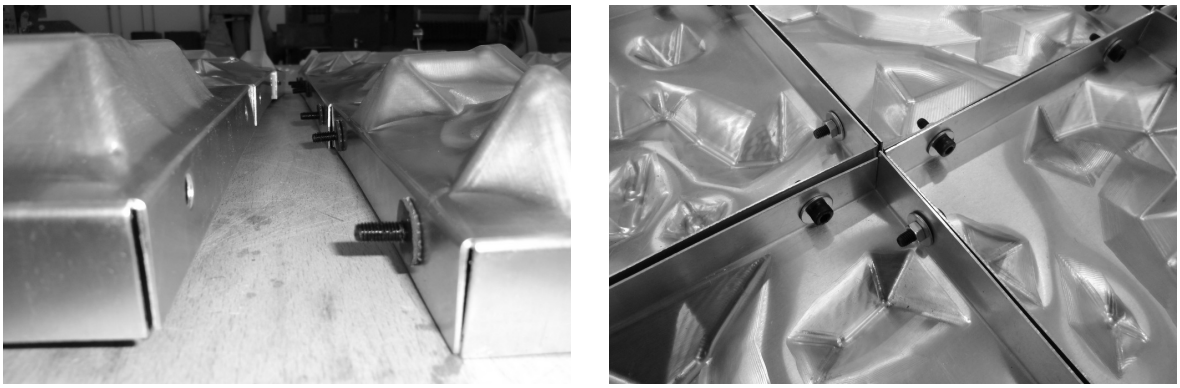

(a) (b)

Figure 5.39: Architecture panels assembling: (a) connection alignment, (b) assembled panels

The pilot installation with nine unique panels surpass the expectation, achieving very interesting aesthetics and exclusivity through a final shape, both influenced by the project and the process. This shared signature, configuring each part with a mix design and process driven geometry, adds value to each piece, endowing it with distinctive historical characteristics from a industrial craft process. Figure 5.40 presents the complete installation with the nine individual and unique panels.

Figure 5.40: Architecture SPIF panels installation

With regard to the full process analysis, each panel development takes on average one and an half hours do complete, with a total energy consumption of 6 kW.h, a total manufacture cost of 75€, where only 2€ are spend in building materials and 26€ on forming operation itself. Tables 5.8 and 5.9 summarises the considered operation for the full process analysis. Although the panel development time and consequently cost is significant, preparation and finishing operations can be done during the forming operation of different parts, and so increasing the achievable production rate.

Table 5.8: Architecture panels full process analysis

Operation	Time	Energy	Cost
CAM programing and post processing	0:10	n.a.	8€
Blank cut	0:01	n.a.	2€
Blank clamping	0:05	n.a.	4€
Tool change	0:05	n.a.	4€
Container forming		view table 5.9	
Tool change	0:05	n.a.	4€
Edge creasing		view table 5.9	
Part release and cleaning	0:05	n.a.	4€
Measure, marking and hole punch	0:05	n.a.	4€
Bending	0:10	n.a.	4€
Finishing and cleaning	0:02	n.a.	2€
Complete process	1:15 to 1:45	4 to 9 kW.h	66 to 86€

Table 5.9: Architecture panels forming operation analysis

	Forming			Edge creasing		
Panel	Time	Energy	Cost	Time	Energy	Cost
0	16:23	2.55 kW.h	15€	10:05	1.59 kW.h	11€
1	22:17	3.56 kW.h	19€	14:45	2.44 kW.h	14€
2	24:52	3.84 kW.h	21€	12:25	1.98 kW.h	12€
3	30:46	3.23 kW.h	25€	13:33	2.20 kW.h	13€
4	18:37	3.01 kW.h	17€	10:17	1.66 kW.h	11€
5	20:09	3.17 kW.h	17€	13:29	2.18 kW.h	13€
5*	15:12	0.83 kW.h	15€	n.a.	n.a.	n.a.
6	25:19	3.93 kW.h	21€	17:40	2.86 kW.h	16€
7	40:09	6.30 kW.h	31€	15:49	2.60 kW.h	15€
8	26:55	4.15 kW.h	22€	17:57	2.98 kW.h	16€

* extra time due to reverse forming, include part flip and tool change

Apart from validating the use of SPIF process for the development of unique parts in architectural applications, the case study development contributed with relevant knowledge on forming multiple cavities and on the design of free form shapes to be manufactured without a backing plate.

The current installation's major drawback concerns with the panels production cost, both in time and material. On each panel development, side operations have larger influence on the part cost than SPIF itself. This dues partly to a very individual fabrication process, adapting tools for each different part. In addition, the case study feature one of less favourable scenarios where sharp edges limit the forming speed and call for a second creasing stage, increasing manufacturing time. Nevertheless, the operation time and cost is compatible with small to medium size batches. For a mass customisation process, changes in the manufacturing process must be done. By pre bending the panels and hold them in a dedicated blank jig for the SPIF operation it is possible to speedup the overall process. In what concerns the

material, a thickness reduction could have a beneficial result not only on cost but also on the forming operation, allowing the use of faster but lower strength forming machines.

With regard to the geometry design, the forming test contributed to the design guidelines for multi container parts or for general parts to be formed without a backing plate. Despite the possible free form surface forming, the SPIF process faces difficulty dealing with very circuitous top perimeters. Mainly when forming with no backing plate, the definition of "peninsula" type configuration harms the part accuracy. When using multiple containers in a part, their proximity improves the geometry transition between them, resulting on a better part.

For the forming operation of multiple container parts without a backing plate, it is concluded that the forming order has strong affect on the end part. Thus, a care definition of the forming strategy and features order could benefit the part quality. Generally, the smaller features are formed with better definition, thus should be preferred. Besides, the nearness of the peripheral blank support also benefits the forming operation, thus giving priority to the pieces near the clamping device.

Chapter 6

SPIF for Rapid Tooling Applications

Due to the pressure of highly competitive markets, industry is driven to compete effectively by reducing manufacturing times and costs while assuring high quality products and service. Besides, environment responsible goals also affect the decisions on industrial manufacturing systems. It is now generally acceptable rapid changes in product volume and model mix calls for a redefinition of the product design and development techniques and the conventional manufacturing processes [10].

Product development takes advantage on the use of CAD systems to define the geometry and its various dimensional characteristics. Besides, the products feasibility can be predicted using computer aided engineering (CAE) software for the analysis of product performance and for the simulation of manufacturing processes without the need of physical prototypes. While these iterations strongly improves the probability of success, in many cases a physical assessment of the real component is still needed. This often requires the creation of prototypes and tools to be produce, becoming one of the most time consuming and costly phases in the development of new products [9, 10, 138].

During the last decades several new smart manufacturing processes have been developed, with great potential for the fabrication of unique parts, commonly named rapid manufacturing methodologies. This process include improvements on traditional manufacturing process such as in CNC milling and the emergence of new technologies like the additive manufacturing systems (AM) and the ISF processes. These manufacturing systems find their applicability not only in the development of prototypes or small volume production, but also for tooling fabrication. These new applications are referred as rapid tooling (RT) techniques and aim to reduce time to market and increase the competitive edge [139]. The leading characteristics of a rapid tooling process should ensure [140]:

- Tooling time is much shorter than for a conventional tool. Typically, time to first articles is below one-fifth that of conventional tooling.
- Tooling cost is much less than for a conventional tool. Cost can be below five percent of conventional tooling cost.
- Tool life is considerably less than for a conventional tool.
- Tolerances are wider than for a conventional tool and have worst surface finishing.

The rapid tooling find its applicability for the development of prototype parts, for small batches production or for first products fabrication before the development of full production tools. By definition, a true prototype is an object produced in the intended material, by the final method of production. The use of RT allows the development of true prototypes, otherwise hard or impossible to obtain. For production scenarios, it is not reasonable to develop production tooling for small volume production. Thus, low cost rapid tooling fill this gap between unique products and large volume mass production. Finally, the development of production tools is typical a time consuming process that can delay a product launch. In these cases, RT can assume an important paper in the manufacturing of the first units, assuming the concept of bridge tooling [9].

Two main classifications of RT are indirect and direct methods. Indirect tooling processes use patterns to produce tools. Direct tooling imply the ability to fabricate a tool directly from a rapid manufacturing machine. Besides, the tooling process can also be classified according to the used materials. If the tooling material can only be used to produce few production copies before it wears, such process is referred as soft tooling. Hard tooling on the other hand involves the production of tools capable of producing thousands of parts. [10, 139]

Mainly due to their novelty and the technologies used in most processes, the RT haven been majorly associated with AM, commonly called as fast free form fabrication (FFF). SPIF and other ISF process can be seen as rapid prototyping processes [37], and so also considered rapid manufacturing methodologies or FFF processes. Besides, being compatible with FMSs, with parts manufactured from CAD models without considerable dedicated tools in short time, ISF processes can be seen analogously to AM technologies. Thus, it is reasonable to apply the RT therm when describing the fabrication of tools for different industrial processes using ISF techniques.

The use of sheet metal and other thin walled structures has considerable application in industrial development of tooling, particularly for processing thermoplastics and composite materials. The sheet materials have usually attractive wight/strength ratios with low material costs and, when applicable, low thermal inertia. Thus, their application in production tools, mainly for small to medium volume production is compelling. However, conventional manufacturing processes have limited geometric freedom or imply the use of very time consuming and expensive tools, thus limiting the use of sheet metal in mould making.

Traditional RT techniques, using AM processes, struggle to achieve thin geometric features, becoming weak competitors for the mould manufacture, at least in a direct method. On the other hand, ISF processes, in particular SPIF, have great appetence for the fabrication of these geometries. In such a way, ISF assume a role of great potential for the development of rapid tooling, particularly for the development of direct hard tooling systems.

The fundamental research on SPIF based RT techniques involves the study of moulds used for different manufacturing processes. For each hypothesis, the research consists of the mechanical and thermal design of the mould, the forming of the mould itself and the test of the mould operation. The mould manufacturing process and operation performance is analysed, evaluated and, when possible, compared against conventional tooling.

A reference geometry is design to support the RT development for different technologies. As the research work aims for a proof of concept, the reference geometry is designed to ensure a feasible forming operation by a single stage SPIF strategy. Thus, a reference geometry derives from a drafted volume with a maximum wall angle of 70^{o}. To avoid a full symmetry, one side wall is sloped at a smaller angle. The part is sized to fit in a 200×200 mm forming window for operational convenience.

The reference geometry is designed with flat areas in order to cut test specimens to use in tensile tests. Since the rapid tooling research seeks the development of thermoplastics and thermoset materials, type IV specimens [141] are chosen to be used in a direct comparison between materials. This allow not only to analyse the moulded material but adds the potential to compare it against the use of conventional tooling.

The specimen, illustrated on figure 6.1, has 115 mm by 19 mm overall dimensions. For the part design, 2 flat areas are chosen with at least 120 mm by 25 mm to cut the specimen for tensile tests. The reference geometry for the new RT techniques development is presented in figure 6.2.

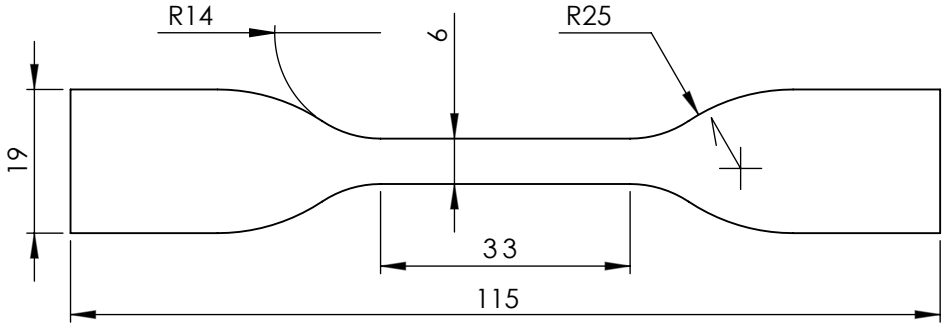

Figure 6.1: Type IV specimen for direct comparison of tensile test on rigid and semi rigid materials

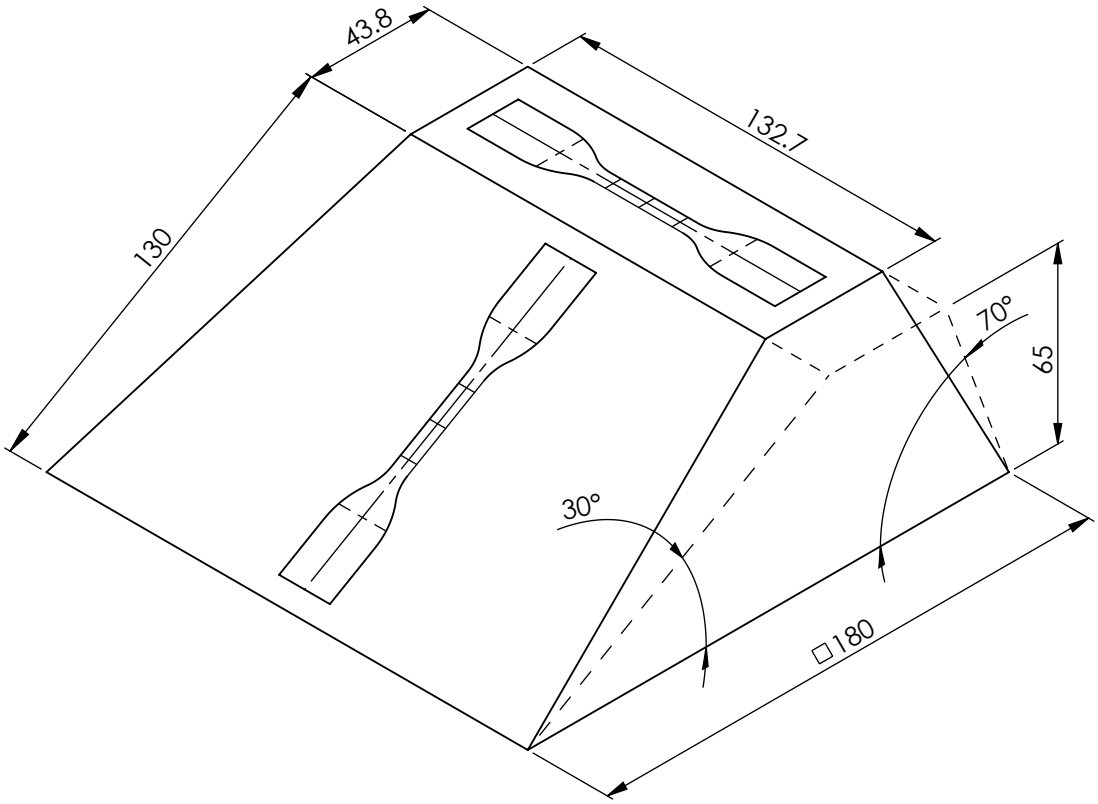

Figure 6.2: Reference geometry for the rapid tooling development

Since the research aims to develop hard tooling techniques, the material properties used in the mould making have a strong influence on its performance. Due to its high formability and to the ease of availability, AA1050 H111 aluminium sheet is selected for the tool development. The alloy is a popular grade of aluminium for general sheet metal work where moderate strength is required. Sheets can be found between 0.2 mm to 6.0 mm. The alloy temper is annealed and slightly strain-hardened, given a minimum yield strength of 85 MPa and an ultimate strength between 105 MPa and 145 MPa. The sheet has a density of 2710 kg/m^3, a Young Modulus of $71GPa$ and a Poisson ratio of 0.33.

To analyse the influence of the forming operation on the material, tensile tests are performed to measure the true yield after strain. Plate type 1 specimens [142] are cut from an incrementally formed part shaped from the reference geometry. Figure 6.3 present the specimens used for the metal characterisation. Three different sets of specimens are cut: from an unformed sheet, from the 30º slope wall and from the 70º slope wall. The analysis of the mechanical properties of the material at each strain hardening state is a key element for an appropriate mould thickness sizing. The cut of the specimens not only allow to characterise the material, but also confirm the final thickness at the different formed angle of the part and compare it against the sine-law estimation.

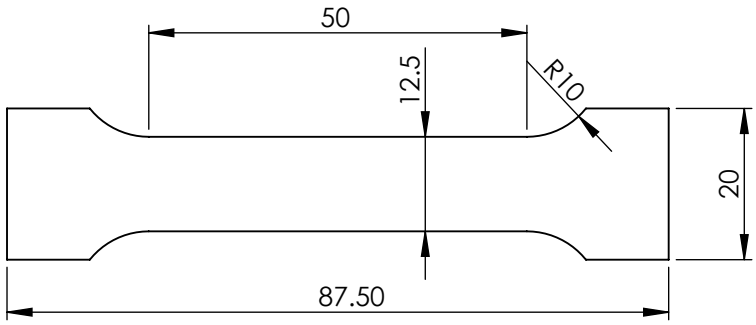

Figure 6.3: Plate type 1 specimen for metallic materials characterisation

For the fulfilment of the mechanical characterisation tests, three parts based on the reference geometry are formed out of AA1050 H111 2 mm sheet. The edge between walls is filleted with a 20 mm radius to allow the forming operation to run at 3000 mm/min without machine vibration issues. The forming operation uses a 12 mm spherical punch in a single stage helical tool path strategy with a 0.5 mm vertical step down. The forming operation is completed without any sheet damage apart from a slight skinning.

Figure 6.4 (a) presents the cut operation of the specimens which thickness are presented in table 6.1. Three sets of specimens are cut from the three different parts, registering the same thickness in all parts. The cut is performed using a 6 mm milling tool operating perpendicular to the sheet. The specimens are finished by deburring, sanding and polishing the trim cuts before performing the tensile tests.

Table 6.1: Aluminium specimens thickness

part area	estimated thickness	measured thickness
unformed top	2.00 mm	1.90 mm
smaller slope wall	1.73 mm	1.65 mm
higher slope wall	0.68 mm	0.60 mm

From a geometric point of view, the cut of the specimens and thickness measurement validates the use of the sine-law for the prediction of the thinning effect in the AA1050 sheet. The sine-law estimates a thickness reduction of 13.5% on the 30º slope wall and 66% on the 70º slope wall and the measure registers a respective thickness reduction of 13.2% and 68.4%. This small difference supports the use of the sine-law for the sizing mould thickness for different material processing technologies.

The tensile tests are performed in a Shimadzu AG-IS 10kN universal testing machine at 5 mm/min. Figure 6.4 (b) presents the tensile test of one of the specimens cut from the higher slope wall. The test on the thicker specimens takes just over 30 seconds to break, the specimens from the smaller slope walls take close to 40 seconds to break and the specimens from the higher slope wall take only just over 10 seconds to break. The specimens cut from the unformed areas fail by neck down break and the ones cut from the formed areas tend to break at 45º. Figure 6.5 present the three sets of specimens after the tensile test, organised from the thicker to the thinner of each formed part. The specimens cut from the higher slope break almost without additional permanent stain. In the remaining specimens, a material elongation is visible in the testes specimens.

(a) (b)

Figure 6.4: Tensile tests of aluminium specimens at different strain strength states: (a) specimen cut at the smaller slope wall (b) tensile test with the specimen cut from the higher slope wall

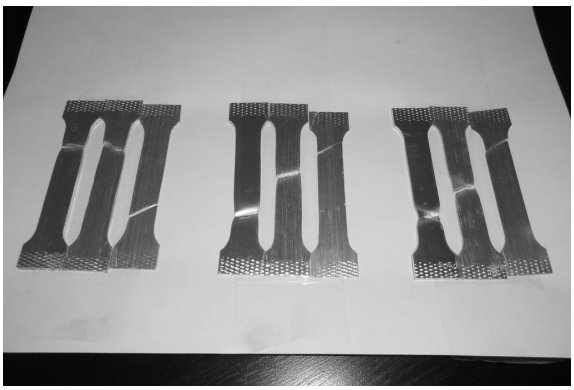

Figure 6.5: Aluminium specimens after tensile tests

The readings from the tensile are treated and presented in the graphic of figure 6.6. Despite no registering a well defined proportional and plastic area, an increase of the yield point is noticeable. The yield value on the unformed specimens is 103 MPa. In what considers the specimens from the smaller slope, no significant variation is found. On the other hand, the yield occur at 130 MPa on the specimens cut from the higher slope. In addition, the thinner specimens material stiffness appears to be slightly higher and breaks without any plastic deformation since the forming operation already induced the maximum admissible strain.

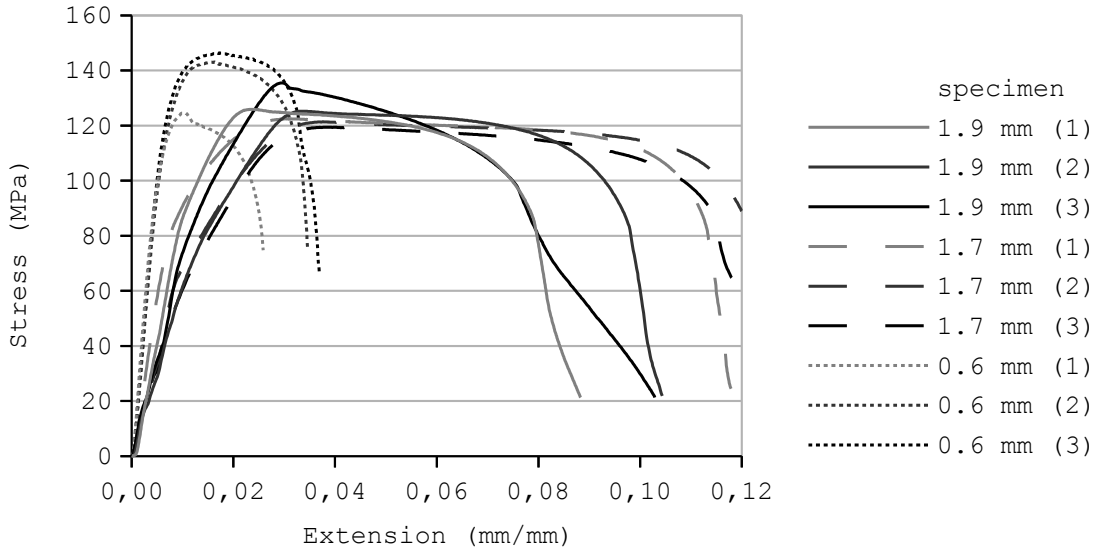

Figure 6.6: Tensile test result of aluminium 1050 specimen at different strain strength: unformed and after SPIF operation forming 30° and 70° walls.

The evaluation of the mechanical properties of the material, particularly the perception of an increase in the yield value from $\sigma_y = 103$ MPa to $\sigma_y = 130$ MPa, support the mechanical design of hard rapid tooling. Although it is expected that thinner walls are under higher stress values, the understanding yield behaviour after strain hardening is crucial for a thickness sizing of a rapid tooling mould.

6.1 Development and test of SPIF thermoforming moulds

6.1.1 Thermoforming process and mould geometry definition

The thermoforming process allows the production of plastic parts by shaping a polymer sheet or film to a mould. The polymer is heated to a pliable state and then pushed to the mould surface. Almost any thermoplastic can be thermoformed, where the most common is the use of High Impact Polystyrene (HIPS), acrylonitrile butadiene styrene (ABS), high-density polyethylene (HDPE) and polymethyl methacrylate (PMMA), commonly know as acrylic. Different methods exist, being vacuum forming one of the most used to the production of small series of 3D shaped plastic parts. Despite using a much simpler mould than other polymer processing technologies as injection, mould cost and development time still has a considerable weight in the development of a product.

Figure 6.7 represent the basic operation concept of a vacuum forming process. A flat thermoplastic sheet is fixed on the forming machine granting an peripheral air sealing. The plastic sheet is heated either before or after the clamping, depending on the machine used. After being heated, the plastic sheet is stretched by a blowing operation before the mould rise, mainly when forming with core moulds. Forming with cavity moulds can dismiss the pre stretching. Vacuum is used to shape the material against the mould before being cooled by an air blower. After cooling, air is blown to help demoulding and the mould descent before part release. The moulding process is relatively slow, with cycle times up to 5 minutes.

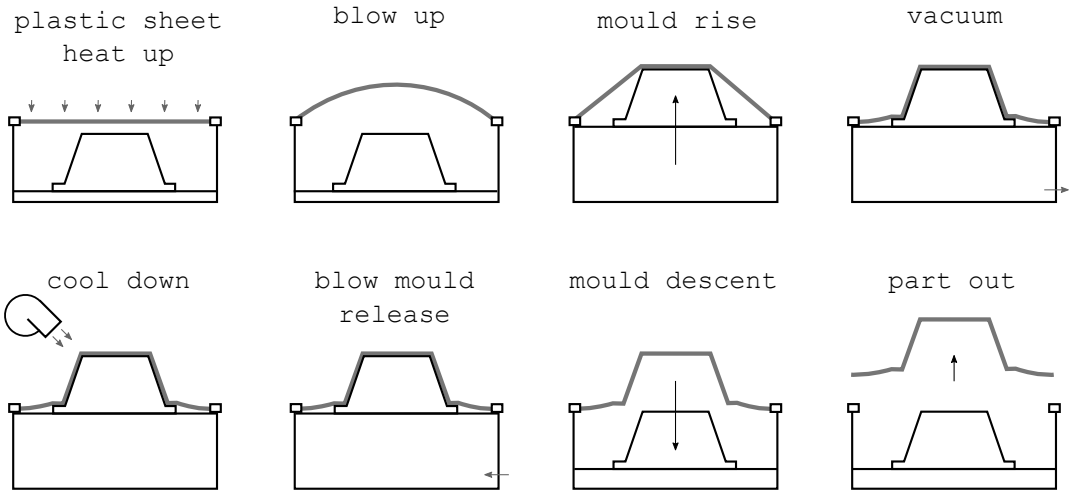

Figure 6.7: Thermoforming operation principle.

Most thermoforming moulds are single surfaced. One surface of the plastic sheet if forced against the mould and the other surface remains unimpeded. Both male and female moulds can be use in vacuum thermoforming operations. Both mould types have complementary geometries of the plastic part, controlling either inside or outside surface of the part. Moulds are usually made by casting aluminium or most frequently milling aluminium, high density rigid polyurethane foams and wood. Sprayed metal, electroformed nickel, hydrocal, and other materials and technologies are also used to make thermoforming moulds. [143] These processes and materials make most mould designs expensive and they take a long time to be build. Besides, high thermal inertia moulds can spoil the continuous operation if cooling is not performed.

The female or negative mould uses a cavity with the complementary geometry of the outside of the plastic part. It is used when the outside of the plastic part is to be controlled. The male or positive mould uses a boss with the complementary geometry of the inside of the plastic part. It is used when the inside of the plastic part is to be controlled. Both mould configurations must be drilled in the lower points to allow the vacuum to pull the plastic sheet. Highly complex parts can include both positive and negative features in the same mould. The opposite side of the mould tolerance in inferior as thinning occurs during thermoforming. Besides, due to the strain during the forming operation, textured plastic sheets are highly affected by thermoforming operation, mainly when forming tall parts.

As vacuum thermoforming pressure is low, it is possible to replace conventional tooling materials and designs by sheet metal based moulds. SPIF can be used to shape sheet metal to the desired surface becoming possible to design sheet metal moulds. Apart from be a potential faster and more economical tooling process, a low thermal inertia may benefit the mould operation. Nevertheless, the fabrication of the sheet metal mould as some geometry related issues.

6.1.2 Part design

Thermoforming parts are shaped like open shell structures from small as a few millimetres to a few meters. Most parts use thickness up to 3 mm thickness, while thicker sheets up to 5 to 6 mm can be used. A minimum 5° draft angle should be used in order to me possible do form parts with any material namely crystalline polymers, mainly when forming with positive moulds. As the mould may have texture due to technological reasons, 1° additional draft should be added for every 5 μm in texture depth. Due to material compression during cooling, parts from negative moulds could have smaller or even zero draft. Lastly, one can say that the larger the draft angle, the better for the finished part [143].

The moulding process allows to shape the plastic sheet to a free form surface, with limitation of obtaining sharp edges. In what concerns fillet radius, to minimise corner stress concentration on the formed part, internal corner radii should have a recommenced minimum of 80% of the plastic thickness [144]. Like in draft, the bigger the fillets on both side and top faces are, the better for the finished part. Fillet radius can also be influenced by technological limitations on the mould making process.

Lastly, a draw ratio of the part geometry also influence its feasibility, where the draw ratio is determined by the surface Area of the part over its footprint. Generally, every feature on a part should avoid being more narrower than it is tall. Besides, as the draw ratio gets larger the radii will almost always have to be increased.

A part is designed based on the reference geometry, aiming to allow both a geometric and a mechanical comparative analysis between the thermoforming process using a formed sheet metal mould and conventional moulds. For the geometric approach it is intended to test flat horizontal areas, different draft angles and different fillet radius. As both positive and negative moulds are intended to be tested, a minimum draft angle is needed.

The test part is designed as a single symmetric part with a projected area of 180 mm by 180 mm and a maximum height of 65 mm with 3 mm of material thickness. It is shaped as a 5 sides box with a minimum draft angle of 20° used on the higher slant sides and one side with a smaller slide. The internal radius used between side faces is 15 mm and between side and top faces is 6 mm. The top has a 120 mm by 35 mm flat area and the smaller slope side has a 127, 6 mm by 106, 6 mm flat area to cut specimens. Figure 6.8 presents the drawing

of the test part with a 3 mm constant thickness. The part is dimensioned in both sides, with inner dimensions to be controlled when thermoforming using a positive mould and outer dimensions to be controlled when using a negative mould.

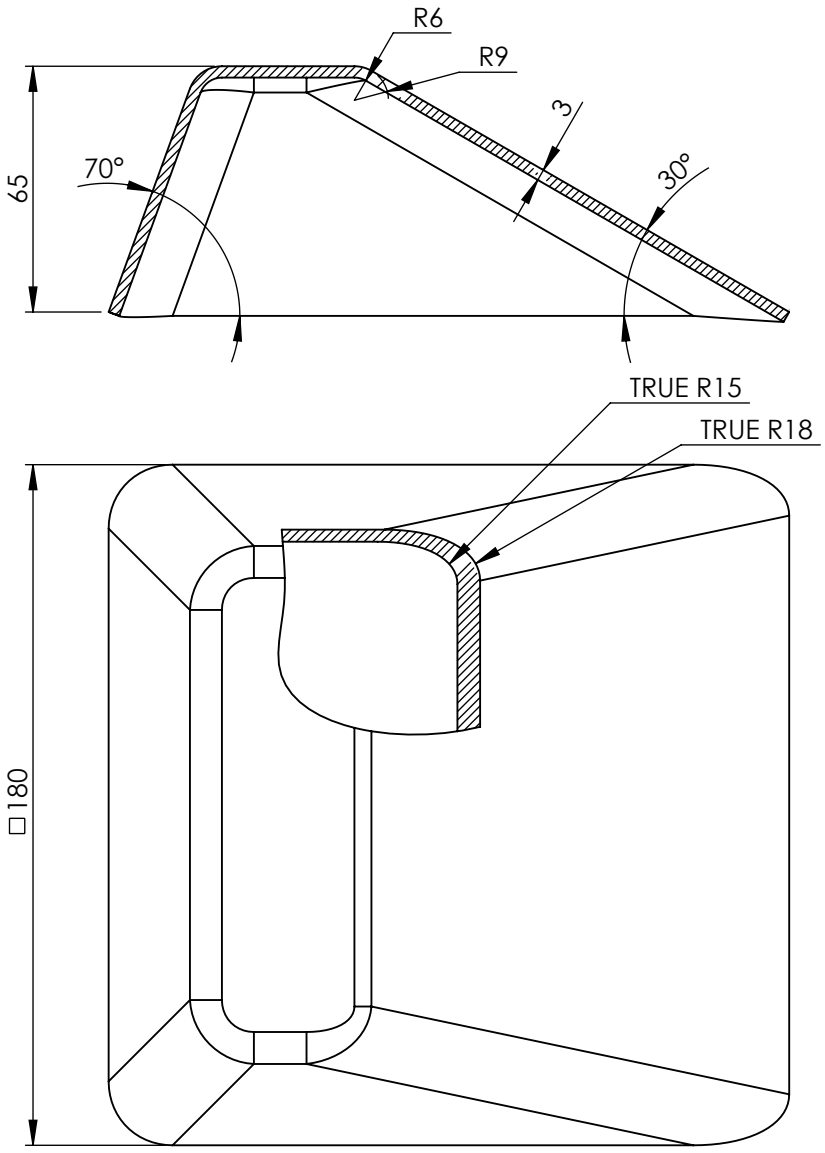

Figure 6.8: Part design for the SPIF rotomoulding concept validation with 3mm constant thickness to thermoform controlling either inside or outside surface, scale 1:2

6.1.3 Mould design and manufacturing

For the evaluation of the use of stand alone sheet metal moulds for thermoforming operations two approaches are followed, operating with a positive and with a negative mould. To test the new fabrication method, two aluminium Alloy 1050 sheet moulds are designed. Sheet metal moulds are designed according with conclusion of previous tests [111]. A SPIF sheet shapes the mould surface and it is supported by a MDF box. For both positive and negative moulds a similar approach is taken, using a 230 mm square sheet supported by a MDF box.

As the SPIF process is better suited to the manufacturing of cavities, the definition of the geometry to be formed for the negative mould is straightforward. The side of the metal sheet facing the forming tool is used as the contact surface for the thermoformed plastic sheet. Thus, thickness variation on the sheet metal doesn't cause major influence on the thermoformed part.

On the other hand, when developing a positive mould, as the SPIF produces cavities, the reverse side of the metal sheet must be used as the contact surface of the mould. As metal sheet stretches it gets thinner. Despite controlling the tool path that forms the sheet metal, due to sheet shrinkage there is no precise control of the outside geometry. Therefore, the definition of the mould geometry is much devious, depending on the thickness estimation by the sine law (equation 2.1).

The negative mould is shaped by the complementary surface of the outer side of the test part. This results on a 180 mm by 180 mm cavity on the mould. The positive mould is shaped by expanding the complementary surface of the inner side off the test part, getting to a 180 mm by 177 mm boss on the mould in order to achieve a more similar base area.

In order to allow the manufacture and use, the positive mould is complemented with a flat base with drafted sides. Both the sheet metal mould and the support board are drilled to allow vacuum to shape the thermoplastic material. The negative mould is assembled over a drafted support box. The negative mould hollow cavity is drilled in the bottom corners to enable vacuum. Figure 6.9 represents the concept of the moulds.

Mould mechanical behaviour

Due to SPIF limitations, previous SPIF mould thermoforming tests proposed a reinforcement of the sheet metal mould by either adding a grid of support points or lines or filling the mould box with a porous mixture [111]. This need due to the lack of stiffness of most ISF machines which limits the maximum sheet thickness. The SPIF-A machine [6, 12] has fewer strength limitations and allows the use of thicker sheets or more rigid materials. Therefore, it is possible to produce a mould without inner reinforcements.

As refereed, thermoforming is a low pressure process. Some thermoforming techniques may use additional pressure up to 0.3 MPa [145]. In the case of vacuum forming, the maximum moulding force occurs at full vacuum. Accordingly, mould pressure is limited to a reference value of 0.1 MPa.

The simulation of mould mechanical behaviour considers a worst case scenario for a vacuum forming operation, where the full moulding surface is under the maximum plausible pressure. The sizing of the sheet thickness for the case should grant the mould strength and stiffness for thermoforming operation. Thus, a uniform pressure of 0.1 MPa on material contact surfaces is considered for the mechanical analysis.

Finite element method is used to determine minimum sheet thickness by a static analysis using the FFEPlus implicit integration solver on solidworks simulation. Simulation is done considering isotropic AA1050 H111 sheet metal with $E = 69$ GPa, $G = 26$ GPa and $\nu = 0.33$. The support box is defined by 16 mm MDF, considering isotropic material with $E = 4$ GPa, $\nu = 0.25$ and $\sigma_y = 17$ MPa.

The sheet thickness on mould walls is determined by the sine law as a function of the top (blank) thickness. Simulations are performed considering nominal thickness value from 1 mm thickness. The analysed thickness are present in tables 6.2 and 6.3. Apart from the blank thickness, it is noted the expected thinner thickness after forming operation.

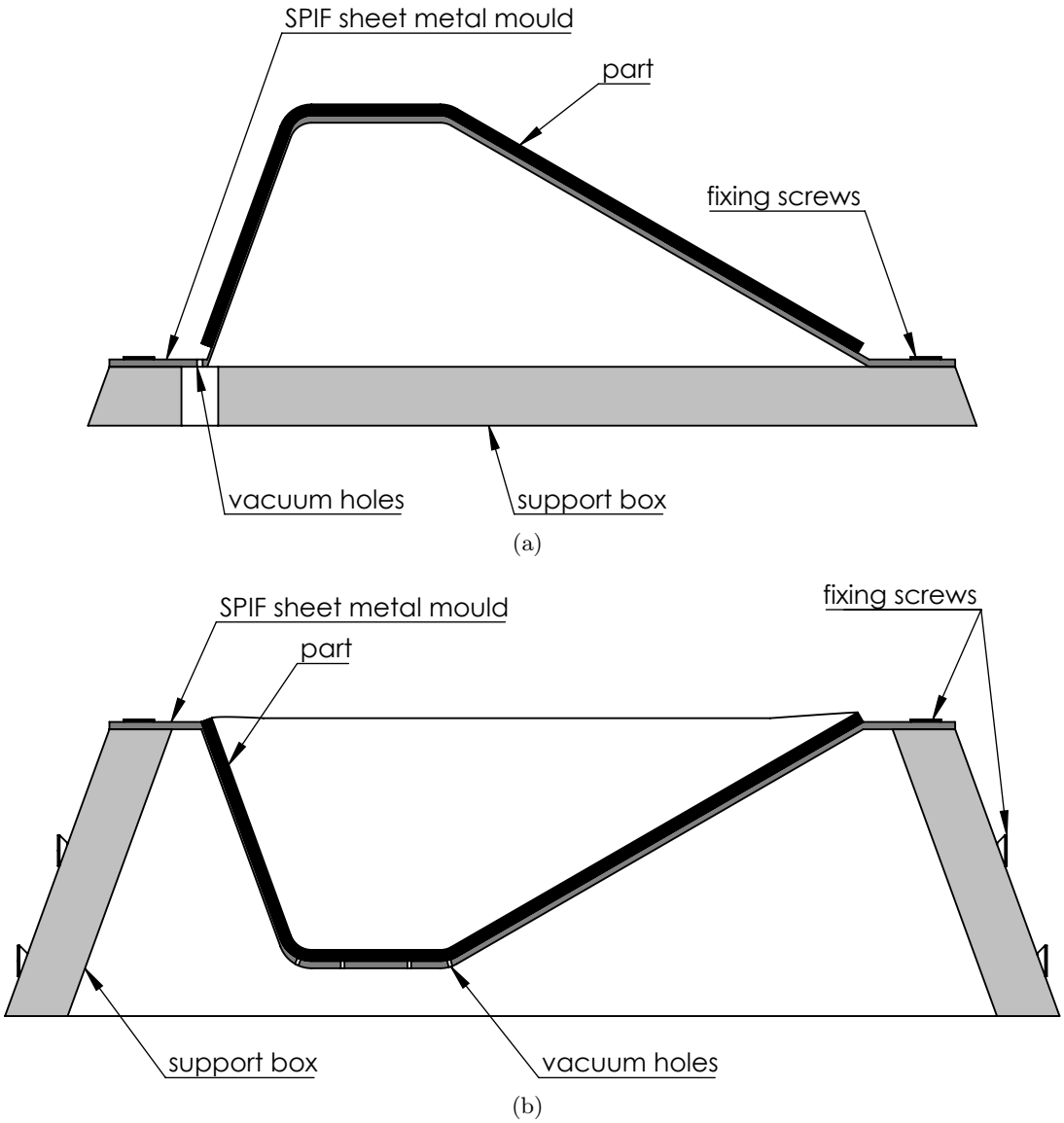

Figure 6.9: SPIF Thermoforming mould concept: (a) positive mould, (b) negative mould

Meshing is done considering a solid mesh using tetrahedral elements with four integration points. The used element size is allowed to range the initial sheet thickness to one sixth of its value, leading to a maximum possible element aspect ratio of 6. The maximum element size lower bound is limited to 2 mm to avoid excessive number of elements. The mesh distribution is defined using curved based mesh, granting a minimum of eight element in a circle and considering a maximum element size grow ratio of 1.6. The meshing details are presented in tables 6.2 and 6.3.

For simulation, mould base is considered fixed in bottom of the MDF. A uniform pressure of 0.1 MPa on all outer surfaces is applied. Global contact between parts is defined with no penetration and a static frictional coefficient of 0.2.

Table 6.4 refers the stress and displacement values of the positive mould and table 6.5 refers the values of the negative mould.

Table 6.2: Mesh details on thermoforming positive sheet metal mould

Blank thickness (mm)	Min. thickness (mm)	Max. element size (mm)	% elements with aspect ratio < 3	Number of elements
1.0	0.34	2.0	95	828510
2.0	0.68	2.0	98.2	843645
3.0	1.03	3.0	97.0	253739
4.0	1.37	4.0	92.5	116740

Table 6.3: Mesh details on thermoforming negative sheet metal mould

Blank thickness (mm)	Min. thickness (mm)	Max. element size (mm)	% elements with aspect ratio < 3	Number of elements
1.0	0.34	2.0	89.8	1645538
2.0	0.68	2.0	98.3	1655574
3.0	1.03	3.0	97.1	349351
4.0	1.37	4.0	96.3	159229

Table 6.4: Stress and displacement on positive sheet metal mould

Thickness (mm)	Max. Stress (MPa)	Max. Displacement (mm)
1.0	1015	17.9
2.0	360	2.53
3.0	144	0.70
4.0	131	0.63

Table 6.5: Stress and displacement on negative sheet metal mould

Thickness (mm)	Max. Stress (MPa)	Max. Displacement (mm)
1.0	908	15.6
2.0	322	2.27
3.0	128	0.75
4.0	67	0.37

A sheet thickness of 3 mm is selected for the manufacture. Stress and displacement distribution is presented on figure 6.10 for the positive mould and on figure 6.11 for the negative mould. Although the calculated displacement is significant, it is lower then the SPIF typical accuracy. Thus, increasing the mould thickness should not benefit the thermoformed part accuracy as despite being more rigid, may be less accurate. With regard to stress, although the value is close to yield, it only occurs on specific points and small areas. Furthermore, calculus considered a pressure of 0.1 MPa (pure vacuum), situation that is never fully achieved in thermoforming process. The drawings of the moulds are presented on appendix E.1.

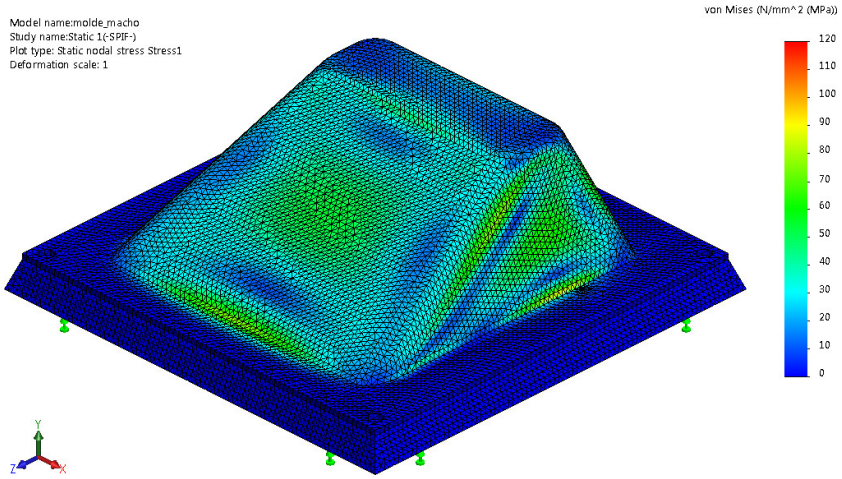

(a)

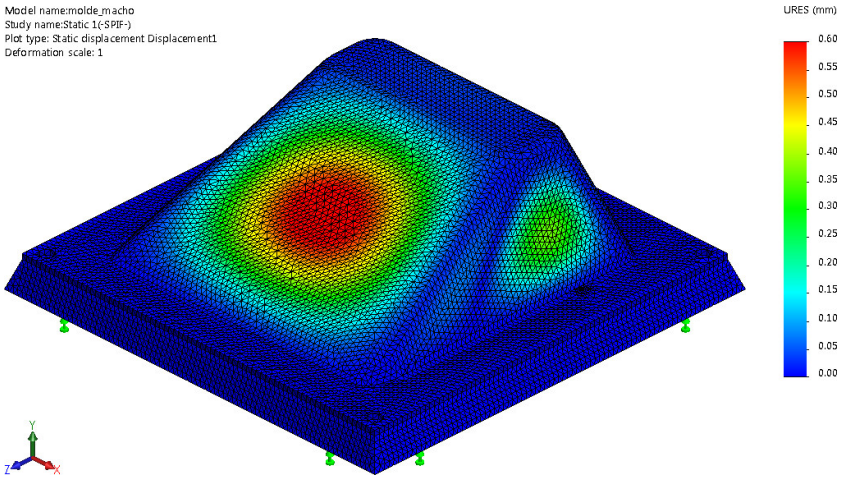

(b)

Figure 6.10: FEM test results on a 3mm sheet positive mould: (a) stress (b) displacement

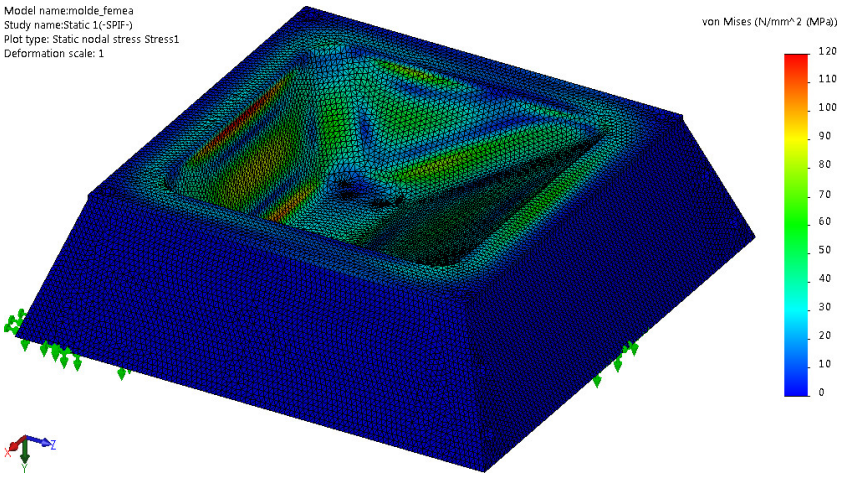

(a)

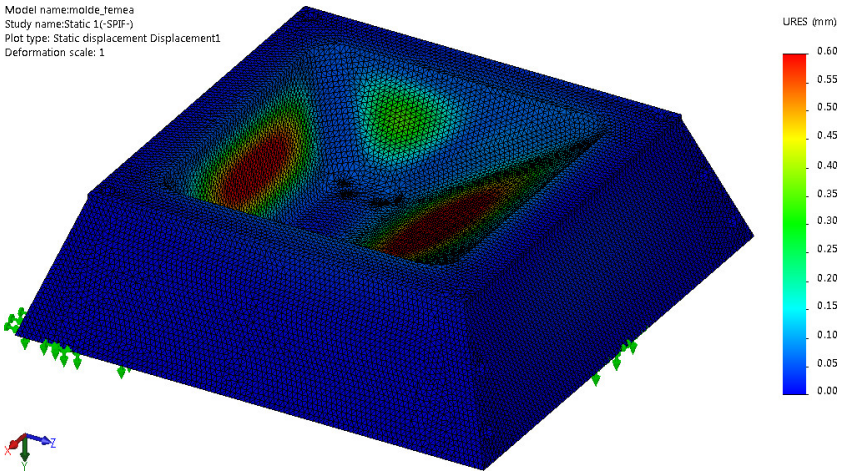

(b)

Figure 6.11: FEM test results on a 3mm sheet negative mould: (a) stress (b) displacement

Mould manufacturing

The SPIF mould manufacturing process included the fabrication of a backing plate, cut of the blank, incremental form of the mould surface, support box part cut and assembly and vacuum holes drilling. Both the negative and the positive moulds manufacture are made while measuring the development and the fabrication time, as well as the material cost and energetic cost.

The manufacturing of a mould by single point incremental forming starts with the cut of a backing plate. The drawing of the backing plate is made by offsetting the outline of the sheet part by 1 mm. A waterjet cutting process is used in order to cut the backing plate from a 5 mm steel sheet, with a material cost of 40€/m^2. The same backing plate is used for both positive and negative mould. Nevertheless, cutting time, material cost and energy consumption is totally accounted for each mould type. The backing plate cutting operation, including preparation, is considered for the overall mould manufacturing operation as it is essential to achieve good forming results.

Second step of the process involves the cut of the aluminium sheet. The 230 mm by 230 mm 3 mm thickness blank is cut from a flat aluminium sheet using an hydraulic guillotine. Two blanks are cut to be used in each mould with a material cost of 80€/m^2. Due to the fast operation time for the blank cut, the energetic consumption is neglected.

For the SPIF operation, a single stage spiral constant Z tool path with a vertical increment of 0.5 mm using a 12 mm ball tip tool is programed. This strategy produces better surface finishing and better accuracy then dropping each z step at one point. The forming operation includes the preparation and machine set up, forming and handling the blanks. The programming and nc program compiling time is considered to the overall evaluation. The SPIF machine set up includes changing backing plate, changing tool and changing sheet holders. The blank is then held to the frame by screwing the sheet holders. The machine is powered up and the sheet position is referenced by moving to tool tip to the centre of the sheet surface. The forming process ran at 3000 mm/min feed rate during an average time of 22 minutes, with a total energy consumption of 4 kW.h. Figure 6.12 illustrates one of the final z increments of each mould SPIF operation. After forming, the parts are released and the lubrication oil is cleaned.

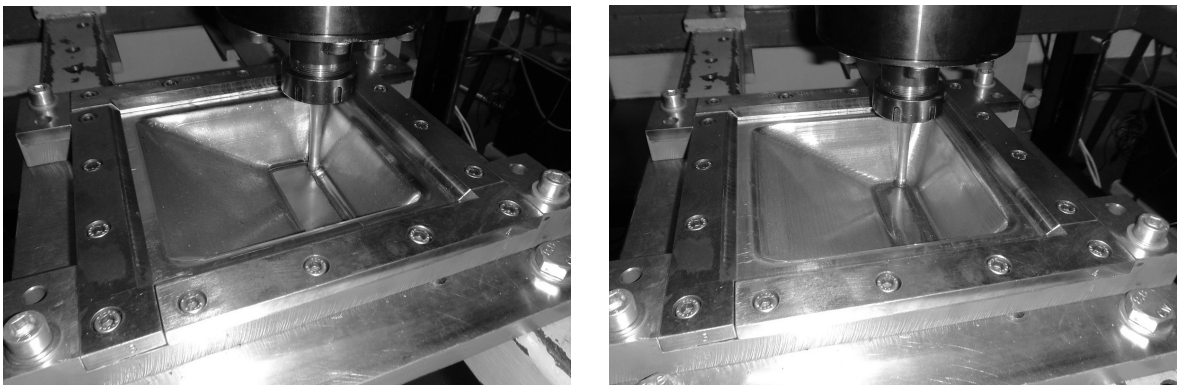

(a) (b)

Figure 6.12: SPIF operation forming sheet metal thermoforming moulds: (a) positive (b) negative

After forming operation, the mould sheets are drilled to allow vacuum during thermoforming when the plastic sheet seals to the mould surface. Drilling is performed with a cordless drill, boring 8 1 mm holes on the negative mould and 3 1.5 mm holes on the positive mould.

To finish the moulds, the base MDF board for the positive mould and MDF box for the negative bold are made to assembled. Angle cuts are made with a circular power saw and parts assembled with self tapping screws. Sheet moulds are screwed to the MDF to be held in place. The average material cost for the material is 10€/m^2.

During the mould manufacture, operation time and energy consumption is measured. As the work is carried out at different locations and with in between pauses to analyse the process evolution, the measurement is done for individual tasks instead of continuously.

Tables 6.4 and 6.5 resume the time and energy consumption for positive and negative moulds. Backing plate cutting and blanks cutting is taken into account for both moulds as it is a mandatory operation if only one of the approaches is made.

Total fabrication time for the positive mould is 1h27min being only 58% for SPIF process. The total energy consumption is 6.63 kW.h, although a large proportion is derived from the water jet cutting. The total material cost is just 8.00€, being 2.50€ for the backing plate, 4.50€ for the aluminium sheet and 1.00€ for the MDF.

The negative mould fabrication time is 1h55min with only 46% of the time for SPIF process. The total energy consumption is 6.66 kW.h, despite the same large proportion at expense of the water jet cutting. The total material cost is 8.50€ due to a larger amount of MDF board.

Figure 6.13 represent a pie graphic display of the time and energy consumption in the SPIF mould manufacture for a better reading.

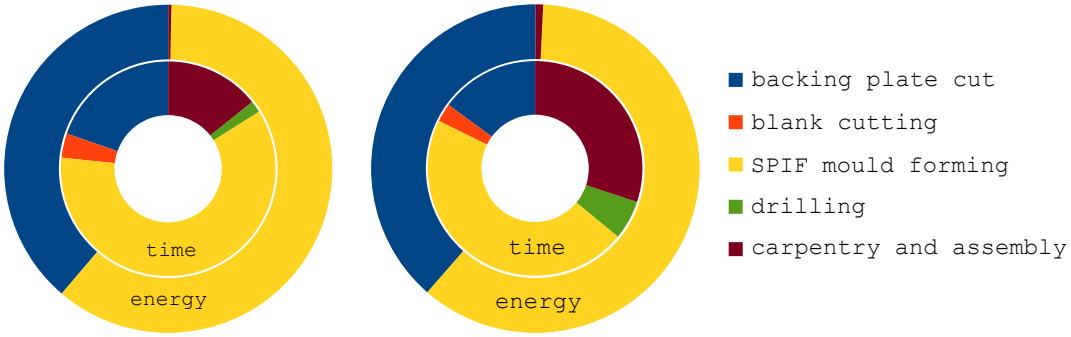

(a) (b)

Figure 6.13: Time and energy consumption in the SPIF thermoforming mould manufacture: (a) positive (b) negative

After manufacture, SPIF sheet moulds are measured by contact using a touch-trigger probe on a 3 axis co-ordinate measuring machines (CMM). Figure 6.14 illustrates the measuring operation of the sheet metal moulds and figure 6.15 shows the comparison between the SPIF part and the CAD. Maximum deviation is +2.9 mm on the positive mould and +6.8 mm on the negative mould. Average deviation is +0.3 mm on the positive mould and +1.8 mm on the negative mould.

Table 6.6: Time and energy consumption in the SPIF positive mould making

Operation	Sub operation	Time (min)	Energy Consumption
Waterjet backing plate cut	backing plate drawing	2:06	-
	cut programing	5:02	-
	machine set up and start up	2:55	0.02 kW.h
	define cut position and parameters	1:55	0.01 kW.h
	cut	4:29	2.54 kW.h
	part removal and clean	0:42	-
Guillotine blank sheet cutting	machine set up	0:28	-
	4 piece cutting	2:43	-
SPIF mould forming	CAM preparation	7:58	-
	compile CAM	3:12	-
	machine set up and start up	7:48	0.20 kW.h
	sheet holding	6:46	-
	define zero	1:33	0.34 kW.h
	forming positive mould	21:57	3.50 kW.h
	part removal and clean	3:34	-
Drilling	sheet drilling	1:32	-
Carpentry	working area and machine set up	4:58	-
	cutting parts	5:15	0,02 kW.h
	assembly	2:14	-

Table 6.7: Time and energy consumption in the SPIF negative mould making

Operation	Sub operation	Time (min)	Energy Consumption
Waterjet backing plate cut	backing plate drawing	2:06	-
	cut programing	5:02	-
	machine set up and start up	2:55	0.02 kW.h
	define cut position and parameters	1:55	0.01 kW.h
	cut	4:29	2.54 kW.h
	part removal and clean	0:42	-
Guillotine blank sheet cutting	machine set up	0:28	-
	4 piece cutting	2:43	-
SPIF mould forming	CAM preparation	8:09	-
	compile CAM	3:12	-
	machine set up and start up	7:48	0.20 kW.h
	sheet holding	6:46	-
	define zero	1:33	0.34 kW.h
	forming negative mould	22:09	3.50 kW.h
	part removal and clean	3:34	-
Drilling	sheet drilling	6:45	-
Carpentry	working area and machine set up	4:58	-
	cutting parts	23:05	0.05 kW.h
	assembly	6:28	-

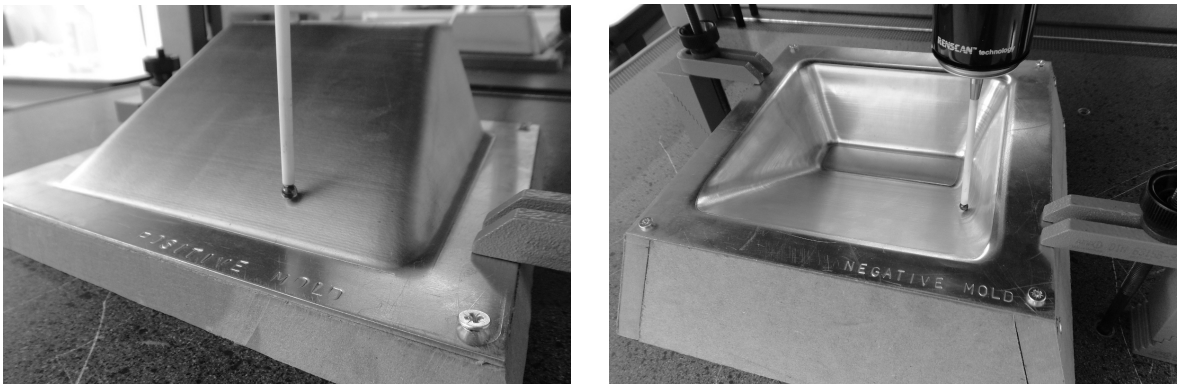

(a) (b)

Figure 6.14: Sheet metal thermoforming moulds dimensional measurement: (a) positive (b) negative

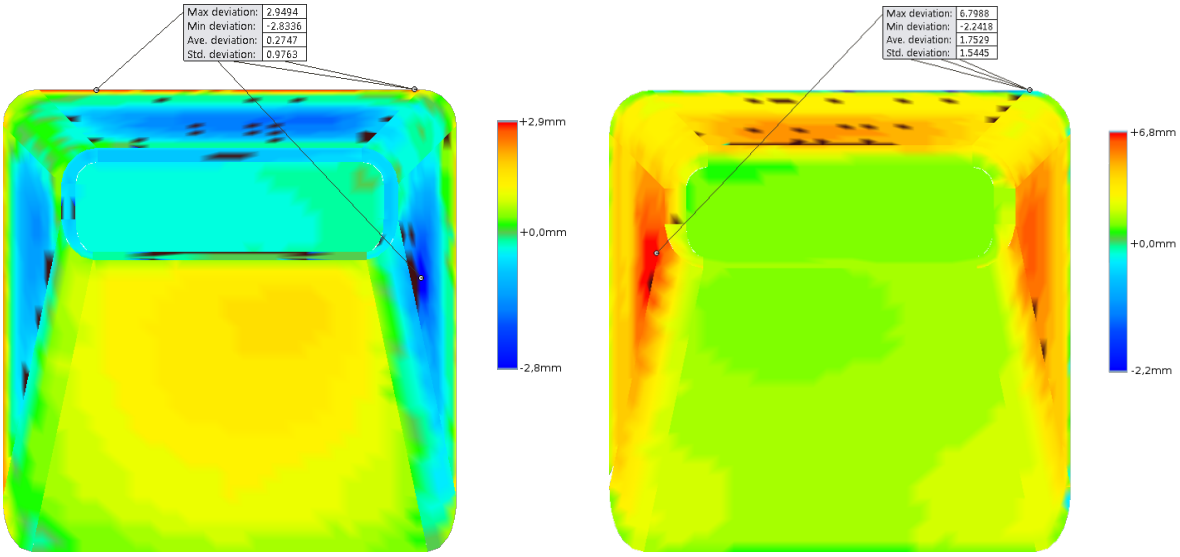

(a) (b)

Figure 6.15: Sheet metal thermoforming moulds dimensional measurement results: (a) positive (b) negative

Furthermore, both moulds are remeasured after being used to check for permanent deformations caused due to vacuum. No major variations are found with average 0.05 mm between first measurement and the one done after use.

Conventional mould design and manufacturing

To establish a benchmark reference for the sheet metal mould, a conventional milled NECURON® 651 mould is designed. The benchmark moulds are designed to have the same overall dimensions as the SPIF moulds so that the differences in thermoforming operation are restricted to the mould accuracy, surface finishing and strength.

The conventional mould manufacturing process included block preparation and machining, including milling and drilling operations. As in the SPIF mould manufacture, the tool development operation is registered measuring time, energy and material cost.

The manufacture of the conventional milled NECURON®651 starts with the cut of a material block using a vertical bandsaw. The blocks are cut from a standard 100 mm NECURON plate with a 5 to 10 mm clearance to the part overall dimensions, with and average cost of 430€/m^2. The part up side is then milled and drilled in a CNC machining center. The part is then flipped and the bottom part is milled to achieve the final base thickness and drilled. Area clearance milling operations used a modular toroidal mill with 25 mm diameter and 2 mm tip radius. Cutting parameters used are 20 mm sidestep, 0.6 mm vertical step, 2300 rpm spinning and 5600 mm/min feed rate, leaving a 0.5 mm offset. Side finishing used a 12 mm ball tip mill with a spiral constant Z tool path with a vertical step of 0.5 mm, the same tool path used for SPIF operation. Side finishing ran at 3000 mm/min feed rate and 9000 rpm spin. For the bottom face finishing and top finishing a 20 mm modular mill with a 0.8 mm tip radius is used. The operation ran at 2400 mm/min feed rate with a 3000 rpm spin and a 18 mm sidestep. Figure 6.16 show the side finishing operation for both moulds manufacture. Although the mold design for the conventional moulds is the same as the SPIF moulds, there are some dimensional differences between them due to different process accuracies.

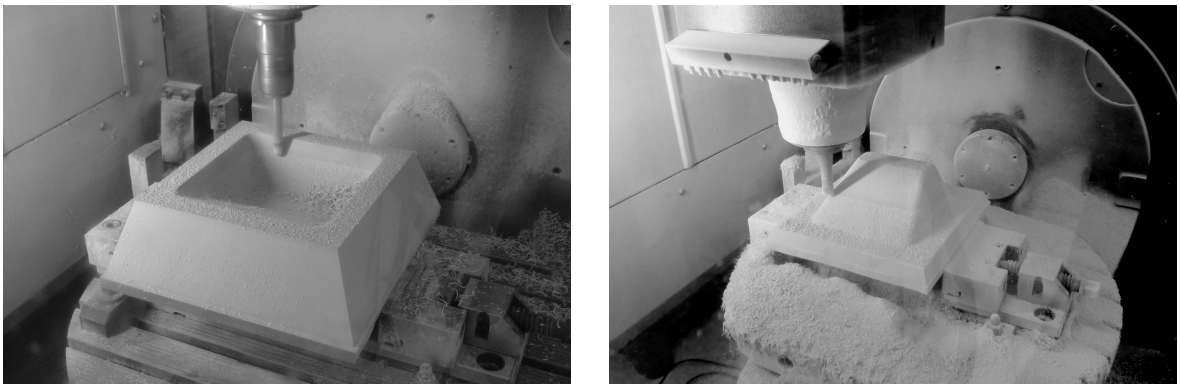

(a) (b)

Figure 6.16: Conventional mould manufacturing: (a) negative (b) positive

As in the SPIF moulds manufacture, operation time and energy consumption is measured, with the measurement done for individual tasks instead of continuously. Table 6.8 and 6.9 resume the time and energy consumption for positive and negative moulds.

Total fabrication time for the positive mould is 5h16min, total energy consumption is 9.32 kW.h and total material cost is 35€. The negative mould fabrication time is 4h42min, total energy consumption is 8.00kW.h and total material cost is 40€. The time and energy consumption of the conventional mould manufacture is presented in the figure 6.17.

Table 6.8: Time and energy consumption in the conventional positive mould making

Operation	Sub operation	Time (min)	Energy Consumption
Block preparation	Block measurement	1:14	-
	Machine set up	0:16	-
	block cut	5:31	0.06 kW.h
mould machining	CAM preparation	13:43	-
	compile CAM	1:34	-
	machine set up and start up	2:21	0.04 kW.h
	fixing block up side	0:40	-
	define zero up side	2:36	0.07 kW.h
	machining up side	239:57	7.83 kW.h
	fixing block down side	3:56	-
	define zero down side	2:30	0.07 kW.h
	machining down side	37:23	1.25 kW.h
	part removal and clean	4:38	-

Table 6.9: Time and energy consumption in the conventional negative mould making

Operation	Sub operation	Time (min)	Energy Consumption
Block preparation	Block measurement	1:16	-
	Machine set up	0:16	-
	Block cut	7:58	0.10 kW.h
mould machining	CAM preparation	16:39	-
	compile CAM	1:36	-
	machine set up and start up	2:21	0.04 kW.h
	fixing block up side	0:48	-
	define zero up side	3:08	0.09 kW.h
	machining up side	187:48	6.03 kW.h
	fixing block down side	2:38	-
	define zero down side	2:38	0.06 kW.h
	machining down side	50:46	1.68 kW.h
	part removal and clean	3:52	-

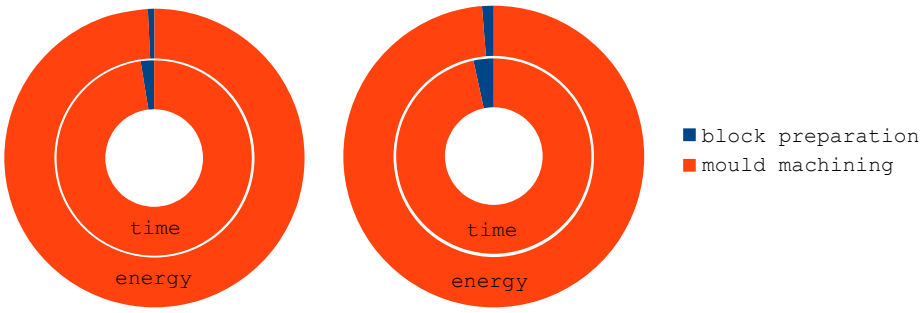

(a) (b)

Figure 6.17: Time and energy consumption in the conventional mould manufacture: (a) positive (b) negative

Mould manufacture comparison

Generally speaking, SPIF mould manufacture is faster then the conventional approach and with a lower expenditure on materials and on energy consumption. Table 6.10 resumes the analysed data of the moulds manufacturing.

On average, the SPIF moulds took 70% less time to produce than the conventional ones. In what concerns material cost, the SPIF manufacture allowed a reduction of almost 80%. In terms of energy consumption, the SPIF process allowed a reduction of 20%.

Table 6.10: Mould manufacture comparison

mould	Manufacture time	Energy consumption	Material cost
SPIF positive	1h27min	6.63 kW.h	8.00€
Conventional positive	5h36min	9.32 kW.h	35.00€
SPIF negative	1h55min	6.66 kW.h	8.50€
Conventional negative	4h42min	8.00 kW.h	40.00€

Relatively to the energy cost of the sheet metal mould fabrication, it is noticeable that a large parcel is related to the backing plate cut. The energetic effectiveness of the overall process could be even more enhanced by replacing the water jet cutting for other processes, for say bandsaw cutting of the outer frame and Wire EDM cutting of the interior window.

In what concerns the manufacturing time, it is noticeable that on average the forming process only take 50% of the total time. The total time spent for the fabrication of sheet metal moulds, and consequently the energy consumption, could be further reduced by avail the backing plate and the MDF box for more then one mould.

Figure 6.18 represent comparative bar graphic display of the material cost, time and energy consumption in the four moulds manufacture for a better reading.

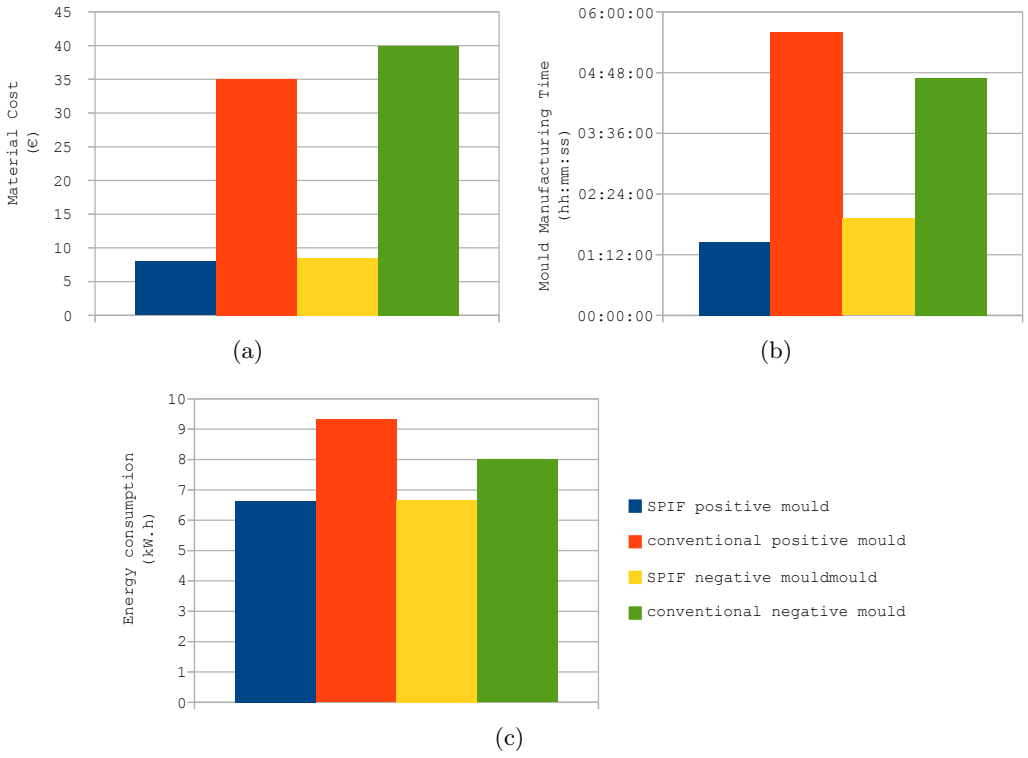

Figure 6.18: Mould manufacture comparison: (a) material cost (b) time (c) energy consumption

6.1.4 Mould operation

For mould validation, various tests are performed using both the SPIF sheet metal moulds and the conventional moulds. The thermoforming tests are performed in a Formech 1772 machine. The moulding surface is spay up with silicone based demoulding agent. Figure 6.19 presents one of the first thermoforming tests performed with the positive sheet metal mould, thermoforming with 3 mm HIPS plastic sheet.

The forming operation works without major noticeable differences between the sheet metal moulds and the conventional moulds. The plastic sheet forms properly to the moulding surface and the mould suffers no visible deformation during the vacuum. The vacuum holes allow to pull the material against the mould and no issue is caused by the material contact. When forming a series of parts, minor heat increase occurs in the sheet metal moulds, resulting on a faster cooling rate of the plastic parts. After forming, the parts release with ease from the moulds. In the sheet metal moulds no harm is enforced neither to the moulds or the parts when no demoulding agent is used.

In a second series of tests, for mould validation, a 3 mm PMMA (acrylic) sheet sheet is used for thermoforming operation. Experiment take place with 100 sec of heat time at 100% power on one side of the sheet and additional 200 sec of heat time on the other. Vacuum is held for 15 sec and cooling by air blowing is held for 30 sec. Figure 6.20 illustrates the thermoforming process using the sheet metal moulds. Despite the increased difficult to thermoform the material, operation succeeds in both the positive and negative moulds.

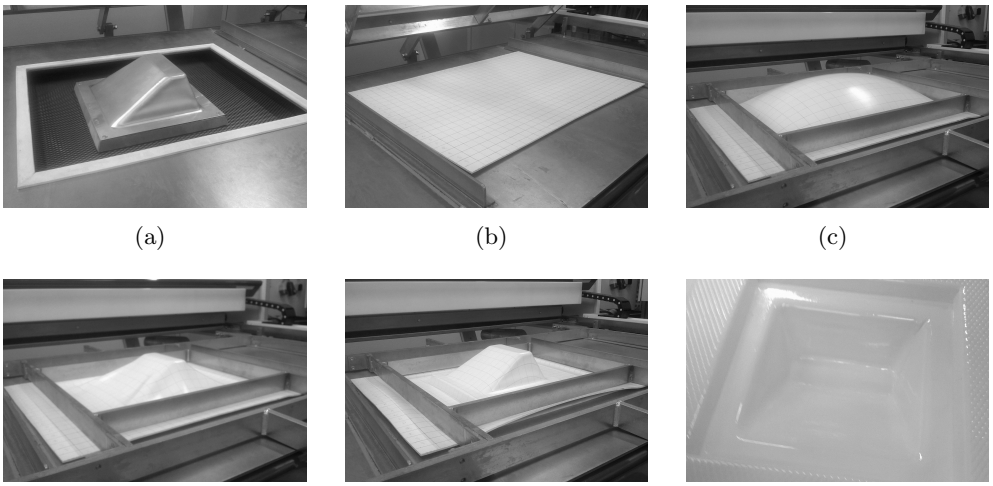

(a) (b) (c)

(d) (e) (f)

Figure 6.19: Thermoforming with SPIF sheet metal moulds using HIPS

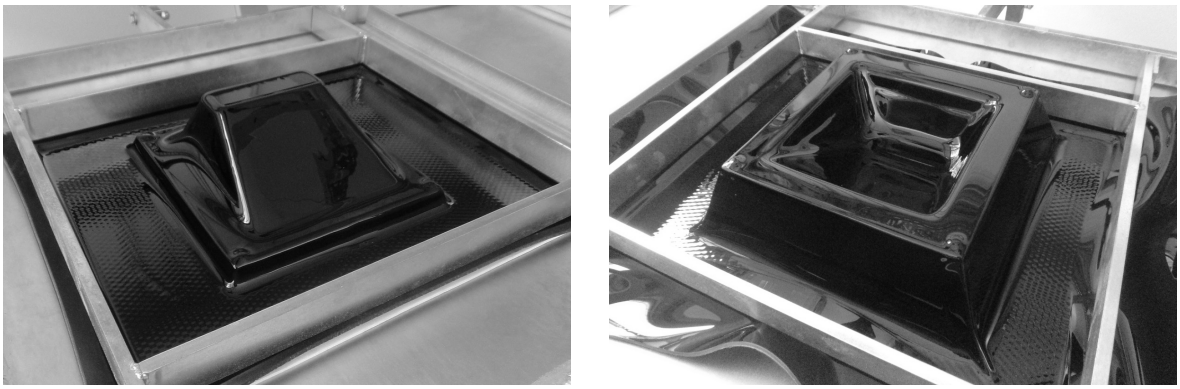

(a) (b)

Figure 6.20: Thermoforming with SPIF sheet metal moulds: (a) positive mould on thermoforming machine during vacuum; (b) negative mould on thermoforming machine during vacuum

After moulding operation, the part are finished. Finishing operation includes the release agent cleaning and trimming. The trimming operation is performed using a bent saw and the cut are manually deburr.

In order to be allow an operational comparison, the conventional moulds are also used in thermoforming operations. From the operation point of view, there aren't significant differences between the use of the SPIF moulds and the conventional tools until the end of the process. The differences are only found during demoulding. Depending on the heat and cooling time, due to its light weight, the SPIF mould stick to the plastic part when the table is moved down for demoulding. Nevertheless, the part releases with ease from the moulds. On the other hand, the heating affect is less significant in the sheet metal moulds, recooling faster and allowing a shorter process time.

6.1.5 Thermoforming parts validation

The plastic parts formed in both the sheet metal moulds and the conventional moulds are first evaluated trough visual inspection. The evaluation is mainly based on the PMMA parts for being the harder to form. All the four moulds succeed to shape the plastic to the desired geometry. Nevertheless, small differences are noticeable both between the positive and the negative moulds and between the sheet metal and the conventional moulds. Figure 6.21 presents two parts formed using the sheet metal moulds.

In the plastic parts formed using the positive moulds, major differences between the sheet metal mould and the conventional deal with the surface flatness. The tent effect lack of accuracy in the sheet metal parts has a slight negative influence on the parts aesthetics. In what regards the surface, both the punch skinning marks from the sheet metal mould and the milling increments from the conventional mould are visible in the finished part, without major differences.

The plastic parts formed in the negative mould have inferior result in shaping the geometry due to lack of material stretching. This slight noticeable miss defined geometry at the inner corners occurs in both moulds. However, this lack of thermoforming accuracy decreases the noticeable differences between the parts formed in the sheet metal and the conventional moulds.

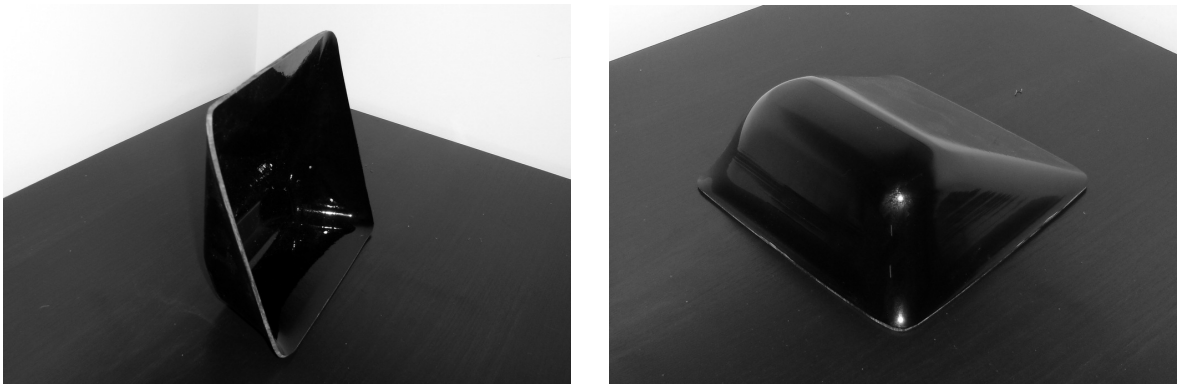

(a) (b)

Figure 6.21: Thermoforming parts formed with SPIF sheet metal moulds: (a) formed with the positive mould; (b) formed with the negative mould

For dimensional control, the thermoformed parts are measured by contact on a CMM. On each part, the surface in contact with the mould is measured. On the part formed on the positive mould, maximum deviation between formed part and CAD model is 14.7 mm with an average of 0.7 mm. On the part formed on the negative mould, maximum deviation is 11.4 mm with an average of 1.8 mm. When comparing parts to the real mould geometry, maximum deviation is 5.8 mm on the positive and 10.6 mm on the negative with respective average of 0.1 mm and 0.2 mm.

In what concerns the mechanical behaviour, the formed parts are tested and compared against the ones developed using the conventional moulds. For that, specimens are cut from parts formed with 2 mm clear acrylic formed with the positive moulds. Four specimens are cut from each part, three from the lower slope wall and one from the top wall. Due to the

material brittleness, one specimen cut from the part formed with the conventional mould shattered during the cut. Figure 6.22 (a) presents the cutting operation of the type IV plastic specimens.

A tensile test is used to compare the two parts. The tensile test is performed at 5 mm/min, with an average time of 70 seconds per test. All tested specimens follow the same profile stress strain curve. However, due to edge cut defects, differences are found at the specimen break strain. Figure 6.22 (b) presents the part form with the SPIF mould at the left and the part formed with the conventional mould at the right with the tested specimens taped in the original position. Figure 6.23 presents the stress strain plot from the tested specimens. No differences are found between the mechanical behaviour of the two parts. All curves follow the same profile with similar ultimate strength value. However, the specimens cut from the part formed with the conventional mould tend to break sooner due to bigger cut defects.

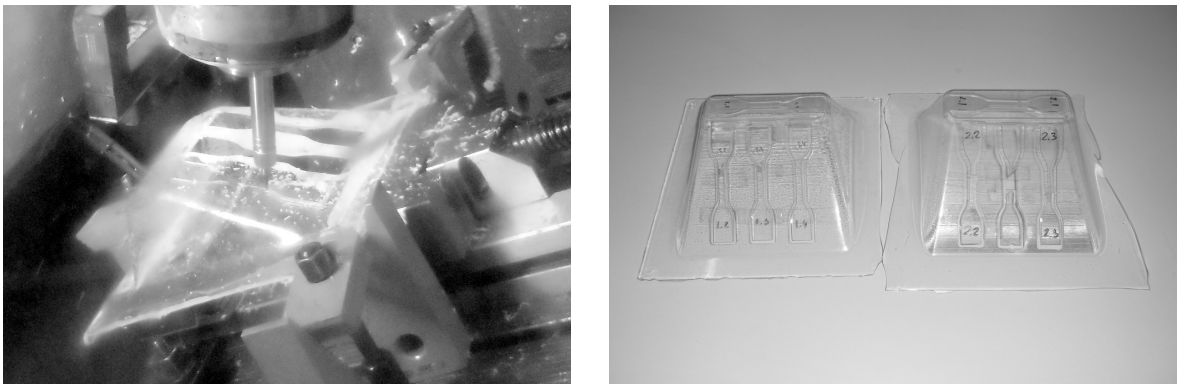

(a) (b)

Figure 6.22: Thermoforming parts specimens: (a) cut of the part formed with the SPIF mould; (b) parts with specimens after tensile tests

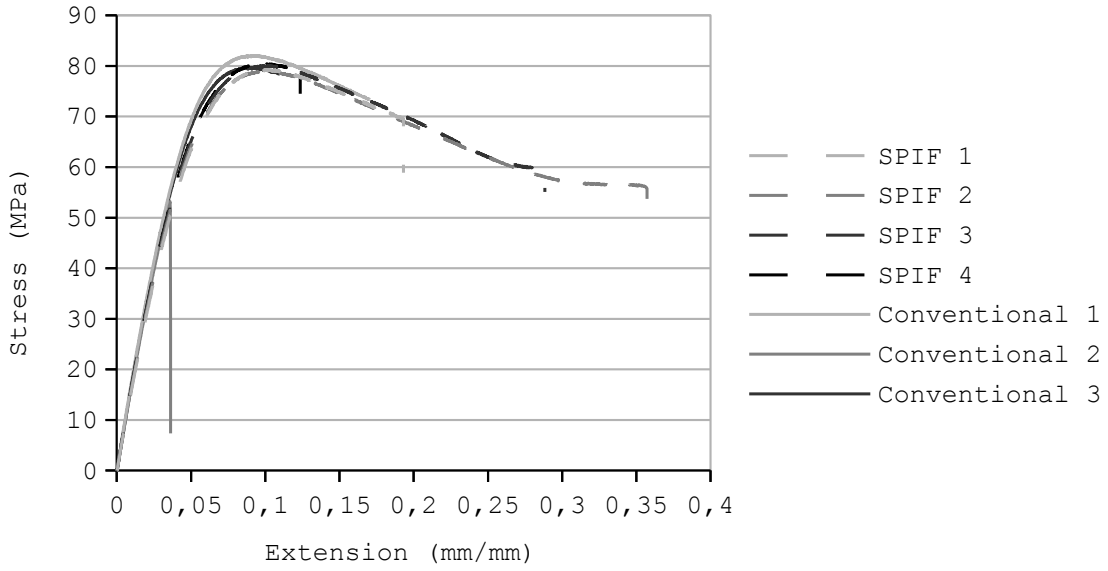

Figure 6.23: Thermoforming parts material mechanical behaviour.

6.1.6 Conclusion

The proof of concept preliminary tests validate the use of the SPIF process as a rapid tooling process for thermoforming operations. Sheet metal moulds made by SPIF are a reliable alternative to the conventional moulds. Despite some significant deviations still occur at some points (mostly peripheral), general appearance of plastic parts is reasonably good and average dimension is accurate.

Both the mechanical and thermal behaviour of the sheet metal moulds are well suited for the thermoforming operation. Regarding the thermal performance, the low thermal inertia due to the little volume of material may have advantages in the temperature cycles, mainly in the cooling process of the plastic. From the mechanical point of view, stand alone sheet metal moulds using medium to thick sheets can support the plastic forming forces on small and medium size moulds.

When comparing the sheet metal moulds manufacturing process against conventional moulds, the new approach is more economical in both development time, energy consumption and material cost.

Besides, moulds total manufacture time and material cost are low and yet largely influenced by some parallel operations. As accessories like backing plate for SPIF operation and MDF support boxes can be used for more than one mould with similar projected area, the use of sheet metal moulds assumes even a more interesting panorama. Relatively to energy, a slight reduction is achieved, although not as significant as the time and material savings for the work done.

On the other hand, despite being acceptable, the thermoformed parts quality is superior in the conventional moulds, mainly in what concerns geometric and dimensional tolerances. However, the major differences between the operation with the different mould concepts may be reduced by finishing operations on the sheet metal moulds allowing the improvement of the part accuracy.

From the mechanical point of view, no differences are found between the parts formed in sheet metal moulds and in conventional tools. The only discrepancy found occur at the cutting process, where the part formed with the conventional mould lead to larger edge defects and a failed cut. Despite not being positive, it is found that this issue relates to the surface texture due to the mould contact. The part formed with the conventional mould has more defined milling marks that affect the finished part surface.

In such a way, the SPIF rapid tooling applications for thermoforming operations is promising, mainly for the development of prototype tools or small series production.

6.2 Development and test of SPIF rotomoulding moulds

6.2.1 Rotomoulding process and mould geometry definition

The rotational moulding processes allows the production of hollow plastic one-pice parts. Two different approaches can be used in rotational moulding. On rotocasting, a thermoset material is used. On rotomoulding, a thermoplastic polymer is charged in a mould and then melted while the mould rotates axially or biaxially inside a forced convention oven. No pressure is used apart from a low contact pressure during the rotation of the heated melt. After the heat up cycle, the mould is cooled down at room temperature or under a water spray while rotation continues before being demoulded. The moulding process leads to stress free parts despite the poor dimensional tolerance control and low mechanical properties. Figure 6.24 illustrates the rotomoulding operation principle. Typical process cycle take between 10 to 20 minutes for the heat up and 10 to 20 minutes for the cool down. The total process time adds the material loading and the part removal. The most common materials use is low density polyethylene (LDPE) in both pellets and powder size mesh, with a melting point around 100°C. The average wall thickness is determined by the amount of material in the mould. The most common rotomoulding machines are the batch and the carousel types. The carousel type use multiple stations for the material loading, heating, cooling and product removal, are usually automated and used for larger productions. The batch type is manually operated to produce a part at a time and is typically used for a low production. During the rotomoulding process, the rotation speed is usually kept constant with typical values between between 3 and 15 rpm. The ratio between the major axis and the minor axis is varies between 8 : 1 and 1 : 5, according to the part configuration and orientation. [145–147]

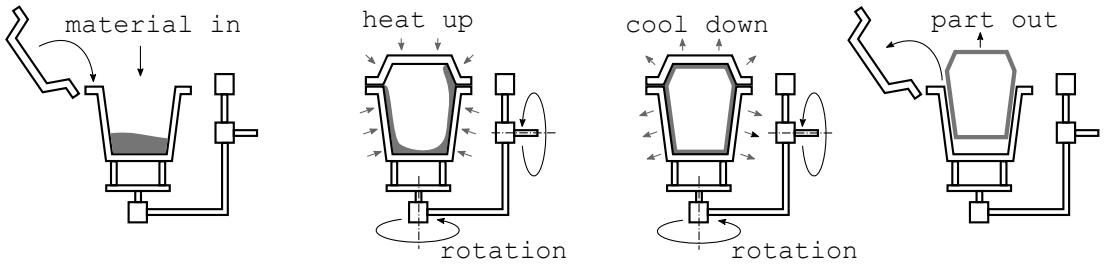

Figure 6.24: Rotomoulding operation principle.

The moulds used for rotomoulding are usually thin shell-like metal structures manufactured by electroforming nickel, casting aluminium, aluminium sheet or steel sheet. Electroformed mould are mainly used for small detailed parts. Casting aluminium is used for medium size moulds. Sheet metal moulds are also commonly used in large moulds, particularly steel due to the ease of welding. The mould assembly may include the molding surface to be mounted on a mould frame to help its assembly and clamping. Two part moulds are mainly used, defining a hollow surface with the straightest parting line possible. More complex assemblies are possible to allow more intricate geometry parts. The mould assembly must include a clamping system, as well as closing guiding features. The mould typically uses a venting channel to allow air to exit the inside during the heating process and reenter during cool off, minimising the risk of creating blowholes in the part or distorting the mould. Different mould surface including texture can be used while polished surfaces should be avoided. For an effective moulding, a release agent must be used. [145, 146]

The rotomoulding temperature cycle can be traced by a graph. Figure 6.25 [146] represents a typical temperature trace for a rotomoulding operation, which describes the mould outer and inner surface temperature, as well as the air temperature outside and inside the mould. During the heat up period, the inner surface is slight cooler than the outer surface and the air temperature inside the mould is even cooler. Until point A, the material hasn't reach the tacky temperature and the speed rotations are nor critical. When the inner air temperature reaches point A, the material starts to melt and absorb most of the heat. This lead to a flat plateau on the internal air temperature until point B. During this period, the rotation speed and speed ratio are critical to allow an uniform thickness distribution. At point B, all material has adhered to the mould wall and the melt is almost complete. Near the mould walls, the plastic have started to coalesce and densify. The coalescence process is completed to a uniform melt until point C. During the period A to C, air bubbles are trap in the plastic. the cooking time should be enough to allow the air to exit but must prevent over-cooking as degradation starts rapidly once the bubbles disappear. At point C, the mould in removed from the oven and the cooling process begins. The air temperature drops quickly until point D where the material starts to solidify. The cooling rate affects the material properties. Between point D and E the plastic solidifies and crystallises, giving off heat and leading to a second plateau in the internal air temperature trace. A final stage in the cooling occurs after point E when the plastic shrinks and creates an isolating layer of air between the mould and the material. At point F the part can be removed from the mould. [146, 147]

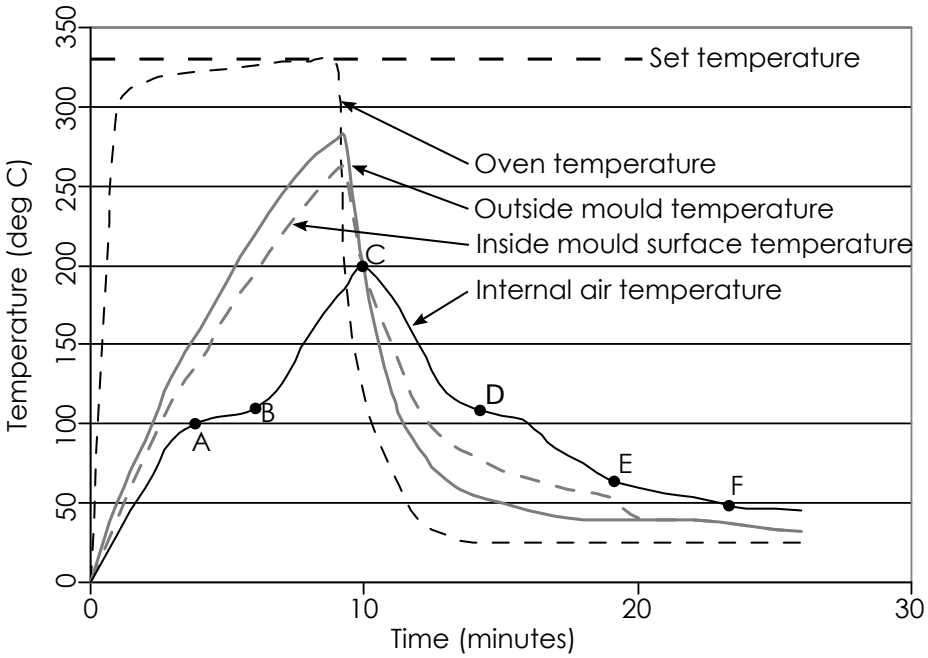

Figure 6.25: Typical temperature trace for a rotomoulding cycle.

As rotomoulding uses mostly thin walled moulds, it is possible to replace the conventional mould manufacturing process by ISF processes. SPIF parts can either define a full mould or to integrate other parts for a more complex assembly. In both cases, the geometric considerations that allow a feasible SPIF part should be taken into account, in addition to the guidelines for the rotomoulding part design.

The proposed system hypotheses considers a two part mould manufactured using aluminium sheet from flat blanks. Thus, the mould uses two different parts, both formed using SPIF to a freeform shape. The remaining flat area around the formed cavity is used as a parting line. Since the research seeks a proof of concept, the mould uses manual alignment between parts and a threaded connection for clamping. The mould sealing is granted by adding high temperature cold welding mass to the formed parts. A venting channel is added to the mould and fixed using high temperature cold welding mass.

Apart from the geometric limits of the SPIF process, the new proposed mould concept is subject to two possible issues, both due to the thinning phenomena that occurs during forming. One the one hand, the thin side walls must be dimensioned to withstand the contact stresses from the plastic load, as well as the possible gain of pressure during heating is venting is insufficient. On the other hand, the different thickness walls may lead to an uneven heating distribution, causing problems is the rotomoulded part thickness homogeneity.

One can estimate the final thickness t_f as a function of the initial thickness t_i using the sine-law (eq. 2.1). However, the sine-law assumes that the material only has vertical movement which theoretically limits the α angle to 90^o. This consideration is reductive as it neglects strain due to stretching or bending, and can only be applied to single stage incremental forming. Nevertheless, this approximation is plausible to be considered in the CAD definition of the mould parts to be evaluated to both mechanical and thermal behaviour. [6]

6.2.2 Part design

Rotomolded parts are closed hollow shaped of all possible sizes. Thickness varies from 1.5 mm to 5 mm and the part is detailed only in the outer side. Draft angle is recommended to facilitate the part removal, however, parts can be manufactured with only a small draft angle or even slight undercuts as the material shrinks away from the cavity mould surface during cooling. Intersecting planes should avoid sharp edges, with recommended radii equal to the thickness. Parting lines should be as straight as possible and large flat areas should be avoided. The high stress areas of the parts should be kept away from the parting line and the part can be reinforced using corrugated surfaces, stand up bosses or kiss off structures. These geometric features require the use of a draft as the material shrinks to the mould in the male geometric features of the mould during cooling. [145, 146, 148]

For the evaluation of the SPIF rotomoulding mould concept, a part is design based one the reference geometry. The rotational moulding part is designed as a hollow part with a projected area of 180 mm by 180 mm and a maximum height of 65 mm. It is shaped as a six sides close box with a minimum draft angle of 20^o used on the higher slant sides and one side with a smaller slope. The internal radius used between side faces is 15 mm and between side and top faces is 6 mm. The top and smaller slope sides keep a flat area sufficient to allow cutting type IV specimens [141], with 115 mm by 19 mm overall dimensions.

The rotomoulding part design is completed by closing the previous geometry to a six sides box. Since flat areas should be avoided, a quarter circle arc shaped slot 20 mm deep deboss with a 20^o draft angle is enclosed in the bottom side. The upper side of the part is also changed from a simple flat configuration to create an opened kissoff with a 22 mm by 30 mm area, 25 mm distant from the bottom side. This linkage between two part sides is common in rotomoulded parts to serve as a structural reinforcement and can lead to only a contact point or an open window. The interface between the upper and bottom sides is rounded with a small fillet. Figure 6.26 represents the drawing of the designed part.

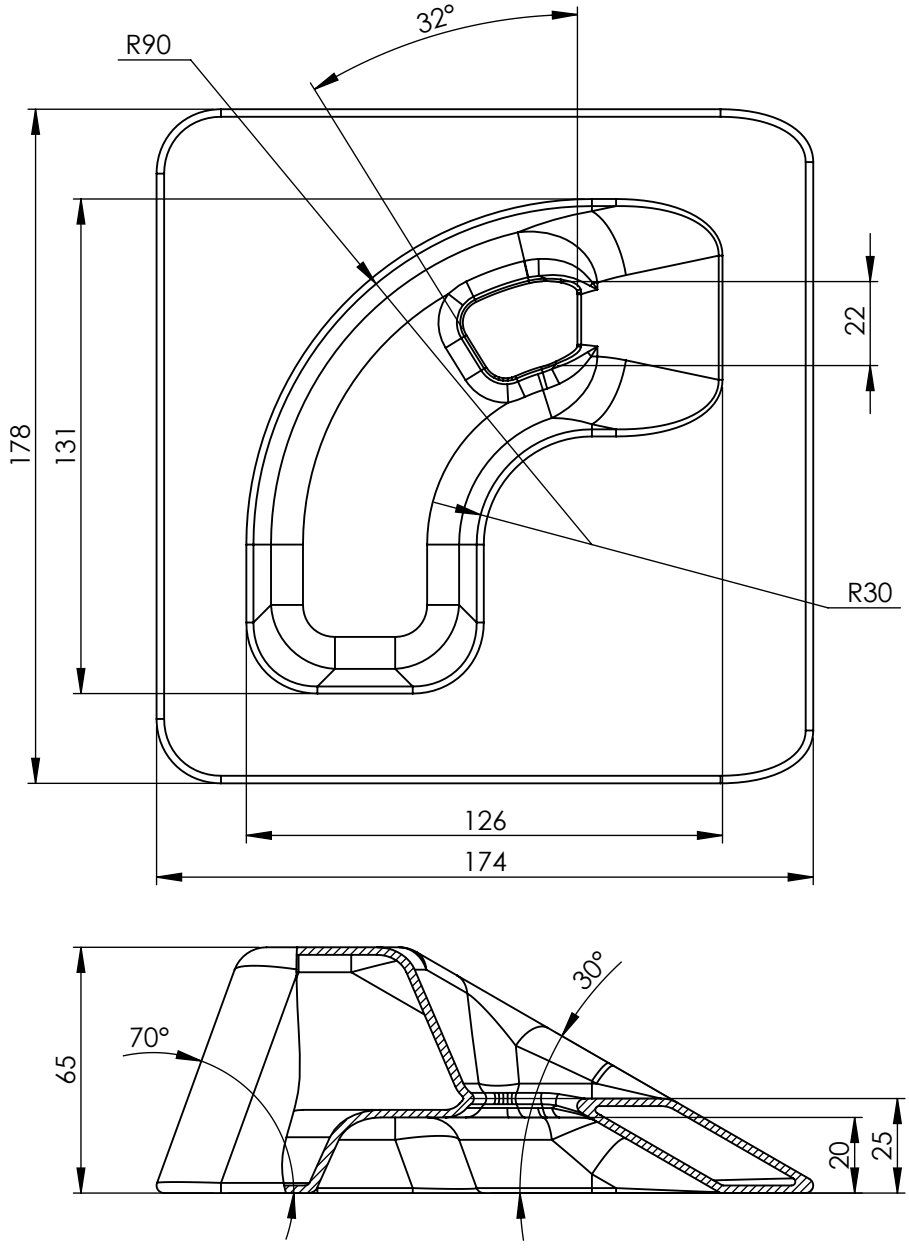

Figure 6.26: Part design for the SPIF rotomoulding concept validation, scale 1:2

6.2.3 Mould design and manufacturing

The mould for the designed rotomoulding part is a two part mould fabricated in aluminium sheet metal by SPIF, as defined in the mould geometry definition section. The moulding surface is derived from the designed part and extended into a flat area at the split line. This straight extension allows a safe SPIF process as it keeps the angle under the maximum forming angle. After forming, cold welding mass is used to better define the mould part joining and improve slit line geometry. The mould assembly uses a set of screws and nuts for the clamping and four screws and washers which position can be tuned to serve as a jig for manual alignment. Figure 6.27 represent the mould concept principle.

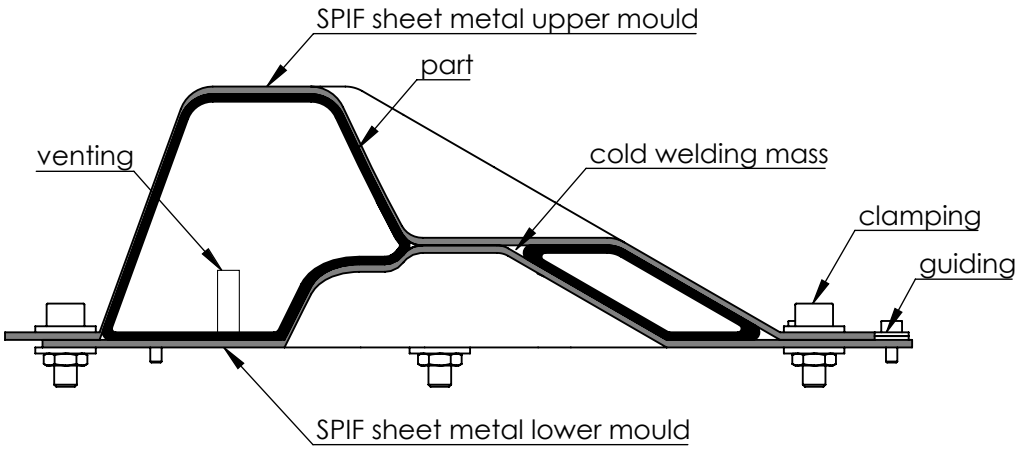

Figure 6.27: SPIF rotomoulding mould concept.

The mould metal parts are modelled according to the sine-law. This approximation allows a acceptable definition of the manufactured geometry, allowing the CAD model to be used to accurate determine the total mould mass and analyse its behaviour through computational methods.

As referenced, the sheet thinning due to the SPIF process may affect the mould behaviour in both a mechanical and thermal level. To complete the mould design process, computational simulations are used to predict the mould behaviour and pre validate the use of SPIF for the development of rotomoulding tools.

In the first stage, static behaviour analysis is perform to size the initial sheet thickness required to support the moulding loads. Notwithstanding the low rotational moulding pressure, one must ensure the sheet metal parts can support the loads without yielding or suffering excessive displacement. It is reasonable to exclude the clamping and guiding fasteners from the analysis, since their high stiffness and strength. Thus, simulation is simplified to sheet metal parts alone. This optimisation allows the conscious selection of the best sheet thickness to be used from the mechanical point of view.

During the second simulation stage, thermal analysis is accomplished to determine differences in the heating time due to the thickness variation. For this, thermal behaviour analysis is first performed on a simplified model and validated by relate with analytical models results. Thermal analysis is then performed using a constant thickness model as a primer reference. The sine-law model defined using the achieved initial thickness is studied for comparison. The analysis seeks for major differences in the mould heat time, material heat time and internal air heat time since this variations may result in defaults in the rotomoulded parts.

Mould mechanical behaviour

As referred, rotational moulding is a low pressure modelling process. Operation loads include only the moulding material weight and the surface pressure. Accordingly, mould pressure is limited to a reference value of 0.1 MPa [145]. This pressure is the addition of the material contact pressure and gain of pressure due to the temperature increase and inefficient venting.

Considering the ideal gas law, in a ventingless environment pressure over temperature is constant. Thus, the internal pressure difference during heating can be defined by equation 6.1, where ΔP is the gain of pressure, P_i is the initial pressure, T_i is the mould initial temperature and T is the internal air temperature. Considering a mould closing at room temperature and atmospheric pressure and heating to an internal air temperature of 200°C, the gain of pressure without venting is 0.06 MPa.

$$\Delta P = P_i - \frac{P_i.T}{T_i} \tag{6.1}$$

In what concerns the contact pressure, along the mould rotation, the significant values occurs mostly on the faced down surfaces moulding surfaces. This fact leads to a uneven pressure distribution. This way, two possible scenarios are plausible: worst real case happens either when the plastic material is most concentrated or when the biggest surface area is faced down. In the first case, the concentrated material may lead to a bigger moulding pressure, but typically in a small area. In the second case, a larger area may be under pressure but typically with a smaller value.

The simulation of mould mechanical behaviour considers a worst case scenario where the full moulding surface is under the maximum plausible pressure. The sizing of the sheet thickness for the case should grant the mould strength and stiffness for rotomoulding operation. Thus, a uniform pressure of 0.1 MPa on all inner surfaces is considered for the mechanical analysis.

Finite element method is used to determine minimum sheet thickness by a static analysis on Solidworks Simulation. Simulation is done considering isotropic AA1050 H111 sheet metal with $E = 69$ GPa, $G = 26$ GPa and $\nu = 0.33$.

Sheet thickness on mould walls is modelled according to the sine-law (2.1) as a function of the blank initial thickness. Analysis are performed using only nominal initial thicknesses between 1 mm and 3 mm. The analysed thickness are presented in table 6.11.

Meshing is done considering a solid mesh using tetrahedral elements with four integration points. The used element size is allowed to range the initial sheet thickness to one sixth of its value, leading to a maximum possible element aspect ratio of 6. The maximum element size lower bound is limited to 2 mm to avoid excessive number of elements. The mesh distribution is defined using curved based mesh, granting a minimum of eight element in a circle and considering a maximum element size grow ratio of 1.6. Meshing the model leads to an average under 300000 elements with the majority of the elements with an aspect ratio under three. Table 6.11 resumes information about the defined meshes.

Fixtures are established to have minimal influence on the behaviour of the moulding surface. The outside edges of the parting line plane are restricted along plane directions allowing only the perpendicular movement resulting from the mould expansion. The mould assembly is performed with an inconsequential gap between the mounding surfaces to avoid the influence of surface-to-surface contact. The component contact is defined by a bounded limited area under the influence of the clamping screws. The screws are defined as preloaded using alloy steel with 6 mm diameter and 16 mm head.

Table 6.11: Mesh details on rotomoulding sheet metal mould

Blank thickness (mm)	Min. thickness (mm)	Max. element size (mm)	% elements with aspect ratio < 3	Number of elements
1.0	0.34	2.0	76.7	239161
2.0	0.68	2.0	96.1	296918
3.0	1.02	3.0	94.5	139783

The simulation runs using FFEPlus iterative solver using implicit integration method. Table 6.12 refers the stress and displacement maximum values of the mould with different initial thickness. Figure 6.28 presents the stress and displacement distribution of the 2 mm sheet metal mould analysis.

Table 6.12: Stress and displacement on rotomoulding sheet metal mould

Blank thickness (mm)	Max. Stress (MPa)	Max. Displacement (mm)
1.0	1200	14.1
2.0	220	2.3
3.0	120	0.8

By analysing the simulation results, a sheet thickness of 2 mm is chosen for the mould manufacture. In what concerns displacement, although the calculated maximum displacement value is significant, it is only located. Furthermore, it has the same magnitude as the SPIF typical accuracy with decreases with the gain in thickness. Thus, increasing the mould thickness should not benefit the rotomoulding part accuracy since despite being more rigid, the mould may be less accurate. With regard to stress, although the maximum value is greater than the reference yield value for the aluminium alloy, it only occurs on specific points and small areas of the formed walls. Greatest stress results are concentrated near sharp edges of the CAD model, which suffer a certain radii during forming, thus reducing the stress value. Moreover, strain hardening occurs during forming in the sloped walls, which raises the yield stress value. Furthermore, calculus considers a pressure of 0.1 MPa, situation that is defined as a worst case scenario in rotomoulding process.

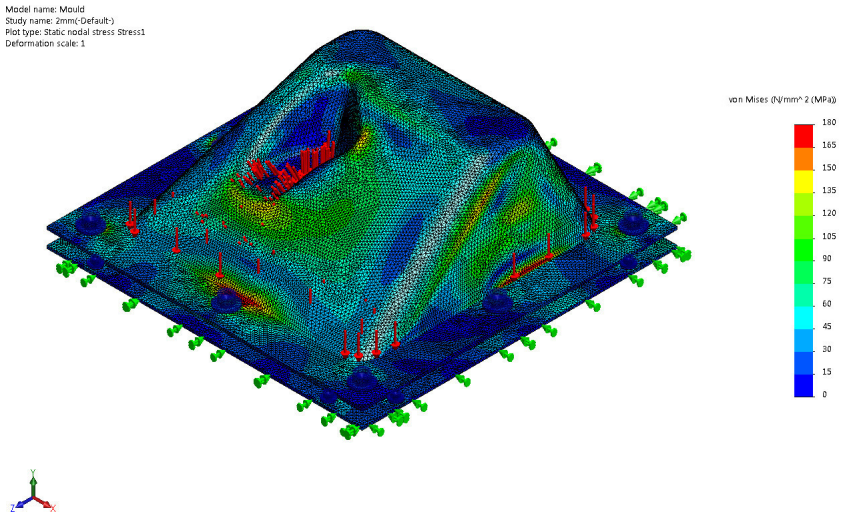

(a)

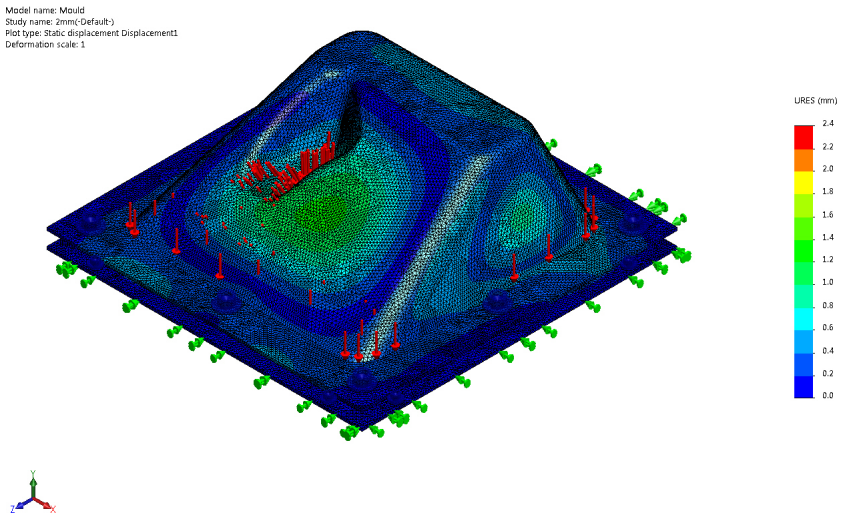

(b)

Figure 6.28: 2 mm rotomoulding mould mechanical behaviour simulation: (a) stress distribution (b) displacement

Mould thermal behaviour

The rotational moulding working principle involves the mould heating inside an oven while rotating until the plastic melt followed by a recooling to shape the material. Consequently, the thermal behaviour of the mould has influence on the rotomoulding process.

The energy transfer from the oven to the mould walls occurs by convection. By integrating the convective heat gain rate over time, one can determine the heating time by equation 6.2, where Δt is the mould heat time, $\rho.c_p$ is the volumetric heat capacity, h is the forced convection coefficient, T is the mould wall intended temperature, T_0 is the oven temperature and T_i is the mould initial temperature. V represents the mould material volume and A the surface area, where $V/A = t$, the mould thickness. Through wall thickness temperature gradient can

be neglected since resistance to heat conduction for a thin-walled mould is much smaller than convective heat flow resistance. The plastic material heat is slower due to the higher heat flow resistance and the energy used for the change of state. [148–150]

$$\begin{aligned} T &= T_i + (T_0 - T_i) \times \left(1 - e^{-\frac{h.A}{\rho.c_p.V}.\Delta t}\right) \\ \Leftrightarrow \Delta t &= -\frac{\rho.c_p.V}{h.A}.\ln\left(1 - \frac{T - T_i}{T_0 - T_i}\right) = -\frac{\rho.c_p.t}{h}.\ln\left(1 - \frac{T - T_i}{T_0 - T_i}\right) \end{aligned} \tag{6.2}$$

Since the plastic heating occurs mainly by heat conduction from the mould surface, the uniform heating of the mould benefits the moulded part thickness distribution. However, as referenced, the SPIF mould has uneven thickness distribution due to thinning. An evaluation of the mould heating time and distribution is performed to validate the SPIF rotomoulding mound concept.

Accordingly to equation 6.2, it is possible to determine the mould heat time. Considering the aluminium properties $\rho = 2705$ kg/m^3, $c_p = 1386$ J/(kg.K) and $h = 20$ W/(m^{2}K) for aluminium on air under common rotomoulding conditions, a mould with a wall thickness of 2 mm ($t = 0,002$), takes around 570 seconds to heat from 20°C to 200°C in a 250°C oven. The graphic in figure 6.29 represents the heat time up to 200°C in an oven from 200°C to 300°C of different thickness aluminium plates. The thinner walls on the mould with 0.68 mm thickness take only around 200 seconds of heat time on the same conditions. However, the heat conduction along the mould walls contributes to more balanced heating. In an ideal setting, the mould heat time could be estimated by equation 6.2 considering an average $V/A = t_{average} = 1.46$ mm, leading to an average heating time of 420 seconds in the same conditions.

In addition, equation 6.2 can also be used to determine the expected mould temperature after a certain amount of heat time. This evaluation can be useful to predict the mould temperature in the thinner areas at the moment the thicker walls reach 200°C. When heated in a 250°C oven for 570 seconds needed to reach 200°C in the 2 mm walls, the thinner walls of the mould may reach almost 250°C. The average mould temperature rounds 220°C. The graphic in figure 6.30 represents the mould temperature over time in a 250°C oven.

With the reference value known, numerical simulation is performed to analyse the thermal behaviour of the full mould. Simulation runs on Solidworks Simulation using FFEPlus

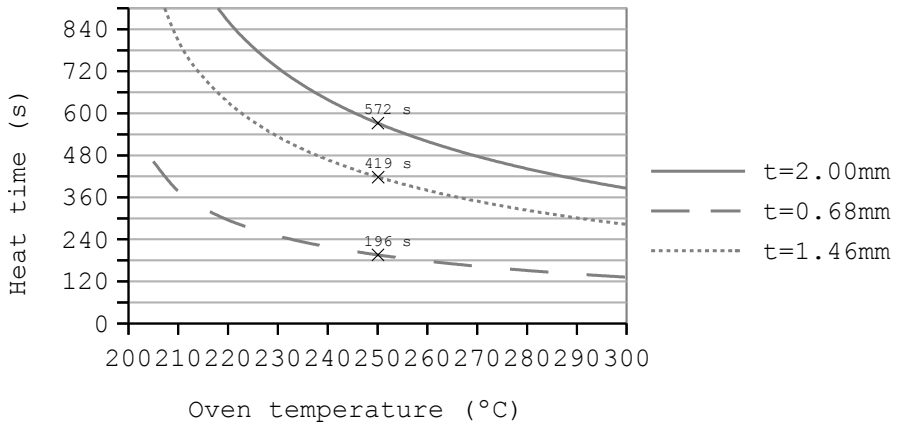

Figure 6.29: Aluminium sheet metal mould heat time up to 200°C.

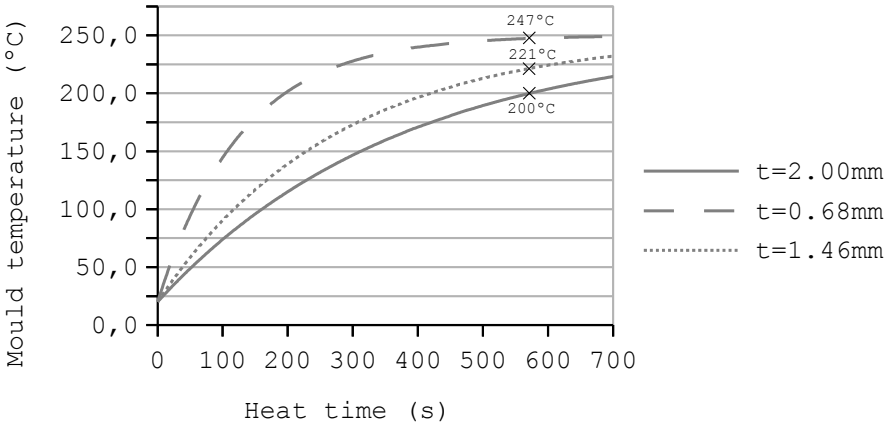

Figure 6.30: Aluminium sheet metal mould temperature in a 250°C oven.

iterative solver, calculating transient type solution up to 600 seconds with time increments of 20 seconds. Meshing is performed using 16 integration points tetrahedral elements.

The simulation consider AA1050 H111 sheet metal with $\rho = 2705$ kg/m^3, $c_p = 1386$ J/(kg.K) and $k = 0.2256$ W/(m.K) inside a volume of air with $\rho = 1.1$ kg/m^3, $c_p = 1000$ J/(kg.K) and $k = 0.027$ W/(m.K). The contact surface between the sheet metal and air is defined using a distributed thermal resistance of $\frac{1}{h} = \frac{1}{20} = 0.05$ (K.m^2)/W. Test conditions consider an initial temperature of 20°C on the sheet metal and a constant temperature of 250°C on the air.

The first thermal simulations are performed using a small sample in order to validate the testing conditions against the analytical solution. A 30×30 mm sample with 2 mm thickness is used. Different air thickness around the sheet are tested. The computed sheet temperature on the thickness centre is 196°C after 580 seconds, no mater the air thickness. The temperature gradient across thickness varies from 200°C is the outer surface and 193°C in the inner surface. The simulation is performed with 2mm elements to represent the mould thickness without distorted elements. Considering the systematic fair approximation to analytical calculus, both the simulation parameters and the mesh size are first validated. Further, the air thickness is sized to 2 mm to allow a good mesh adjustment with minimal increase of the number of elements.

The second simulation extends the previous sample to a second are with the same size and the 0.68 mm minimal mould predicted thickness. Figure 6.31 present the temperature results after 580 seconds of heating time. The temperature in midthickness of the most far apart areas of the sample is 196°C in the 2 mm side and 246°C in the 0.68 mm side, close to the predicted values. As expected, a continuous temperature change is noticeable in the thickness variation due to heat conduction. In fact, the gradient effect is noticeable on 15 mm both aways from the thickness variation edge. This effect not only speeds up the heat time of the thicker area but also reduces the achieved temperature on the thinner side.

The simulation is repeated using different size mesh elements to perform a mesh convergence analysis. Meshing is performed using element size from 12.0 mm to 0.5 mm. Greater dimension fail to mesh due to over distorted elements and smaller dimensions lead to excessive simulation time. Table 6.13 and the graphic in figure 6.32 show the temperature results after 580 seconds of heating time in a 250°C oven calculated with different size mesh. The previous approach of using 2 mm elements, meshing the mould geometry without major de-

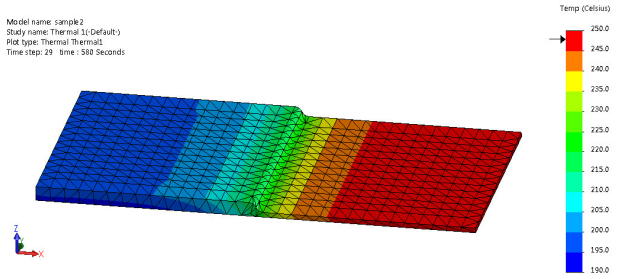

Figure 6.31: 2 mm sample thermal behaviour simulation at 580 seconds in a 250°C oven

formed elements, proof to be the best compromise between result accuracy and simulation time. Due to the small temperature gradient over thickness, it is not profitable to descritize the geometry with more than one element in thickness. Although in the thinner areas the 2 mm mesh leads to elements with an aspect ratio close to 3, they are compatible with the even smaller temperature gradient.

Thus, the simulation of the thermal behaviour of the rotomoulding mould is performed using 2 mm mesh in both the mould material and the 2 mm air layer around the mould. Thermal properties and contact is defined as described above, considering the 0.05 $(K.m^2)/W$ thermal resistance surface contact between aluminium and air.

Table 6.13: Sample temperature at 580 seconds of heating time in a 250°C oven calculated with different mesh size

		2.0mm thick area			0.68mm thick area		
mesh size (mm)	total elements	outer surface (°C)	midthickness (°C)	inner surface (°C)	outer surface (°C)	midthickness (°C)	inner surface (°C)
14.0	fail	-	-	-	-	-	-
12.0	233	205.9	200.0	195.7	246.7	246.6	246.5
10.0	304	205.3	200.1	195.1	246.7	246.5	246.3
8.0	555	208.6	199.0	194.4	246.6	246.5	246.4
6.0	747	201.9	197.9	192.7	246.4	246.3	246.2
5.0	1103	201.8	197.1	192.4	246.5	246.4	246.2
4.0	1636	199.8	195.8	192.0	246.5	246.4	246.3
3.0	6018	199.8	196.1	192.4	246.4	246.3	246.2
2.0	6974	199.1	195.7	192.4	246.4	246.3	246.1
1.0	41365	198.4	194.0	192.8	246.4	246.3	246.2
0.5	312978	198.1	194.2	193.0	246.4	246.3	246.2

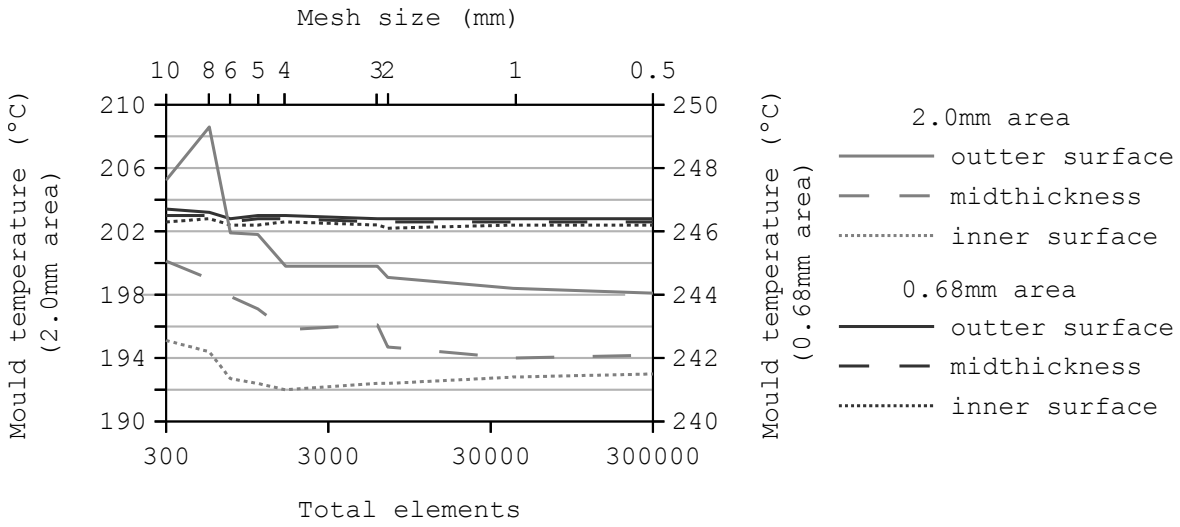

Figure 6.32: Sample temperature at 580 seconds of heating time in a 250ºC oven mesh convergence plot

The transient state thermal simulation uses a 500739 elements mesh, where 96.3% have an aspect ratio inferior to 3. The calculated heat time to reach a minimum 200°C in all mould area mid thickness is 600 seconds, with the thinner areas ending at 247°C. The overall average mould temperature is 218°C. The needed time to heat the thinner walls to 200°C is just 220 seconds. However, this heat time lead to an average temperature of 150°C and only 120°C on the thicker walls. With 480 seconds of heating time, the mould reaches an average temperature of 205°C, with local value varying from 180°C to 240°C. Figure 6.33 shows the temperature distribution in the mould after 220 seconds, 480 seconds and 600 seconds.

The presented results show only areas with temperature bellow 250ºC, excluding the air layer around the mould. The posterior surfaces, in both the upper and the lower side of the mould, have the same behaviour as the visible ones.

The overall temperature distribution follows the expected behaviour. The thickness variations leads to an uneven temperature distribution. However, also as expected, the heat rate of the thicker areas is faster than the estimated by equation 6.2 due to the heat conduction. Still, the uneven temperature distribution leads to 60ºC differences when the mould reaches 200ºC average. Thus, due to the unwanted hot spots, one can assume the SPIF mould could be used for rotomoulding operations, with possible thickness distribution issues.

The performed thermal analysis takes into account only the mould heating. However, the rotomoulding process involves the heating of the moulding material and the subsequent internal air heating as well. To improve the simulation reliability, the thermal simulation is completed considering those materials. [151, 152]

For the new simulation, a simplified model of the thermoplastic material with a constant thickness of 2 mm is modelled around the inside mould surface. This approximation simulates an even material distribution by the mould rotation. A solid core model is also modelled inside the polyethylene layer and defined as air. The assembly keeps the same mould parts and the 2 mm thickness outer air layer.

The thermal properties of the polyethylene are defined in order to describe its heating behaviour, including the melting phenomena. The total heat flow of the low density polyethylene increases to a four times of the value absolute value during the melting. This sharp peak dues

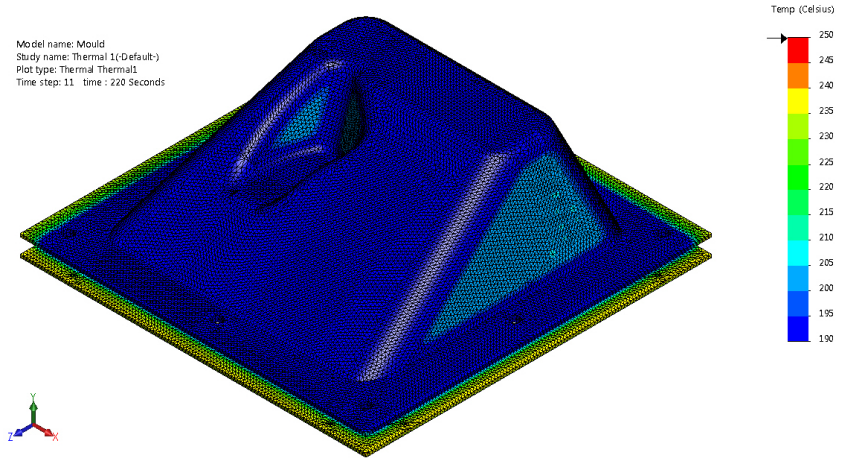

(a)

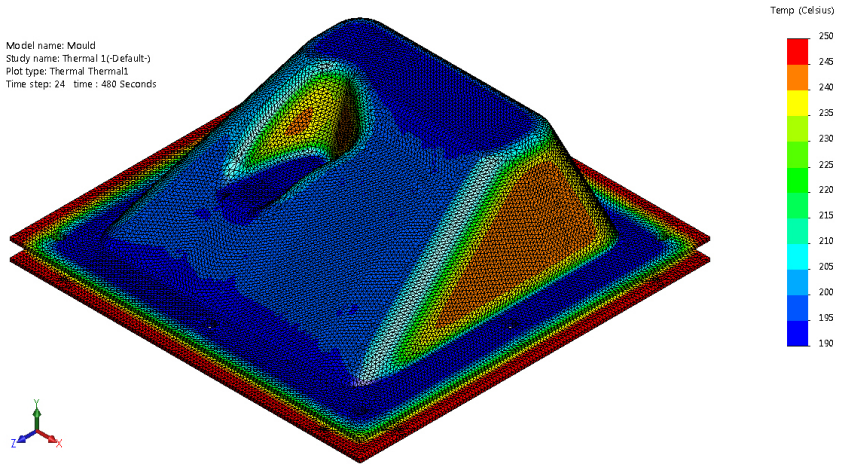

(b)

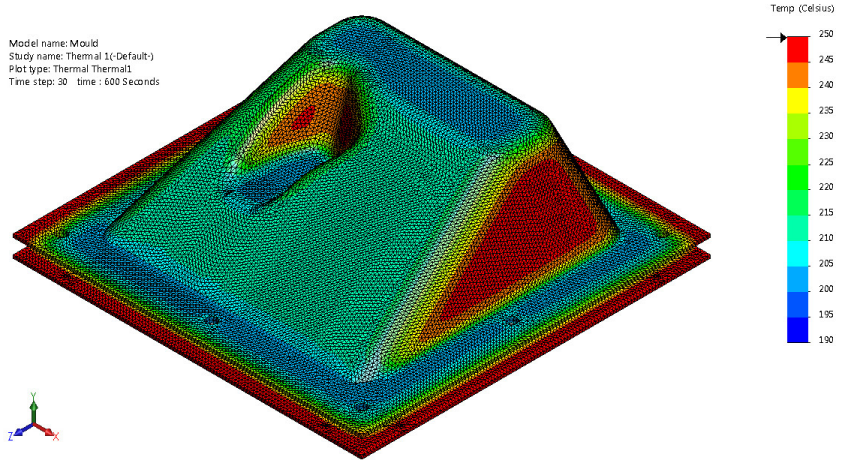

(c)

Figure 6.33: 2 mm rotomoulding mould thermal behaviour simulation in a 250°C oven: (a) after 220 seconds, (b) after 480 seconds, (c) after 600 seconds

to the endothermic melting. For the simulation, the thermal material behaviour is described by the specific heat, the thermal conductivity and density. The polyethylene is defined with $\rho = 917$ kg/m^3 and $k = 0.322$ W/(m.K). The specific heat is defined on a temperature dependent bases instead of a fixed value, with the value varying from $c_p = 1842$ J/(kg.K) to $c_p = 7368$ J/(kg.K), as described in the graphic of figure 6.34. [153]

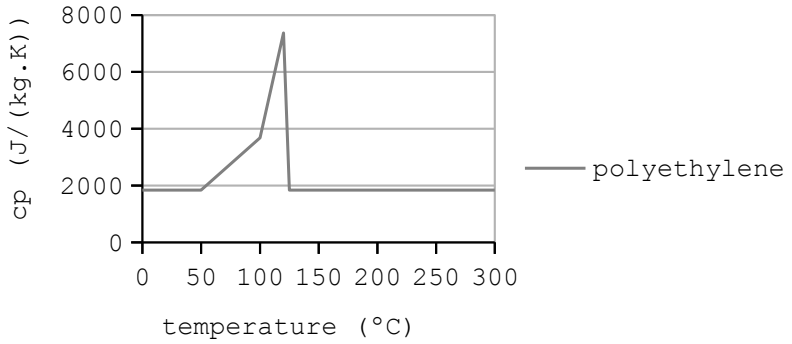

Figure 6.34: Polyethylene specific heat over temperature

The core volume of air is settled with $\rho = 1.1$ kg/m^3, $c_p = 1000$ J/(kg.K) and $k = 0.027$ W/(m.K). The contact surface between the sheet metal and the outside air and between the polyethylene and the inside air is defined using a distributed thermal resistance of $\frac{1}{h} = \frac{1}{20} = 0.05$ (K.m^2)/W. No thermal resistance is considered between the mould inner surface and the moulding material.

The mesh uses the same element type mesh with the same dimension, granting a fine adjustment to the model geometry. The new thermal simulation uses a 1190025 elements mesh, where only 1.7% have an aspect ratio superior to 3. Due to the mesh size, it is not possible to run the simulation for the full period of analysis. Thus, the simulation is split in two stages. The first transient state calculates the thermal behaviour up to 480 seconds with a 20 seconds time increment. This stage considers an initial temperature of 20°C in the mould, moulding material and inner air and a constant temperature of 250°C in the outer layer of air. The second stage also works with a 20 seconds time basis transient state, defining the initial state from the result of the last time step of the first simulation and maintaining the outer air constant temperature. The calculus simulates 480 additional seconds, corresponding to a full period of 960 seconds of heating time. The additional analysis time overdue an expected longer heating period.

The new calculated heat time to reach a minimum 200°C in all mould area mid thickness is 840 seconds, with the thinner areas ending at 231°C. The overall average mould temperature is 218°C. After this heat period, the polyethylene reaches temperature between 191°C and 230°C, with an average value of 210°C. Due to the higher quantity of material to heat and subsequent higher thermal inertial, it is both noticeable a longer heating time but a smaller temperature gradient over the mould surface.

The needed time to heat the thinner walls to 200°C is 480 seconds. However, this heat time lead to an average temperature of 180°C and only 140°C on the thicker walls. The moulding material reaches an average temperature of 165°C, with a maximum value of 197°C.

With 660 seconds of heating time, the mould reaches an average temperature of 204°C, with local value varying from 185°C to 218°C. At this heating time, the moulding material reaches an average of 192°C, varying from 180°C to 218°C.

The moulding material average temperature reaches 199°C after 720 seconds of heating time, with values from 184°C to 222°C. At this time the mould reaches an average temperature of 209°C and the inner air reaches an average temperature of 197°C.

Figure 6.35 shows the temperature distribution in the mould after 480 seconds, 660 seconds and 840 seconds for comparison with the first simulation results after 220 seconds, 480 seconds and 600 seconds, presented in figure 6.33. The smaller temperature difference along the mould surface is noticeable, mainly on the headmost time steps. In addition to the higher temperature value being lower, the affected area is smaller. As in the first simulation, the lower side of the mould has a similar temperature distribution as the shown side.

Figure 6.36 (a) presents a section cut of the mould and polyethylene after 720 seconds of heating time. Both the outside air layer and the inner air are hided for a better reading of the mould and material temperature. The temperature distribution shows both a difference in the different areas and a small through thickness gradient. Figure 6.36 (b) shows the temperature distribution on the polyethylene material. The similarities between figures 6.35 (b) and 6.36 (b) due to the additional 60 seconds of heating. Although the uneven temperature distribution, the bellow 40°C interval is acceptable for a rotomoulding operation, thus validating the 2 mm sheet metal mould manufactured by SPIF, as presented in the drawings of appendix E.2.

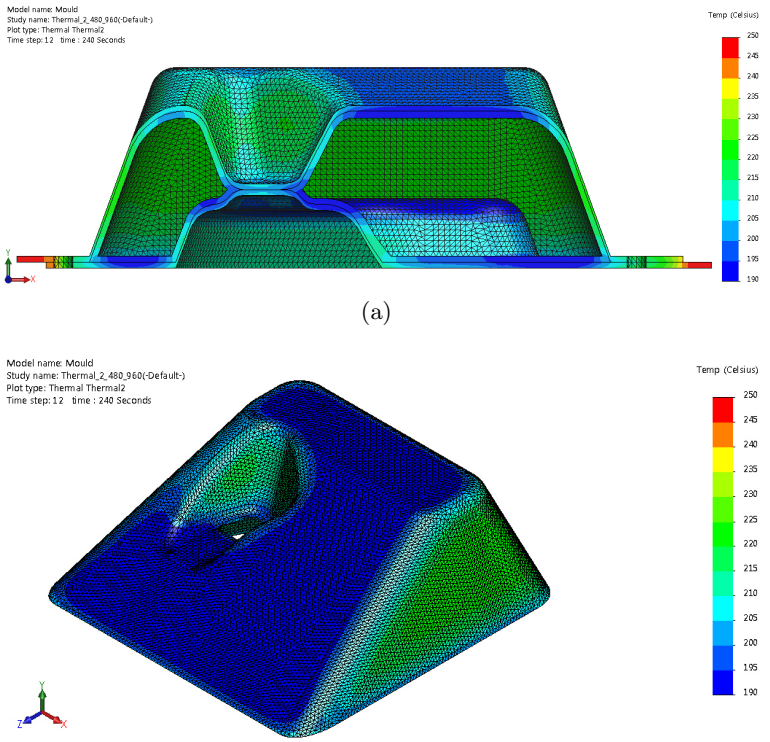

Figure 6.36: 2 mm rotomoulding mould thermal behaviour simulation in a 250°C oven moulding 2 mm thickness of polyethylene after 720 seconds: (a) section view, (b) polyethylene material

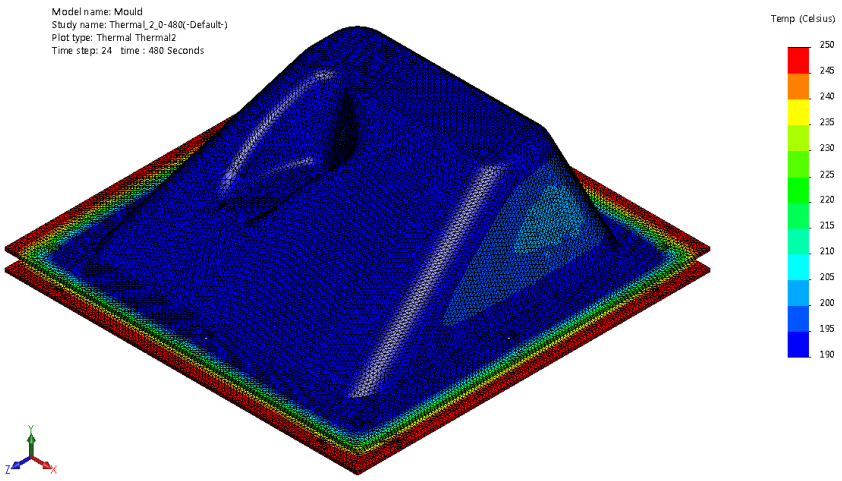

(a)

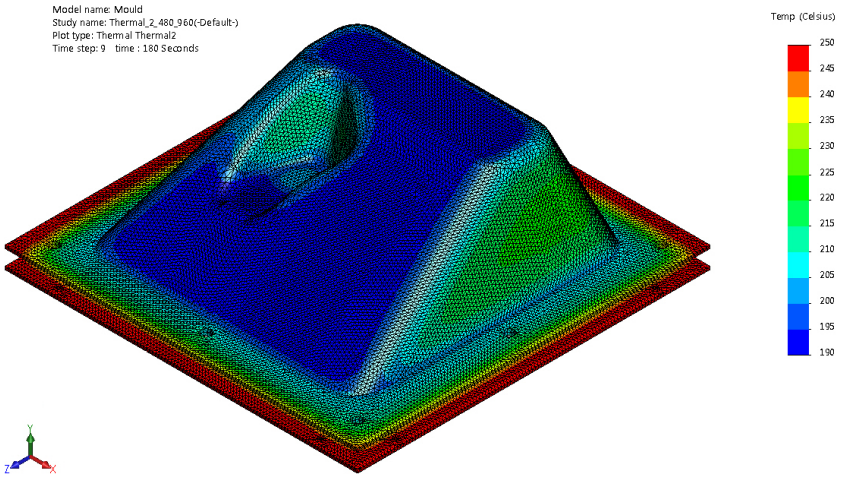

(b)

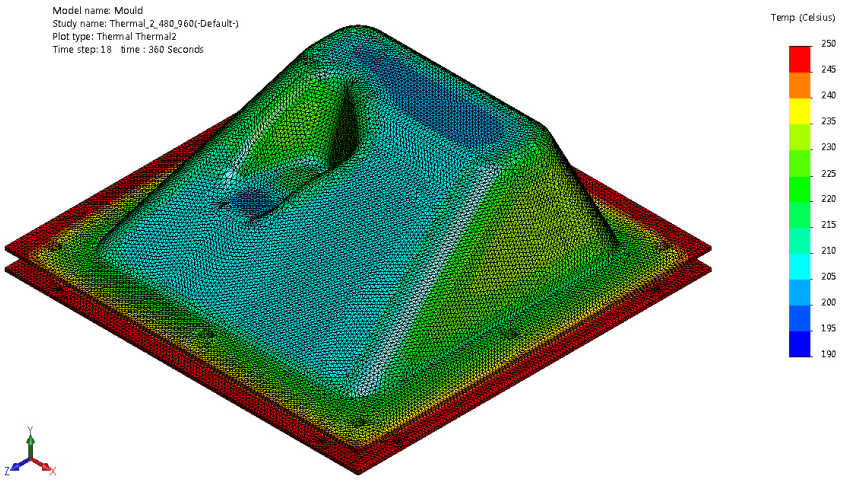

(c)

Figure 6.35: 2 mm rotomoulding mould thermal behaviour simulation in a 250°C oven moulding 2 mm thickness of polyethylene : (a) after 480 seconds, (b) after 660 seconds, (c) after 840 seconds

Mould manufacturing

The manufacturing of a mould by SPIF starts with the backing plate cutting operation. The drawing of the backing plate is made by offsetting the outline of the sheet part by 1 mm. As each mould part cavity leaves the black plane with a different geometry, one backing plate must be cut per mould part. Due to the test part design being based on prior parts geometry, previously cut backing plates are used for the rotomoulding mould manufacture. Nevertheless, the cutting operation and backing plate material is considered for the comprehensive analysis of the mould manufacturing process. A waterjet cutting process is used in order to cut the backing plate from a 5 mm steel sheet, with a material cost of 40 €/m^2, expending 225×225 mm of sheet per backing plate.

The second step of the process involves the cut of the aluminium sheet. The 230 mm by 230 mm banks are cut from a 2 mm thickness AA1050 H111 aluminium sheet, with a material cost of 60 €/m^2. The straight cuts are performed on a hydraulic guillotine. Two blanks are cut to be used in each mould side. The blank corners are also cut to allow a better fitting in the rotomoulding device used for the mould test.

For the SPIF operation, a single stage helical tool path with a vertical constant increment of 0.5 mm using a 15 mm ball tip tool is used. The spherical tip follows the perimeter of the hallow shape on a continuous movement, dropping 0.5 mm at each loop, at a feed rate speed of 3000 mm/min. The helical movement is chosen for producing better surface finishing and better accuracy then dropping each z step at one point. The overall forming process considers the machine power up, machine set up and forming itself. The machine set up includes changing backing plate, changing tool and changing sheet holders. During the set up the blanks are held to the frame by screwing the sheet holders. The sheet position is referenced by moving to tool tip to the centre of the sheet surface. The forming operation runs, adjusting the tool motion to the defined feed rate. Besides, to improve the accuracy of the kiss off area, a local support is used, being manually positioned under the blank at the moment the punch reaches -20 mm. After forming, the process includes the part release and cleaning. Figure 6.37 illustrates one of the final z increments of each part of the rotomoulding mould SPIF operation.

(a) (b)

Figure 6.37: SPIF operation forming the rotomoulding sheet metal mould: (a) lower side part (b) upper side part

After forming operation, the mould sheet parts are drilled to allow the mould venting and the assembly of the clamping and guiding screws. Drilling is performed using a cordless drill. Eight 6.5 mm holes are bored on each part for the clamping crews, four $M3$ holes are bored and tapped on the lower part for the guiding ishers fixture. Four $M3$ screws with eight ishers and eight $M6$ with screws with sixteen washers and nuts are added to the mould assembly.

The mould is finished by filling up the undesired small radius created at the blank edge during the forming operation using cold welding mass, with a total material cost of 5 €. The mass application must be accomplished withing a 5 minutes working time. The epoxy reaction takes 30 additional minutes and the mould fabrication ends with a sanding operation. The mass curing period is not considered for the mould manufacturing time.

During the mould manufacture, operation time and energy consumption is measured. As the work is carried out at different locations and with in between pauses to analyse the process evolution, the measurement is done for individual tasks instead of continuously. Table 6.15 resume the time and energy consumption for the rotomoulding mould. Although the backing plate has been reused, its cutting operation is considered. Table 6.14 resume each manufacturing stage process time, energy consumption and material cost. Figure 6.38 represent a pie graphic display of the time and energy consumption in the SPIF mould manufacture for a better reading.

Total fabrication time for the mould is 2h26min being only 54% for SPIF process. The required time to use the mould adds the cold welding mass curing time. The total energy consumption is 10.98 kW.h, although a large proportion is derived from the water jet cutting. The total material cost is just 20.00 €, being 5.00 € for the backing plates, 7.50 € for the aluminium sheet, 5.00 € for the cold welding mass and 2.50 € in fasteners.

Table 6.14: Time, energy and cost of the mould manufacture

Operation	Time (min)	Energy (kW.h)	Material Cost
backingplate cut	29:28	5:11	5.00 €
blank cutting	02:43	-	7.50 €
SPIF mould forming	78:52	5:87	-
drilling and fastening	26:31	-	2.50 €
cold welding	08:08	-	5.00 €

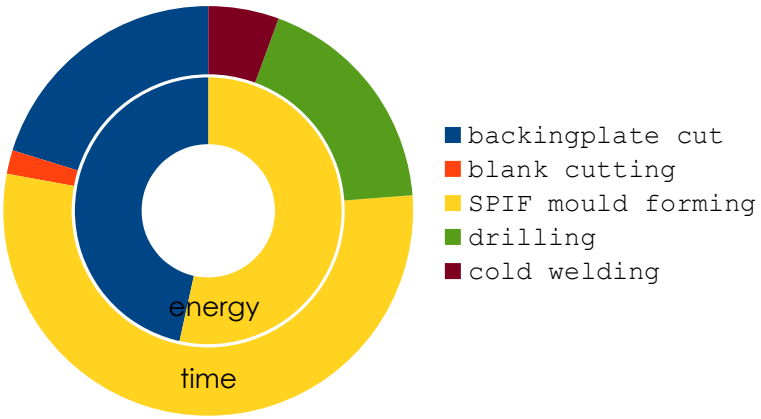

Figure 6.38: Time and energy consumption in the SPIF rotomoulding mould manufacture

Table 6.15: Time and energy consumption in the SPIF positive mould making

Operation	Sub operation	Time (min)	Energy Consumption
Waterjet backing plates cut	backing plate drawing	4:12	-
	cut programing	10:04	-
	machine set up and start up	2:55	0.02 kW.h
	define cut position and parameters	1:55	0.01 kW.h
	cut	8:58	5.08 kW.h
	part removal and clean	1:24	-
Guillotine blank sheet cutting	machine set up	0:46	-
	2 piece cutting	1:57	-
SPIF upper mould forming	CAM preparation	8:21	-
	compile CAM	3:22	-
	machine set up and start up	8:28	0.02 kW.h
	sheet holding	4:58	-
	define zero	1:32	0.29 kW.h
	forming positive mould	24:39	4.06 kW.h
	part removal and clean	5:12	-
SPIF lower mould forming	CAM preparation	4:05	-
	compile CAM	2:49	-
	sheet holding	3:31	-
	define zero	0:40	0.12 kW.h
	forming positive mould	7:15	1.20 kW.h
	part removal and clean	4:00	-
Drilling	measure and marking	12:27	-
	sheet drilling	11:34	-
	threading	2:30	-
Cold welding	radii filling	3:48	-
	sanding	4:20	-

After manufacture, SPIF sheet moulds are measured by contact using a touch-trigger probe on a 3 axis co-ordinate measuring machines (CMM). Figure 6.39 illustrates the measuring operation of the sheet metal moulds and figure 6.40 shows the comparison between the SPIF part and the CAD. Maximum deviation is +2.9 mm on the positive mould and +6.8 mm on the negative mould. Average deviation is +0.3 mm on the positive mould and +1.8 mm on the negative mould.

The improved accuracy when comparison with the typical values dues both to attention to the forming procedure and to the addition of the cold welding mass. The local support used in the top part forming grants an acceptable accuracy in the flat area that creates the kiss off, otherwise unreachable. The adjacent area in the bottom part is granted using 3 mm overforming operation. The typical radii at the SPIF part boundary is eliminated through the mass filling, as noticeable in figure 6.39 (b) due to the darker colour. One can also improve the surface quality using the same epoxy mass. The filling can both correct flatness or surface profile and decrease roughness.

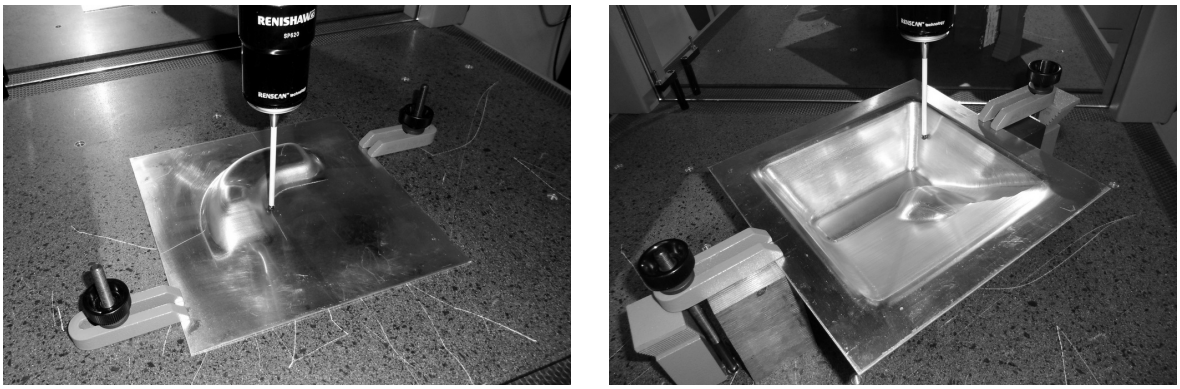

(a) (b)

Figure 6.39: Rotomoulding sheet metal moulds dimensional measurement: (a) lower side (b) upper side

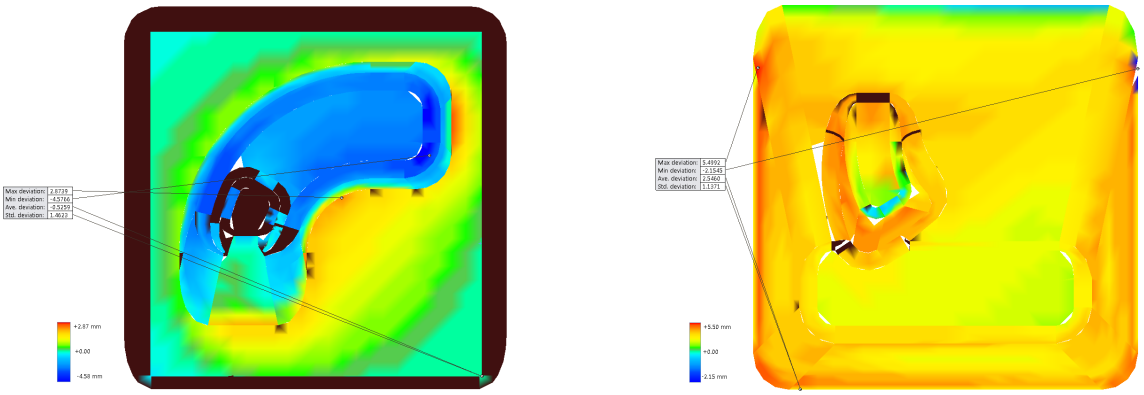

(a) (b)

Figure 6.40: Rotomoulding sheet metal moulds dimensional measurement results: (a) lower side (b) upper side

After measured, the mould is closed and heated up to 250°C to check for stiffness issues due to the internal air heating. No failure occurs during the heating and cooling process. The parts are remeasured without registering dimensional changes. In such a way, the manufactured mould is validated and approved for operation tests.

6.2.4 Mould operation

For the mould operation test, a three stage procedure is performed. At the first stage, the mould is tested using polyurethane thermoset resin (PU) in a rotocasting operation. In the second stage, the mould is used for a rotomoulding operation using low density polyethylene thermoplastic (LDPE) pellets. The third test aims of industrial rotomoulding process using LDPE powder. This approach start with room temperature operation to only test material distribution and set the reference geometry moulded part. The second and third stages deal with heat, testing the material distribution and resulting part geometry.

Rotomoulding system development

In order to test the new rotomoulding mould concept, due to the unavailability of a rotomoulding machine, a batch type rotomoulding system is developed. The system consists of two curved aluminium tubes as frames, mounted on two perpendicular axis. Figure 6.41 represents the developed rotomoulding system. A fixed frame has a 60 teeth modulus 6 gear which is bolted to the oven door. The x frame is supported on the fixed frame with the power shaft passing through the door. The yz frame is mounted on the x axis with a 10 teeth spur gear at the power shaft. The rotation of the x frame transmits the rotation to the yz frame through a passive 22 teeth spur gear. Thus, the rotation ratio between the main and the secondary axis is 1:6. The speed ratio can be adjusted by replacing the spur gears up to 1:3.

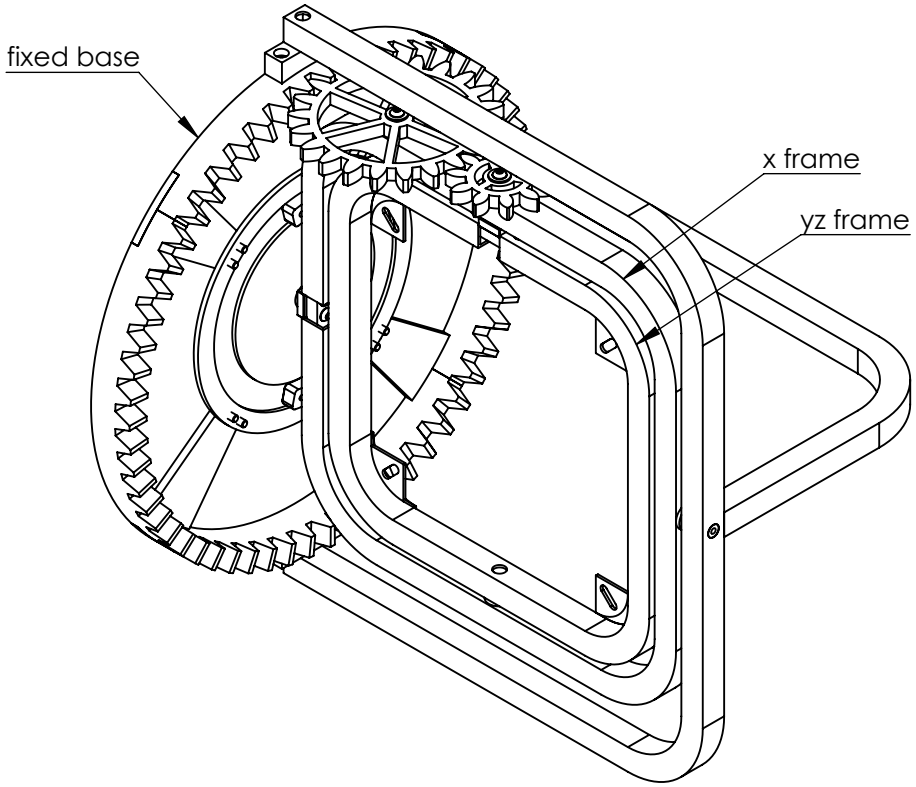

Figure 6.41: Rotomoulding system.

Due to being developed for the mould operation validation only, the system is simplified, dispensing bearing and dampers and leading to additional wear. In addition, the power shaft is manually driven by a crank, avoiding the application of a motor and reduction gears.

The rotomoulding system frames are produced by hand bending 20×20 mm aluminium tubes, closed by milled connectors. The frame axis are turned out of steel rod and all remaining assembly parts, including gears, are cut and milled out of aluminium blocks. The frames compounded by multiple parts are riveted and all remaining connections use M5 screws.

The mould mounting in performed by a quarter of a truncated cone in each corner of the yz-axis frame to allow a centred fixture of the mould. The mounting part consists on a by a incrementally formed truncated cone with 80 mm of diameter, cut if four equal parts.

Rotocasting operation

The functional test is performed in a rotocasting operation, using polyurethane resin. A preliminary test is performed in an inaccurate mould manufactured without the local support and without applying the epoxy mass to fill to the radii, testing the rotational moulding system for material distribution and the mould assembly for possible leakages. Figure 6.42 present the rotocasting operation, presenting the mould fill up process and the mould rotation. The test is performed before fixing the rotomoulding system to the oven to validate its operation.

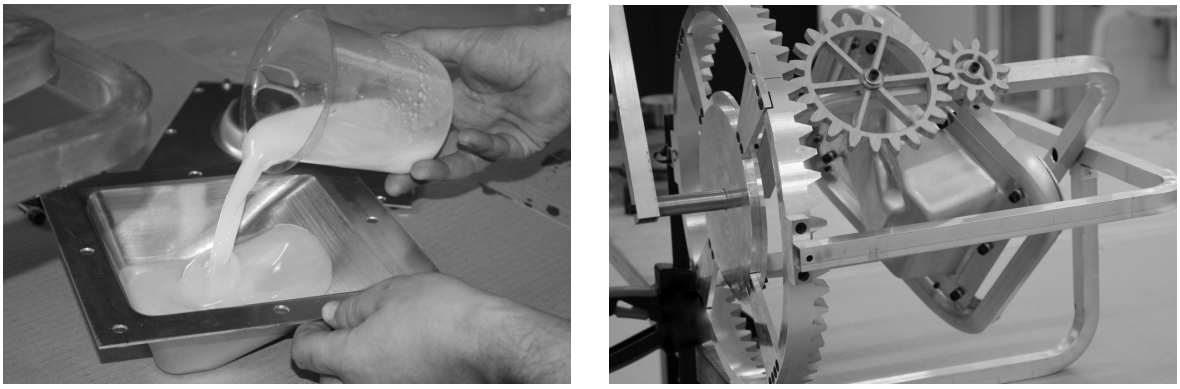

(a) (b)

Figure 6.42: Rotocasting operation with the unfinished SPIF mould: (a) resin fill up (b) mould rotation

The rotation system works as expected. Despite the fact that bearings are not used, the system rotates easily. The uneven weight distribution due to the spur gears does not affect the motion continuity. The rotation is kept between 4 and 10 r.p.m. during the 30 minutes of pot life. During the 3 hours of gel time the mould is regularly rotated by 180°. Despite the unfinished mould, the assembly lead to no leakages and the material spread is acceptable, with only a slight run due to insufficient rotation during the gel time. Figure 6.43 presents the first rotocasting part as removed from the mould. The part geometry reproduces in detail every design element. An over thickness is noticeable at the part thinner edge due to the material run during the gel time. Despite the low resin viscosity and the unfinished mould assembly, no leakage occurs. However, a concave structure with small burrs is noticeable at the parting line due to the mould unfilled radii.

The preliminary results validate the rotational moulding system performance and confirmed the possibility of manufacture moulds by SPIF. Along these lines, the rotomoulding system is mounted on the oven and the mould manufacture is repeated according to the described techniques to improve accuracy.

Rotomoulding operation

Being prevalidated, the sheet metal mould manufactured by SPIF is tested for rotomoulding operations. In a first test, the moulding process is performed using LDPE in pellet form.

The moulding is performed using 150 g of LDPE pellets, corresponding to a 2 mm thickness part after densification. The mould is rotated for 12 minutes in the oven with temperature between 210°C and 250°C. Figure 6.44 shows the mould filling with LDPE pellets and the

Figure 6.43: Rotocasting part manufactured with the unfinished SPIF mould as demoulded

open mould after the moulding process. During the rotomoulding, polyethylene sample in left at sight inside to oven for an approximate visual inspection on the melting stage. Although the sample is not isolated inside the mould, its observation gives relevant intel about the melting stage. In addition, the material stage can be anticipated sonorously as the pellets stop to roll inside the mould.

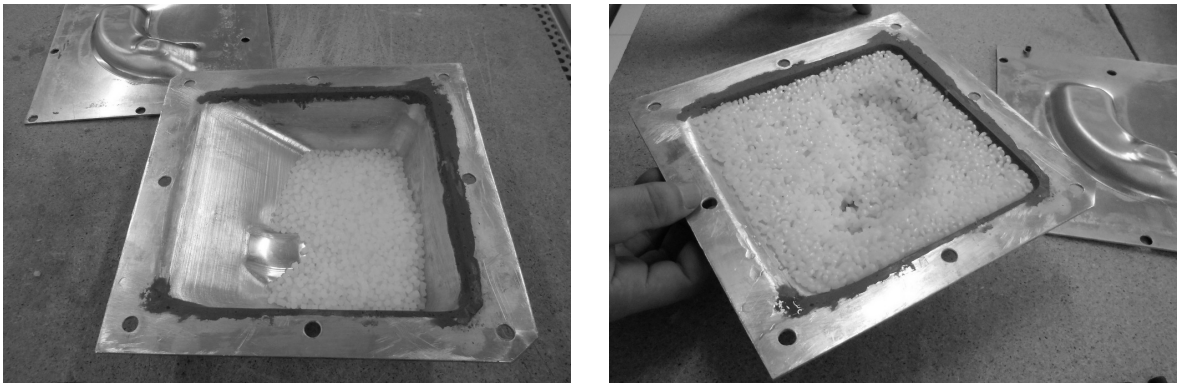

(a) (b)

Figure 6.44: Rotomoulding operation with the unfinished SPIF mould: (a) LDPE pellets fill up (b) open mould after moulding operation

As expected, material densification is not achieved due to the oversize particles used. However, melting occurs around all mould walls, forecasting a fair rotomoulding operation. The part geometry is consistent to the mould geometry with a fair material distribution. The kissoff structure opens despite a low boundary accuracy. Thus, the second stage rotomoulding tests is performed using convenient material particle size.

The rotomoulding operation is performed using LDPE powder superior than 35 mesh, where each particle size is under 500 μm [147]. The moulding operation is performed using 150 g of LDPE powder, corresponding to a 2 mm even thickness part after densification. The mould is rotated for 12 minutes in the oven with temperature between 210°C and 250°C and cooled down at room temperature for 15 additional minutes. Due to the fast heat time when compartment to usual oven operation, an external thermocouple close to the mould exterior

surface is used for temperature reading. Figure 6.45 (a) shows the open mould filled with LDPE powder inside the oven before beginning the moulding process. The rotomoulding operation occur as expected without any noticeable issue due to temperature variations along the moulding surface. Figure 6.45 (b) presents the close mould before demoulding the part. The material shrinkage during the cool down promote an easy demoulding from all moulding surface expect the kiss off structure, where the material compress the mould. The moulded plastic releases with extreme ease from the aluminium surface and is also does not adhere to the epoxy mass because of the use of a silicon based release agent.

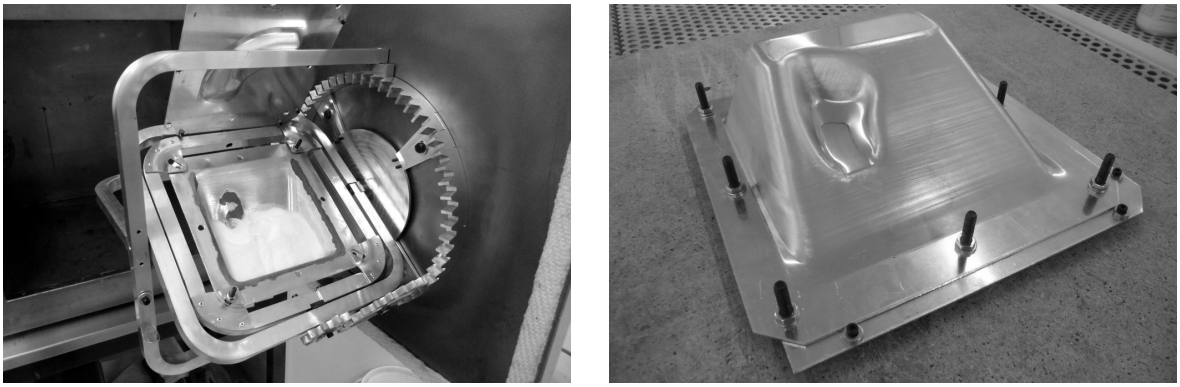

(a) (b)

Figure 6.45: Rotomoulding operation with the finished SPIF mould: (a) LDPE powder fill up mounted on the rotomoulding device (b) close mould after moulding operation

The overall material distribution along the moulding surface is faultless, forecasting a fair thickness distribution. The surface finishing is acceptable and the overall geometry is moulded as expected, as presented in figure 6.46. No significant burrs are found along the parting line although a small undensified volume occurs due to the cold spots caused by the filling mass. The open kiss off at the part centre has better results than the ones from the rotocasting operation, with an open structure despite the miss defined boundary. Some undensified material is also found near the kiss off and along the parting line due to a cold spot caused by the filling material used to improve accuracy. The mould parts are not harmed by internal air pressure due to heating nor the thermal extension. The epoxy mass filing is also consistent with the mould heating. The material shrinkage against the kiss off structure also do not cause any damage on the mould.

After moulding operation, the part is finished. Finishing operation includes the release agent cleaning, deburring and improving external fillets. Deburring operation is done using manual tools, improving the fillets along the parting line, including the open kiss off. Along the operation, major volume of undesified material is removed.

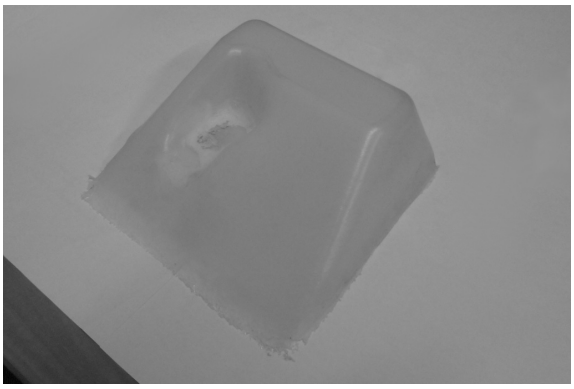

Figure 6.46: Rotomoulding LDPE part manufactured with the SPIF mould as demoulded

6.2.5 Rotomoulding parts validation

In a first term, the plastic parts are visually evaluated, showing decent results. The overall material distribution is faultless, forecasting a fair thickness distribution. The surface finishing is acceptable and the overall geometry is moulded as expected, although the SPIF tool marks on the mould are noticeable. Figure 6.47 present three finished parts, moulded by rotocasting, and by rotomoulding using pellets and powder.

For dimensional control, the rotational moulded parts are measured using a hand laser scanner and compared to the CAD model. The LDPE part is on average 2.8 mm smaller than the CAD model, with deviation varying from -9.7 mm to $+5.5$ mm. The part under dimension occurs both due to mould inaccuracy and material shrinkage. When comparing to the real mould geometry, parts are on average 1.3 mm smaller then the mould, being only bigger in the slot features. The average accuracy is proper of typical rotomoulding process although some deviations, mainly on the bottom side are slightly greater then desired. This deviation occur due to the impossibility of improving top radius of the lower mould size and due to a slight inaccuracy at the moulding surface contact to create the kiss of structure.

For a thickness evaluation, parts are cut by a quarter, as presented in figure 6.48. The LDPE parts present and average thickness along the cut of 2.3 mm, with wall thickness varying from 1.7 mm and 3.0 mm. The average thickness of the base plane and the lower slope wall is 2.1 mm. The higher slope walls average thickness is 2.7 mm. The higher thickness on the part is found at the corners between the base and the higher slope wall, with a maximum value of 7.5 mm. It is noticeable that the unidentified material is only found at the outside surface and the corner has a 4.6 mm solid thickness, minimising the undesired effects of the cold spot. The edge between the base and the lower slope wall features the worst thickness distribution, with thickness down to 0.8 mm and failing to close the surface at some points. This matter occurs mostly because of material distribution issues due to the part close angle.

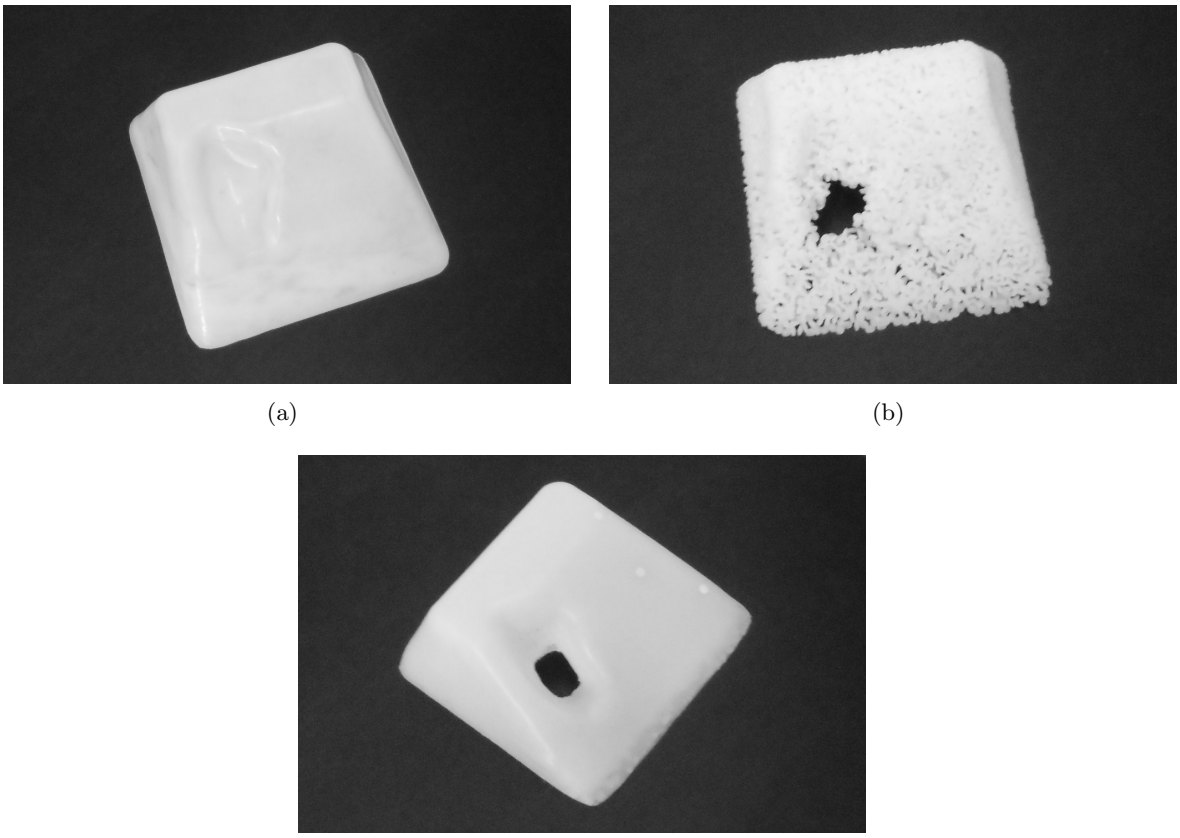

(a) (b)

(c)

Figure 6.47: Rotational moulding parts manufactured by: (a) rotocast PU resin, (b) rotomoulded LDPE pellets, (c) rotomoulded LDPE powder

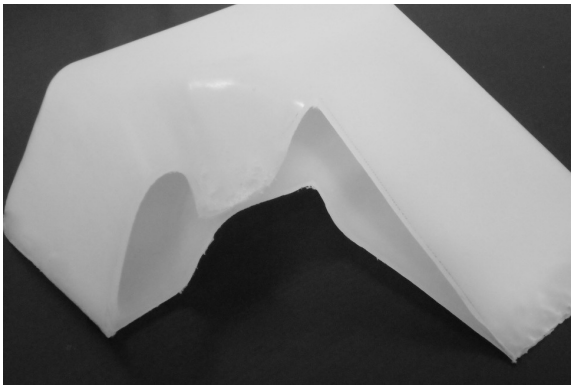

Figure 6.48: Rotational moulding parts cut for thickness evaluation

6.2.6 Conclusion

Although only some preliminary tests have been done yet, one can validate the SPIF process as a rapid tooling process for both rotocasting and rotomoulding operations. Sheet metal moulds made by SPIF are a reliable alternative to the conventional moulds. Despite some significant deviations due to the inaccuracy of the forming process, general appearance of plastic parts is reasonably good and average dimension is accurate.

The sheet metal mechanic and thermal behaviour are suitable to rotomoulding operations, being confirmed both numerically and experimentally. The selection of a sheet thickness for a given mould design can be performed using numerical studies, using simple elements sized as the sheet thickness to define a model geometrically achieved by the sine-law. The thermal behaviour and process time prediction can be done assuming a similar mesh with additional integration points.

The mould total manufacture time and material cost are low and yet largely influenced by some parallel operations. As some tools like backing plate for SPIF operation can be used for more than one mould with similar projected area, the use of sheet metal moulds assumes even a more interesting panorama. The performed test uses two different backing plates while in parts with a more typical parting line could share the backing plate for both mould parts.

If comparing the mould manufacture with typical process, one can predict the SPIF sheet metal approach is both more economical in an energetic and material point of view, as well as in the development time. However, the mould accuracy is lower and leads to worst surface quality.

Yet, the process accuracy and surface finishing can be improved. The accuracy, and surface quality as well, can be improved by using multistage or other forming techniques, although they lead to a longer forming time. A fair compromise must be pursue. Besides, complementary operations can also improve the mould quality. Sanding operation alone can improve the surface quality. A full coverage of the moulding surface with epoxy mass associated to sanding and milling operations could lead to additional manufacturing time and cost but grant great results, although attention must be paid to avoid the creation of cold spots.

This new approach for the manufacture of sheet metal rotational moulding moulds allows to increase the possible geometric complexity. The developed case study used a mould fully developed by SPIF for proof of concept. Nevertheless, the incremental sheet forming technologies can be mixed with other process, achieving great design possibilities.

The uneven thickness distribution on the mould walls due to the incremental forming process lead to a small uneven thickness along the moulded part due to faster heating times. Nevertheless, those differences do not unfeasible the rotomoulded parts and are minor than the ones caused by material distribution.

6.3 Development and test of SPIF composite open contact moulding moulds

6.3.1 Open mould processing and mould geometry definition

Open mould thermoset composite processes produce components with a good strength to weight ratio, with a fair design flexibility and a low do moderate tooling cost. The basic techniques generally use room temperature low-pressure cure of low-viscosity resins, shaping reinforcement fibbers to the parts geometry. A large variety of open mould processes can be used for the fabrication of composite parts, using both dry fabrics and wet resins or preimpregnated fabrics denoted prepregs. The most common moulding techniques are spray-up and hand-lamination, also known as hand layup or wet layup. Figure 6.49 presents the basic hand layup process. In the hand lay-up technique, fibers are positioned on or into the mold and wetted by liquid resin. Brushes are often used to distribute the resin evenly onto the fibbers and rollers are employed to work air bubbles out of the reinforcement and to ensure complete wet out. Before applying the fibbers and resin, the moulding surface can be prepared using release agents or release films, and covered in gel coat. The process is highly skilled dependent and only suited to low production rates due to slow cure times of room temperature resins. The contact moulding techniques can be improved by applying pressure to improve consolidation of the laminate by extracting excess resin and included air. This is mainly achieved by using vacuum bagging, covering and sealing the hand-laid laminate inside a vacuum film over a peel play, a perforated release film and a breather/bleeder fabric. [154, 155]

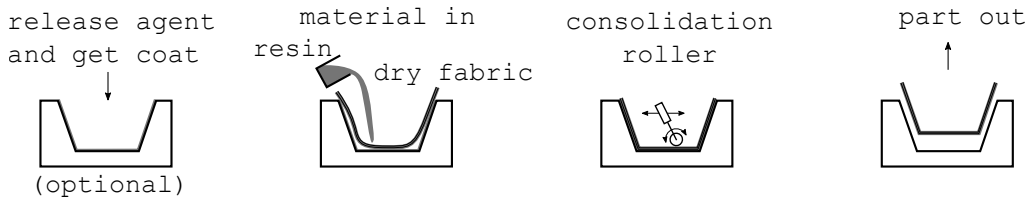

Figure 6.49: Hand layup operation principle.

Different approaches can be used for positioning the reinforcement material, allowing a proper suiting to the mould surface. On the one hand, tapering pieces of fabric allows great structural tailoring capabilities, damage tolerance, and potential for creating significant weight savings. However, stress concentrations at the drop-offs of the fabric pieces may lead to delamination in resin rich areas referred to as resin pockets. The stacking of the reinforcement plies, both in number of layers and positioning has strong influence on the part properties. [156] On the other hand, the fabric can be sheared, allowing a better fit to the mould surface. Different techniques like one handed guiding or two handed guiding, manual folding, hoop shearing, double-tension shearing, tension-secured shearing and mold interaction shearing both before and during the fabric positioning allow a better adjust on the mould surface. [157]

The materials used as reinforcements are typically aramid, carbon, or especially glass fibers. These are available in chopped strand mat and in woven, knitted, stitched or bonded fabrics. The most used thermosets in contact moulding are polyester, vinylester and epoxy resins. The moulding techniques to use are selected depending on the intended part qual-

ity and on the selected materials. The curing procedure is also selected depending on the thermoset resin, either at ambient temperature or autoclave curing. [154]

The moulds used for contact moulding are found in both a core or cavity configuration, where the moulding process aims to control the accuracy and surface finishing of the inner or outer face. The tool should have adequate rigidity to maintain dimensional tolerance and a surface finish to reflect that required of the component to be produced. The moulds used for contact moulding are commonly manufactured in-house, using fiberglass-reinforced skin, and supported by a framework, commonly welded steel structure or wood section box. These are typically manufactured from models of the final part built in wood, plaster, foam, or other materials. The master is completed, polished and waxed and the mold is built up on it with fabrication technique similar to the parts manufacturing. [154]

Depending on the part complexity and size, the mould can be a single part or a complex assembly. However, regardless the mould complexity, the moulding techniques produce continues surfaces. Thus, the contact moulding techniques must be followed by trimming, drilling or other finishing operations.

Although the single side moulds only allow to control the dimensional tolerance and surface finishing of one part side, it is possible to smooth out and gel coat paint the non tool side.

Despite the possibility of developing low to moderate cost tools, the manufacturing process is typically longstanding and commonly generates non recyclable waste. As the moulding pressure is low, it is possible to replace conventional moulds by sheet metal moulds, manufactured by ISF processes [158]. SPIF allows to form parts with geometric complexity compatible to reinforced plastics moulds, with sufficient strength to be used in stand alone application. SPIF parts can be used for both core or cavity type moulds.

The study hypothesis tests the use of SPIF for the development of a cavity mould to be used in a fiber glass hand layup process. The mould is developed in a single part, formed from a single aluminium flat blank. Since sheet metal rigidity is sufficient to support the moulding pressure, the mould dispenses the need for a framework, being mounted only on a simple support to ensure stability.

6.3.2 Part design

Plastic reinforced parts are mostly free form shell like structures with thickness from 1.5 to 15 mm. The tailoring of the fibbers allow to distribute the part strength as desired in both constant or variable thickness parts. Besides, the part design can use sandwich construction to achieve lighter and stiffer parts. The moulding processes are suited for medium to large size parts, allowing close to vertical walls and deep draws. The shaping of more complex parts, particularly with undercuts is possible while requiring more complex moulds, including slides or split parts. The composite parts should have generous curvature at corners to avoid fibber bridging, mainly when using cavity moulds. A minimum radius of 5 to 10 mm and greater than the part thickness is recommended between sides. While it is possible to create reinforcement structures like ribs and bosses, it is more common to corrugate the surface for increased strength parts. Besides, the parts can include metallic inserts both as reinforcement or for assembly purposes. [155]

For the evaluation of the SPIF hand layup mould concept, a part is design based one the reference geometry. The new part is shaped with typical features from fibber glass parts. The hand layup part uses the base single symmetric shape with a projected area of 180 mm by 180 mm and a maximum height of 65 mm, with a minimum draft angle of 20^{o}. The

radius between side faces is 15 mm and between side and top faces was 6 mm. The part design is completed by adding reinforcements indents to the larger sloped walls. Two indents are shaped centred in the opposite sides based on 10 mm diameter slots along the vertical direction of the part. Four additional indents are positioned symmetrically, oriented by the mid plan between the vertical direction and the side walls slope. Given the different wall angles, the indents depth is 2.4 mm in the smaller slope and 4.5 mm in the larger slope. Figure 6.50 represents the drawing of the designed part. The part thickness is not defined as it depends on the number of plies and amount of resin. Given the part radii, the thickness should be kept bellow 3 to 4 mm.

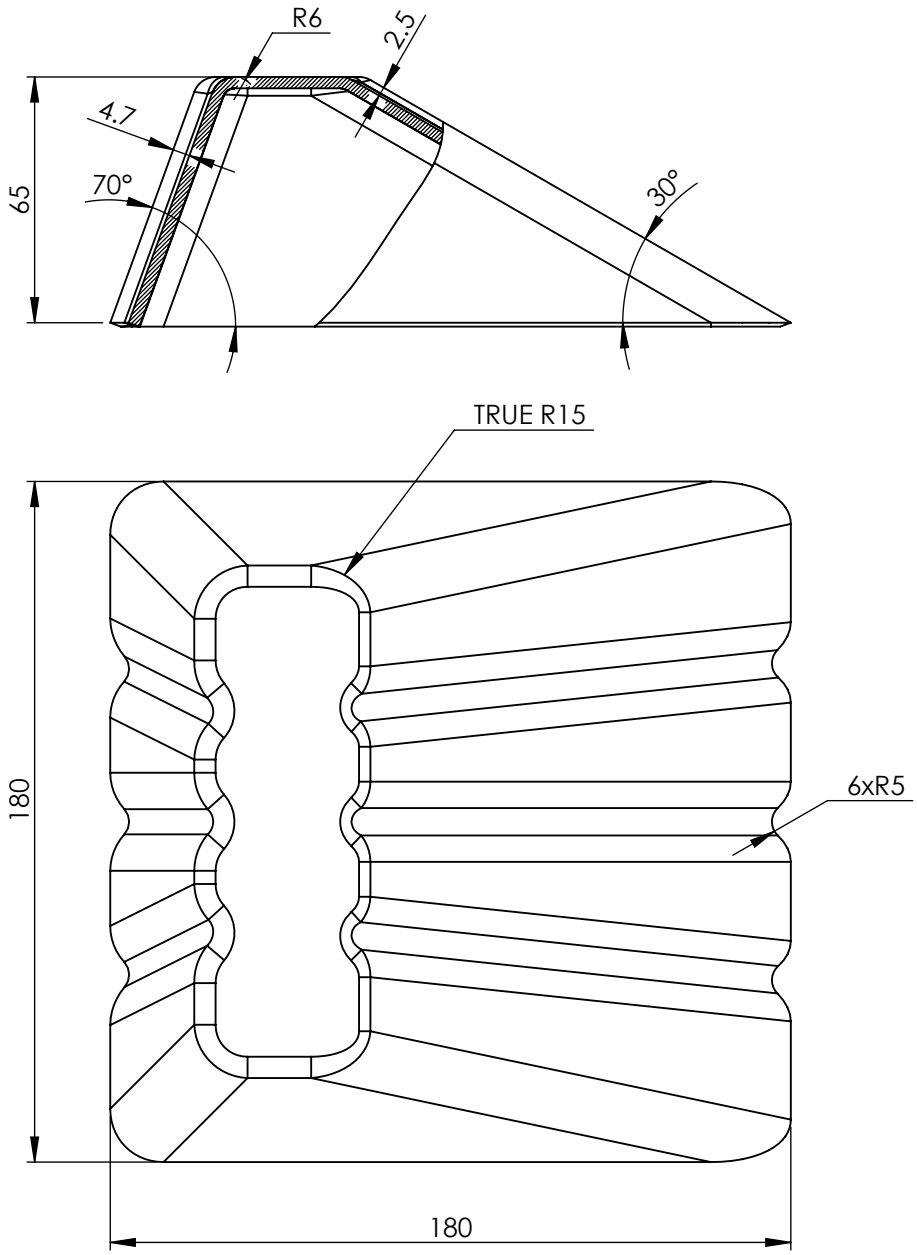

Figure 6.50: Part design for the SPIF hand layup concept validation, scale 1:2

6.3.3 Mould design and manufacturing

The hand layup mould is formed from a single part in aluminium sheet metal by SPIF. The moulding surface is derived from the outer side of the designed part. After forming, the mould is assembled on a simple MDF box for better handling. The mould assembly uses a set of self tapping screws to both mount the support box and fix the metal part. Figure 6.51 represent the mould concept principle.

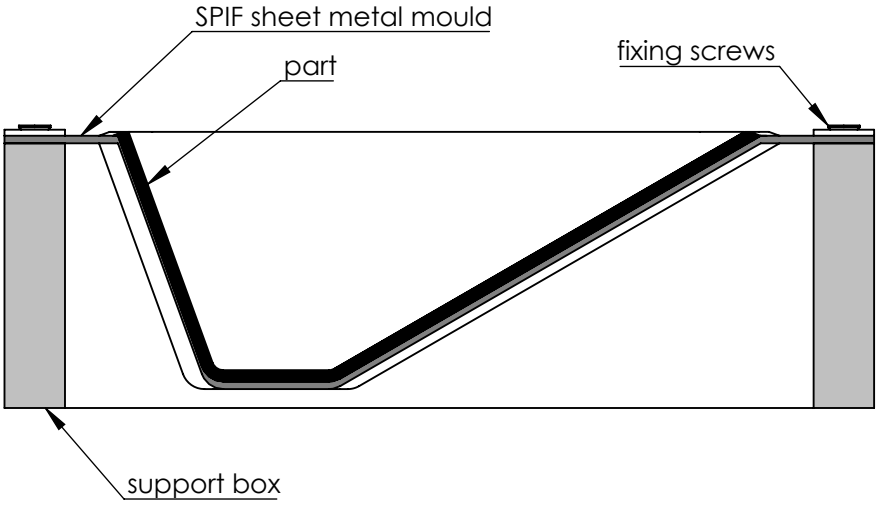

Figure 6.51: SPIF hand layup mould concept.

Since the moulding force is only hand applied and yet low, the load support capability is not an issue. In what concerns bear loading, a 1 mm thickness aluminium sheet should be sufficient to support the moulding operation, despite an estimated final thickness of 0.34 mm on the larger slope walls. However, the thin blank is unsuited for a 70^{o} wall angle, with some local areas going up to 80^{o}. Thus, the sheet metal thickness is only sized to allow a feasible mould manufacture. A 2 mm thickness sheet is selected for the mould manufacture, allowing both a feasible forming process using a single stage operation and providing great mechanical performance for the moulding operation.

The hand layup mould assembly and its parts drawings are presented in appendix E.3.

Mould manufacturing

The manufacturing process of the hand layup mould starts with the cut of a backing plate. Despite the forming operation being made with the same backing plate from the previous tests, the cut is considered to the complete manufacturing analysis. A 225 $\times$ 225 mm 5 mm steel sheet, with a material cost of 40 €/m^2 is used for the backing plate, cut by a water jet process.

The 2 mm AA1050 H111 aluminium blanks are cut in a hydraulic guillotine. The mould uses one 230 $\times$ 230 mm blank with a material cost of 60 €/m^2.

The forming operation is performed using a 12 mm spherical punch, with forming step of 0.5 mm in a single stage helical tool path strategy. Because of the short moves due to the small indents, the forming operation is performed at a 2500 mm feed rate, avoiding vibration related issues. The forming process considers the CAM preparation and NC program compiling to

the SPIF-A machine, machine set up, sheet clamping, machine power up, sheet referral, forming operation and part release, cleaning and hole punching. The process takes just over an hour and a total energy consumption of 6.5 kW.h including close to 40 minutes of effective forming operation. Figure 6.52 (a) illustrates one of the final z increments of the mould SPIF operation. After forming, the sheet metal part is hole punch at the corner to allow its assembly on the support box.

A simple MDF box is built out from four equal pieces, assembled by side screwing. The average material cost for the MDF is 10€/m^2. The sheet metal part is fixed to the mould support box using self tapping screws through the punch holes. The support box is mounted using eight ST4.2 $\times$ 32 screws and the sheet metal part fixed with four ST4.2 $\times$ 19 screws and four 6 mm washers.

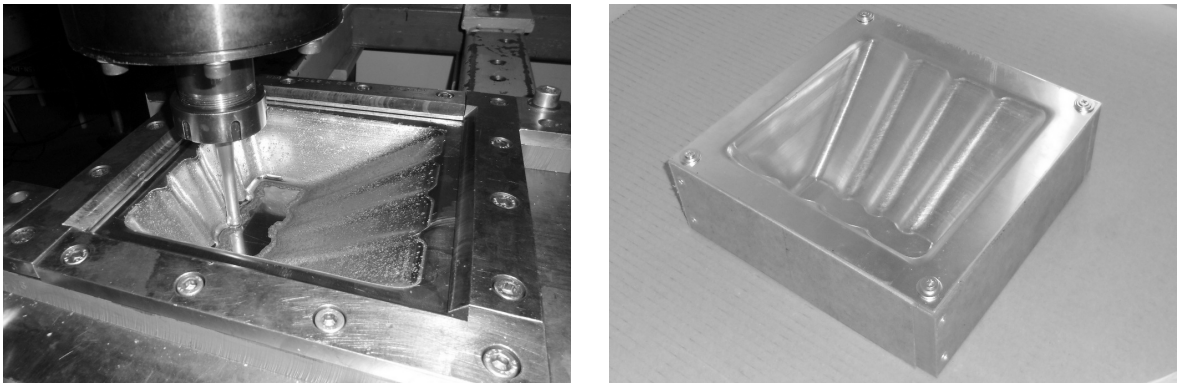

(a) (b)

Figure 6.52: Manufacture of the hand layup sheet metal mould: (a) forming operation (b) assembled mould

During the mould manufacture, operation time and energy consumption is measured considering each individual task. Table 6.17 resume the time and energy consumption for the hand layup mould manufacturing. Table 6.16 resume each manufacturing stage process time, energy consumption and material cost. Figure 6.53 represent a pie graphic display of the time and energy consumption in the SPIF mould manufacture for a better reading.

Total fabrication time for the mould is 1h38min being 67% for the SPIF process. The total energy consumption is 9.13 kW.h, although a large proportion is derived from the water jet cutting. The total material cost is just 7.00 €, being 2.50 € for the backing plates, 3.50 € for the aluminium sheet and 1.00 € for the MDF parts and fasteners.

Table 6.16: Time, energy and cost of the hand layup mould manufacture

Operation	Time (min)	Energy (kW.h)	Material Cost
backingplate cut	17:09	2.57	2.50 €
blank cutting	01:51	-	3.50 €
SPIF mould forming	66:07	6.51	-
carpentry and fastening	13:03	0.05	1.00 €

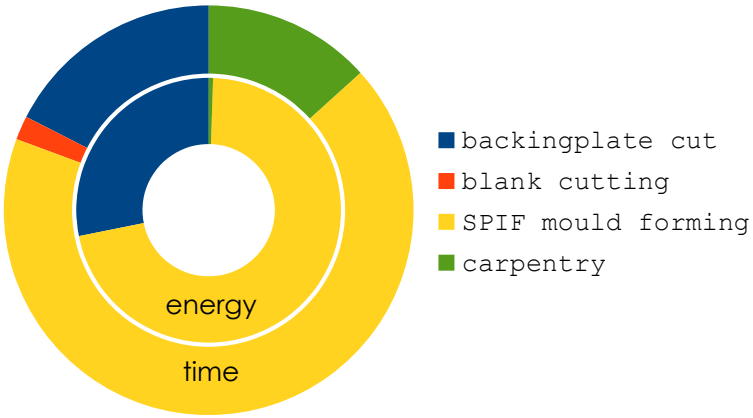

Figure 6.53: Time and energy consumption in the SPIF hand layup mould manufacture

Table 6.17: Time and energy consumption in the SPIF hand layup mould making

Operation	Sub operation	Time (min)	Energy Consumption
Waterjet backing plate cut	backing plate drawing	2:06	-
	cut programing	5:02	-
	machine set up and start up	2:55	0.02 kW.h
	define cut position and parameters	1:55	0.01 kW.h
	cut	4:29	2.54 kW.h
	part removal and clean	0:42	-
Guillotine blank sheet cutting	machine set up	0:58	-
	blank cutting	0:53	-
SPIF mould forming	CAM preparation	7:22	-
	compile CAM	2:56	-
	machine set up	4:33	-
	sheet holding	3:59	-
	machine start up define zero	2:05	0.35 kW.h
	forming positive mould	38:56	6.16 kW.h
	part removal, clean and punch	6:16	-
Carpentry	measure and marking	2:17	-
	cut	3:59	0.05kW.h
	assembly	6:47	-

After manufacture, SPIF sheet mould is measured by contact using a touch-trigger probe on a 3 axis CMM. Figure 6.54 illustrates the measuring operation of the sheet metal moulds and figure 6.55 shows the comparison between the SPIF part and the CAD. Maximum deviation is +6.4 mm on the side walls of the mould, with an average deviation of +1.5 mm. The measurement analysis show and accuracy improvement at the indent reinforced walls. When analysing the reinforced walls and part bottom only, maximum deviation is −3.0 mm at the part top, with an average deviation of +0.9 mm.

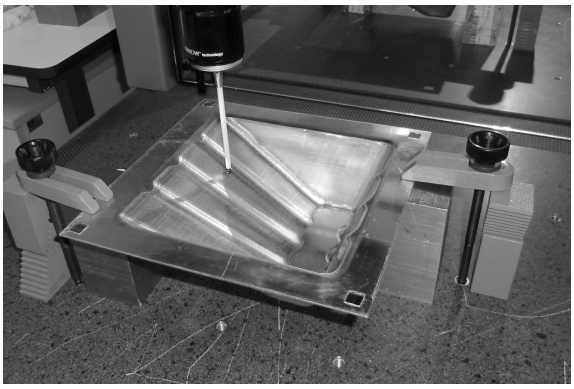

Figure 6.54: Hand layup sheet metal mould dimensional measurement

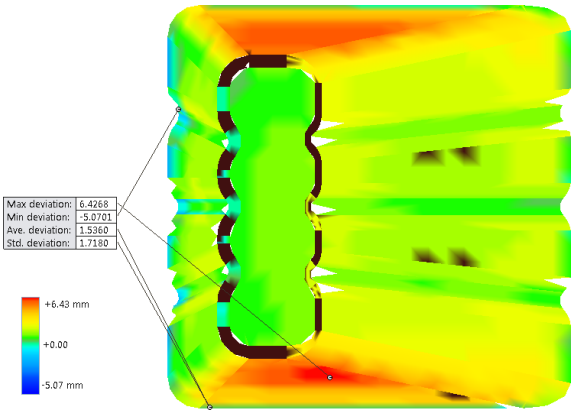

Figure 6.55: Hand layup sheet metal moulds dimensional measurement results

6.3.4 Mould operation

The mould operation test is made in a hand layup process using 400 g/m^2 fiber glass chopped strand mat impregnated with epoxy resin. The part is laminated in a three plies composite, using mainly tapering pieces techniques with two handed guiding and manual folding.

The mould is spray covered with silicone based demoulding agent. No gel coat is used for the part manufacture.

The fiber glass mat is tailored so that each layer can cover different areas of the part without cuts. The first and the third plies use a larger mat piece extended from the top of the smaller slope wall, by the parts bottom to the top of the opposite wall and two smaller pieces on the remaining side walls. Small pieces of mat are also placed in the radii between side walls. The second ply has a perpendicular mat distribution.

All pieces of fiber glass are soaped in resin before being assembled in the part lamination. The pieces are positioned one at a time and pressed against the mould using a barrel type roller and hand pressure. The mould rigidity is plenty sufficient for the hand layup operation. Figure 6.56 (a) presents the SPIF hand layup mould before the lamination operation, with the chopped strand mat pieces distribution tested inside the mould. Figure 6.56 (b) present the mould after lamination operation.

(a) (b)

Figure 6.56: Hand layup operation with the SPIF mould: (a) moulding tools and chopped mat inside mould (b) mould after lamination

The laminate is left for curing overnight before demoulding. The demoulding operation is performed easily, with the part leaving the mould without major effort or causing any damage. Figure 6.57 shows the fibber glass part after being demoulded and after trimming operation.

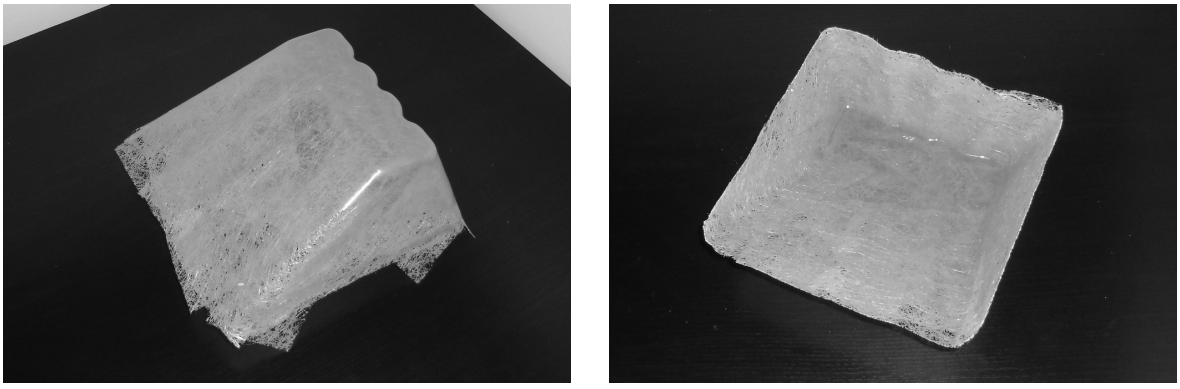

(a) (b)

Figure 6.57: Finishing operation of the hand layup part moulded in the SPIF mould: (a) part as demoulded (b) part after trimming

6.3.5 Hand layup parts validation

In a first evaluation by visual inspection, the fiber glass part succeed to shaped the model geometry, with a fair surface quality. No major issue is noticeable because of the use of a SPIF mould instead of a conventional mould, although some forming punch marks are still visible at the finished part. Some lost of contact point can be spotted near the ribs, although they relate to faults in the lamination operation an not to the mould itself.

For dimensional control, the hand layup moulded parts are measured using a hand laser scanner and compared to the CAD model. The maximum deviation between the fibber glass

part and the CAD model is +5.1 mm, with and average of +1.2 mm. When comparing to the real mould geometry, the maximum deviation is −2.6 mm.

In what regards the surface quality, some failures are found along the part, mainly on the higher slope reinforced wall. However, these faults are related to laminating issues and not to the use of the sheet metal mould. The faces moulded with tool contact have some minor marks from the sheet metal SPIF related irregularities mainly on the lower slope wall. Notwithstanding these issues, the surface quality is generally considered fair along all part.

6.3.6 Conclusion

The possibility of using stand alone sheet metal parts for the development of open contact moulds is validated. Sheet metal mould are a reliable alternative to conventional tools for the manufacture of composite parts and compatible with typical accuracy levels. It is possible to achieve a reasonably good part quality even when laminating composites on unfinished SPIF sheet metal tools.

The research tested and validated the use of a fully SPIF sheet metal mould for hand layup operation. Nevertheless, it is considered that it is also reliable to use SPIF tools for other process like spray-up, and the tools can benefit from combining SPIF with other manufacturing processes, namely for the development of highly complex geometries.

From the mechanical point of view, the sheet metal is sufficiently rigid and tough to support the moulding loads. Thus, The selection of the mould thickness only need to take into account the SPIF process itself. The blank sheet thickness must be selected to in order to be compatible with the maximum forming angle. When designing a core mould, the sine law can be used to estimate the thinning with sufficient accuracy to define the mould geometry.

The mould total manufacture time and material cost are much lower than the ones in conventional fiber glass tools development. In addition, the environmental footprint from the sheet metal mould manufacture is much lower as it only uses easily recyclable materials. Finally, due to the material properties, the sheet metal mould as the potential to be reshaped to accommodate additional design features.

From the financial point of view, one can predict the SPIF sheet metal approach is more economical. However, the mould accuracy is lower and leads to worst surface quality. This weakness can be overtaken by finishing operation, despite their impact in the development time and cost.

Both the mould accuracy and surface finishing can be improved. Considering the SPIF process alone, improvements can be achieved by using multistage or other forming techniques, although they lead to a longer forming time. Besides, finishing operations can also be performed to improve surface quality. Coating option are also valid for the improvement of both accuracy and surface finishing despite the negative impact on the time to first use and recyclability ease.

6.4 Development and test of SPIF compression moulding moulds

6.4.1 Compression moulding process and mould geometry definition

The compression moulding technologies are suitable for processing different materials. One of the most common usages is found in processing thermoset materials, fiber-based plastic composites and cellular materials. Different compression moulding techniques can be applied, using moulding materials in different states: bulk, sheet or granulate. In such a way, different techniques are better suited to mould anything from thick, solid shapes to thin-walled shapes. Generally, the compression moulding process involves applying pressure to force the material into contact with all mold areas, while heat and pressure are maintained until the material cures. Beyond the free form moulding capability, a major advantage when comparison to other manufacturing processes is the possibility of moulding variable thickness parts. [109, 155, 159]

Compression moulding operation typically uses two part moulds, defined by a cavity and a core. Figure 6.58 represents the basic operation of the moulding process. Depending on the used materials, the process may use heated moulds or a two step process where the material is first compressed and then cured in a oven. The first approach is usually performed on hot press machines and the second approach is a regular press and a oven. Some moulding procedures, namely when using thermoplastic matrices, pre heat the material at a specific temperature to soften it, promoting and easier compression and mould filling. Throughout the process heat and pressure are maintained until the polymer has cured. During the compression cycle, it is common to reopen the tool to let vapour escape. The mould may include venting features to better deal with this phenomenon. [145, 160]

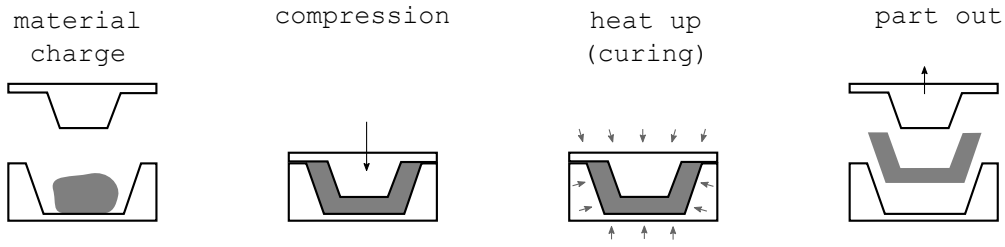

Figure 6.58: Compression moulding operation principle.

A relevant benefit of the compression moulding is that it discards relatively small waste, thus providing advantages when moulding with costly materials. Besides, compression moulding techniques are capable to mould extra large and complicated components. Finally, a major benefit of the compression moulding process, particularly when moulding foams or other cellular materials is the ability to control the material compression ratio and achieve a specific part density. [160]

Compression moulding of cork

A particular application of the compression moulding technology deals with the processing of cork composites. These materials commonly use 0.5 to 1.0 mm grain size granules, bounded by a polyurethane (PU) based resin. The granulated cork density varies from 60 to 160 kg/m^3 and can be agglomerated to 140 to 600 kg/m^3 by compression moulding operations. Due to the absence of waste material, this manufacturing process allows to achieve fairly complex geometries for medium to high quantities [161].

The compression moulding of cork may be performed in a two step moulding operation, since the resin curing time is significant. Material mixtures used in compression moulding use corkresin ratios around 9:1. The material mixture adds water to the cork granules and binder for moisture cured polyurethane, enabling the aggregation of the powder and aiding compression and mould filling. Due to the great density difference between the material mixture and the finished part, the mould cavity must assure the volume for the bulk material. The compression is performed and the mould is locked in the final position to be heated for binder cure [162, 163].

6.4.2 Part design

Typical compression moulding parts thickness can vary from only 1 mm to over 25 mm, allowing to shape thicknesses variations along the part. The compression moulding part require the use of a minimum draft angle from 3º and a minimum 2 mm radius in all edges. The process allows the shaping of free form surfaces, allowing the inclusion of corrugated features, bosses or ribs. [155]

The definition of a part geometry for a cork piece moulded by compression moulding follows this general guidelines. Special care must be taken regarding the minimum thickness to avoid fragile areas. In addition, minimum detail should also be sized according to the used granulate size.

For the evaluation of the SPIF cork compression moulding mould concept, a part is design based one the reference geometry. The cork part uses the base single symmetric shape with a projected area of 180 mm by 180 mm and adds corrugated features to all walls. The radius between side faces is 15 mm and between side and top faces was 6 mm. The material volume is reduced by designing the part as a thick shell. Along the smaller slope wall direction the part uses a 26 mm thickness which increases to 37 mm in the lateral walls. Figure 6.59 represents the drawing of the designed part.

6.4.3 Mould design and manufacturing

The designed tools for the cork compression moulding SPIF rapid tooling research uses a two pieces mould with a flat parting line. The mould is design for a vertical operation, with the part being moulded upside down. One part of the mould is formed by a cavity with the complementary surface of the upper side of the designed part. The opposite part is formed by a core with the complementary geometry of the part hollow to mould the thick wall part. These two parts are the moulding essentials, designed as sheet metal containers. Since the raw material volume is much higher than the empty cavity, the mould assembly is completed with a frame box to allow the placing of all the uncompressed cork mixture. This frame box is defined to be manufactured by a flange type SPIF part with a manually bent extension. The manufacture and assembly detail is presented on the drawings of the appendix E.4. Finally, for a more convenient operation, a support box is included in the mould design. Besides, a clamping system is added to allow locking the closed mould under pressure for oven resin curing. Figure 6.60 presents a simplified concept of the compression moulding tool.

The presented mould concept not only responds to the designed part but also follows a common guideline for any flat parting line part. Moulds with a higher cavity volume over part volume ratio may dispatch the frame box extension. Compression moulding tools for other materials where the material compression ratio is lower may also dismiss the frame box.

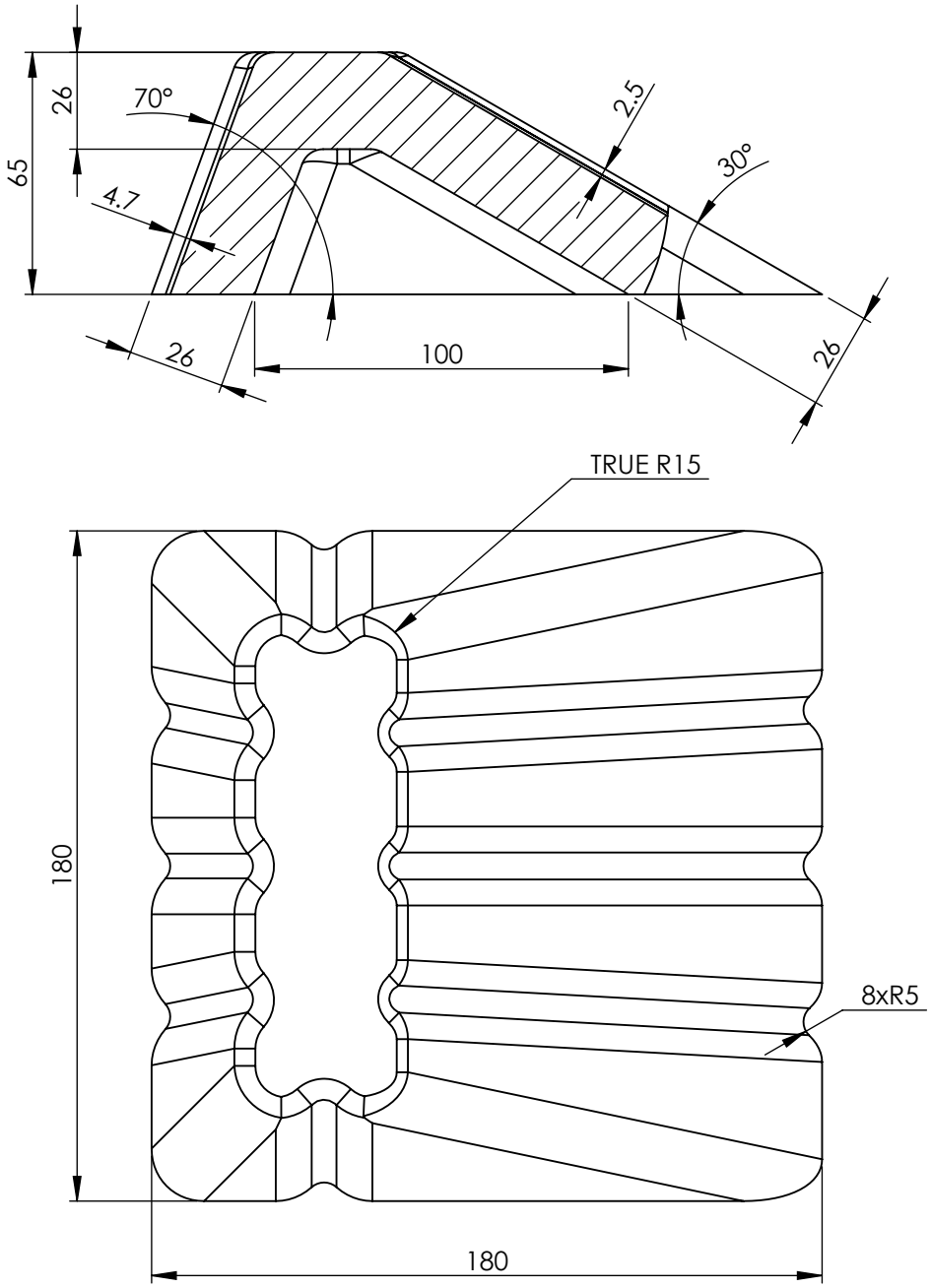

Figure 6.59: Part design for the SPIF compression moulding concept validation, scale 1:2

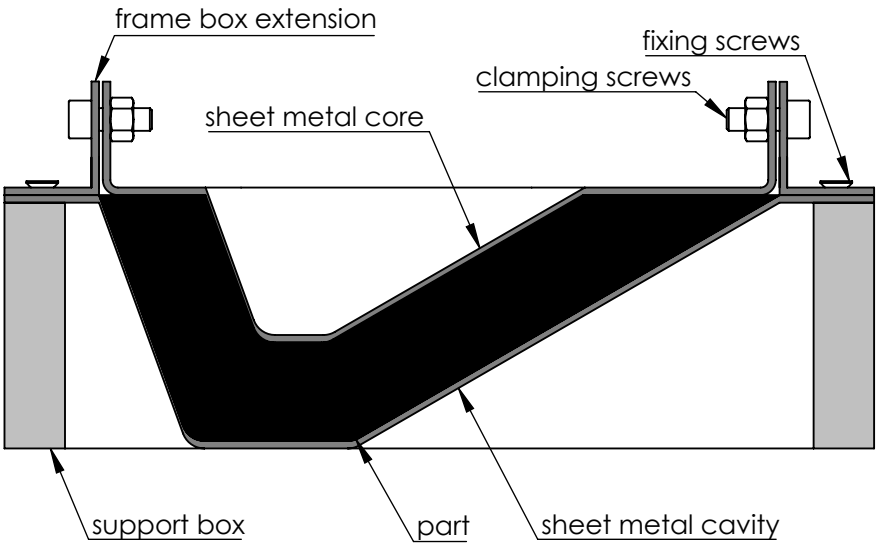

Figure 6.60: SPIF cork compression moulding mould concept.

The designed part has a 930000 mm^3 volume. The mould cavity volume is 1133000 mm^3, resulting on a maximum volume compression ratio of 1.22. In order to allow a moulding operation with a compression ratio up to 2, the cavity volume must be extended to 2 $\times$ 930000 mm^3, resulting on an additional of 727000 $-$ mm^3. Given the cavity top surface 32000 mm^2 area, the extension box must be 23 mm height.

Like the previous proof of concept studies, the mould parts are modelled according to the sine-law. This approximation allows a acceptable definition of the manufactured geometry, allowing the CAD model to be used to accurate determine the total mould mass and analyse its behaviour through computational methods. Besides, this approximation allows a better definition of the core part shape, as it uses the formed flip-side for the moulding operation.

In what concerns the thermal behaviour, since the resin cure time in the cork compression moulding, as well as is other material processing, is significant, no need for a thermal analysis is relevant. The resin curing deals with temperature bellow 200°C and cure times from 2 to 12 hours. These values are compatible with any mould thickness and, due to the long heating time, the heat up rate is little significant.

From the mechanical point of view, the compression moulding operation deals with quite significant loads. In such a way, the support box is dimensioned so that the cavity sheet metal part is both supported around the perimeter and in the bottom. In what concerts the moulding load application, the core top allows a table top support through a back plate. Considering this principle of operation, the sheet metal initial thickness is sized according to the mechanical behaviour of the mould under stress.

Mould mechanical behaviour

Generally, the compression moulding loads varies from 0.1 to 10 MPa, increasing up to 15 MPa for some specific materials [155,159]. This huge variation depends mainly on the compression moulding technology variant used and the moulding material. In the case of cork compression moulding, moulding loads are typically kept in the lower range of the refereed interval. Depending on the intended moulded part density, the moulding load may go up to 2.0 MPa [162].

Considering the compression of the cork alone, applications where the compression ratio is kept bellow 2 the differences in the compressive stress are not noticeable. In these cases, the moulding load in typically inferior to 0.6 to 0.7 MPa. In higher compressive ratios densification occurs and the compressive stress increases abruptly. In compressive rations bellow 1.1 the moulding load is much lower. As the cork granulated mixture density is much lower than the cork itself due to the air between material granules, the moulding loads is even lower. [163].

As the research aims for a proof of concept for the development of tools for prototypes manufacturing, the moulding pressure is considered for a low reference value. This consideration is further supported by a moulding operation aiming for a low density part. In such a way, the mechanical analysis considers a distributed load of 0.2 MPa. The test load considers the moulding compression itself. The mould locking is not considered since the force reduces after compression is stabilised in low to medium density parts.

Finite element method is used to determine minimum sheet thickness by a static analysis on Solidworks Simulation. Simulation is done considering isotropic AA1050 H111 sheet metal with $E = 69$ GPa, $G = 26$ GPa and $\nu = 0.33$.

Sheet thickness on mould walls is modelled according to the sine-law (2.1) as a function of the blank initial thickness. Analysis are performed using only nominal initial thicknesses between 1 mm and 3 mm. The analysed thickness are presented in table 6.18.

Meshing is done considering a solid mesh using tetrahedral elements with four integration points. The used element size is allowed to range from the initial sheet thickness to one sixth of its value, leading to a maximum possible element aspect ratio of 6. The maximum element size lower bound is limited to 2 mm to avoid excessive number of elements. The mesh distribution is defined using curved based mesh, granting a minimum of eight element in a circle and considering a maximum element size grow ratio of 1.6. Meshing the model leads to an average under 300000 elements with the majority of the elements with an aspect ratio under three. Table 6.18 resumes information about the defined meshes.

Table 6.18: Mesh details on cork compression sheet metal mould

Blank thickness (mm)	Min. thickness (mm)	Max. element size (mm)	% elements with aspect ratio < 3	Number of elements
1.0	0.34	2.0	76.6	255684
2.0	0.68	2.0	93.2	319399
3.0	1.02	3.0	92.2	136981

Fixtures are established to represent the moulding operation. The area in contact with the support box is fixed. In addition, the vertical down movement of the cavity bottom and the vertical upward movement of the core top are restricted to simulate contact with the press plates.

The simulation runs using FFEPlus iterative solver using implicit integration method. Table 6.19 refers the stress and displacement maximum values of the mould with different initial thickness. Figure 6.61 presents the stress and displacement distribution of the 2 mm sheet metal mould analysis. The structural reinforcement caused by the corrugated surface is mostly noticeable in the higher slope walls.

Table 6.19: Stress and displacement on cork compression sheet metal mould

Blank thickness (mm)	Max. Stress (MPa)	Max. Displacement (mm)
1.0	525	5.94
2.0	165	1.36
3.0	92	0.62

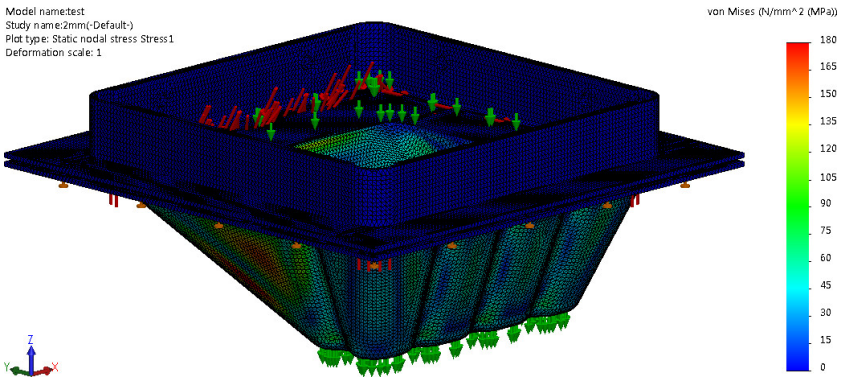

(a)

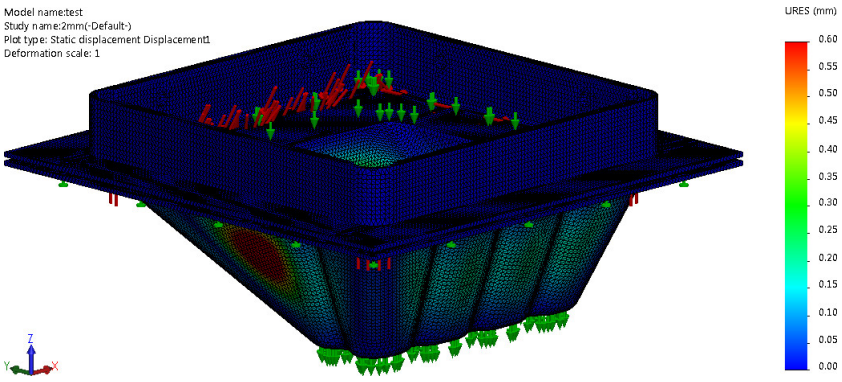

(b)

Figure 6.61: 2 mm cork compression mould mechanical behaviour simulation: (a) stress distribution (b) displacement

By analysing the simulation results, a sheet thickness of 2 mm is chosen for the mould manufacture. In what concerns displacement, although the calculated maximum displacement value is significant, it is only located. Furthermore, it has the same magnitude as the SPIF typical accuracy with decreases with the gain in thickness. In what concerns the stress, although the maximum the values are just above the yield, even after strain hardening, they are only spoted in small areas. Further, despite being run with a small load, the simulation considers a loading perpendicular to the surface, which is the worst case scenario.

The cork compression mould assembly and its parts drawings are presented in appendix E.4, considering the manufacture of the formed parts in 2 mm sheet metal and the frame box extension in 1 mm sheet.

Mould manufacturing

The manufacturing process of cork compression moulding tools starts with the cut of dedicated backing plates for each mould side. Despite the forming operation being made with the same backing plate from the previous tests, the cut is considered to the complete manufacturing analysis. Two 225×225 mm 5 mm steel sheet, with a material cost of 40 €/m^2 are used for the backing plate, cut by a water jet process. One backing plate is cut with a 182×182 mm window to form the mould cavity and the frame box and the other is cut with a 102×102 mm window to form the mould core.

The 2 mm AA1050 H111 aluminium blanks are cut in a hydraulic guillotine. The mould uses three 230×230 mm blank with a material cost of 60 €/m^2. The mould assembly uses an addition strip of 1 mm aluminium sheet with 40×720 mm with a material cost of 40 €/m^2.

The forming operation of the three SPIF parts is done using a 12 mm spherical punch with a 0.5 mm vertical forming step in a helical tool path strategy. The container configuration parts are formed in a single stage tool path strategy and the flange configuration part is formed using a multi stage strategy. Figure 6.62 shows the forming operation of the three SPIF parts.

As in the hand layup mould, because of the short moves due to the small indents, the forming operation of the mould cavity is performed at a 2500 mm/min feed rate. The forming process considers the CAM preparation and NC program compiling to the SPIF-A machine, machine set up with a tool change and backing plate change, sheet clamping, machine power up, sheet referral, forming operation and part release and cleaning. The process takes just over an hour and a total energy consumption of 7.2 kW.h including close to 45 minutes of effective forming operation.

The core mould side is formed using the same tool path strategy and increment, at a 2000 mm/s feed rate because of the reduced wall length and side radii. The forming process considers the same parameters where the tool change in not required. The process takes just under half an hour and a total energy consumption of 2.2 kW.h including close to 12 minutes of effective forming operation.

The incremental flanging operation of the frame box part a 140×140 mm window is opened on the blank, leaving 20 mm around the 180×180 mm boundary. Four 8 mm wide cut reliefs are open, leaving just 10 mm of material inside the part boundary at the corners. The SPIF operation is performed using a three stage strategy. The first stage forms the sheet to a 45º wall, the second to a 70º wall and the firth to a vertical wall. The forming operation is performed at 3000 mm/min feed rate. The flange forming is perform in under 50 minutes, including 20 minutes of effective forming operation, with a total energy consumption of 3.8 kW.h.

Complementary forming operations are performed to finish the frame box and the core side of the mould. The core part blank corners are cut and the sides are bent using a manual sheet metal bender. The frame box height extension is manually bent around the frame box flange while riveting.

After forming, additional operations are perform to complete the mould assembly. A support box is built using four equal MDF pieces. Both the cavity part and the frame box are drilled to be fixed in the support using self tapping screws. The frame box and the core part are also drilled in position for the mould locking mechanism.

Total fabrication time for the mould is 4h22min being 56% for the SPIF process. The total energy consumption is 17.21 kW.h and the total material cost is 20.00 €.

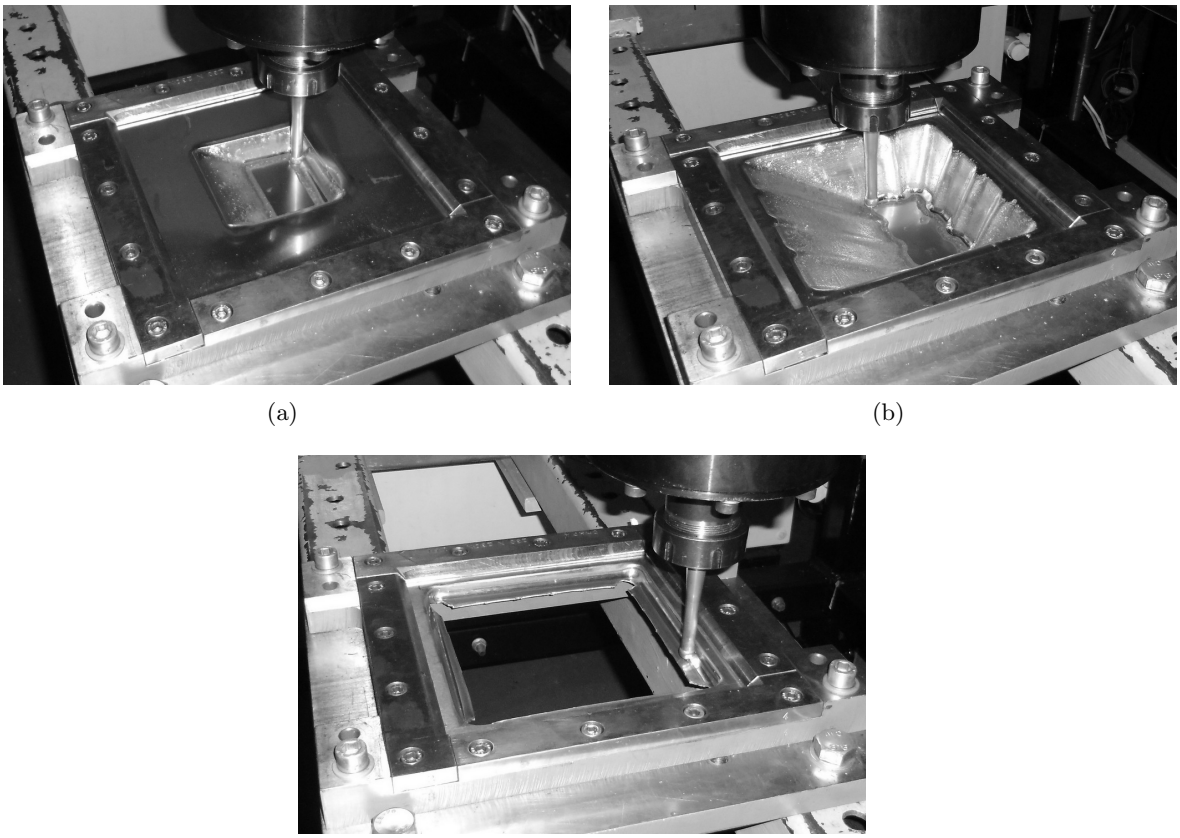

(a) (b)

(c)

Figure 6.62: SPIF operation forming sheet metal cork compression mould: (a) core side, (b) cavity side, (c) frame box flanged part

Table 6.21 resume the time and energy consumption for the cork compression moulding mould manufacturing. Table 6.20 resume each manufacturing stage process time, energy consumption and material cost. Figure 6.63 represent a pie graphic display of the time and energy consumption in the SPIF mould manufacture for a better reading.

Table 6.20: Time, energy and cost of the cork compression mould manufacture

Operation	Time (min)	Energy (kW.h)	Material Cost
backingplate cut	26:00	3.98	5.00 €
blank cutting	19:25	-	12.50 €
SPIF mould forming	147:03	13.16	-
Drilling and other forming operations	13:03	-	-
Carpentry and assembly	25:24	0.07	2.50 €

Figure 6.64 present the finished cork compression mould cavity and core side by side. No trimming is performed in the flanged frame box part since it has no effect on mould performance.

Table 6.21: Time and energy consumption in the SPIF cork compression mould making

Operation	Sub operation	Time (min)	Energy Consumption
Waterjet	backing plate drawing	3:12	-
backing plates	cut programing	8:36	-
cut	machine set up and start up	2:55	0.02 kW.h
	define cut position and parameters	1:55	0.01 kW.h
	cut	6:58	3.95 kW.h
	part removal and clean	2:24	-
Guillotine	machine set up	0:31	-
blank sheet	three blanks cutting	1:28	-
cutting	machine set up	0:56	-
	one strip cut	1:23	-
	blank measuring and marking	3:16	-
	blank pre cut hole	11:51	-
SPIF	CAM preparation	7:52	-
cavity	compile CAM	3:27	-
mould	machine set up	4:33	-
forming	sheet holding	3:42	-
	machine power up and define zero	1:15	0.22 kW.h
	forming positive mould	43:47	6.95 kW.h
	part removal, clean and punch	4:58	-
SPIF	CAM preparation	6:14	-
core	compile CAM	2:09	-
mould	machine set up	0:23	-
forming	sheet holding	3:39	-
	machine power up and define zero	1:32	0.28 kW.h
	forming positive mould	11:48	1.94 kW.h
	part removal and clean	3:46	-
SPIF	CAM preparation	13:03	-
mould	compile CAM	2:52	-
frame box	machine set up	0:34	-
forming	sheet holding	4:21	-
	machine power up and define zero	2:35	0.42 kW.h
	forming frame box	20:21	3.35 kW.h
	part removal and clean	4:12	-
Auxiliary	core mould measure and cut	10:18	-
forming	core mould bending	8:48	-
operations	core mould trimming	8:21	-
	frame box extension bending	2:23	-
Drilling	measure and marking	12:05	-
	sheet drilling and punch holing	1:42	-
Carpentry	measure and marking	2:26	-
	cut	5:19	0.07 kW.h
	assembly	4:48	-
Mould assembly	frame box mount	9:48	-
	mould assembly	3:03	-

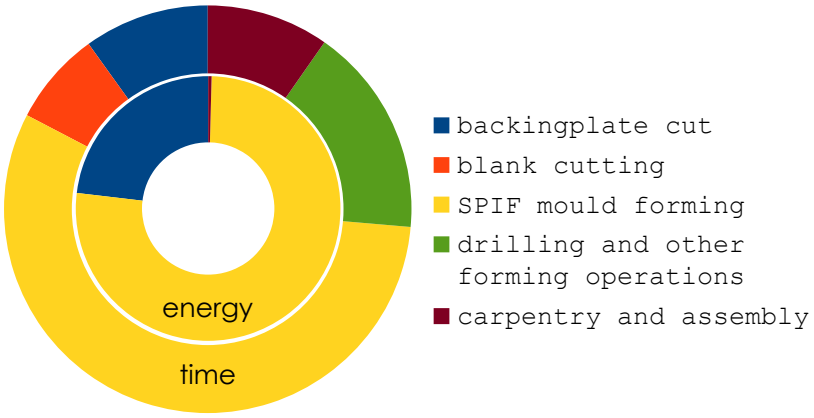

Figure 6.63: Time and energy consumption in the SPIF cork compression mould manufacture

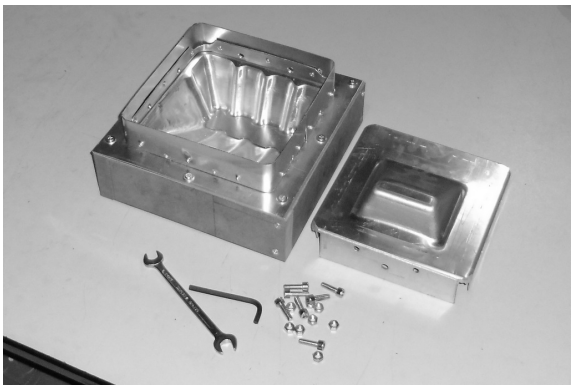

Figure 6.64: Sheet metal cork compression mould

After forming operation, the mould sheet metal parts are measured by contact using a touch-trigger probe on a 3 axis CMM. Figure 6.65 illustrates the measuring operation of the sheet metal parts and figure 6.66 shows the comparison between the SPIF parts and the CAD model. Maximum deviation on the core side of the mould is +6.0 mm at the top edge of the longer higher slope wall. The average deviation is +1.0 mm. On the cavity side of the mould, the maximum deviation is +7.2 mm, with an average deviation of +1.1 mm. As in the hand layup mould, the measurement analysis show and accuracy improvement at the indent reinforced walls. Besides, the addition of the reinforcement indents also benefits the wall flatness.

(a) (b)

Figure 6.65: Sheet metal cork compression mould dimensional measurement: (a) core side (b) cavity side

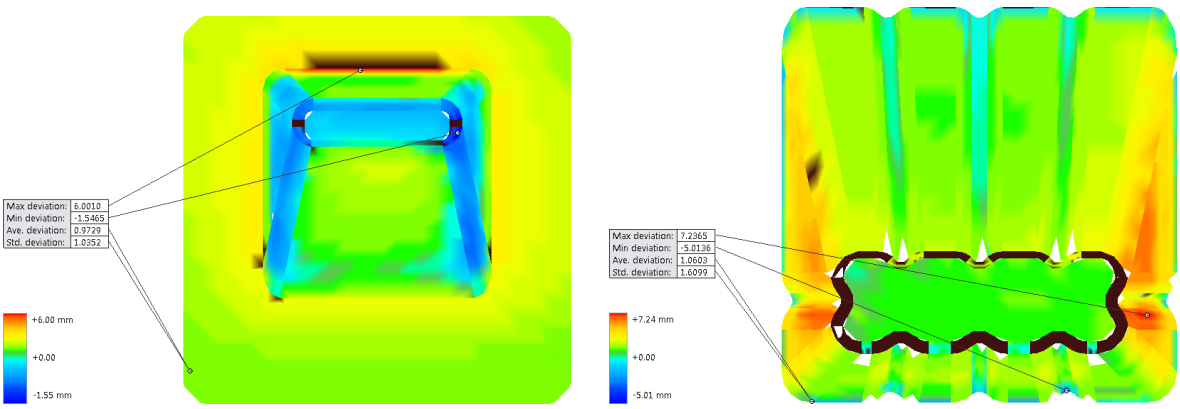

(a) (b)

Figure 6.66: Sheet metal cork compression mould dimensional measurement results: (a) core side (b) cavity side

6.4.4 Mould operation

The mould operation is performed in two stages. In the first test, only the mould essential parts are used and the mould clamping is performed using screws and nets between the mould cavity and the core blank planes. In the second test, the complete mould is used, performing the compression on a hydraulic press before locking the mould. In both test a silicone base release agent is used in both mould sides. A 9:1 weight ratio is used for the cork granules and PU resin mixture. The mixture adds water for moister activated binder curing and the curing is performed with the closed mould in a oven.

The first mould operation test is performed in between the mould manufacturing for preliminary validation. Figure 6.67 present the preparatory cork compression moulding test, using only the two main sheet metal parts. In this test, the cork mixture uncompressed volume is limited to the cavity side of the mould. Thus, a small compression ratio of 1.22 is implied. The moulding force is quite low, being applied manually. No deformation is visible on neither side of the mould. The closed mould is cured in a oven for two hours at 140°C. During the mould opening, is hard to cause no damage to the moulded part due to the lack of density. Besides, the cork mixture fails to aggregate in all filled volume. Nevertheless, the mould suffers no damage and the material releases with easy from the aluminium surface.

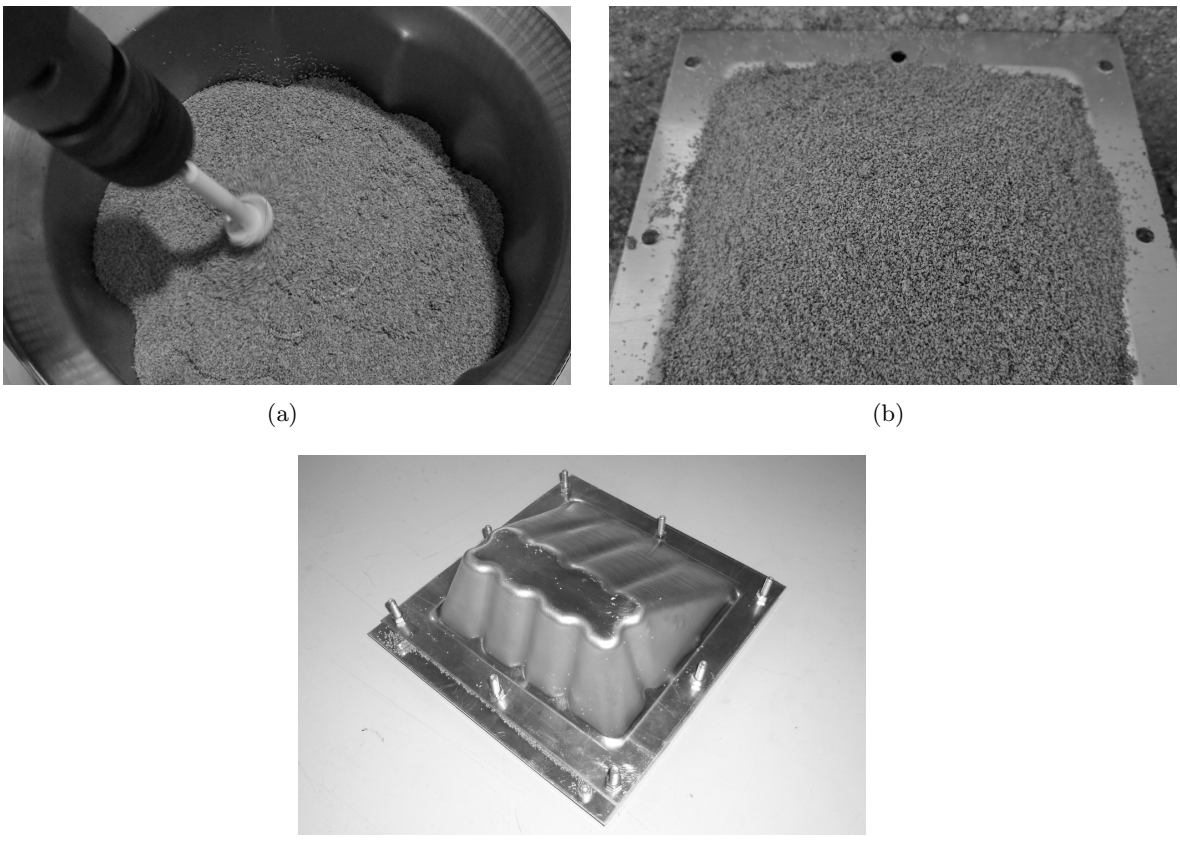

(a) (b)

(c)

Figure 6.67: Cork compression moulding with simplified SPIF sheet metal mould: (a) cork mixture preparation; (b) cork mixture inside mould cavity; (c) closed mould

On a second cork compression moulding approach, the compete mould is used. Aiming for a 180 kg/m^3, the part weight is 167 g. Considering a 9:1 weight ratio, the cork composite mixture uses 150 g of cork powder and 17 g of bounding resin. In order to add some moisture to the powder mixture, 10 g of water are added.

A silicone based demoulding agent is used and demoulding paper pieces are positioned in plannable areas to help the part release. The cork mixture is added to the mould cavity with the frame box extension, filling it to approximately 30 mm height. The core sheet metal part is placed on top of the mould and pressed in a 15 tones manual hydraulic press. During the compression operation, the maximum applied force reach close to 500 kg.f corresponding to a moulding pressure of 0.15 MPa when considering the 180×180 mm projected area. No visible deformation is noticeable during the moulding operation. During the mould compression, a small amount of material is lost by the side locking holes. Yet the amount can be despised when compared with the moulding material volume. The mould is locked while under pressure using the side screws. The frame box support the closed mould without core part slide during the press force release. The closed mould is removed from the press and cured on an oven for two hours with a temperature set for 140°C with maximum peak of 150°C. Figure 6.68 present the four major steps along the cork compression moulding operation.

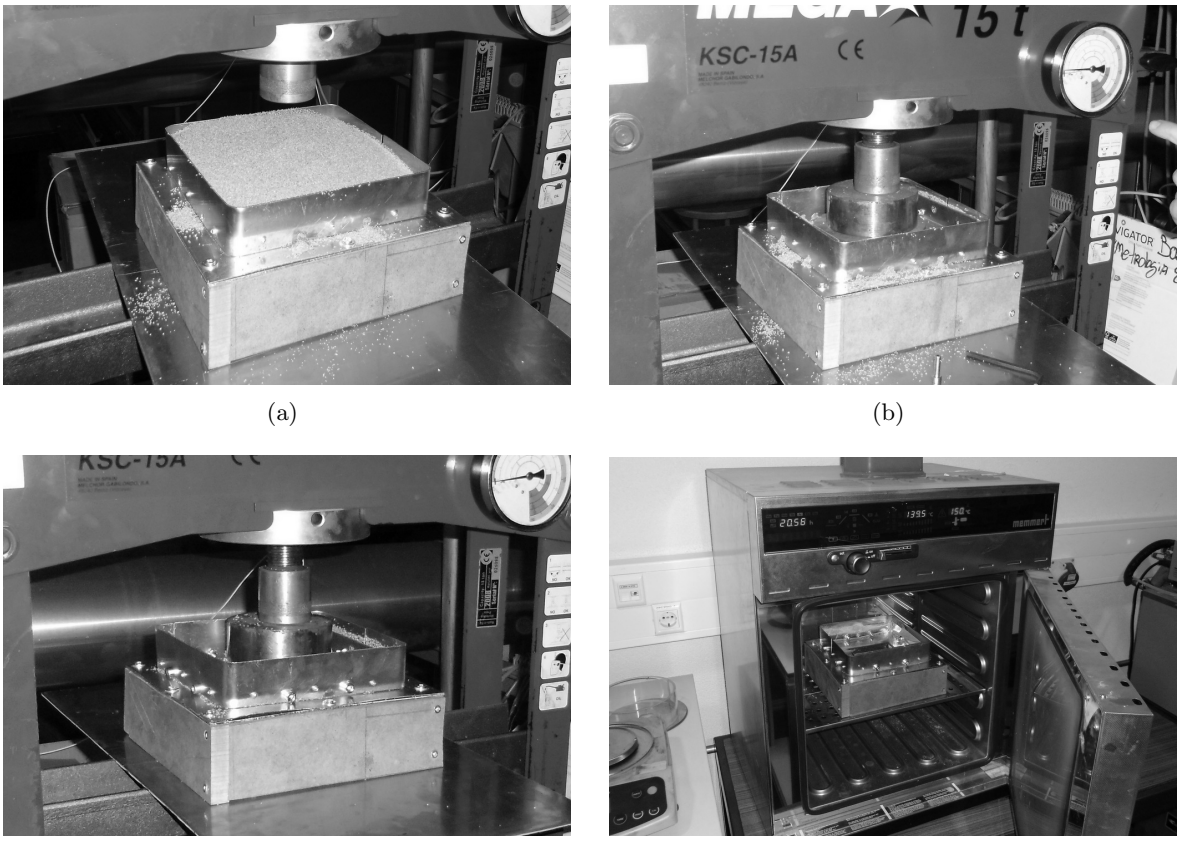

(a) (b)

(c) (d)

Figure 6.68: Cork compression moulding with complete SPIF sheet metal mould: (a) cork mixture inside mould cavity and frame box extension; (b) mould under pressure; (c) locked mould after pressure release; (d) closed mould inside oven

The moulded part releases with ease from the mould due to the use of the demoulding paper. Nevertheless, some wrinkles are formed in the paper during the compression moulding than harm the part surface. Hovever, the use of the silicone demoulding agent alone proof to be insufficient for the cork compression moulding operation with the compression ratio of 1:2, causing damage at the part surface during demoulding operation.

After operation, the mould parts are measured to check for permanent deformation. The core side of the mould suffers a permanent deformation close to 3.5 mm at the centre of the edge more far from the core feature. Besides, a mark from the pressure distribution plate of the press in noticeable at the part. The cavity side is deformed by 4.0 mm at the centre of the lower slope wall. All remaining walls suffer no permanent deformation.

6.4.5 Compression moulding parts validation

For the part evaluation, a first visual inspection is performed. The evaluation assesses the mould filling, part apparent density and general part quality.

In what concerns the preliminary tests using the simplified mould, the results are unsatisfactory. Figure 6.69 present the demoulded part. Due to the lack of material caused by the low compression ratio, the cork mixture fails to agglomerate in all the mould volume. Furthermore, the extreme low density leads to an extreme fragile part due to insufficient cork particle aggregation. Still, the part overall geometry is achieved and the part surface quality in the well defined areas is good.

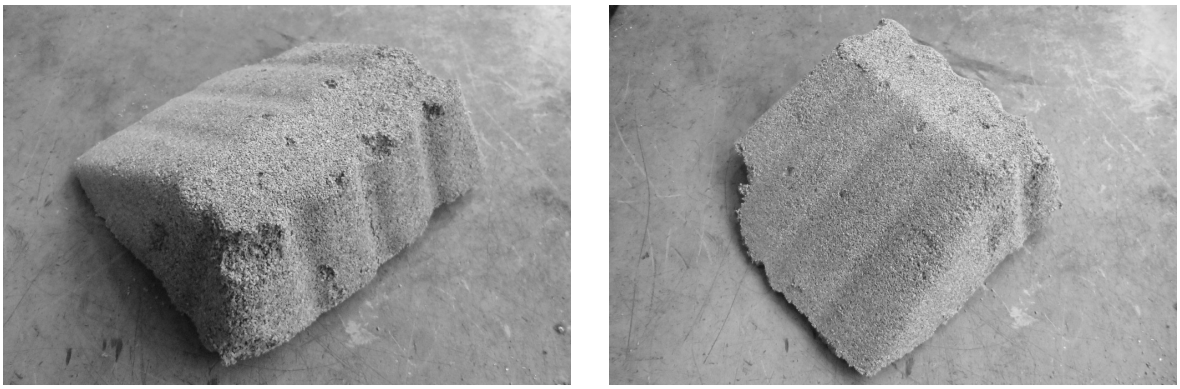

(a) (b)

Figure 6.69: Simplified mould cork compression moulding part

The use of the complete part leads to considerable better results. Figure 6.70 present the demoulded part after cleaning the disperse cork particles. The part success to define the overall geometry definition, with only minor failures at the sharp edges, small defects due to wrinkles in the demoulding paper at the bottom side of the part and some high concentration binder spots noticeable at surface. Nevertheless, the surface quality is good and cork granulated congregate apparent distribution is uniform.

The part is weight for density evaluation. The total part weight is 166 g, resulting on and effective global density of 180 kg/m^3. During the moulding process the material lost is negligible. A manual compression of the part surface suggest an uniform material behaviour, an so a uniform material density.

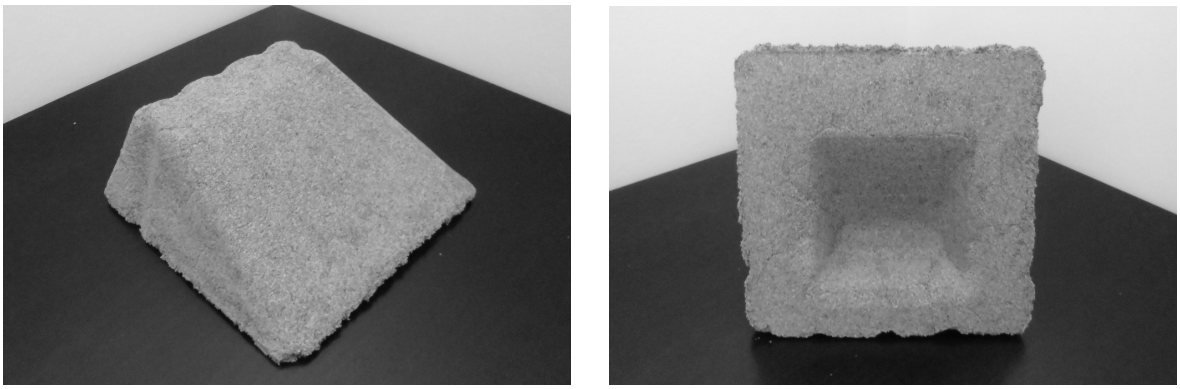

(a) (b)

Figure 6.70: Complete mould cork compression moulding part

The part is measured for accuracy evaluation. Despite some significant deviations, the cork part is moulded with an average deviation of -0.4 mm. However, the largest deviation along the part surface goes up to 6.3 mm at the centre of the lower slope wall, due to the mould deformation. A biggest deviation is found at the lower edges with the real part -13 mm smaller than the CAD model. This large value is partly due to the failure in defining the part bottom edge.

6.4.6 Conclusion

The use of sheet metal moulds for cork compression moulding operation is validated. Some relevant issues are found at the moulded parts. Nevertheless, some of these problems, particularly the binder spots and the wrinkle marks result from the compression moulding operation and not to the mould itself. Only the miss definition of the part edge is affected by the mould, due to the considerable gap between the frame box and the core side. Even so, the use of sheet metal moulds is an attractive solution for compression moulding of cork or other powder and binder based composites, mainly when the production volume requires low cost tooling.

The mould fabrication has reduced time and cost, and has the potential to achieve relatively complex parts. The inclusion of sheet metal parts with other parts increases the geometry limits and, in specific situations, lead to a faster mould development and lower tooling cost.

From the mechanical point of view, the 2 mm sheet metal alone is sufficiently rigid although not tough enough to support the moulding loads, leading to permanent deformation. On the core side of the mould, the permanent deformation result from an uneven pressure distribution. The addition of a correct size pressure plate could eliminate this issue. On the cavity side, the deformation dues to the geometry itself. The mechanical behavior could be improved by either use a thicker sheet or by adding a filling support by using sand or other porous mixture.

Apart from the defects that result from the mould deformation and oversized gap between the core and the frame box and operation issues, the part quality is good. The unaffected surfaces have an accuracy of ± 2 mm and a good surface finishing. The punch marks on the sheet metal surface are not visible on the moulded part.

Chapter 7

Conclusions

In this thesis an overall analysis of the SPIF process and applications is perform, with experimental work being done based on the SPIF-A machine. Enhancement are made to the SPIF process promoting its industrial applicability, case study parts are manufactured for validating its use and new rapid tooling concepts are proposed and proof.

Contributions are made to the SPIF process by proposing new possible part configurations and investigating on the most adequate forming parameters, and by systematise the possible part configurations and design guidelines for the development of parts thought for SPIF. In addition, particular contributions to the development of the SPIF-A machine are set by improving its instrumentation and data analysis, developing an energy consumption model, as well as developing computational tools for the use of commercial CAM software.

The development of case study analysis test the use of SPIF in different fields of application, dealing with parts representative of the possible configurations. The formed parts are finished and evaluated and, when necessary, the forming process is improved to meet the design requirements.

Finally, SPIF sheet metal moulds are designed and developed for multiple manufacturing technologies, validating its use for processing thermoplastics and composite materials. Moulds are design to have minimum demand on additional materials besides the formed sheet metal, and requiring minimum finishing or side operations. Thus, SPIF process is validated as a direct rapid tooling process. Besides validating its use, the mould cost and performance are evaluated and, when possible, compared to conventional tooling development processes.

The research work provides considerable improvements to the SPIF industrialisation, achieving the intended contribution to the technology readiness level. The contributions made to the SPIF process succeed to cement the TRL4 index, providing new possible features to the technology and validating them in lab. Along the development of the case studies, despite the use of laboratory installations, industrial like considerations were followed, advancing the TRL index to a potential level 5. The rapid tooling proposal was validated, bringing new concept ideas to a TRL3 level. In such a way, despite not leading to any applied true industrial installation, the goals are considered to be fulfilled. Different principles of application are validated for SPIF proofing the viability of using ISF for the manufacture of end products or other technical parts. The achievable part accuracy and surface finishing, as well as the attainable part mechanical properties, are inferior than other forming processes. Yet, the obtainable part quality is accordant with many product requirements and the tooling cost, material cost, energetic cost and process time are very competitive.

In what considers an energetic study of the SPIF process, an investigation is made by analysing the SPIF-A machine. Being hydraulically actuated with a fix displacement pump, the energy consumption is mainly dependent on the process time, increasing in a almost proportional way. Forming force insignificant influence on the energy consumption. Thus, higher feed rates and forming steps lead to quicker forming processes and consequently less energy dependent. In most cases, the forming parameters selection should privilege achievable part quality rather than energy consumption. Other ISF hardware may have different energy consumption models since alternative power sources lead to a more force dependant behaviour. A theoretical energy consumption model is defined. An internal report with the energy consumption conclusion and all collected experimental data has been written with the title "Spif energy consumption - experimental evaluation of single point incremental forming consumption on the SPIF-A machine" [134]. Along with the energy analysis, the SPIF-A machine data logging and data analysis has been improved.

A relevant contribution to the SPIF process improvement is the possibility of forming tunnel type parts. This new approach uses a semi constrained blank, increasing the capability of adapting to channel parts while increasing the possible useful work volume, decrease material consumption and minimising side operations. Tunnel and semi tunnels are feasible with similar free form liberty as container part, although the forming limits are lower. The results of the tunnel incremental forming study have been submitted and accepted to be presented at the International Conference on Sheet Metal - SheMet conference, 10 to 12 April 2017, with the title "Incremental forming of tunnel type parts" and published in the Procedia Engineering journal [164].

SPIF is now a viable process for sheet material forming. Major applications of the process are the prototyping of sheet metal parts, the fabrication of unique parts or small batches, the fabrication of old parts replacements and some rapid tooling operations. For the selection of SPIF process to form a part, it is important to study the feasibility of the shape design, as well as understand the accuracy and surface finish reachable by ISF. The proposed extended design guidelines, as well as the definition of possible part configurations and proposal of a modeling method are key tools for the SPIF leveraging and dissemination. The bibliographic review, as well as the fulfilment of some experimental test lead to a systematic understand on the SPIF possibilities and limitations. With this information as background, a proposal for the possible part configuration types as well as a list of design guidelines for SPIF has been defined. This information is considered structural both for the definition of geometries for benchmark parts for scientific tests and as an orientation for applied works.

Six different possible part configurations are identified. Apart from the conventional single container type parts and new proposed tunnel and semi tunnel parts, part configuration may include curvature changes leading to island type parts, flanged faces, preformed or postformed parts and traced features. Different configurations may be included in one part. In what concerns design guidelines, apart from the well stated maximum forming angle and part size, orientations refer to possible feature size, radii, changes in curvature and designs to improve part quality.

The work on Design Guidelines and part configuration types has been synthesised in a paper format and presented in the Sustainable Smart Manufacturing Conference, 20 to 22 October 2016 with the title "Defining Design Guidelines for Single Point Incremental Forming - Rules to a good design of container and tunnel like parts manufactured by incremental forming" and published in the Challenges for Technology Innovation: An Agenda for the Future book [165]. A more extensive paper including not only the part design guidelines and possible

part configurations but also key notes on the process assessment has been published on The International Journal of Advanced Manufacturing Technology with the title "Integration of Design Rules and Process Modelling within SPIF technology - a review - On the industrial dissemination of Single Point Incremental Forming" [166]. An internal report has been writen with information about practical applicability of SPIF using the SPIF-A machine to support future work with the name "SPIF CAD CAM - Manual for preparing SPIF tool paths using PowerMill - Post-processing for the SPIF-A machine" [123].

Sheet metal parts have been designed and manufactured using SPIF. Parts have been selected to answer to different industrial fields requirements, using different materials and being formed with different part configuration. Parts are manufactured and validated. Apart from validating the use SPIF for the manufacture of industrial parts, the applied work includes the development of simpler tools and techniques to improve the achievable part quality.

A abstract of a case study paper on product design and development thought for SPIF has been submitted to the 1st MTD Conference - Meaningful Technology and Design, 20 to 21 July 2017, with the title "Single Point Incremental Forming, Product Design by Process" [167] although the conference has been cancelled.

A poster with the case studies on design and architecture parts has been presented in the Ciência 2017 - Encontro com a Ciência e Tecnologia em Portugal with the title "Case studies on industrial applicability of single point incremental forming" [168].

In what concerns the contributions made to the use of SPIF as a rapid tooling process, sheet metal moulds were designed and validates for thermoforming operations, composite hand layup, rotomoulding and rotocasting. Sheet metal molds made by SPIF are a reliable alternative to the conventional molds. Despite some significant deviations still occur at some points, general appearance of plastic or composite parts is reasonably good and average dimension is accurate. Mould manufacture time and cost are low yet largely influenced by some parallel operations. As accessories like backing plates for SPIF operation can be used for more then one mould part with similar projected area, the use of sheet metal moulds assumes even a more interesting panorama.

Sheet metal moulds have reasonable strength capacity due to the combination of the material properties and the typical surface geometry. In addition, in the processes that deal with heat, a low thermal inertia allows a fast heat up and cool down.

In a mechanical point of view, the mould strength depends mostly on the sheet thickness and the mould size. Since most processes deal with distributed pressure allover the moulding surface, the mould size has huge influence on the load support capacity. Two approaches can be followed in the mould design to allow a feasible operation. The sheet thickness can be sized to support the moulding pressure. However, this can lead to oversize, difficult to form thicknesses. An alternative approach is to use reinforcements. This option, using either ribs or other support structures or a full filling allow a great increase of the mould toughness at the cost of a more complex mould manufacture process or assembly.

In a thermal point of view, the thickness differences caused by thinning during the forming operation lead an uneven thermal distribution. Still, the thickness differences influence on the heat or cool down time is compatible with thermoplastics processing. The thermal gradient is minimised due to the thermal conduction along the sheet. The behaviour can be improved by adding isolation to the thinner walls or by applying heat sinks on the thicker areas.

The designed moulds for validating the rapid tooling concept are manufactured exclusively by SPIF in single part moulds. The mould thickness is sized to deal with the moulding forces without the use of reinforcements or inner filling. The SPIF-A machine has high strength

capacity that allow to form thick sheets leading to simpler moulds. The experimental work is performed on a simple benchmark part for proof of concept. The combination of SPIF with other technologies for the development of more complex mould assembly have greater potential in both the allowable geometry and the achievable results.

The use of SPIF as a direct rapid tooling process is validated by pilot operation in laboratory installations. Both industrial equipment and simpler purpose built systems are used for the mould operation. For each of the refereed technologies some parts are manufactured and evaluated. All developed moulds manage to produce decent quality parts, with an accuracy closer to the typically achieved with conventional moulds despite a poorer surface quality.

The achievable accuracy during the mould manufacture through SPIF goes down to ± 1 mm and adds to the thermoplastic and thermoset processing accuracy. The result is compatible with most parts processed by low pressure manufacture processes, mainly during a preliminary evaluation stage. The surface quality attain during SPIF has fair roughness but has typically scratch marks due to material skinning on tool contact. These marks turn to be the biggest set back in the use of SPIF sheet metal moulds. Finishing operations can be used to improve surface quality.

A alternative method for improving accuracy and surface quality has been proposed by adding epoxy mass to the moulding surface. The filling up mass can improve the inaccuracies of the SPIF process, particularly the undesired top radius between the forming cavity and the flat blank. A full converge of the moulding surface, together with manual sanding or even automated finishing processes or milling could lead to great geometrical results, competitive to conventional processes. The application of the epoxy mass is compatible with both mould strength and service temperature. The mass application must avoid the formation of large volumes since they can lead to cold spots that have negative influence on the moulding process and finished parts.

In a global point of view, it is considered that the rapid tooling applications with SPIF moulds are viable, mainly for the manufacture of evaluation parts and initial production batches. The use of SPIF for the production of rotational moulding moulds has great industrial potential, both for rotomoulding or rotocasting. The association of SPIF to other forming processes and welding can be very beneficial the plastics industry, allowing more flexible design in sheet metal moulds. In what concerns composite material manual processes, SPIF moulds also have great applicability both in stand alone applications and in combination with other materials. The thermoforming operations with SPIF sheet metal moulds is the least promising process, since the achievable geometries impose greater limitations to the typical part designs. Still, the operation is feasible and the moulds are a fast an inexpensive alternative to conventional process for simpler parts.

The proof of concept work on the development of sheet metal moulds by SPIF for thermoforming operations has been presented and published as a paper at the 19th ESAFORM Conference, 27 to 29 April 2016 with the title "Testing single point incremental forming molds for thermoforming operations" [169] and presented on the Research Trends in Mechanical Engineering 2016 Conference, 11 to 13 July 2016 with the title "Developing Low Cost Time Saving Molds for Thermoforming Operations" [170].

The work on the development of theet metal moulds by SPIF for rotomoulding and rotocasting operations has been submited as a paper to the 20th ESAFORM Conference, 26 to 26 April 2017, with the title "Testing Single Point Incremental Forming Moulds For Rotomoulding Operations" [171].

As a final conclusion, it is considered that the SPIF process is at an industry ready

stage, granting a feasible and consistent results. During the research work, tools to grant good manufactured parts have been detailed, being considered a satisfactory contribution to the process application and dissemination. Conventional uses have been validated and new applications developed, contributing to the technology potential growth.

7.1 Future work

Aiming for a continuous improvement of the ISF process performance and applicability, some future work is proposed. Aside from the proposed outlines, it is suggested to continue using SPIF and other ISF process in industrial parts.

In order to give continuity to the process research work, it is suggested to enlarge the energetic analysis to other hardware capable of performing SPIF operations and develop a generalised energy consumption model. This analysis could be use to contribute to a more accurate process cost model.

The most significant future work proposed follows the SPIF rapid tooling application field. In this line of action, it suggested to work on the development of techniques to improve the achievable mould quality when using SPIF for rapid tooling operations. In addition, it is proposed to analyse the formed sheet metal mould ware and determine expected life. Final suggestion consist on the development of case study applications with the use SPIF sheet metal moulds for the production of industrial parts.

Appendix A

CAD/CAM for the SPIF-A

A.1 Post Processor Details

1. Option File Settings
1.1. Information
1.1.1. General

Option File	SPIF-A
Delcam PostProcessor Version	6.8.4
Machine Tool Manufacturer	SPIF-A
Machine Tool Model	V1
Controller Manufacturer	MatLab
Controller Series	XPCTarget
Customer	UA
Notes	Daniel Afonso Dan@ua.pt

1.2. Program Generation
1.2.1. General

NC Program Tolerance	Use CLDATA Tolerance
Output Linear Units	Metric
Output Angular Units	Degrees
Output File Extension	nc

1.2.3. Arcs And Splines

arc support		
Plane	3axis	3+2
XY	Off	Off
XZ	Off	Off
YZ	Off	Off

1.2.4. Multi-axis

Euler Angles Style	Winding and Unwinding
Linearise Multi-Axis Moves	No
Reset Axes	Before Pure 3 Axis
Use Constant Surface Speed	No
Calculation Method	Euler
Ignore Toolpath Workplane Shift	No
Euler Convention	XYZ Static (default)
Adjustment Move For Axial Reset	No

1.3. Machine Kinematics

Type	5-Axis Head Head

Axis	Type	Vector	Limits
Machine X	Linear axis	-1 0 0	-400 400
Machine Y	Linear axis	0 -1 0	-400 400
Machine Z	Linear axis	0 0 1	-400 0
Machine B	Rotary axis	0 1 0	-45 45
Machine C	Rotary axis	1 0 0	-45 45

1.4. Format

1.4.1. General

Duration Format	hh 'H -' mm 'M -' ss 'S'
Decimal Separator	.
Exponent String	e
Text Case	Not Changed

1.4.2. Blocks

Output Block Number	Yes
Number Of Start Block	111
Maximum Block Number	Unlimited
Block Increment	1

1.4.3. NC Comments

Enable NC Comments	Yes
Comment Start	;
Comment End	
Enable Multiline Comments	No
Comment Text Case	Not Changed

2. Commands

Name	State	Preview
Program Start	Active	% Program made for SPIF-A % Program: % Author: dan % Date:17.06.2016 % Units: MM % Tool type: % Tool Diameter: 0.0 % Tool Tip Radius: 0.0 % Tool Lenght: 0.0
Toolpath Start	Inactive	
Toolpath End	Active	
Program End	Active	N111 M30
Move		
First Move After Toolchange	Active	
Motion Mode Change	Active	
Move Linear	Active	N111 G1 X0 Y0 Z0
Move Rapid	Active	N111 G1 X0 Y0 Z0
Tool		
Load Tool	Inactive	
User Commands		
First_Move_3AX	Active	N111 G1 X0 Y0 N112 G1 Z0
Move_3AX	Active	N111 G1 X0 Y0 Z0
Move_3P2	Active	N111 N111 G1 X0 Y0 Z0 B0 C0
Move_5AX	Active	N111 N111 G1 X0 Y0 Z0 B0 C0

3. Parameters
3.1. Standard

Name	Type	Units	State	Value
Program				
CAM System Name	String	Undefined		
Input Linear Units	Group		MM INCH	MM INCH
NC Program Name	String	Undefined		
Program X Max	Real	Linear		
Program X Min	Real	Linear		
Program Y Max	Real	Linear		
Program Y Min	Real	Linear		
Program Z Max	Real	Linear		
Program Z Min	Real	Linear		
Safe Z	Real	Linear		
Controller Switches				
Motion Mode	Group		CCW CW LIN RAP	G3 G2 G1 G1
Move				
Toolpath Axis Mode	Group		3+2 3AXIS 5AXIS	
X	Real	Linear		
Y	Real	Linear		
Z	Real	Linear		
Euler A	Real	Angular		
Euler B	Real	Angular		
Euler C	Real	Angular		
Tool				
Tool Diameter	Real	Linear		
Tool Tip Radius	Real	Linear		
Tool Length	Real	Linear		
Tool Overhang	Real	Linear		
Tool Type	String	Undefined		
Tool Name	String	Undefined		
Workplane				
Workplane Euler A	Real	Angular		
Workplane Euler B	Real	Angular		
Workplane Euler C	Real	Angular		

Appendix B

Measure and calculus scripts

B.1 Script to calculate consumption and generate power over time graphics

```
clc
close
//Title
%title = "Energy consumption measurement";
L = 4; //number of measuring lines: 1, 3 or 4

//read data logger file and remove headers and comments
M = csvRead("dat00001.csv", ",", [], 'string');
M = M(2:size(M,1),2:(2+L));

//reading current values
data = strtod(M(:,2:(L+1)));

//reading time
time = strstr(M(:,1)," ");
time = strsubst(time,":"," ");
for i=1:size(time,1)
    t(i,:)=tokens(time(i,1))';
end
clear i
t = strtod(t);
time=t(:,1)*60*60+t(:,2)*60+t(:,3);
time=time-time(1);
clear t

//total time calculation
duration = time(size(time,1))-time(1);
if round(duration-60*fix(duration/60))<10
    duration = strcat(["Total duration: ", string(fix(duration/60)),
":0",string(round(duration-60*fix(duration/60)))]);
```

```
else
    duration = strcat(["Total duration: ", string(fix(duration/60)),
":",string(round(duration-60*fix(duration/60)))]);
end
disp(duration)

//current and power calculation
if  L==4 then
    amp(:,1) = data (:,1)*50/0.625;
    amp(:,2:4) = data (:,2:4)*100/0.625;
elseif L==3
    amp = data*100/0.625;
else
    amp = data*50/0.625;
end
power = amp*230/1000;

//consumption calculation
if  L==4 then
    C1=intsplin(time,power(:,1))/(60*60);
    C2=intsplin(time,power(:,2))/(60*60);
    C3=intsplin(time,power(:,3))/(60*60);
    C4=intsplin(time,power(:,4))/(60*60);
    C=C1+C2+C3+C4;
elseif L==3
    C1=intsplin(time,power(:,1))/(60*60);
    C2=intsplin(time,power(:,2))/(60*60);
    C3=intsplin(time,power(:,3))/(60*60);
    C=C1+C2+C3;
else
    C=intsplin(time,power(:,1))/(60*60);
end
consumption = strcat(["Total consumption: "
                                    ,string(round(C*100)/100),"kW.h"]);
disp(consumption)

//plot display
plot(time/60,power(:,:))
axis=get("current_axes");
axis.data_bounds=[0,0;max(time/60),(max(max(power)))];
line=gce();
if L==4 then
    captions(line.children,['L';'L1';'L2';'L3']);
elseif L==3
    captions(line.children,['L1';'L2';'L3']);
else
    captions(line.children,['L1'])
```

```
end
xlabel("time (min)", "fontsize", 2);
ylabel("instant power (kW)", "fontsize", 2);
title(%title, "fontsize", 3);
xstring(0,0.90*(max(max(power))),duration);
xstring(0,0.85*(max(max(power))),consumption);
```

B.2 Script to compute force and generate forming power over time graphics

```
clc
close
//Title
%title = "Force measuring test";
disp(%title);

//read data file from matlab:
//t: time | FC: force | FK: XYZABC | VelR: feedrate
loadmatfile('dat00001.mat');
time = t; clear t;

//filter applied on feedrate and force measure data
n = 100;     num = ones(1,n)*(1/n);    den=1;

//total time calculation
time=time-time(1);
duration = time(size(time,1));
if round(duration-60*fix(duration/60))<10
    duration = strcat(["Total duration: ", string(fix(duration/60)),
":0",string(round(duration-60*fix(duration/60)))]);
else
    duration = strcat(["Total duration: ", string(fix(duration/60)),
":",string(round(duration-60*fix(duration/60)))]);
end
disp(duration)

//feed rate components calculation
FK(:,1)=FK(:,1)-mean(FK( FK(:,3)<=0  ,1));
FK(:,2)=FK(:,2)-mean(FK( FK(:,3)<=0  ,2));
vX=(diff(FK(:,1))./diff(time))*60; vX(size(vX,1)+1)=vX(size(vX,1));
vY=(diff(FK(:,2))./diff(time))*60; vY(size(vY,1)+1)=vY(size(vY,1));
vZ=(diff(FK(:,3))./diff(time))*60; vZ(size(vZ,1)+1)=vZ(size(vZ,1));
vZ(1:size(vZ,1)-round(n/2)+1)
                        = filter(num,den,vZ(round(n/2):size(vZ,1)));
vT = sqrt(vX.^2+vY.^2);
vT(1:size(vT,1)-round(n/2)+1)
                        = filter(num,den,vT(round(n/2):size(vT,1)));
feed = strcat(["Average feed rate:
tangential:", string(round(mean(vT(vT>100))*10)/10)," mm/min
vertical:", string(round(mean(abs(vZ(vT>100)))*10)/10)," mm/min"]);
disp(feed);
```

```
//force filter
FC(:,1) = FC(:,1) - mean(FC(1:10,1));
FC(:,2) = FC(:,2) - mean(FC(1:10,2));
FC(:,2) = FC(:,2)*(mean(abs(FC(:,1)))/mean(abs(FC(:,2))));
FC(:,3) = FC(:,3) - mean(FC(1:10,3));
FC(:,5) = sqrt(FC(:,1).^2+FC(:,2).^2);
FC(1:size(FC,1)-round(n/2)+1,4)
                        = filter(num,den,FC(round(n/2):size(FC,1),3));
FC(1:size(FC,1)-round(n/2)+1,5)
                        = filter(num,den,FC(round(n/2):size(FC,1),5));
FC(:,6) = abs(FC(:,5).*sind(atand(FC(:,2)./FC(:,1))
                        + atand(FK(:,2)./FK(:,1))));
FC(1:size(FC,1)-round(n/2)+1,6)
                        = filter(num,den,FC(round(n/2):size(FC,1),6));
force = strcat(["Average force: Fz = ",
string(round(mean(FC(FC(:,4)>(max(FC(:,4)))*0.9,4))*10)/10),
                                    "N Ft = ",
string(round(mean(FC(FC(:,4)>(max(FC(:,4)))*0.9,6))*10)/10),"N"]);
disp(force);

//forming time calculation
ftime = time(FC(:,4)> 10);
ftime = (ftime(size(ftime,1)) - ftime(1));
if round(ftime-60*fix(ftime/60))<10
    ftime = strcat(["Forming time: ",string(fix(ftime/60)),":0",
    string(round(ftime-60*fix(ftime/60)))]);
else
    ftime = strcat(["Forming time: ", string(fix(ftime/60)),":",
    string(round(ftime-60*fix(ftime/60)))]);
end
disp(ftime);

//forming power calculation
powerZ = FC(:,4).*abs(vZ)/(1000*60);
powerT = FC(:,6).*vT/(1000*60);
 power = powerT + powerZ;
fpower = strcat(["Forming power: ",
string(round(mean(power(power>1))*100)/100)," W"]);
disp(fpower);

//forming energy calculation
C = intsplin(time,power(:,1))/(60*60);
consumption = strcat(["Total consumption: ",
string(round(C*100)/100)," W.h"]);
disp(consumption)
```

```
//tool path plot display
scf;
param3d(FK(:,1),FK(:,2),FK(:,3));
title(strcat(["Toll path: ",%title]), "fontsize", 3);

//feed rate components plot display
scf;
plot(time/60,[vZ vT]);
line=gce();
captions(line.children,['Vz';'Vt']);
xlabel("time (min)", "fontsize", 2);
ylabel("feed rate (mm/min)", "fontsize", 2);
title(strcat(["Feed rate: ",%title]), "fontsize", 3);

//force plot display
scf;
plot(time/60,FC);
axis=get("current_axes");
axis.data_bounds=[0,min(FC);max(time/60),max(FC(:,1:3))];
line=gce();
captions(line.children,['Fx';'Fy';'Fz';'Filtered Fz';
'Filtered |Fxy|';'Filtered |Ft|']);
xlabel("time (min)", "fontsize", 2);
ylabel("Forming force (N)", "fontsize", 2);
title(strcat(["Forming force: ",%title]), "fontsize", 3);

//forming power plot display
scf;
plot(time/60,power(:,:))
axis=get("current_axes");
axis.data_bounds=[0,0;max(time/60),(max(max(power)))];
line=gce();
captions(line.children,['Power'])
xlabel("time (min)", "fontsize", 2);
ylabel("instant power (W)", "fontsize", 2);
title(strcat(["Forming power: ",%title]), "fontsize", 3);
xstring(0,0.95*(max(max(power))),duration);
xstring(0.018,0.90*(max(max(power))),ftime);
xstring(0,0.85*(max(max(power))),consumption);
```

B.3 Script to calculate energetic efficiency prediction

```
clc
close
deltaZ = [0.1  0.5  1.0];        //mm
feedrate = [1000  3000  5000]; //mm/min
t0 = [0  1  2  3];                //mm
dtool = 12;      //mm
sigma_u = 105; //MPa
alpha = 45;      //°
time = [15  5  2
         7  2  1
         4  1  0.5];              //min
a = -1; b = dtool; c = -((deltaZ)/(2*sind(alpha))).^2;
deltaH = (-b+sqrt(b^2-4*a*c))/(2*a);   //mm

n=0
for i = 1:4
    for j = 1:3
        for k = 1:3
          n=n+1;
          Fz = 0.0716*sigma_u*(t0(i)^1.57)*(dtool^0.41)*
(deltaH(j)^0.09)*alpha*sind(alpha);
          beta = asind(deltaZ(j) / (dtool * sind(alpha)));
          Fr = Fz*tand((alpha + beta + 17.2*((dtool/10 )^(-2.54)))/2);
          Ft = Fr*(360*(alpha^(-1.23))*(dtool^(-0.62)));
          w = Ft*feedrate(k)/(1000*60) + Fz*(20/time(j,k))/(1000*60);
          W = w * time(j,k)/60;
          C = 15 * 0.7 * time(j,k)/60;
          u = (W/(C*1000))*1000;
          disp(strcat(["test",string(n)]))
          disp(strcat(["deltaZ = ",string(deltaZ(j)),"mm",
                              "t0 = ",string(t0(i)),"mm",
                    "feedrate = ",string(feedrate(k)),"mm/min",
                        "time = ",string(time(j,k)),"min"]));
          disp(strcat(["force: F_z = ",string(round(Fz)),"N",
                                  "F_r = ",string(round(Fr)),"N",
                                  "F_t = ",string(round(Ft)),"N"]));
          disp(strcat(["form power:",string(round(w*100)/100),"W"
                       "form energy:",string(round(W*100)/100),"W.h"
                "energy consumption:",string(round(C*100)/100),"kW.h"
                         "efficiency:",string(round(u*100)/100),"‰"]));
          disp("--------------------------//--------------------------");
      end
    end
end
```

Appendix C

Modular baking plate drawings

C.1 Modular backing plate for tunnel and semi tunnel tests

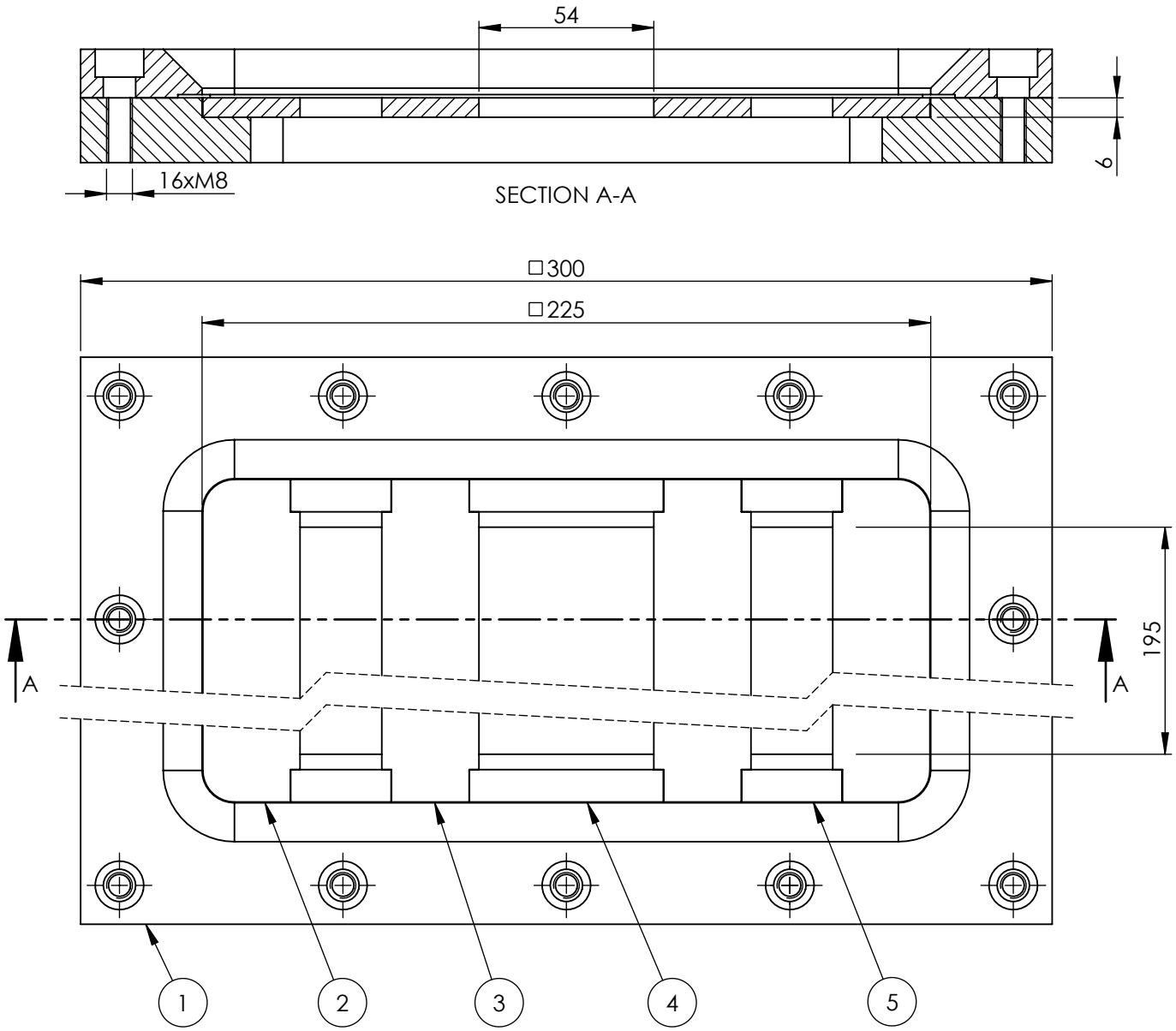

Item	Part	Configuration	Qty.
1	sheet holder		1
2	end bridge		2
3	movable bridge		2
4	central spacer	60, 85, 110	3x2
5	lateral spacer	31, 18.5	2x4

Modular backing plate for tunnel and semi tunnel test, scale 1:2

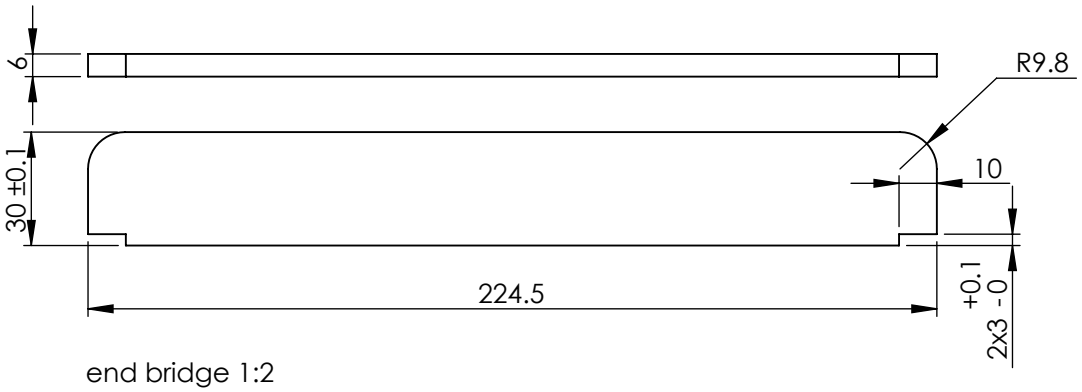

end bridge 1:2

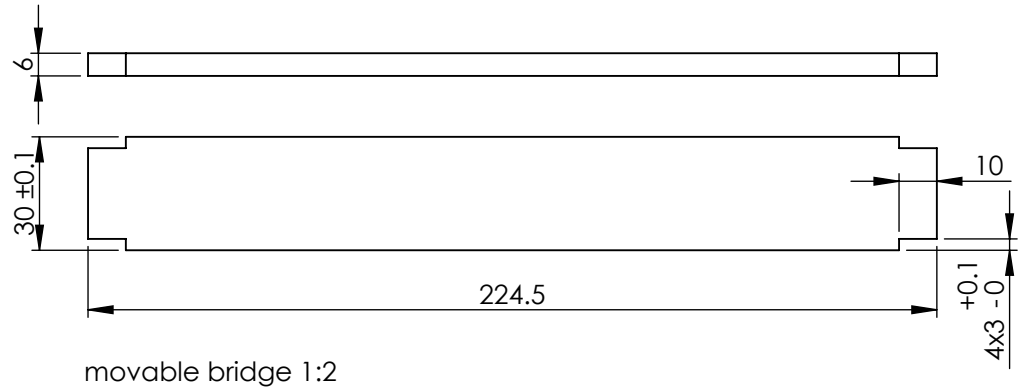

movable bridge 1:2

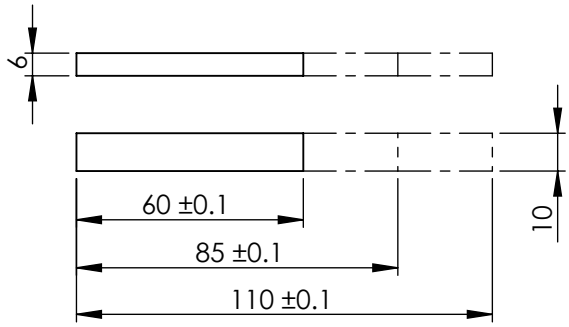

central spacer 1:2

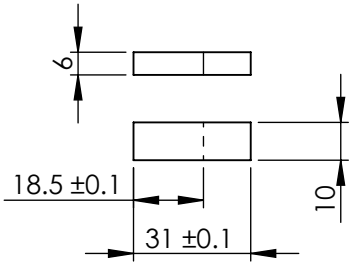

lateral spacer 1:2

Modular backing plate parts for tunnel and semi tunnel test, scale 1:2

Appendix D

SPIF cost model

D.1 Model parameters

```
tools.diameter = [6 10 12 15 20 24];

time.setup = 30; //min (set up time for a different blank size)
time.toolchange = 5; //min
time.program = 15; //min/stage
time.powerup = 0.5; //min
time.zero = 1;
time.clamp = 1.25;          //min/side
time.clampextra = 0.25;     //min/50mm
time.release = 1.0; //min/side
time.clean = 0.5;     //min
time.formingfallowup = 10; //min

energy.powerup = 0.1;   //kW.h
energy.zero = 0.15;     //kW.h
energy.forming = 0.16; //kW.h / min

environment.carboneletric = 0.144; //kgCO2/kW.h
environment.carbonoil = 0.5/100; //kgCO2/cc
environment.carbonmachine = 0.5*400/9000; //kgCO2/min
environment.carbonmaterial = 10; //kgCO2/kg

cost.labour = 50; //euro/h
cost.machine = 40; //euro/h
cost.energy = 0.0999; //euro/kW.h
cost.environment = 25/1000; //euro/kgCO2
```

D.2 Cost model

variables geometry, material and parts are read and defined from the input data.

```
//vertical step down
if (parts.accuracy==1) then
    tool.backinplate = 1;
    toolpath.finishing = 1;
elseif (parts.accuracy==2) then
    tool.backinplate = 1;
    toolpath.finishing = 0;
else
    tool.backinplate = 0;
    toolpath.finishing = 0;
end

if (parts.finishing==1) then
    toolpath.finishing = 1;
    toolpath.finalstepdown = 0.1;
    toolpath.stepdown = 0.5;
elseif (parts.finishing==2) then
    toolpath.stepdown = 0.5;
    toolpath.finalstepdown = 0.5;
else
    toolpath.stepdown = 1;
    toolpath.finalstepdown = 1;
end

if (material.sigmau>=800) then
    toolpath.stepdown = 0.1;
    toolpath.finalstepdown = 0.1;
elseif (material.sigmau>=400 & toolpath.stepdown > 0.5) then
    toolpath.stepdown = 0.5;
    toolpath.finalstepdown = 0.5;
end

//number of forming stages
if (geometry.angle>material.angle) then
   toolpath.stage = 1 + ceil((geometry.angle - material.angle)/5)...
   + toolpath.finishing;
else
   toolpath.stage = 1 + toolpath.finishing;
end

//tool diameter
tool.force = 3.8*material.sigmau;
```

```
tool.number = 1;
tool.min = sqrt((tool.force/35)/%pi)*2;
dmin = tools.diameter-tool.min;
tool.min = dmin(find(dmin==min(dmin(dmin>=0)))) + tool.min;

tool.diameter = (geometry.sideradii-1)*2;
d = tools.diameter-tool.diameter;
tool.diameter = d(find(d==max(d(d<=0)))) + tool.diameter;

if((tool.diameter/2)>=geometry.bottomradii) then
    if[geometry.bottomradii>=(tool.min/2)] then
        tool.diameter = (geometry.bottomradii)*2;
        d = tools.diameter-tool.diameter;
        tool.diameter = d(find(d==max(d(d<=0)))) + tool.diameter;
    else
        tool.radius = floor(geometry.bottomradii);
        if(toolpath.stage == 1) then
            toolpath.stage = 2;
            toolpath.finishing = 1;
        end
        tool.number = 2;
    end
end

if (tool.backinplate == 1) then
    toolmsg = strcat([toolmsg, " + backing plate"]);
end

//Feedrate
toolpath.feedrate = 750+250*(geometry.sideradii-(tool.diameter/2));
toolpath.feedrate(find(toolpath.feedrate>9000)) = 9000;

//Toolpath length
toolpath.avperimeter = round((geometry.area / geometry.depth) ...
- (%pi*tool.diameter));
toolpath.length  = round(toolpath.avperimeter ...
* (geometry.depth / toolpath.stepdown));

if (toolpath.finishing == 0) then
    toolpath.totallength = toolpath.length * toolpath.stage;
else
    toolpath.totallength = (toolpath.length * (toolpath.stage-1))...
    + (round(toolpath.avperimeter ...
    * (geometry.depth / toolpath.finalstepdown)));
end
toolpath.time = toolpath.totallength/toolpath.feedrate;
```

```
//blank size and material cost
material.lenght = ceil(geometry.lenght/100)*100;
if(material.lenght<machine.minlenght) then
    material.lenght = machine.minlenght;
end

if (geometry.config=="Container") then
    material.width = ceil(geometry.width/100)*100;
    if(material.width<machine.minwidth) then
        material.width = machine.minwidth;
    end
elseif(geometry.config=="Tunnel") then
    material.width = geometry.width;
elseif(geometry.config=="Semi_Tunnel") then
    material.width = ceil(geometry.width/50)*50;
else
    material.width = ceil(geometry.width/100)*100;
    if(material.width<machine.minwidth) then
        material.width = machine.minwidth;
    end
end
material.cost = material.cost ...
* material.lenght * material.width * material.thickness;

//process time and energy
if (geometry.config=="Tunnel") then
    process.handlingtime = time.clamp*2 + time.release*2 ...
    + time.clean + (tool.number-1)*time.toolchange;
    if (material.lenght>machine.minlenght) then
        process.handlingtime = process.handlingtime ...
        + 4*time.clampextra * ((material.lenght ...
        - machine.minlenght) / 50);
   end
    process.poweruptime = (time.powerup + time.zero)*tool.number;
    process.energy = (energy.powerup + energy.zero)*tool.number;
elseif (geometry.config=="Semi_Tunnel") then
    process.handlingtime = time.clamp*3 + time.release*3 ...
    + time.clean + (tool.number-1)*time.toolchange;
    if (material.lenght>machine.minlenght) then
        process.handlingtime = process.handlingtime ...
        + 4*time.clampextra * ((material.lenght ...
        - machine.minlenght)/50);
    end
    if (material.width>machine.minwidth) then
        process.handlingtime = process.handlingtime ...
        + 2*time.clampextra * ((material.width ...
        - machine.minwidth)/50);
```

```
    end
    process.poweruptime = (time.powerup + time.zero)*tool.number;
    process.energy =    (energy.powerup + energy.zero)*tool.number;
elseif (geometry.config=="Island") then
    process.handlingtime = time.clamp*8 + time.release*8 ...
    + time.clean*2 + (tool.number-1)*time.toolchange;
    if (material.lenght>machine.minlenght) then
        process.handlingtime = process.handlingtime ...
        + 8*time.clampextra * ((material.lenght ...
        - machine.minlenght)/50);
   end
    if (material.width>machine.minwidth) then
        process.handlingtime = process.handlingtime ...
        + 8*time.clampextra * ((material.width ...
        - machine.minwidth)/50);
    end
    process.poweruptime = (time.powerup*2+time.zero*2)*tool.number;
    process.energy = (energy.powerup*2+energy.zero*2)*tool.number;
else
    process.handlingtime = time.clamp*4 + time.release*4 ...
    + time.clean + (tool.number-1)*time.toolchange;
    if (material.lenght>machine.minlenght) then
        process.handlingtime = process.handlingtime ...
        + 4*time.clampextra * ((material.lenght ...
        - machine.minlenght)/50);
   end
    if (material.width>machine.minwidth) then
        process.handlingtime = process.handlingtime ...
        + 4*time.clampextra * ((material.width ...
        - machine.minwidth)/50);
    end
    process.poweruptime = (time.powerup + time.zero)*tool.number;
    process.energy = (energy.powerup + energy.zero)*tool.number;
end
process.formingtime = toolpath.time;

//process energy
process.energy = process.energy ...
+ process.formingtime*energy.forming;
process.energycost = process.energy * cost.energy;

//process start time and end time
if (material.lenght > machine.minlenght ...
                        | material.width > machine.minwidth)  then
    process.starttime = time.setup + time.toolchange ...
    + time.program*toolpath.stage;
    process.endtime = time.setup;
```

```
else
    process.starttime = time.toolchange+time.program*toolpath.stage;
    process.endtime = 0;
end
process.starttime = process.starttime + process.endtime;

//process cost
process.startcost = cost.labour*(process.starttime)/60;
process.handlingcost = cost.labour*(process.handlingtime)/60;
process.powerupcost =  cost.labour*(process.poweruptime )/60 ...
+ cost.machine*(process.poweruptime )/60;
if (process.formingtime<time.formingfallowup) then
    process.formingcost =  cost.labour*(process.formingtime )/60 ...
    + cost.machine*(process.formingtime )/60;
else
    process.formingcost = cost.labour*(time.formingfallowup)/60 ...
    + cost.machine*(process.formingtime )/60;
end

//tooling cost
process.bakinplatecost = tool.backinplate ...
* (geometry.topperimeter*10/1000 ...
+ (material.width*material.lenght*5*  5*300/125500000));
process.toolwearcost = tool.diameter * tool.force ...
* toolpath.totallength * 1D-10;

//environment
process.co2 = (environment.carboneletric * process.energy) ...
+ (environment.carbonoil * geometry.area / (100*100)) ...
+ (environment.carbonmachine * process.formingtime) ...
+ (environment.carbonmaterial * material.density ...
* material.width * material.lenght * material.thickness);
process.co2cost = process.co2* cost.environment;
```

Appendix E

Rapid tooling drawings

E.1 Thermoforming mould drawings

ITEM NO.	PART NUMBER	QTY.
1	mould core	1
2	support	1
3	ST4.2x16 screw	4

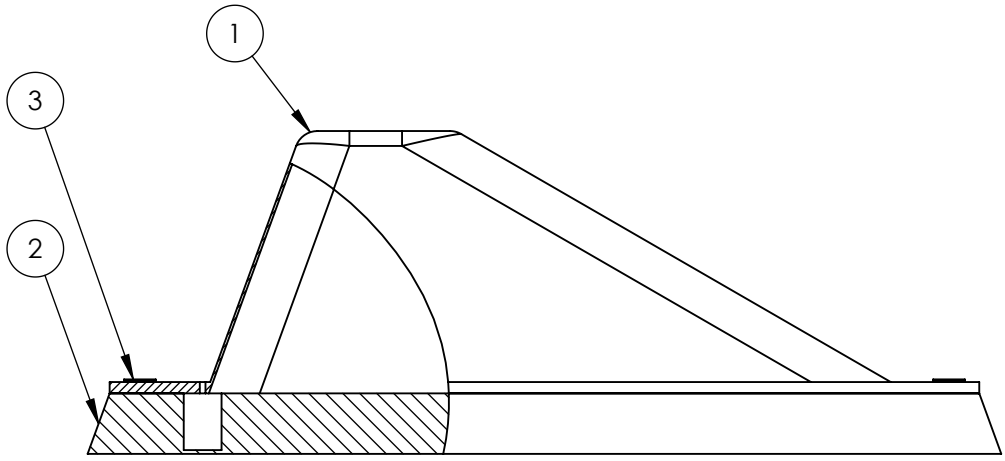

SPIF thermoforming positive mould, scale 1:2

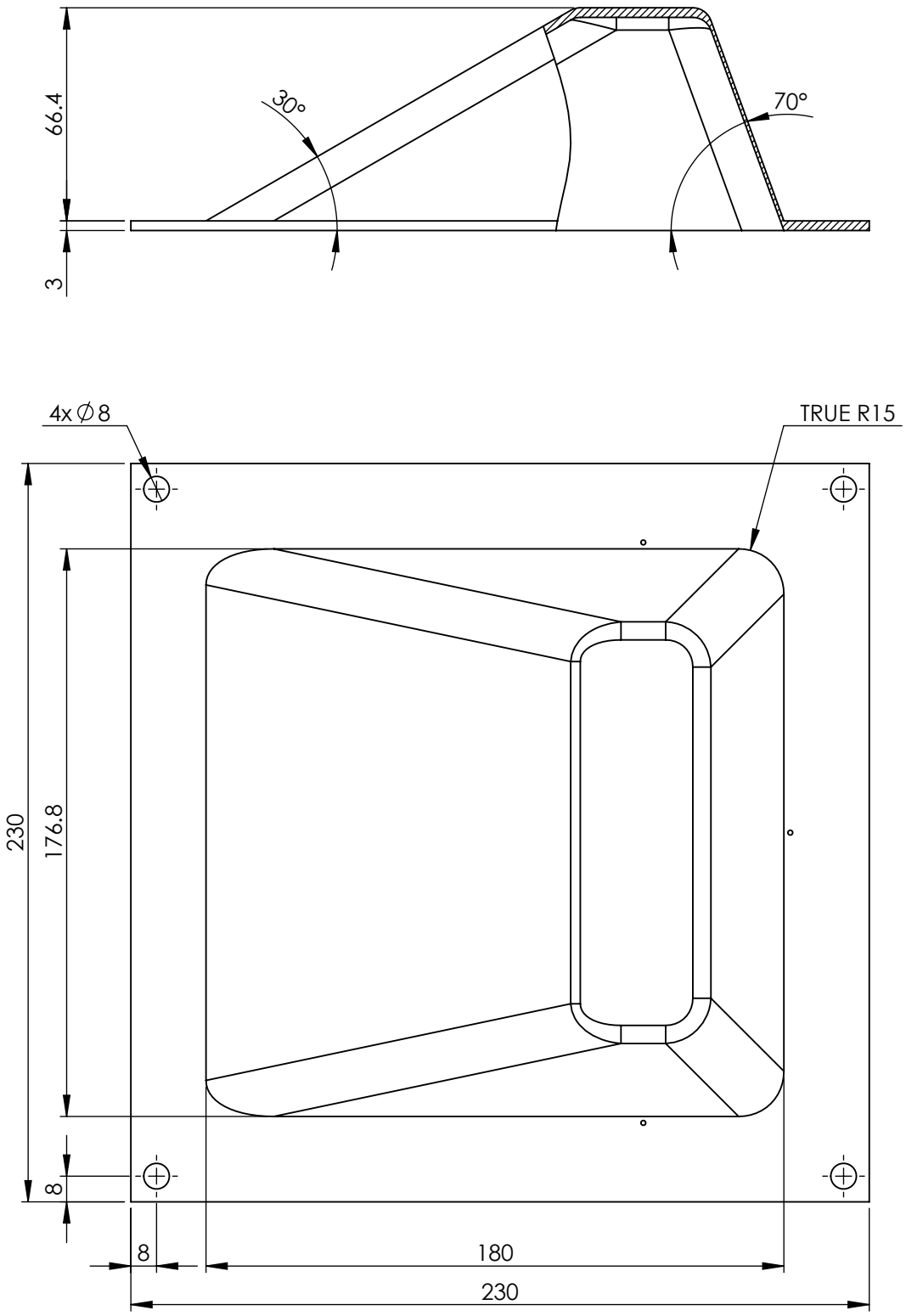

SPIF thermoforming positive mould core, scale 1:2

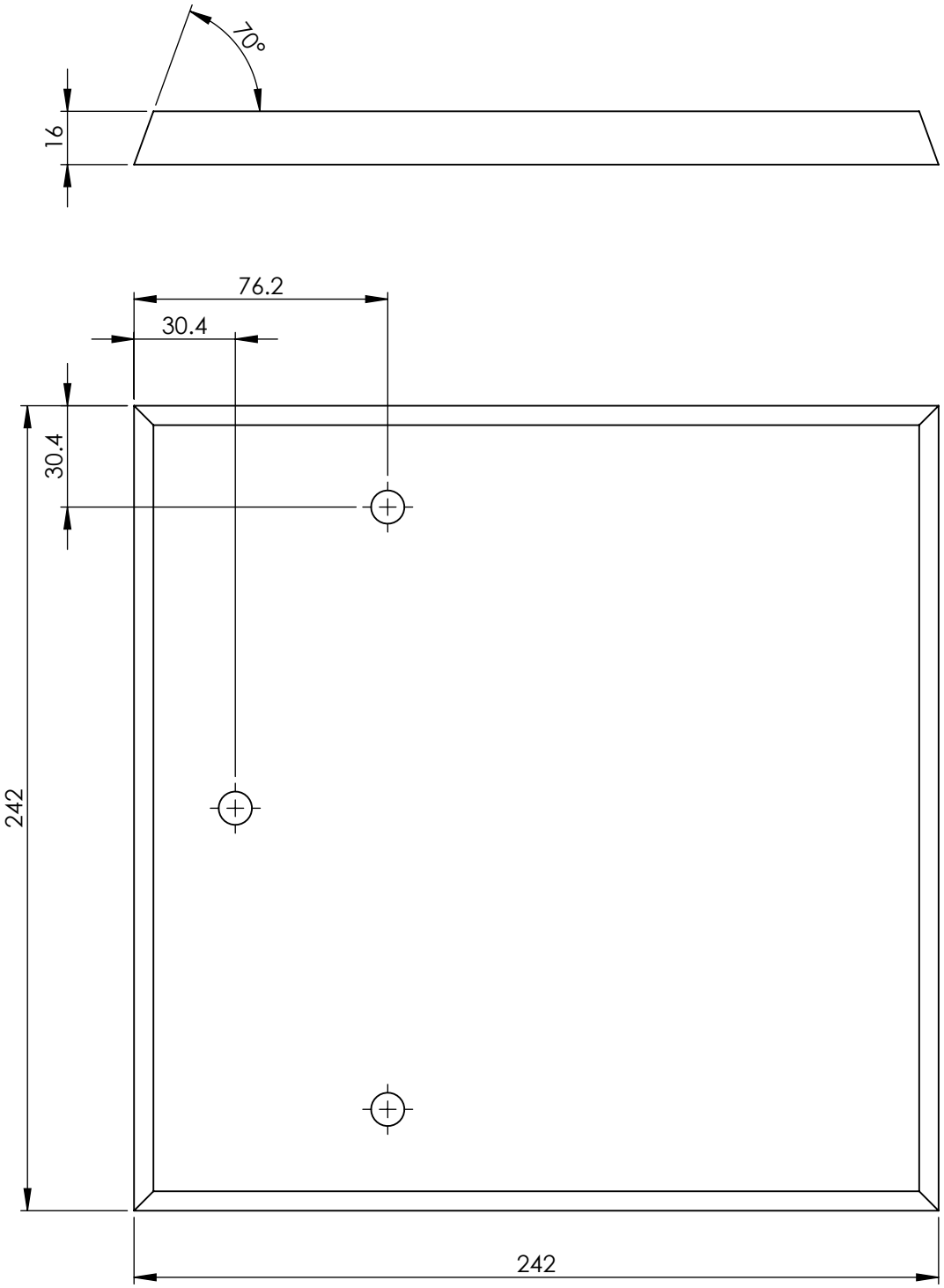

SPIF thermoforming positive mould support, scale 1:2

ITEM NO.	PART NUMBER	QTY.
1	mould cavity	1
2	support long	2
3	support short	2
4	ST4.2x16 screw	4
5	ST4.2x32 screw	8

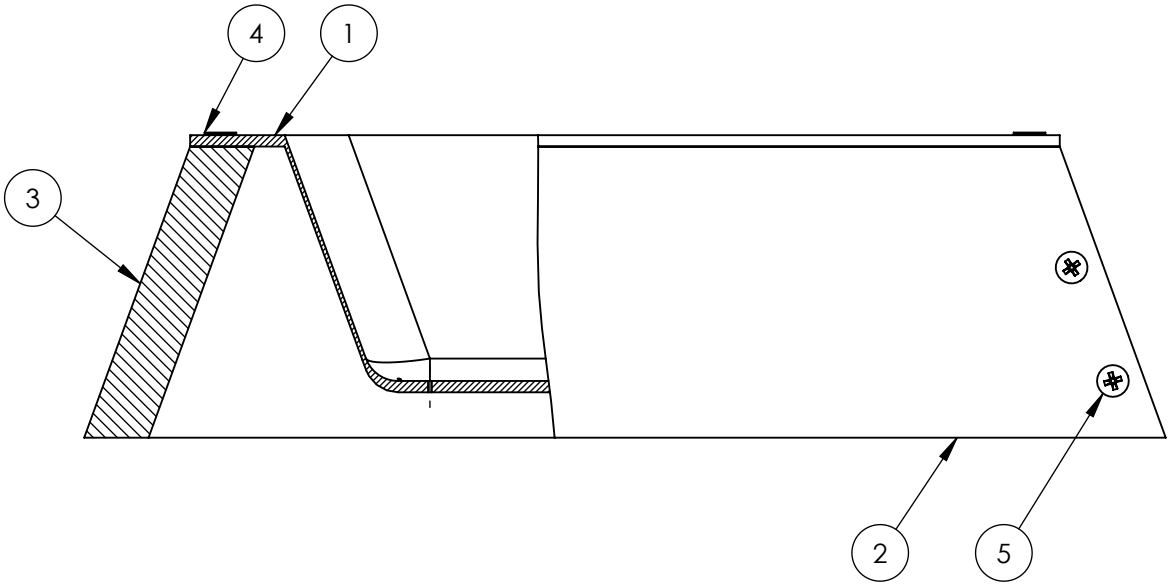

SPIF thermoforming negative mould, scale 1:2

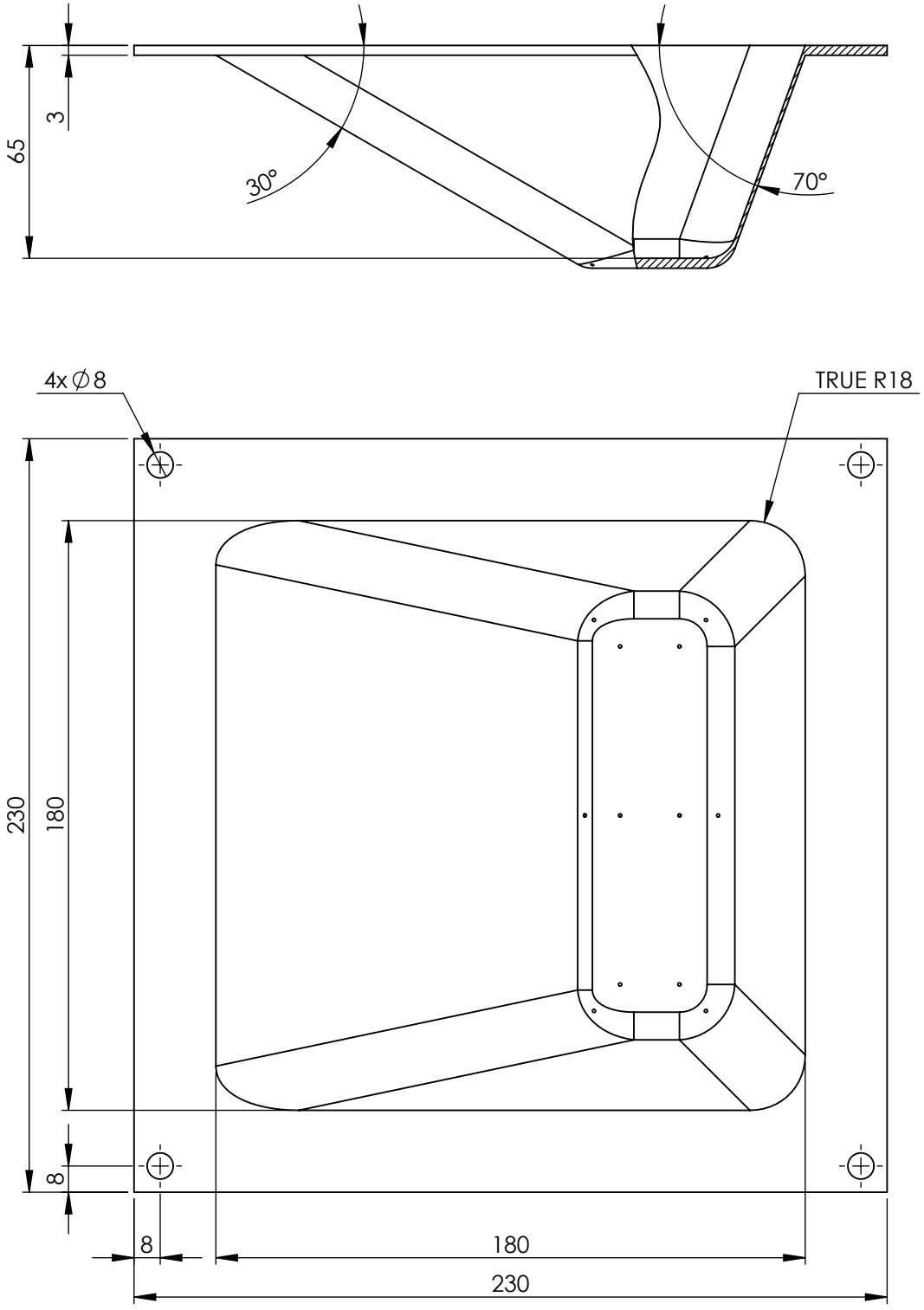

SPIF thermoforming negative mould cavity, scale 1:2

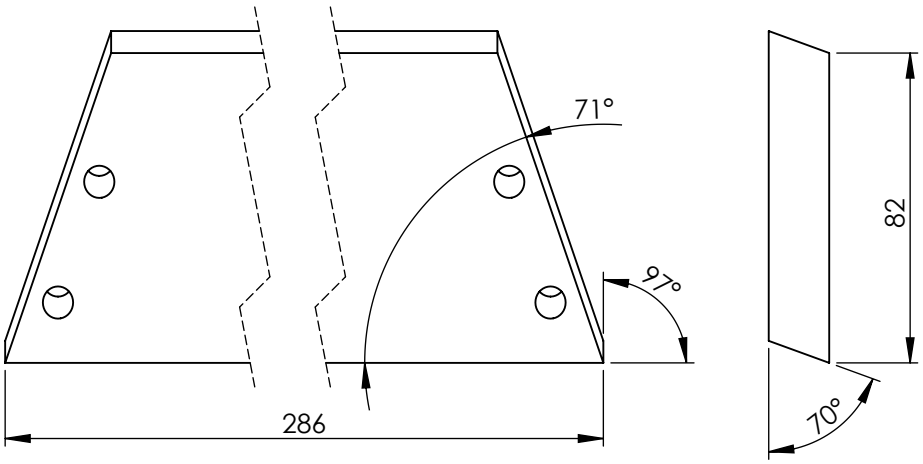

SPIF thermoforming negative mould support long, scale 1:2

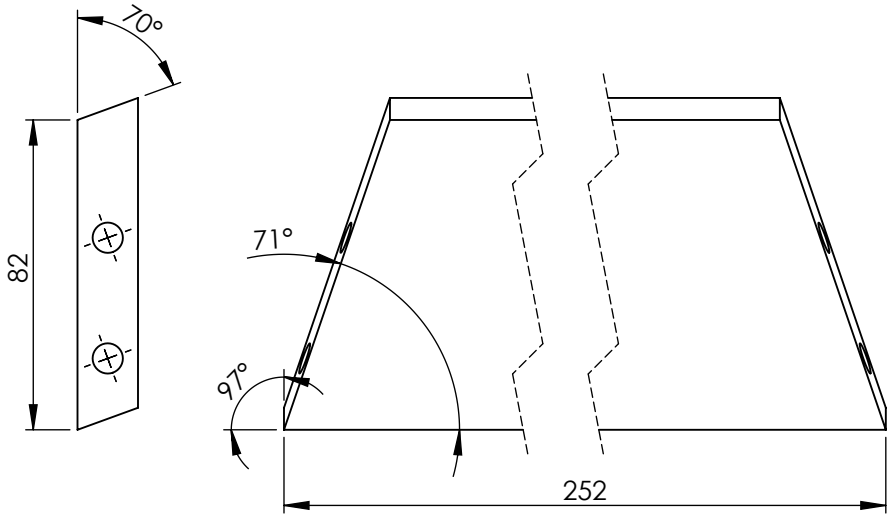

SPIF thermoforming negative mould support short, scale 1:2

E.2 Rotomoulding mould drawings

ITEM NO.	PART NUMBER	QTY.
1	lower_mould	1
2	upper_mould	1
3	washer 6mm	16
4	M6 x 16 screw	8
5	M6 Thin Nut	8
6	washer 3mm	8
7	M3 x 8 screw	4

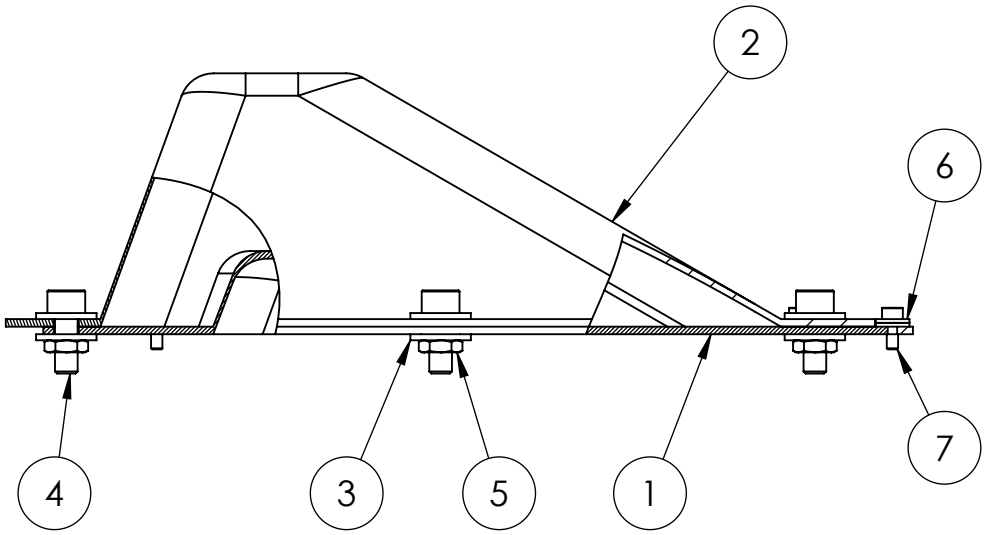

SPIF rotational moulding mould, scale 1:2

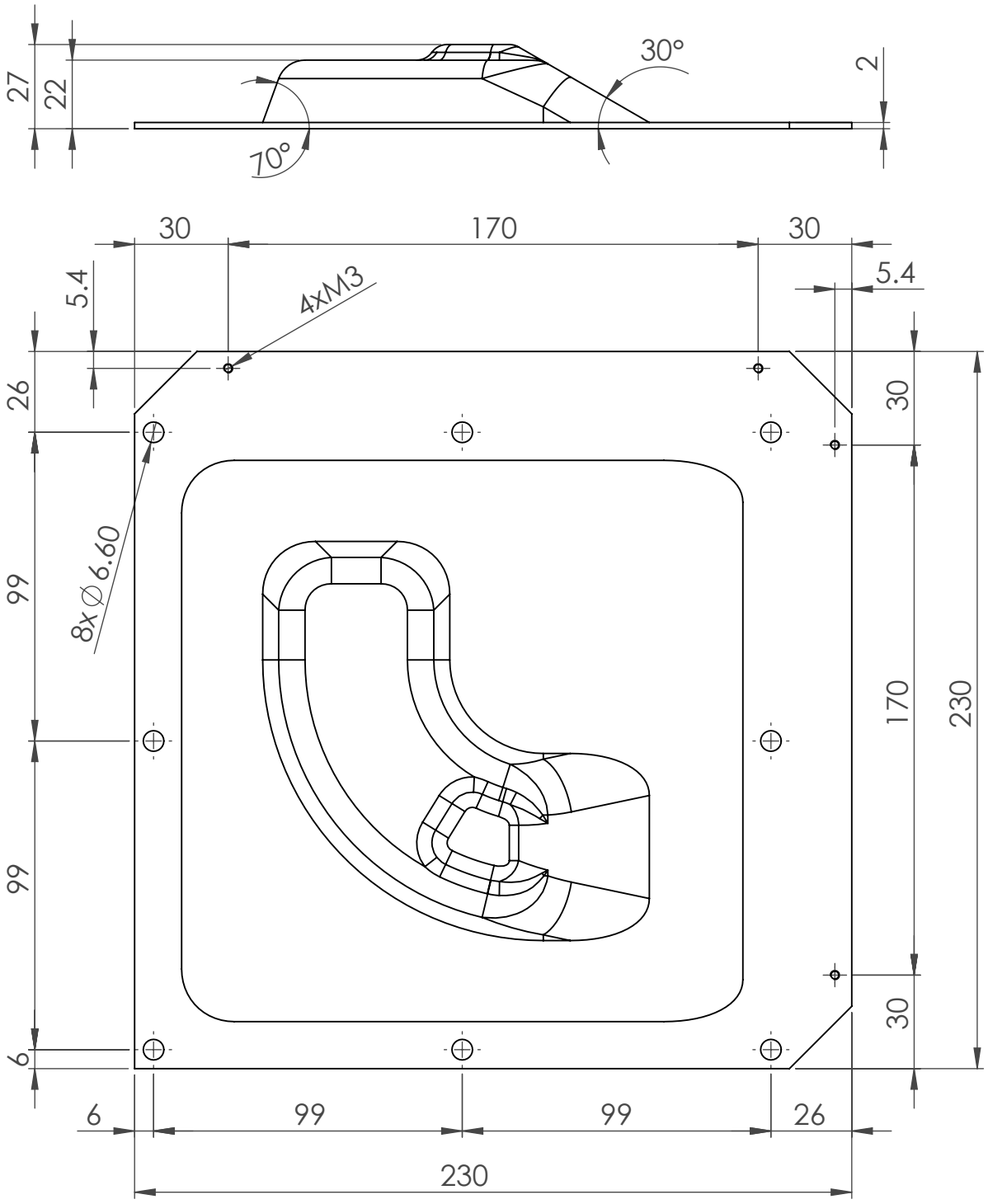

SPIF lower side mould part, scale 1:2

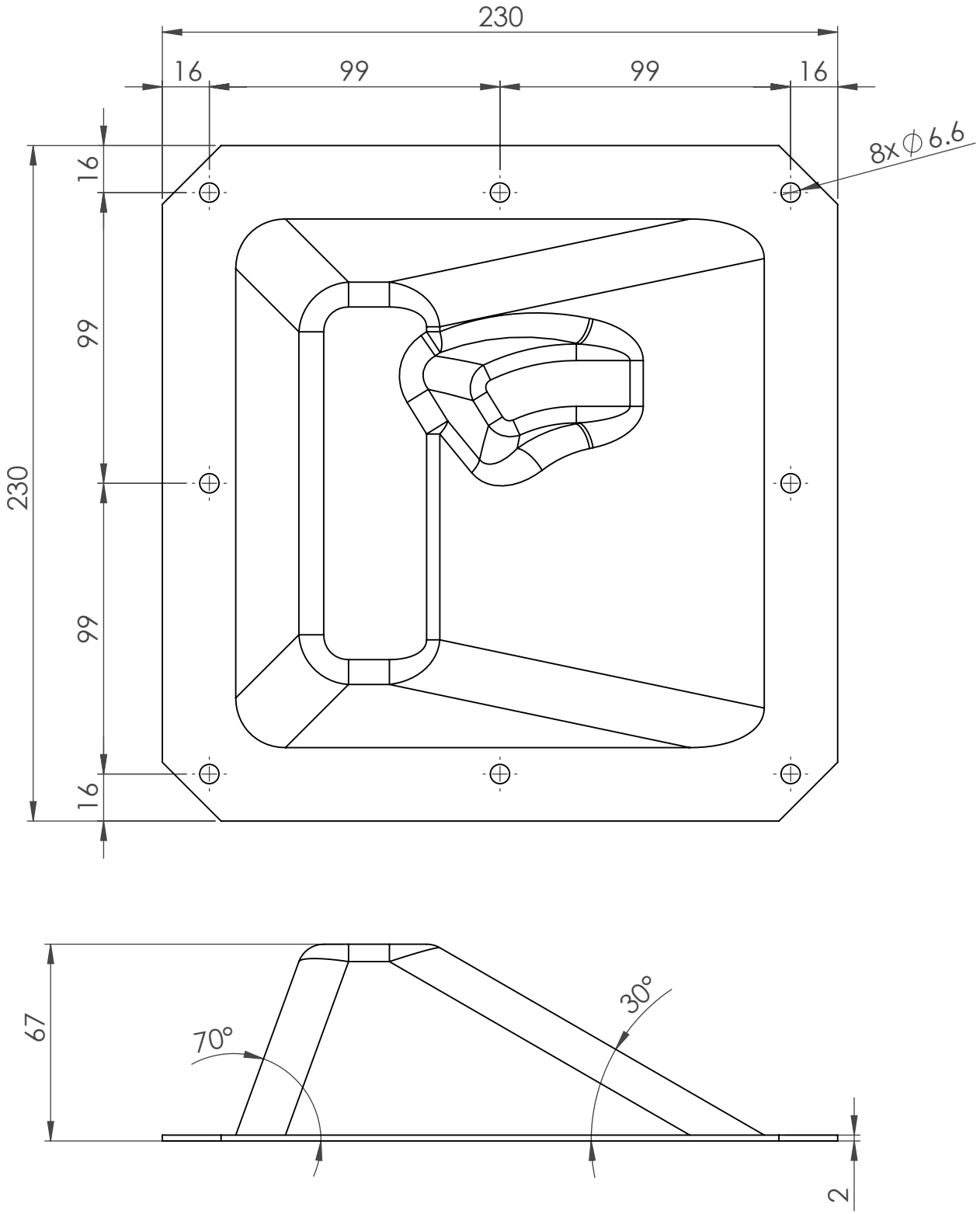

SPIF upper side mould part, scale 1:2

E.3 Hand layup mould drawings

ITEM NO.	PART NUMBER	QTY.
1	mould cavity	1
2	support	4
3	washer 6mm	4
4	ST4.2x19 screw	4
5	ST4.2x32 screw	8

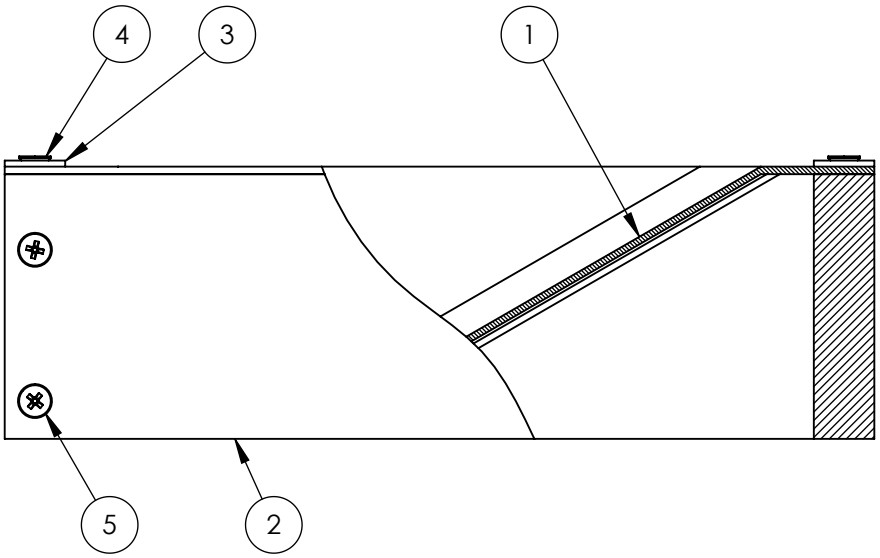

SPIF hand layup mould, scale 1:2

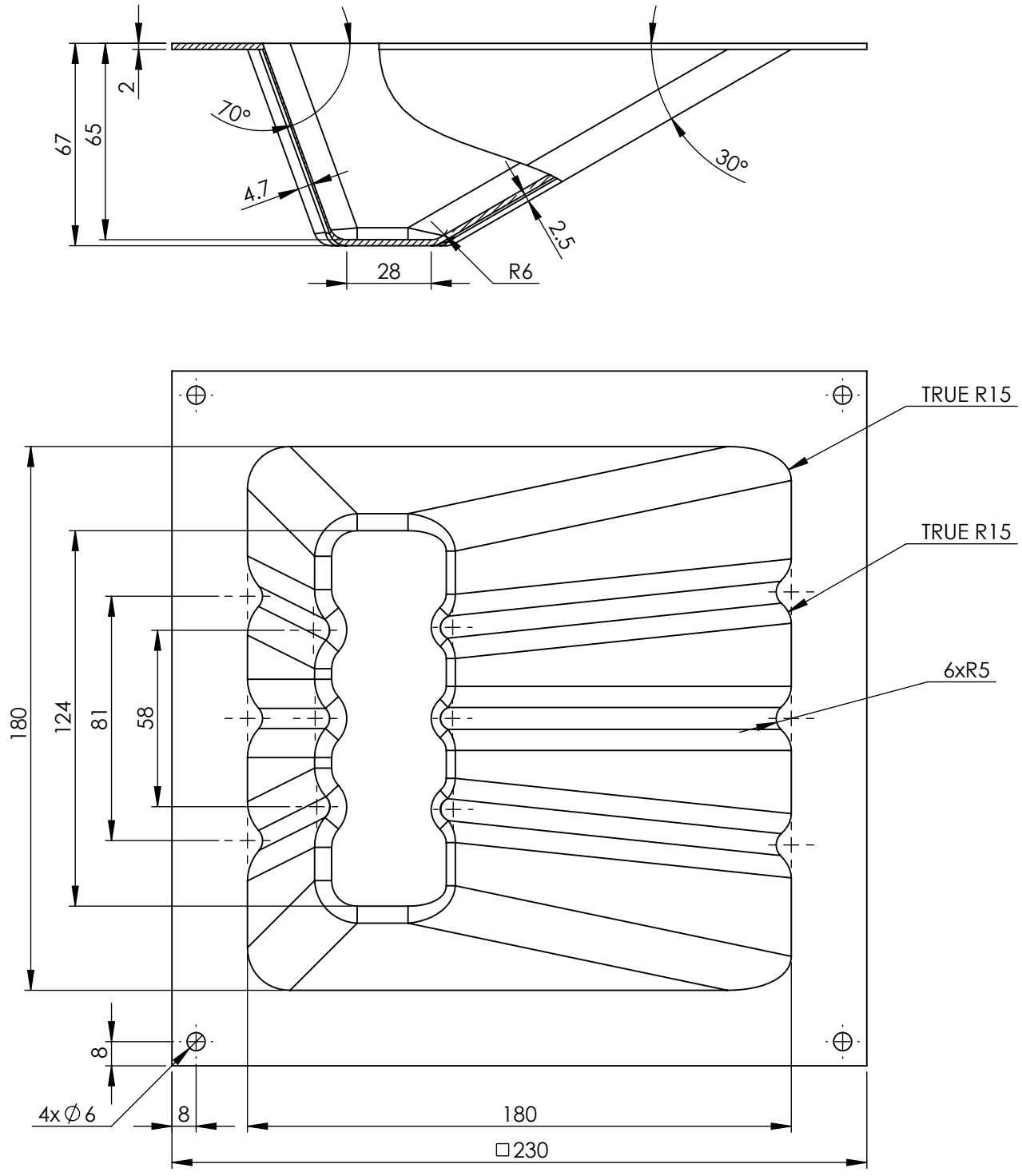

SPIF hand layup mould cavity, scale 1:2

E.4 Cork compression moulding mould drawings

ITEM NO.	PART NUMBER	QTY.
1	mould cavity side	1
2	mould core side	1
3	frame box	1
4	support	4
5	ST4.2x32 screw	8
6	ST4.2x19 screw	8
7	M6 x 16 screw	8
8	M6 nut	8

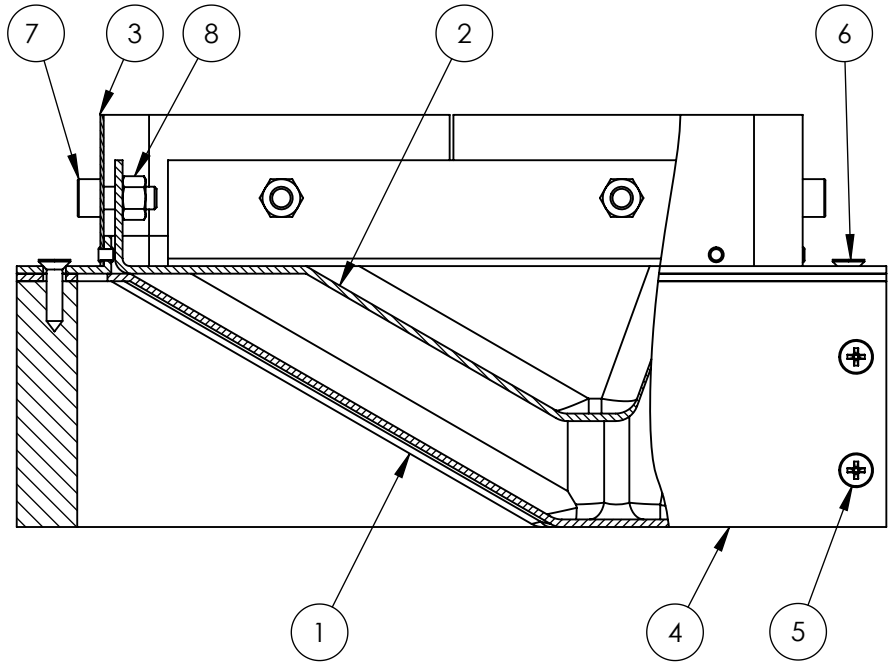

SPIF cork compression moulding mould, scale 1:2

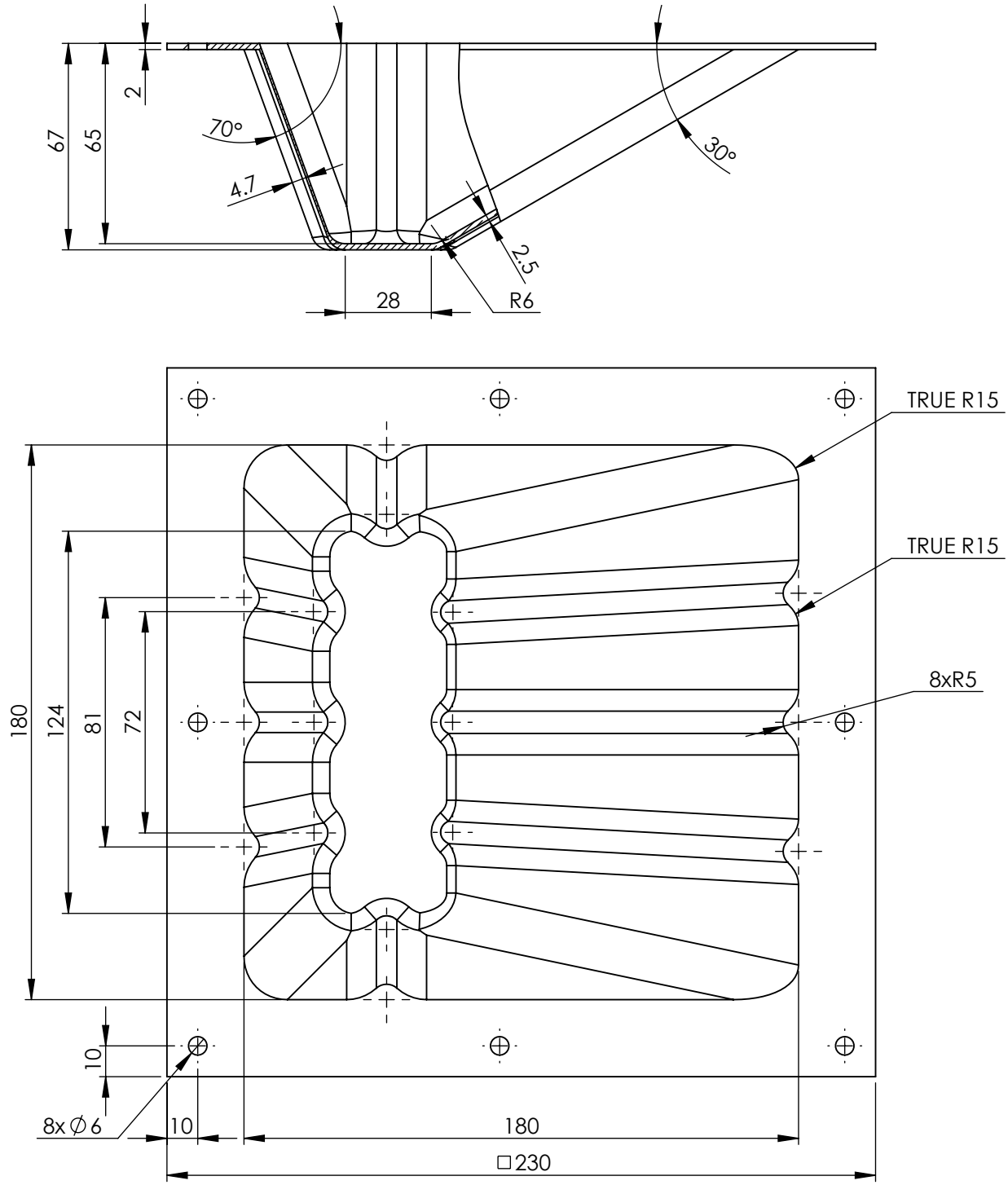

SPIF cork compression moulding mould cavity mould part, scale 1:2

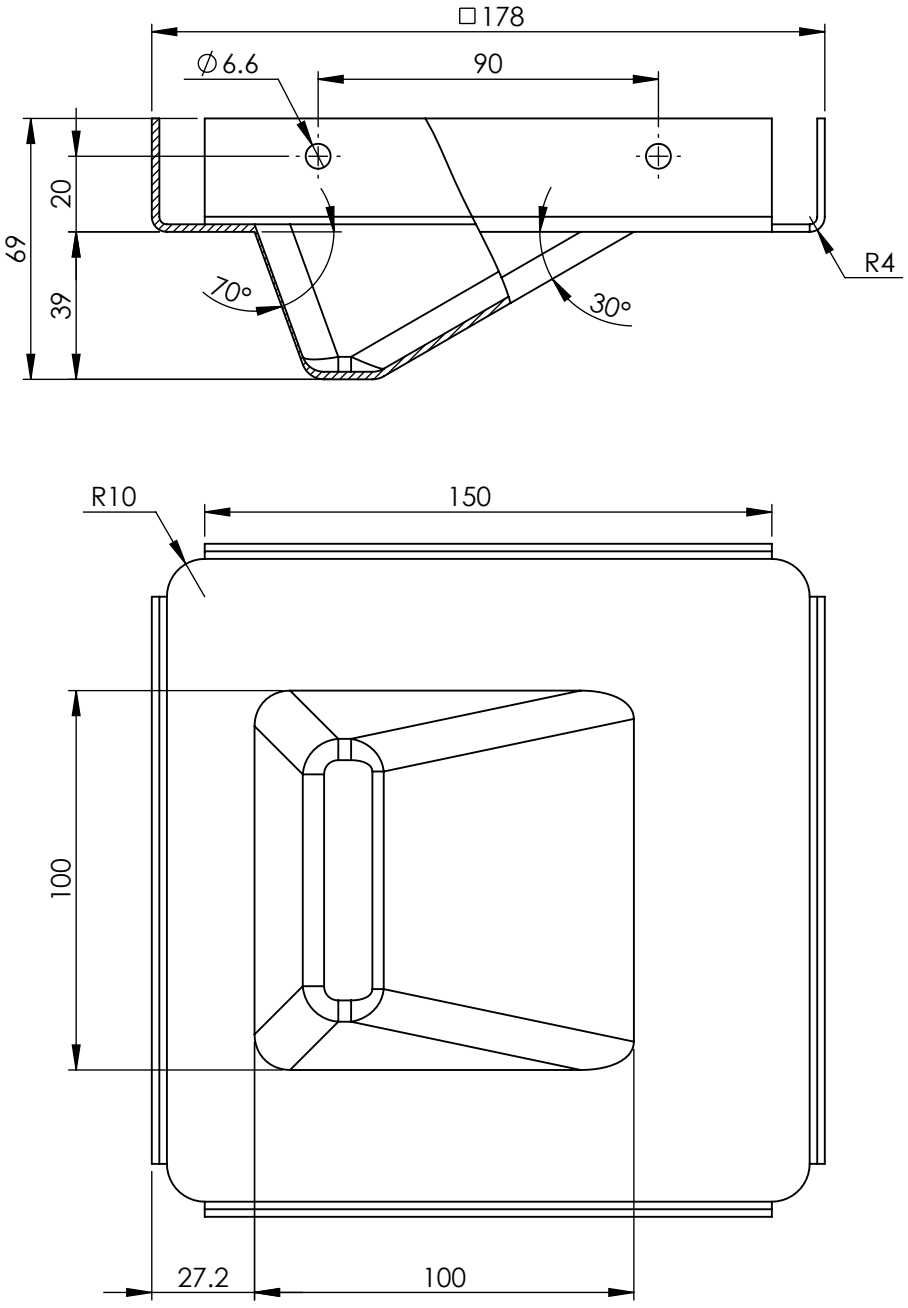

SPIF cork compression moulding mould core mould part, scale 1:2

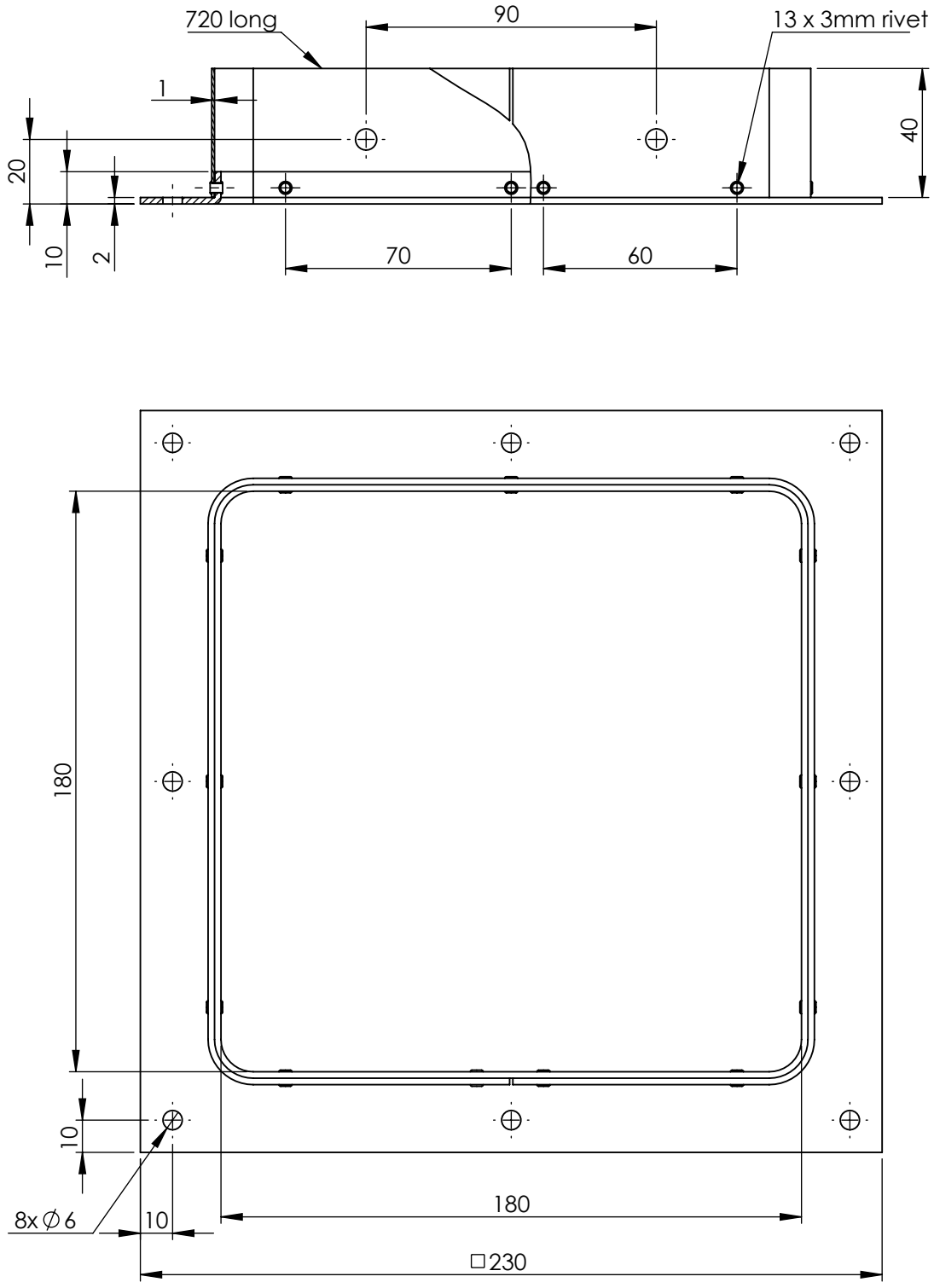

SPIF cork compression moulding mould frame box mould part, scale 1:2

Bibliography

[1] J. A. Schey. *Introduction to Manufacturing Processes.* McGraw-Hill, 3^{th} edition, 2000.

[2] E. Leszak. Apparatus and process for incremental dieless forming. *E. Patent US3342051A1*, 1967.

[3] W.C. Emmens, G. Sebastiani, and A.H. van den Boogaard. The technology of incremental sheet form ing - a brief review of the history . *Journal of Materials Processing Technology, Volume 210*, pages 981–997, 2010.

[4] J. Jeswiet, F. Micarib, G. Hirtc, A. Bramleyc, J. Dufloue, and J. Allwoodf. Asymmetric single point incremental forming of sheet metal. *CIRP Annals - Manufacturing Technology, Volume 54, Issue 2*, pages 88–114, 2005.

[5] S. Smith, G. C. Smith, R. Jiao, and C. H. Chu. Mass customization in the product life cycle. *Journal of Intelligent Manufacturing, Vol. 24, Issue 5*, pages 877–885, 2013.

[6] R. J. Alves de Sousa, J. A. F. Ferreira, J. B. Sá de Farias, J. N. D. Torrão, D. Afonso, and M. A. B. E. Martins. Spif-a: on the development of a new concept of incremental forming machine. *Structural Engineering and Mechanics, Volume 59, no. 5*, pages 645–660, 2014.

[7] C. Poli. *Design for Manufacturing: A Structured Approach.* Elsevier Inc., 1^{st} edition, 2001.

[8] L. Elg. *Innovations and new technology - what is the role of research? Implications for public policy.* VINNOVA - Swedish Governmental Agency for Innovation Systems, 1^{st} edition, 2014.

[9] P. D. Hilton and P. F. Jacobs. *Rapid Tooling: Technologies and Industrial Applications.* Marcel Dekker, Inc., 1^{st} edition, 2010.

[10] A. Equbal, A. Kumar Sood, and M. Shamim. Rapid tooling: A major shift in tooling practice. *Journal of Manufacturing and Industrial Engineering, Volume 14, no. 3-4*, pages 1–9, 2015.

[11] R. J. Alves de Sousa, J. A. F. Ferreira, S. R. Marabuto, and D. Afonso. Máquina para estampagem incremental de chapa. *PT_105888-1*, 2013.

[12] S. R. Marabuto, D. Afonso, J. A. F. Ferreira, F. Q. Melo, M. Martins, and R. J. Alves de Sousa. Finding the best machine for spif operations - a brief discussion. *Key Engineering Materials, Volume 473*, pages 861–868, 2011.

[13] J. B. S. Farias, M. A. B. E. Martins, D. G. Afonso, S. R. Marabuto, J. A. F. Ferreira, and R. J. Alves de Sousa. Cad/cam strategies for a parallel kinematics spif machine. *Key Engineering Materials, Volumes 554-557*, pages 2221–2229, 2013.

[14] R.P. Bastos, R.J. Alves de Sousa, and J. A. F. Ferreira. Enhancing time efficiency on single point incremental forming processes. *International Journal of Material Forming*, pages 1–10, 2015.

[15] N. Azevedo, J. Sá Farias, R. Bastos, P. Teixeira, J. P. Davim, and R. Alves de Sousa. Lubrication aspects during single point incremental forming for steel and aluminum materials. *International Journal of Precision Engineering and Manufacturing, Volume 16, Issue 3*, pages 589–595, 2015.

[16] T. Frederick Waters. *Fundamentals of Manufacturing for Engineers.* Taylor & Francis Ltd, 2^{nd} edition, 2001.

[17] M. El Sherbiny, H. Zein, M. Abd-Rabou, and M. El shazly. Thinning and residual stresses of sheet metal in the deep drawing process. *Materials & Design, Volume 55*, pages 869–879, 2014.

[18] A. Hedrick. Key design principles for successful deep drawing. *Stamping Journal, March/Abril*, 1999.

[19] Z. Marciniak, J. L. Duncan, and S. J. Hu. *Mechanics of Sheet Metal Forming.* Butterworth-Heinemann, 2^{nd} edition, 2002.

[20] Erichsen. *Sheet Metal Testing, testing equipment for quality management.*

[21] GOM Optical Measuring Techniques. *Application Example: Material Testing - Material Properties: Determination of Process Limitations in Sheet Metal Forming - Forming Limit Diagram.* Measuring Systems: ARAMIS.

[22] Dantec Dynamics. *DIC - Digital Image Correlation, DIC Measurement Principle.*

[23] A. Talic-Cikmis, T. Pepelnjak, and S. Hasanbegovic. Experimental determination of forming limit diagram. 4^{th} *International Research/Expert Conference "Trends in the Development of Machinery and Associated Technology"*, pages 605–608, 2010.

[24] H. Lundh, P. Bustad, B. Carlsson, G. Engberg, L. Gustafsson, and R. Lidgren. *Sheet Steel Forming Handbook - Size shearing and plastic forming.* SSAB Tunnplat AB, 1^{th} edition, 1998.

[25] E. Degarmo, J. Black, and R. Kohser. *Materials and Processes in Manufacturing.* Wiley, 9^{th} edition, 2003.

[26] O. Music, J. M. Allwood, and K. Kawai. A review of the mechanics of metal spinning. *Journal of Materials Processing Technology - Volume 210, Issue 1*, pages 3–23, 2010.

[27] Z. Y. Cai and M. Z. Li. Multi-point forming of three-dimensional sheet metal and the control of the forming process. *International Journal of Pressure Vessels and Piping - Volume 79, Issue 4*, pages 289–296, 2002.

[28] Z. Y. Cai, M. Z. Li, and Y. W. Lan. Three-dimensional sheet metal continuous forming process based on flexible roll bending: Principle and experiments. *Journal of Materials Processing Technology - Volume 212, Issue 1*, pages 120–127, 2012.

[29] S. M. Tabibian and M. K. Najafabadi. Review on various kinds of die less forming methods. *International Journal of Engineering and Advanced Technology (IJEAT)*, pages 24–28, 2014.

[30] J. Downie. *Power Hammer Techniques and Applications for Creating Compound Curves in Sheet Metal*. International Specialised Skills Institute, Melbourne, 2010.

[31] T. Schafer and R. D. Schraft. Incremental sheet metal forming by industrial robots. *Rapid Prototyping Journal, Vol. 11 Issue 5*, pages 278–286, 2005.

[32] P. O'Hara. Peen-forming - a developing technique. *International Conferences on Shot Peening 8*, pages 217–226, 2002.

[33] A. J. Fischer. Embodied computation: Exploring roboforming for the mass-customization of architectural components. Master's thesis, Carnegie Mellon University, 2015.

[34] M. Tisza. General overview of sheet incremental forming. *Journal of Achievements in Materials and Manufacture Engineering, Volume 55, Issue 1*, pages 113–120, 2012.

[35] W. F. Hosford and J. L. Duncan. Sheet metal forming: A review. *Journal JOM, Volume 51, Issue 11"*, pages 39–44, 1999.

[36] S. Kalpakjian and S.R. Schmid. *Manufacturing Processes for Engineering Materials*. Pearson Education, 5^{th} edition, 2008.

[37] M. Skjoedt, N. Bay, and T. Lenau. *Rapid Prototyping by Single Point Incremental Forming of Sheet Metal*. PhD thesis, Technical University of Denmark, 2008.

[38] L. Lamminen, B. Wadman, R. Küttner, and T. Svinning. Prosheet - prototyping and low volume production of sheet metal components - research report. Technical report, Nordic Industrial Fund - Center for innovation and commercial development, NI Project number: 03028.

[39] G. Hussain, G. Lin, and N. Hayat. Pyramid as test geometry to evaluate formability in incremental forming: Recent results. *Journal of Mechanical Science and Technology, Volume 26, Issue 8*, pages 2337–2345, 2012.

[40] A.K. Behera, R.J. Alves de Sousa, G. Ingarao, and V. Oleksik. Single point incremental forming: An assessment of the progress and technology trends from 2005 to 2015. *Journal of Manufacturing Processes, Volume 27*, pages 37–62, 2017.

[41] M. B. Silva. *Single Point Incremental Forming*. PhD thesis, Instituto Superior Técnico Universidade Técnica de Lisboa, 2008.

[42] T. Marques. Estampagem incremental de polímeros. Master's thesis, Instituto Superior Técnico Universidade Técnica de Lisboa, 2010.

[43] Amar K Behera and Hengan Ou. Effect of stress relieving heat treatment on surface topography and dimensional accuracy of incrementally formed grade 1 titanium sheet parts. *International Journal of Advanced Manufacturing Technology, Volume 87, Issue 9-11*, pages 3233–3248, 2016.

[44] A. Lozano, G. Bermúdez, and F. Correa. Comparative analysis between the spif and dpif variants for die-less forming process for an automotive workpiece. *INGE CUC , vol. 11 no. 2*, pages 68–73, 2015.

[45] Amino North America Corporation. Dieless nc machine, Dec. 2015. *www.aminonac.ca/presses-and-equipment-dieless-nc.asp*.

[46] D. Bailly, M. Bambach, G. Hirt, T. Pofahl, G. Della Puppa, and M. Trautz. Investigation on the producibility of freeform facade elements made of sheet metal as self-supporting structures by means of incremental sheet forming. *The METEC and 2nd European Steel Technology and Application Days*, 2015.

[47] I. Paniti. A novel, single-robot based two sided incremental sheet forming system. *Conference ISR ROBOTIK*, pages 547–553, 2014.

[48] J. Allwood, N. E. Houghton, and K. P. Jackson. The design of an incremental sheet forming machine. *Advanced Materials Research, Volume 6, Issue 8*, pages 471–478, 2005.

[49] J. Câmara. Single point incremental forming. Master's thesis, Instituto Superior Técnico Universidade Técnica de Lisboa, 2009.

[50] R. Bastos. Control of a servo-hydraulic platform using parallel kinematics for incremental forming. Master's thesis, University of Aveiro, 2014.

[51] J. Torrão. Control and execution of incremental forming using parallel kinematics. Master's thesis, University of Aveiro, 2013.

[52] G. Hussain, H. R. Khan, G. Lin, and N. Hayat. Guidelines for tool-size selection for single-point incremental forming of an aerospace alloy. *Materials and Manufacturing Processes, Volume 28, Issue 3*, pages 324–329, 2013.

[53] V. Sajn, B. Jurisevic, and F. Kosel. Water jet incremental sheet metal forming: pressure distribution analysis. *International Journal on Interactive Design and Manufacturing (IJIDeM)*, pages 95–102, 2011.

[54] I. Paniti. New solutions in incremental sheet forming. Master's thesis, Hungarian Academy of Sciences Institute for Computer Science and Control, 2014.

[55] A. Gottmann, J. Diettrich, G. Bergweiler, M. Bambach, G. Hirt, P. Loosen, and R. Poprawe. Laser-assisted asymmetric incremental sheet forming of titanium sheet metal parts. *Production Engineering, Volume 5, Issue 3*, pages 263–271, 2011.

[56] J. Asghar. Importance of tool configuration in incremental sheet metal forming of difficult to form materials using electro-plasticity. *Proceedings of the World Congress on Engineering, Volume III*, 2013.

[57] M. Skjoedt, M. B. Silva, N. Bay, P. A. F. Martins, and T. Lenau. Single point incremental forming using a dummy sheet. *proceedings of the 2nd ICNFT - 2nd international conference on new forming technology*, pages 267–276, 2007.

[58] A. Blaga and V. Oleksik. A study on the influence of the forming strategy on the main strains, thickness reduction, and forces in a single point incremental forming process. *Advances in Materials Science and Engineering, Volume 2013*, 2013.

[59] M. Skjoedt, M. H. Hancock, and N. Bay. Creating helical tool paths for single point incremental forming. *Key Engineering Materials, Proceeding of SheMet07*, pages 583–590, 2007.

[60] M. Callegari, D. Amodio, E. Ceretti, and C. Giardin. *Industrial Robotics: Programming, Simulation and Applicationl*, chapter Sheet Incremental Forming: Advantages of Robotised Cells vs. CNC Machines, pages 493–514. Pro Literatur Verlag, 2006.

[61] J. B. Sá de Farias, R.P. Bastos, J. A. Ferreira, and R. J. Alves de Sousa. Assessing 3 and 5 degrees of freedom toolpath strategy influence on single point incremental forming. *Key Engineering Materials Vols. 651-65*, pages 1159–1162, 2015.

[62] M. Skjoedt, N. Bay, B. Endelt, and G. Ingarao. Multi stage strategies for single point incremental forming of a cup. *Proceedings of the 11 conference on Material Forming ESAFORM*, 2008.

[63] S. B. M. Echrif and M. Hrairi. Process simulation and quality evaluation of incremental sheet forming. *IIUM Engineering Journal, Special Issue, Mechanical Engineering*, pages 185–196, 2011.

[64] M. Bambach, B. Taleb Araghi, and G. Hirt. Strategies to improve the geometric accuracy in asymmetric single point incremental forming. *Production Engineering Research and Development, Volume 3, Issue 2*, pages 145–156, 2009.

[65] H. Vanhove, J. Gu, H. Sol, and J. Duflou. Process window extension for incremental forming through optimal work plane rotation. *Proceeding of the 10th anniversary of the International Conference on Technology of Plasticity*, 2011.

[66] M. B. Silva, M. Skjoedt, A. G. Atkins, N. Bay, and P. A. F. Martins. Single point incremental forming & formability/failure diagrams. *Journal of Strain Analysis for Engineering Design, Volume 43, Issue 1*, pages 15–36, 2008.

[67] J. Jeswiet and D. Young. Forming limit diagrams for single-point incremental forming of aluminium sheet. *Proceedings of the Institution of Mechanical Engineers, Part B: Journal of Engineering Manufacture*, pages 359–364, 2005.

[68] M. B. Silva, M. Skjoedt, N. Bay, and P. A. F. Martins. Theory of single point incremental forming. *Journal of Materials Processing Technology, Volume 57, Issue 1*, pages 247–252, 2008.

[69] M.B. Silva, L.M. Alves, M.L. Alves, and P.A.F. Martins. Fracture forming lines in single point incremental forming. *Proceeding of the IDDRG 2010 - International Deep Drawing Research Group*, 2010.

[70] D. Frizen. *Estudo dos parâmetros de conformabilidade para o processo de estampagem incremental*. PhD thesis, Federal University of Rio Grande do Sul, 2016.

[71] J. Verbert. *Computer Aided Process Planning for Rapid Prototyping With Incremental Sheet Forming Techniques*. PhD thesis, Katholieke Universiteit Leuven, 2010.

[72] P. Martins, L. Kwiatkowski, V. Franzen, A. Tekkaya, and M. Kleiner. Single point incremental forming of polymers. *Cirp Ann-Manuf Techn, 58*, pages 229–232, 2009.

[73] L. Fratini, G. Ambrogio, R. Di Lorenzo, L. Filice, and F. Micari. Influence of mechanical properties of the sheet material on formability in single point incremental forming. *Cirp Ann-Manuf Techn, 53*, pages 207–210, 2004.

[74] K. Jackson and J. Allwood. The mechanics of incremental sheet forming. *Journal of Materials Processing Technology, Volume 209, Issue 3*, pages 1158–1174, 2009.

[75] R. Malhotra, L. Xue, T. Belytschko, and J. Cao. Mechanics of fracture in single point incremental forming. *Journal of Materials Processing Technology, Volume 212, Issue 7*, pages 1573–1590, 2012.

[76] F. Maqbool and M. Bambach. Revealing the dominant forming mechanism of single point incremental forming by splitting plastic energy dissipation. *Procedia Engineering, Volume 183*, pages 188–193, 2017.

[77] A. Petek, K. Kuzman, and J. Kopac. Deformations and forces analysis of single point incremental sheet metal forming. *Archives in Material Science and Engineering, Volume 35, Issue 2*, pages 107–116, 2009.

[78] R. Aerens, P. Eyckens, A. Van Bael, and J. R. Duflou. Force prediction for single point incremental forming deduced from experimental and fem observations. *The International Journal of Advanced Manufacturing Technology, Volume 9, Issue 12*, pages 969–982, 2009.

[79] Y. Li, J.T. D. William, Z. Liu, H. Lu, and P. A. Meehan. Deformation mechanics and efficient force prediction in single point incremental forming. *Journal of Materials Processing Technology, Volume 221*, pages 100–111, 2015.

[80] A. Mohammad, H. Vanhove, A. Van Bael, and J. R. Duflou. Influence of laser assisted single point incremental forming on the accuracy of shallow sloped parts. *AIP Conference Proceedings, Volume 1567, Issue 1*, pages 864–867, 2013.

[81] J. Jeswiet, D. Adams, M. Doolan, T. McAnulty, and P. Gupta. Single point and asymmetric incremental forming. *Advances in Manufacturing, Volume 3, Issue 4*, pages 253–262, 2015.

[82] D. Adams and J. Jeswiet. Design rules and applications of single-point incremental forming. *Proceedings of the Institution of Mechanical Engineers, Part B: Journal of Engineering Manufacture, Volume 229, Issue 5*, pages 253–262, 2014.

[83] J. Duflou, B. Lauwers, and J. Verbert. Study on the achievable accuracy in single point incremental forming. *Advanced Methods in Material Forming*, pages 251–262, 2007.

[84] M. Ham and J. Jeswiet. Dimensional accuracy of single point incremental forming. *11th ESAFORM conference on material forming*, 2008.

[85] A. K. Behera, H. Vanhove, B. Lauwers, and J. Duflou. Accuracy improvement in single point incremental forming through systematic study of feature interactions. *Key Engineering Materials, Volume 473*, pages 881–888, 2011.

[86] A. Mohammadi, H. Vanhove, A. Bael, and J. Duflou. On the geometric accuracy in shallow sloped parts in single point incremental forming. *Key Engineering Materials, Volumes 554-557*, pages 1443–1450, 2013.

[87] M. Skjødt, M. B. Silva, P. A. F. Martins, and N. Bay. Strategies and limits in multi-stage single-point incremental forming. *Journal of Strain Analysis for Engineering Design, Volume 45, no. 1*, pages 33–44, 2010.

[88] Z. Liu, Y. Li, and P. A. Meehan. Vertical wall formation and material flow control for incremental sheet forming by revisiting multistage deformation path strategies. *Materials and Manufacturing Processes, Volume 28*, pages 562–571, 2013.

[89] H. Vanhove, J. Gu, H. Sol, and J. Duflou. Process window extension for incremental forming through optimal work plane rotation. *Proceeding of the 10th anniversary of the International Conference on Technology of Plasticity*, 2011.

[90] L. Thyssen, P. Seim, D. Störkle, and B. Kuhlenkötte. On the increase of geometric accuracy with the help of stiffening elements for robot based incremental sheet metal forming. *19th ESAFORM Conference.*, 2016.

[91] V.C. Do, D.T. Nguyen, J.H. Cho, and Y.S. Kim. Incremental forming of 3d structured aluminium sheet. *International Journal of Precision Engineering and Manufacturing, Volume 17, Issue 2*, pages 217–223, 2016.

[92] CO2PE! Cooperative effort on process emissions in manufacturing, 2015. *www.co2pe.org*.

[93] K. Branker, D. Adams, A. Szekeres, and J. Jeswiet. Investigation of energy, carbon dioxide emissions and cost in single point incremental forming. *Re-engineering Manufacturing for Sustainability: Proceedings of the 20th CIRP International Conference on Life Cycle Engineering*, pages 291–295, 2013.

[94] O. Anghinelli, G. Ambrogio, R. Di Lorenzo, and G Ingarao. Environmental costs of single point incremental forming. *Steel research international 2011, Special Edition*, pages 525–530, 2011.

[95] G. Ambrogio, G. Ingarao, F. Gagliardia, and R. Di Lorenzo. Analysis of energy efficiency of different setups able to perform single point incremental forming (spif) processes. *Proceeding of the 21st CIRP Conference on Life Cycle Engineering*, pages 111–116, 2014.

[96] G. Ingarao, H. Vanhove, K. Kellens, and J. R. Duflou. A comprehensive analysis of electric energy consumption of single point incremental forming processes. *Journal of Cleaner Production, Volume 67*, pages 173–186, 2014.

[97] I. Bagudanch, M. Garcia-Romeu, I. Ferrer, and J. Lupiañez. The effect of process parameters on the energy consumption in single point incremental forming. *The Manufacturing Engineering Society International Conference, MESIC*, pages 346–353, 2013.

[98] S. Gardez. Economic analysis of low volume sheet metal products manufactured by single point incremental forming process. Master's thesis, UET Lahore, 2008.

[99] R. Lendel, M. Milutinovic, A. Ivanisevic, D. Vilotic, D. Movrin, and P. Skakun. Single point incremental forming of large-size components. *Journal for Technology of Plasticity, Vol. 39, Number 1*, pages 59–66, 2014.

[100] J. Ames. Systematische untersuchung des werkstoffflusses bei der inkrementellen blechumformung mit cnc-werkzeugmaschinen. Master's thesis, Rheinisch-Westfaelische Technische Hochschule Aachen, 2008.

[101] M. Elford, P. Saha, D. Seong, MD Z. Haque, and J. Whan Yoon. Benchmark 3 - incremental sheet forming. *AIP Conf. Proc. - NUMISHEET 2014: The 9th International Conference and Workshop on Numerical Simulation of 3D Sheet Metal Forming Processes: Part A Benchmark Problems and Results and Part B General Papers*, 2013.

[102] M. Amino, M. Mizoguchi, Y. Terauchi, and T. Maki. Current status of "dieless" amino's incremental forming. *Procedia Engineering, Volume 81*, pages 54–62, 2014.

[103] Ford sheet-metal-forming technology on journey from lab to application, 2013. *articles.sae.org/12385/.*

[104] K. Reynolds. How the toyota new global architecture will impact mass-car building, 2015. *www.motortrend.ca/en/news/1505-toyota-new-global-architecture-mass-car-building.*

[105] J. Duflou. Production processes - cranial plate, 2006. *www.mech.kuleuven.be/pp/research/spif_cranial.en.html.*

[106] J. Castelan, L. Schaeffer, A. Daleffe, D. Fritzen, V. Salvaro, and F. Pinto da Silva. Manufacture of custom-made cranial implants from dicom®images using 3d printing, cad/cam technology and incremental sheet forming. *Brazilian Journal of Biomedical Engineering, Volume 30, Issue 3*, pages 265–273, 2014.

[107] M. Milutinovic, R. Lendel, M. Potran, D. Vilotic, P. Skakun, and M. Plancak. Application of single point incremental forming for manufacturing of denture base. *Journal for Technology of Plasticity, Vol. 39, Number 2*, pages 15–23, 2014.

[108] J. Duflou. Production processes - solar cooker, 2006. *www.mech.kuleuven.be/pp/research/spif_solar.en.html.*

[109] C. Lefteri. *Making It: Manufacturing Techniques for Product Design.* Laurence King, 2^{nd} edition, 2012.

[110] A. Kalo and M. J. Newsum. An investigation of robotic incremental sheet metal forming as a method for prototyping parametric architectural skins. *Robotic Fabrication in Architecture, Art and Design*, pages 33–49, 2014.

[111] R. Appermont, B. Van Mieghem, A. Van Bael, J. Bens, J. Ivens, H. Vanhove, A.K. Behera, and J. Duflou. Sheet-metal based molds for low-pressure processing of thermoplastics. *Proceedings of the 5th Bi-Annual PMI Conference*, pages 383–388, 2012.

[112] J. P. Holman. *Experimental Methods for Engineers.* McGraw-Hill, 7^{th} edition, 2001.

[113] D. C. Montgomery. *Design and Analysis of Experiments.* Wiley, 6^{st} edition, 2005.

[114] P. Mort, J. Cross, and T. L. Downey. Writing a case study report in engineering. *The University of New South Wales*, 2002.

[115] C. V. McLelland. Nature of science and the scientific method. *The geological Society of America*, 2006.

[116] G. Muller. Systems engineering research validation. *The Gaudí project, Buskerud University College and Embedded Systems Institute*, 2016.

[117] H. Spliid. *Design and Analysis af Experiments with k Factors having p Levels.* Technical University of Denmark, 1^{st} edition, 2002.

[118] D. D Frey and H. Wang. Adaptive one-factor-at-a-time experimentation and expected value of improvement. *Technometrics, Volume 48, Issue 3*, pages 418–431, 2006.

[119] P. Brereton, B. Kitchenham, D. Budgen, and Z. Li. Using a protocol template for case study planning. *12th International Conference on Evaluation and Assessment in Software Engineering*, 2008.

[120] P. A. C. Miguel. Estudo de caso na engenharia de produção: estruturação e recomendações para sua condução. *Produção, Volume 17, número 1*, pages 216–229, 2007.

[121] M. Al-Atabi and S. N. Yam. Introducing research skills through the use of the scientific method in engineering labs. *Journal of Engineering Science and Technology, Special Issue on Engineering Education*, pages 56–61, 2013.

[122] European Commission. *EN Horizon 2020 Work Programme 2016-2017.* European Commission, 2016.

[123] D. Afonso. Spif cad cam - manual for preparing spif toolpaths using powermill - post-processing for the spif-a machine. *University of Aveiro*, 2016.

[124] 120323/14. *Current Transducer HASS 50..600-S.* LEM Components, 2014.

[125] CH 24101. *Isolated current and voltage transducers, Characteristics - Applications - Calculations.* LEM Components, 2015.

[126] 2638A. *HYDRA Series III Data Acquisition Unit - Users Manual.* Fluke Corporation, 2013.

[127] G. E. Urroz. *Numerical Integration Using SCILAB.* UtahState University, distributed by infoClearinghouse.com, 2001.

[128] Model TR3D-A-*. *Round Three Directional Load Cell*. Michigan Scientific Corporation, 2013.

[129] LMU 209 Data Sheet. *LMU 209 Load Monitoring Unit*. Martrol, 2014.

[130] V. Lindberg. *Uncertainties, Graphing, and the Vernier Caliper: Uncertainties and Error Propagation*. Rochester Institute of Technology, 2000.

[131] Scilab Group INRIA Meta2 Project/ENPC Cergrene. *Signal Processing With Scilab*. INRIA - Unité de recherche de Rocquencourt, 1999.

[132] Renishaw Digitising Products Division. *Cyclone Scanning system*. Renishaw, 2014.

[133] Immersion. *MicroScribe G2 Desktop Digitizing Systems*. Solution Technologies, 2004.

[134] D. Afonso. Spif energy consumption - experimental evaluation of single point incremental forming consumption on the spif-a machine. *University of Aveiro*, 2016.

[135] J. Sá de Farias, J. Ferreira, S. Marabuto, A. Andrade Campos, M. Martins, and R. Alves de Sousa. *Smart Manufacturing Innovation and Transformation: Interconnection and Intelligence*, chapter Towards Smart Manufacturing Techniques using Incremental Sheet Forming, pages 159–189. IGI Global, 2014.

[136] F. Field, R. Kirchain, and R. Roth. Process cost modeling: Strategic engineering and economic evaluation of materials technologies. *JOM: the journal of the Minerals, Metals & Materials Society, Volume 59, Issue 10*, pages 21–32, 2007.

[137] R. Kirchain. *Encyclopedia of Materials: Science and Technology*, volume 2, chapter Cost Modeling of Materials and Manufacturing Processes. Elsevier, 2001.

[138] P. Vasconcelos, F. Lino, R. Neto, and M. Vasconcelos. Design and rapid prototyping evolution. *RPD 2002 - Advanced Solutions and Development conference*, 2002.

[139] T. Andrew. Development of an expert system as applied to rapid tooling techniques for injection molding. Master's thesis, Lehigh University, 2005.

[140] E. Tackett. *Rapid Tooling*. Saddleback College Advanced Technology Center.

[141] ASTM. *Standard test method for tensile properties of plastics*. West Conshohocken, PA, 2010.

[142] ISO 10002-1:2009. *Metallic Materials - tensile testing part1: method of test at ambient temperature*, 2009.

[143] J. L. Throne. *Thermoforming 101*. SPE thermoforming division, 2006.

[144] GE plastics. *Thermoforming Processing Guide*. GE Engineering Thermoplastics Processing Guide.

[145] D. Rosato, D. Rosato, and M. Rosato. *Plastic Product Material & Process Selection Handbook*. Elsevier, 2004.

[146] R. J. Crawford and M. P. Kearns. Practical guide to rotational moulding. *Rapra Technology Limited*, 2003.

[147] LyondellBasell. *A Guide to Rotational Molding*. 5717E/0715.

[148] H. Belofsky. *Plastics: Product Design and Process Engineering*. Hanser, 1995.

[149] K. Ghosh. Thermal models and energy saving strategies for rotational molding operation. *Georgia Institute of Technology*, 2004.

[150] S. Banerjee, W. Yan, and D. Bhattacharyya. Modeling of heat transfer in rotational molding. *Polymer Engineering & Science, Volume 48, no. 11*, pages 2188–2197, 2008.

[151] L. G. Olson, R. Crawford, M. Kearns, and N. Geiger. Rotational molding of plastics: Comparison of simulation and experimental results for an axisymmetric mold. *Polymer Engineering and Science, Volume 40, no. 8*, pages 1758–1764, 2000.

[152] A. Greco, A. Maffezzoli, and J. Vlachopoulos. Simulation of heat transfer during rotational molding. *Advances in Polymer Technology, Volume 22, no. 4*, pages 271–279, 2003.

[153] L. C. Thomas. Characterisation of melting phenomena in linear low density polyethylene by modulated dsc$^{\text{tm}}$. *TA Instruments, Thermal Analysis and Rheology*, 2016.

[154] D. Cripps, T. J. Searle, and J. Summerscales. *Comprehensive Composite Materials*, chapter Open Mold Techniques for Thermoset Composites. Elsevier, 2000.

[155] Molded Fiber Glass Companies. *Technical Design Guide for FRP Composite Products and Parts - Techniques & Technologies for Cost Effectiveness*.

[156] C. Santulli. Alternatives for a hand lay-up composite structure: E-glass/epoxy adhesive joint or tapered laminate. *Journal of Materials Science Letters, Volume 21, no. 24*, pages 1959–1963, 2002.

[157] M. Elkington, D. Bloom, C. Ward, A. Chatzimichali, and K. Potter. Hand layup: understanding the manual process. *Advanced Manufacturing: Polymer & Composites Science, Volume 1, no. 3*, pages 138–151, 2015.

[158] J. Bens, B. Van Mieghem, R. Appermont, H. Vanhove, A. Van Bael, J. Duflou, and J. Ivens. Development of material - and energy - efficient metal sheet based tools for composite manufacturing. *Proceedings of the ECCM15 - 15TH European Conference on Composite Materials*, 2012.

[159] Victrex. *Compression Moulding Processing Guide*, 2016.

[160] Ahmad Adlie Shamsuri. Compression moulding technique for manufacturing biocomposite products. *International Journal of Applied Science and Technology, Volume 5, Issue 3*, pages 23–26, 2015.

[161] Amorim Cork Composites. *Cork Solutions & Manufacturing Processes*, 2017.

[162] E. Fernandes, V. Silva, J. Chagas, and R. Reis. Cork-polymer composite (cpc) materials and processes to obtain the same, 2009. WO Patent App. PCT/PT2008/000,051.

[163] S. P. Silva, M. A. Sabino, E. M. Fernandes, V. M. Correlo, L. F. Boesel, and R. L. Reis. Cork: properties, capabilities and applications. *International Materials Reviews, Volume 50, Issue 6*, pages 345–365, 2005.

[164] D. Afonso, R. Alves de Sousa, and R. Torcato. Incremental forming of tunnel type parts. *Procedia Engineering, volume 183*, pages 137–142, 2017.

[165] D. Afonso, R. Alves de Sousa, and R. Torcato. Defining design guidelines for single point incremental forming - rules to a good design of container and tunnel like parts manufactured by incremental forming. *Challenges for Technology Innovation: An Agenda for the Future, CRC press*, 2016.

[166] D. Afonso, R. Alves de Sousa, and R. Torcato. Integration of design rules and process modelling within spif technology - a review. *The International Journal of Advanced Manufacturing Technology*, 2017, (in revision).

[167] D. Afonso, R. Santos, R. Alves de Sousa, and R. Torcato. Single point incremental forming, product design by process. *1st MTD Conference - Meaningful Technology and Design*, 2017 (cancelled).

[168] D. Afonso, R. Alves de Sousa, R. Torcato, J. P. Sousa, R. Santos, and R. Valente. Case studies on industrial applicability of single point incremental forming. *Ciência 2017 - Encontro com a Ciência e Tecnologia em Portugal*, 2017.

[169] D. Afonso, R. Alves de Sousa, and R. Torcato. Testing single point incremental forming molds for thermoforming operations. *The 19th International ESAFORM Conference on Material Forming*, 2016.

[170] D. Afonso, R. Alves de Sousa, and R. Torcato. Developing low cost time saving molds for thermoforming operations. *1st International Conference on Research Trends in Mechanical Engineering*, 2016.

[171] D. Afonso, R. Alves de Sousa, and R. Torcato. Testing single point incremental forming moulds for rotomoulding operations. *The 20th International ESAFORM Conference on Material Forming*, 2017 (accepted).